

**Exploring the relationship between 1-butanol production and  
the pseudohyphal response in *Saccharomyces cerevisiae***

A thesis submitted to The University of Manchester for the degree of Doctor of  
Philosophy in the Faculty of Biology Medicine and Health

**2021**

**David A Leon-Navarro**

**School of Biological Sciences**

## Table of Contents

1.	Abstract.....	13
2.	Declaration.....	14
3.	Dedication .....	15
4.	Acknowledgements .....	16
5.	Introduction.....	17
5.1	Brief summary of the history of microbes in biotechnology .....	17
5.2	<i>Saccharomyces cerevisiae</i> as a model organism .....	19
5.2.1	The legacy of <i>S. cerevisiae</i> as a eukaryotic model organism.....	20
5.2.2	Advantages of <i>S. cerevisiae</i> in the biosynthetic industry .....	22
5.3	Biofuels.....	23
5.3.1	Biofuels as an emergent biotechnological need.....	23
5.3.2	Classification of biofuels by generation .....	25
5.3.2.1	First Generation .....	25
5.3.2.2	Second Generation .....	26
5.3.2.3	Third Generation .....	27
5.3.2.4	Fourth Generation .....	28
5.4	Fusel alcohols as biofuels and chemical commodities.....	28
5.4.1	Industrial uses and production of fusel alcohols.....	29
5.4.2	Butanol as a biofuel.....	31
5.5	Current strategies for 1-butanol biosynthesis .....	32
5.5.1	Butanol biosynthesis through the ABE pathway in <i>Clostridium spp.</i> .....	32
5.5.2	Expression of the ABE pathway in <i>E. coli</i> and <i>S. cerevisiae</i> .....	35
5.5.3	Use of endogenous amino acid catabolic pathways for 1-butanol production in <i>S. cerevisiae</i> .....	35
5.6	2,3-butanediol as an alternative product of fermentation .....	39
5.6.1	Industrial applications of 2,3-butanediol.....	39
5.6.2	2,3-butanediol biosynthesis in <i>S. cerevisiae</i> .....	41
5.6.3	Native bacterial 2,3-butanediol producers.....	42
5.6.4	Metabolic engineering of <i>S. cerevisiae</i> for industrial production of 2,3-butanediol.....	43
5.7	Yeast cellular responses to butanol stress .....	44
5.7.1	Butanol toxicity.....	45

5.7.2	Cellular tolerance and responses to 1-butanol stress .....	45
5.7.3	Metabolic state and quorum-sensing .....	47
5.8	The pseudohyphal response in <i>Saccharomyces cerevisiae</i> .....	48
5.8.1	Signaling pathways involved in yeast filamentation .....	49
5.8.2	Filamentous Mitogen-Activated Protein Kinase pathway .....	49
5.8.3	RAS/cAMP/Protein Kinase A pathway .....	52
5.8.4	SNF1/AMP-dependent Kinase pathway .....	55
5.8.5	Target of Rapamycin (TOR) pathway.....	57
5.8.6	Butanol-induced filamentation.....	60
5.8.7	Novel signaling pathways: the role of mitochondria.....	60
5.9	Aims and objectives of the project .....	61
6.	Materials and Methodology .....	63
6.1	Culture conditions .....	63
6.1.1.	<i>Saccharomyces cerevisiae</i> strains used and growth conditions .....	63
6.1.2.	Antibiotic-based selection media .....	63
6.1.3.	<i>Escherichia coli</i> strains used and growth conditions.....	66
6.1.4.	Cell density in liquid cultures.....	67
6.2.	Nucleic acid manipulation and analysis .....	67
6.2.1.	Purification of plasmid DNA from bacteria .....	67
6.2.2.	Extraction of genomic DNA from yeast cells .....	68
6.2.3.	Extraction of RNA from yeast cells .....	68
6.2.4.	RNA sequencing.....	70
6.2.5.	Determination of DNA and RNA concentrations .....	70
6.2.6.	DNA amplification by Polymerase Chain Reaction (PCR) .....	71
6.2.7.	Agarose gel electrophoresis .....	76
6.2.8.	Digestion of plasmid DNA with restriction enzymes.....	77
6.2.9.	Transformation of yeast cells with plasmid DNA or PCR product.....	77
6.3.	Characterisation of yeast strains.....	79
6.3.1.	Photomicroscopy.....	79
6.3.2.	Stereomicroscopy .....	79
6.3.3.	Growth curves in liquid culture .....	79
6.3.4.	Cell viability assays .....	80
6.3.5.	Agar invasion assay.....	80
6.4.	Protein analysis .....	81

6.4.1.	Preparation of whole cell protein extracts.....	81
6.4.2.	Determination of protein concentration .....	81
6.4.3.	Polyacrylamide gel electrophoresis (PAGE).....	82
6.4.4.	Western Blot .....	82
6.5.	Anaerobic fermentation and metabolite detection by gas chromatography ...	84
6.5.1.	Preparation of gas chromatography standards and glassware .....	84
6.5.2.	Semi-anaerobic fermentation and butanol measurement procedures.....	84
6.6.	Detection of GFP fluorescence in yeast cells.....	85
6.6.1.	Qualitative detection of fluorescence in agar cultures using a laser scanner.....	85
6.6.2.	Microplate assay for the measurement of GFP fluorescence in liquid cultures... ..	86
6.7.	Statistical analysis.....	86
6.8.	Gene Ontology Enrichment analysis .....	87
7.	Development of butanol-responding fluorescent biosensors for <i>S. cerevisiae</i> strains.	88
7.1	Introduction .....	88
7.2	General strategy for biosensor construction .....	90
7.3	Construction and insertion verification of GFP-based biosensor strains.....	91
7.4	Qualitative assessment of GFP fluorescence using a biomolecular imager .....	94
7.5	Microplate assay for quantifying GFP fluorescence in biosensor strains .....	99
7.6	Time-course fluorescence in the GLC7-GFP biosensor strain.....	99
7.6.1	Evaluation of fluorescence from set concentrations of biosensor strains ..	102
7.6.2	Fluorescence intensity of biosensor strains does not increase when exposed to 1-butanol for 4 hours .....	104
7.7	Western Blot reveals strong expression of the Glc7p-GFP fusion protein ....	105
7.8	Construction of <i>SHQ1</i> and <i>NRP1</i> GFP biosensor strains .....	109
7.9	The <i>SHQ1</i> and <i>NRP1</i> biosensor strains had no changes in fluorescence after 1-butanol stress .....	111
7.10	Discussion .....	116
8.	Construction and characterization of <i>adh1Δ</i> mutants in a filamentous strain of <i>Saccharomyces cerevisiae</i> .....	121
8.1	Introduction .....	121
8.2	Deletion of <i>ADHI</i> in a haploid filamentous strain of <i>S. cerevisiae</i> .....	123
8.3	Construction of a diploid <i>adh1Δ</i> filamentous strain .....	125
8.4	Drug sensitivity further verifies the deletion of <i>ADHI</i> .....	128
8.5	Phenotypical characterization of the <i>adh1Δ</i> filamentous strains .....	130

8.6	Loss of <i>ADHI</i> causes changes in colony morphology in haploids .....	130
8.7	Butanol-induced pseudohyphal growth and agar invasion are present in <i>adh1Δ</i> strains.....	133
8.8	<i>adh1Δ</i> strains exhibit slow growth and similar sensitivity to butanol stress to their wild-type.....	135
8.9	The filamentous <i>adh1Δ</i> strain accumulates more butanol than its non-filamentous counterpart .....	137
8.10	Discussion.....	140
9.	Exploring the role of acetaldehyde as a key metabolite in endogenous butanol production.....	143
9.1	Introduction .....	143
9.2	Removal of the Hygromycin B resistance marker in the $\Sigma$ 1278b <i>adh1Δ</i> strain.....	146
9.3	Insertion of the <i>ALD6/ACS2</i> cassette in the $\Sigma$ 1278 <i>adh1Δ</i> strain .....	148
9.4	Expression of <i>ALD6</i> and <i>ACS2</i> reduces the ruffled colony phenotype in the <i>adh1Δ</i> filamentous strain.....	151
9.5	Expression of <i>ALD6</i> and <i>ACS2</i> reduces 1-butanol and acetaldehyde accumulation in an <i>adh1Δ</i> strain .....	153
9.6	Overexpression of <i>ALD6</i> and <i>ACS2</i> in <i>adh1Δ</i> strains reduces R,R-2,3-butanediol accumulation. ....	156
9.7	Investigating the potential of yeast pyruvate decarboxylase enzymes as alternative switches for endogenous butanol production .....	159
9.8	Deletion of <i>PDC1</i> in haploid $\Sigma$ 1278b and W303 strains and construction of a diploid <i>pdc1Δ</i> strain.....	160
9.9	Deletion of <i>PDC1</i> alone does not induce 1-butanol accumulation in either $\Sigma$ 1278b or W303-1A strains. ....	163
9.10	Construction and analysis 1-butanol accumulation in of <i>pdc1,5Δ</i> yeast strains.....	166
9.11	Double deletion of <i>PDC1</i> and <i>PDC5</i> was not able to induce 1-butanol accumulation in either $\Sigma$ 1278b or W303-1A strains. ....	169
9.12	Discussion.....	171
10.	Transcriptomic analysis approach to the identification of potential genes involved in the endogenous production of 1-butanol in <i>S. cerevisiae</i> .....	175
10.1	Introduction .....	175
10.2	Preparation of RNA extracts from anaerobic cultures.....	176
10.3	Sequencing and Quality Control analyses of <i>S. cerevisiae</i> RNA samples.....	176
10.4	Differential expression analysis of RNA-seq data.....	179

10.4.1	Deletion of <i>PDC1</i> results in little transcriptomic change in either the $\Sigma$ 1278b or W303-1A backgrounds.....	180
10.4.2	Transcriptomic profile of <i>adh1</i> $\Delta$ strains of the $\Sigma$ 1278b and W303-1A backgrounds.....	183
10.4.3	Differentially expressed genes in the <i>ALD6/ACS2 adh1</i> $\Delta$ mutants of the $\Sigma$ 1278b and W303-1A backgrounds.....	187
10.4.4	Transcriptomic effect of the overexpression of <i>ALD6</i> and <i>ACS2</i> in the <i>adh1</i> $\Delta$ strains.....	192
10.5	Gene enrichment analysis reveals trends in differentially expressed genes between the <i>adh1</i> $\Delta$ and <i>ALD6/ACS2 adh1</i> $\Delta$ strains.....	195
10.5.1	Aerobic respiration is downregulated in the <i>adh1</i> $\Delta$ strains, while overexpression of <i>ALD6</i> and <i>ACS2</i> partially rescues this downregulation.....	196
10.5.2	Genes of the ergosterol biosynthesis pathway are downregulated in <i>adh1</i> $\Delta$ strains.....	200
10.5.3	Genes involved in glycolysis, glycogen metabolism, and the pentose phosphate pathway are downregulated in the <i>adh1</i> $\Delta$ W303-1A strain.....	203
10.5.4	Sulfur uptake, homocysteine biosynthesis, and glutathione conjugation genes are upregulated in butanol-producing strains.....	208
10.6	Discussion.....	220
11.	General discussion.....	222
11.1	Overview.....	222
11.2	Summary of the main findings of this project.....	223
11.3	Conclusions.....	225
12.	References.....	227

Word Count: 58,431.

## List of Figures

Figure 5.1. The Ehrlich pathway. ....	30
Figure 5.2. The ABE fermentation pathway from Clostridia. ....	34
Figure 5.3. Glycine-dependent 1-butanol biosynthetic pathway of <i>S. cerevisiae</i> . ....	37
Figure 5.4. 2,3-butanediol isomers and their biosynthesis in <i>S. cerevisiae</i> . ....	40
Figure 5.5. Summary of the Filamentous MAPK pathway in <i>S. cerevisiae</i> . ....	51
Figure 5.6. Summary of the RAS/cAMP/Protein Kinase A pathway involved in yeast pseudohyphal growth. ....	54
Figure 5.7. Summary of the SNF1 pathway involvement in the yeast filamentous response. ....	56
Figure 5.8. Summary of the TOR signaling cascade leading to the filamentous response in <i>S. cerevisiae</i> . ....	59
Figure 7.1. General strategy for the construction of potential butanol-responding biosensor strains and verification of c-terminal GFP integration. ....	92
Figure 7.2. Detection of the presence of GFP fusion proteins in living cells by fluorescence microscopy after a 1-hour 1-butanol stress. ....	95
Figure 7.3. Detection of the presence of GFP fusion proteins in living cells by fluorescence microscopy after a 4-hour 1-butanol stress. ....	96
Figure 7.5. Time-course measurement of fluorescence in the <i>GLC7-GFP</i> biosensor strain relative to controls. ....	101
Figure 7.6. Concentrating cells to overcome background strain fluorescence in the fluorescence microplate assay. ....	103
Figure 7.7. Fluorescence of biosensor strains after a 4-hour 1% butanol stress. ....	106
Figure 7.8. Evaluation of GFP fusion protein expression in the constructed biosensor strains. ....	108
Figure 7.9 Verification of GFP tagging of <i>NRP1</i> and <i>SHQ1</i> genes and expression of fusion protein. ....	110
Figure 7.10. Detection of the presence of Nrp1p-GFP and Shq1p-GFP fusion proteins in living cells by fluorescence microscopy. Fluorescent microscopy of the verified biosensor strains treated with 1% (v/v) 1-butanol for 1 hour. Excitation and emission wavelengths used were 470 nm and 525 nm, respectively. Magnification is 100x and scale bar is 5 $\mu$ m in length. ....	112
Figure 7.11. Detection of the fluorescent response of the <i>NRP1</i> and <i>SHQ1</i> biosensor strains in solid media under 1% butanol stress. ....	113
Figure 7.12. The <i>SHQ1</i> and <i>NRP1</i> biosensors do not increase in fluorescence after 1% butanol treatment. ....	115
Figure 8.1. Strategy for the deletion of <i>ADH1</i> in a haploid $\Sigma$ 1278b strain of <i>S. cerevisiae</i> . ....	124
Figure 8.2. Construction and verification of a diploid <i>adh1A</i> strain in the $\Sigma$ 1278b background. ....	127

Figure 8.3. Phenotypical verification of the deletion of <i>ADHI</i> in haploid and diploid strains by drug sensitivity.....	129
Figure 8.4. Deletion of <i>ADHI</i> leads to changes in colony morphology of a $\Sigma$ 1278b haploid strain. ....	132
Figure 8.5 Pseudohyphal growth and agar invasion of <i>adh1A</i> filamentous strains. ....	134
Figure 8.6 Deletion of <i>ADHI</i> causes slow growth but does not affect cell viability on butanol stress.....	136
Figure 8.7 Deletion of <i>ADHI</i> reduces ethanol accumulation and induces butanol production in haploid filamentous strains of <i>S. cerevisiae</i> . ....	139
Figure 9.1. Metabolic fates of acetaldehyde in <i>S. cerevisiae</i> . ....	144
Figure 9.2. The Hygromycin B resistance selection marker was removed from the filamentous <i>adh1A</i> strain.....	147
Figure 9.3. Insertion and verification of Flag-tagged <i>ALD6</i> and <i>ACS2</i> genes in the <i>adh1A</i> filamentous strain.....	150
Figure 9.4. Overexpression of <i>ALD6</i> and <i>ACS2</i> in a $\Sigma$ 1278b <i>adh1A</i> strain disrupts its ruffled colony phenotype.....	152
Figure 9.5 Insertion of the <i>ALD6</i> and <i>ACS2</i> genes abolishes 1-butanol and acetaldehyde accumulation in the non-filamentous <i>adh1A</i> strain. ....	154
Figure 9.6 Overexpression of <i>ALD6</i> and <i>ACS2</i> reduces accumulation of R,R-butenediol in the <i>adh1A</i> strains.....	157
Figure 9.7. Verification of <i>PDC1</i> deletion and mate testing of haploid and diploid $\Sigma$ 1278b strains.....	162
Figure 9.8. Deletion of <i>PDC1</i> does not have an impact on ethanol, butanol or acetaldehyde accumulation in <i>S. cerevisiae</i> . ....	164
Figure 9.10. Verification of <i>PDC5</i> deletion in $\Sigma$ 1278b and W303-1A haploid strains.....	168
Figure 9.11. Deletion of <i>PDC1</i> , <i>PDC5</i> , or <i>PDC1/5</i> does not result in 1-butanol production in <i>S. cerevisiae</i> .....	170
Figure 10.1. Quality Control reports reveal contaminated RNA samples and grouping of samples by strain and genetic background.....	177
Figure 10.2. Transcriptional profile of the <i>pdcl</i> $\Delta$ strains in the $\Sigma$ 1278b and W303-1A backgrounds. ....	181
Figure 10.3. Transcriptional profile of the <i>adh1</i> $\Delta$ strains in the $\Sigma$ 1278b and W303-1A backgrounds. ....	184
Figure 10.4. Expression of <i>HMRA1</i> is decreased in the $\Sigma$ 1278b <i>adh1</i> $\Delta$ and <i>ALD6/ACS2 adh1</i> $\Delta$ strains. ....	186
Figure 10.5. Transcriptional profile of the <i>ALD6/ACS2 adh1</i> $\Delta$ strains in the $\Sigma$ 1278b and W303-1A backgrounds. ....	189
Figure 10.6. Transcriptional changes caused by the overexpression of <i>ALD6</i> and <i>ACS2</i> in the <i>adh1</i> $\Delta$ strains of the $\Sigma$ 1278b and W303-1A backgrounds.....	193

<b>Figure 10.7. Gene Ontology enrichment analysis of differentially expressed genes between mutants and their parental strains across <math>\Sigma</math>1278b and W303 strains. ....</b>	<b>197</b>
<b>Figure 10.8. Downregulation of aerobic respiration in the <i>adh1</i><math>\Delta</math> strains is reversed in the W303-1A strain when <i>ALD6</i> and <i>ACS2</i> are overexpressed.....</b>	<b>198</b>
<b>Figure 10.9. Downregulation of the ergosterol biosynthesis pathway in the <i>adh1</i><math>\Delta</math> strains is reduced in the W303-1A strain when <i>ALD6</i> and <i>ACS2</i> are overexpressed. ....</b>	<b>201</b>
<b>Figure 10.10. Differential expression of glycolytic, glycogen, and pentose phosphate pathway genes in the <i>adh1</i><math>\Delta</math> strains.....</b>	<b>204</b>
<b>Figure 10.11. NADH-producing reactions of the Pentose Phosphate Pathway in <i>S. cerevisiae</i>. ....</b>	<b>206</b>
<b>Figure 10.12. Upregulation of sulfur metabolism genes in the <i>adh1</i><math>\Delta</math> strains decreases when <i>ALD6</i> and <i>ACS2</i> are overexpressed.....</b>	<b>209</b>
<b>Figure 10.13. Sulfate reduction and L-cysteine biosynthesis pathway in <i>S. cerevisiae</i>.....</b>	<b>211</b>
<b>Figure 10.14. Glutathione biosynthesis pathway and role of glutathione in the maintenance of redox homeostasis. ....</b>	<b>212</b>
<b>Figure 10.15. Differential expression of genes involved in glutathione biosynthesis and cellular redox homeostasis. ....</b>	<b>215</b>
<b>Figure 10.16. <i>adh1</i><math>\Delta</math> strains are more resistant to hydrogen peroxide stress than the parental strains.....</b>	<b>219</b>

## List of Tables

<b>Table 5.1. Fuel properties of gasoline, ethanol, and 1-butanol .....</b>	<b>32</b>
<b>Table 6.1. <i>Saccharomyces cerevisiae</i> strains used in this study .....</b>	<b>64</b>
<b>Table 6.2. Plasmids used in this study .....</b>	<b>67</b>
<b>Table 6.3. Oligonucleotides used in this study .....</b>	<b>71</b>
<b>Table 6.4. Antibodies used in this project .....</b>	<b>83</b>
<b>Table 7.1. Candidate genes for the construction of <i>in-vivo</i> 1-butanol biosensors .....</b>	<b>91</b>
<b>Table 3.7. Oligonucleotides used for the verification of GFP tagging of candidate genes..</b>	<b>93</b>
<b>Table 7.3. Expected size of GFP fusion proteins and loading control used in Western Blot .....</b>	<b>107</b>
<b>Table 8.1. Oligonucleotides used for the verification of the deletion of <i>ADHI</i> .....</b>	<b>123</b>
<b>Table 9.1. Oligonucleotides used for the verification of the deletion of <i>PDC1</i> .....</b>	<b>160</b>
<b>Table 9.2. Oligonucleotides used for the verification of the deletion of <i>PDC5</i> .....</b>	<b>167</b>
<b>Table 9.3. Oligonucleotides used for the verification of the deletion of <i>PDC5</i> in the <i>pdc1</i>Δ W303-1A strain .....</b>	<b>167</b>

## List of Abbreviations

2,3-BDO	2,3-butanediol
ABE	Acetone-Butanol-Ethanol
ADH	Alcohol dehydrogenase
ADP	Adenosine diphosphate
AMPK	AMP-dependent protein kinase
AntA	Antimycin A
ATP	Adenosine triphosphate
bp	Base pair
CoA	Coenzyme A
DNA	Deoxyribonucleic acid
DEG	Differentially expressed gene
DEPC	Diethyl polycarbonate
dNTPs	Deoxyribonucleotides
DTT	Dithiothreitol
EDTA	Ethylenediaminetetraacetic acid
fMAPK	Filamentous mitogen-activated protein kinase
GC	Gas chromatography
GAP	GTPase activating protein
GDP	Guanosine diphosphate
GEF	Guanine nucleotide exchange factor
GFP	Green fluorescent protein
GO	Gene ontology
GTP	Guanosine triphosphate
HEPES	(4-(2-hydroxyethyl)-1-piperazineethanesulfonic acid)
HOG	High osmolarity glycerol
HSP	Heat shock protein
HygB	Hygromycin B
LB	Luria-Bertrani
MAPK	Mitogen-activated protein kinase
MMP	Mitochondrial membrane permeability
NAD <sup>+</sup>	Nicotinamide adenine dinucleotide, oxidised
NADH	Nicotinamide adenine dinucleotide, reduced
NADP <sup>+</sup>	Nicotinamide adenine dinucleotide phosphate, oxidised
NADPH	Nicotinamide adenine dinucleotide phosphate, reduced
OD	Optic density
ORF	Open reading frame
PCA	Principal component analysis
PCR	Polymerase chain reaction
PDC	Pyruvate decarboxylase
PEG	Polyethylene glycol
PKA	Protein kinase A
PMSF	Phenylmethanesulfonyl fluoride

PPP	Pentose phosphate pathway
QC	Quality control
RAS	Rat sarcoma
RNA	Ribonucleic acid
RNA-seq	Ribonucleic acid sequencing
RTG	Mitochondrial retrograde
rt-qPCR	Reverse transcription quantitative real-time PCR
SCD	Synthetic complete dextrose
SD	Standard deviation
SDS	Sodium dodecyl sulfate
SDS-PAGE	Sodium dodecyl sulfate Polyacrylamide gel electrophoresis
SDW	Sterile distilled water
TAE	Tris acetid acid EDTA
TBE	Tris boric acid EDTA
TCA	Tricarboxylic acid cycle
ThPP	Thiamine pyrophosphate
TOR	Target of rapamycin
UV	Ultraviolet
v/v	Volume per volume
WT	Wild-type
w/v	Weight per volume

## 1. Abstract

Doctor of Philosophy in the Faculty of Biology, Medicine and Health. 2021

### **Exploring the relationship between 1-butanol production and the pseudohyphal response in *Saccharomyces cerevisiae***

David A. Leon-Navarro

The University of Manchester, Faculty of Biology, Medicine and Health, M13 9PT, United Kingdom.

1-butanol is a promising biofuel due to its energy content, ease to apply in current infrastructure, and ability to be used in a series of industrial processes. Butanol is produced naturally by bacteria of the genus *Clostridia* through the acetone-butanol-ethanol pathway, but due to the difficulties associated with clostridial fermentations, butanol production in industry-friendly hosts like *Saccharomyces cerevisiae* is of high interest. Hence, the aim of this project was to assess endogenous 1-butanol production of a filamentous strain of *S. cerevisiae* and identify potential advantages to the fermentative process found in this genetic background. Endogenous butanol production was induced by deleting the *ADH1* gene in a  $\Sigma$ 1278b strain. The resulting mutant displayed altered colony morphology and produced up to  $114 \pm 19$  mg/l of butanol in anaerobic fermentation, more than an *adh1* $\Delta$  mutant of the W303-1A background. Neither deletions of *PDC1* or *PDC5* were able to induce butanol accumulation. When the *ALD6* and *ACS2* genes were overexpressed in the *adh1* $\Delta$  strains with the aim of reducing intracellular acetaldehyde accumulation, 1-butanol and acetaldehyde accumulation were hindered in the  $\Sigma$ 1278b strain, and completely abolished in the W303-1A strain, suggesting a close relationship between both. RNA-seq analysis of the *adh1* $\Delta$  and *ALD6/ACS2 adh1* $\Delta$  strains revealed a correlation between the induction of glutathione biosynthesis genes, and the repression of aerobic respiration and ergosterol biosynthesis with the ability to produce 1-butanol via the endogenous pathways. The results obtained in this project suggest a role for the glutathione-mediated acetaldehyde stress response in facilitating 1-butanol production when *ADH1* is deleted, as evidenced by the yields of the  $\Sigma$ 1278b strain. However, further research will be required to better understand how these cellular mechanisms interact and result in accumulation of butanol in *S. cerevisiae*.

## 2. Declaration

No portion of the work referred to in this thesis has been submitted in support of an application for another degree or qualification of this or any other university or other institute of learning.

### Copyright statement

- I. The author of this thesis (including any appendices and/ or schedules to this thesis) owns certain copyright or related rights in it (the “Copyright”) and s/he has given The University of Manchester certain rights to use Copyright, including for administrative purposes.
- II. Copies of this thesis, either in full or in extracts and whether in hard or electronic copy, may be made **only** in accordance with the Copyright, Designs and Patents Act 1988 (as amended) and regulations issued under it or, where appropriate, in accordance with licensing agreements which the University has from time to time. This page must form part of any such copies made.
- III. The ownership of certain Copyright, patents, designs, trademarks and other intellectual property (the “Intellectual Property”) and any reproductions of copyright works in the thesis, for example graphs and tables (“Reproductions”), which may be described in this thesis, may not be owned by the author and may be owned by third parties. Such Intellectual Property and Reproductions cannot and must not be made available for use without the prior written permission of the owner(s) of the relevant Intellectual Property and/ or Reproductions.
- IV. Further information on the conditions under which disclosure, publication and commercialisation of this thesis, the Copyright and any Intellectual Property and/or Reproductions described in it may take place is available in the University IP Policy (see <http://documents.manchester.ac.uk/DocuInfo.aspx?DocID=24420>), in any relevant Thesis restriction declarations deposited in the University Library, The University Library’s regulations (see <http://www.library.manchester.ac.uk/about/regulations/>) and in The University’s policy on Presentation of Theses

### **3. Dedication**

I dedicate this work to my family and the memory of my father Guillermo, as I would not be alive writing these words without their stoic support.

#### **4. Acknowledgements**

I would like to offer special thanks to my two supervisors, Prof. Mar Ashe and Prof. Christopher Grant, who through their guidance and transparent feedback have taught me to approach challenges in a straight and inquisitive manner, and to reach to others for aid and return such aid when requested. Additional thanks to Prof. Graham Pavitt for his support as project advisor.

I would like to thank former members of the laboratory Olugbenga Ogunlabi, Sarah Sheaik and Reem Swidah, whose experience with gas chromatography and butanol-producing strains have paved the path to this project, and thanks to their teachings I have been enabled to continue this path.

Special thanks to Zorana Carter for her constant support and for developing the plasmids used to construct the deletion strains used in this project.

To the past and present members of the Ashe-Grant-Pavitt laboratories, I want to extend my thanks for contributing to an amicable and supportive research and social environment. I wish all of you happiness and fulfillment in your life endeavors.

My eternal appreciation to my mother Luciana, my father Guillermo, my brother Pablo, and my love Enzo, as without their trust, support and understanding I would not have had the strength to press on. Thanks for believing in me all these years.

Finally, special thanks to ANID (Agencia Nacional de Investigación y Desarrollo) Chile, whose financial support made this project possible.

## **5. Introduction**

### **5.1 Brief summary of the history of microbes in biotechnology**

Biotechnology is the use and modification of living organisms for the development and manufacture of products for human use, and its associated activities range from the domestication and select breeding of animals and plants, to advanced genetic modifications and metabolic engineering of microorganisms towards specific products.

One of the oldest biotechnological industries is the use of yeasts in the fermentation of sugar-rich foodstuffs to produce alcoholic beverages, as evidenced by archeological findings from prehistoric China and Iran (McGovern et al, 1997; McGovern et al, 2004). During history, almost every culture developed some sort of fermented product, including non-alcoholic foodstuffs such as cheese and milk kefir. Despite its ubiquity, the microbial nature of the fermentation process would remain unknown until technological and scientific advances between the 17<sup>th</sup> and 19<sup>th</sup> century allowed a closer look into microorganisms.

The invention of the microscope by Anthonie van Leeuwenhoek in the 17<sup>th</sup> century (Dobbel, 1923) and further technical improvements by Giovanni Batista Amici (Amici, 1820) led to the birth and early development of microbiology. Between 1836 and 1838, Charles Cagniard-Latour, Friederich Kützing and Theodor Schwann independently reported that yeast ferment contained globular bodies of “vegetal” nature, and attributed sugar fermentation to a physiological process (Barnett, 1998). During the 19<sup>th</sup> century the contributions of multiple microbiologists, including Louis Pasteur and Robert Koch, provided the technical and experimental knowledge to reliably study pure cultures of microbes, extending the range of microorganisms that could be studied and the quality of the experimental data.

Later in the mid 1900's, advances in genetics and molecular biology laid the foundations for one of the biggest biotechnological breakthroughs of the century: the development of recombinant DNA technology. First, the discovery and characterization of extrachromosomal transferable genetic elements in bacteria, named plasmids in 1952 by Joshua Lederberg (Lederberg, 1952), produced the base molecule for gene transfers. Later on, the identification of restriction endonucleases able to cleave specific DNA sequences (Mertz and Davis, 1972) and DNA ligases that could re-join the cleaved fragments (Little et al., 1967) provided the molecular tools to cut and paste the desired genes into plasmid vectors. The first successful recombinant plasmid was constructed by Stanley Cohen and colleagues (Cohen et al., 1973). This technique revolutionized biotechnology by providing the basis to potentially express and produce any gene product in easy to grow microbes, reducing production costs of some drugs, such as insulin (Tikhonov et al., 2001).

Finally, development of the first DNA sequencing techniques by Frederick Sanger and colleagues in 1977 allowed for the first time in history the sequencing of the genomes of viruses and prokaryotes (Sanger et al., 1977), an achievement that paved the way for more ambitious international endeavors like sequencing the genome of the first eukaryotic model organism: *Saccharomyces cerevisiae* in 1996 (Goffeau et al., 1996), and would eventually lead to the first drafts of the human genome in 2001 (IHGSC, 2001; Venter et al., 2001). Assembly and analysis of such large amounts of data would not have been possible without the support of powerful computational tools; hence a close relationship between biology and informatics was pivotal for the development of genomics. The genomic revolution not only provides biotechnology with information on the location, sequence and known mutants of potential genes of interest, but it also provides a global approach to biological systems where it is now possible to examine how different

conditions affect the whole of multiple cellular systems, including metabolic state, transcript levels and protein expression.

A more recent major technological leap in the field of sequencing is the development of next-generation sequencing techniques, which allow for high-throughput sequencing of DNA and RNA samples (Goodwin et al., 2016), increasing sequencing speed while reducing sequencing costs from \$5,292.39 to \$0.006 per megabase since the completion of the human genome project in 2001 (Wetterstrand, 2021). This reduction in costs has enabled the application of high-throughput sequencing in new fields, such as clinical identification of genetic variants in human diseases (Qin, 2019), taxonomic and comparative genomic studies (Cao et al., 2017; Marciniak and Perry, 2017), as well as the biotechnological industry (Costessi et al., 2018).

These recent advances in genetic manipulation have provided the tools and knowledge to turn microbes into biological factories that can synthesize products requiring processes as simple as expressing a single heterologous gene product, to more complex processes involving multiple enzymatic steps. Biotechnology holds the potential to provide solutions in a world where sustainable industries and alternatives to current technologies are required, and fortunately, with the aid of microbes, the possibilities are nearly limitless.

## **5.2 *Saccharomyces cerevisiae* as a model organism**

From its humble origins in prehistoric brewing, *S. cerevisiae* has grown to become a key protagonist in the food industry, biotechnology, and scientific research. To this date, this organism continues to be used in fermentative industry and biological research thanks to a series of traits that will be reviewed in the following sections.

### 5.2.1 The legacy of *S. cerevisiae* as a eukaryotic model organism

Since the initial discoveries on the nature of fermentations in the 19<sup>th</sup> century, *S. cerevisiae* has become a model organism for research on eukaryotic biology. This unicellular organism has been at the front of several breakthroughs in eukaryotic metabolism, genetics, and cell biology.

One of the reasons for this is that *S. cerevisiae* is a eukaryotic organism that is simple and quick to grow and manipulate in the laboratory, making it much easier to work with than many higher organisms, such as mammals. While some scientific questions cannot be answered in yeast, like those regarding the more intricate functions of multicellular organisms, it is an outstanding model for studies on the fundamental mechanisms behind genetics and cell biology because many of these mechanisms are highly conserved among eukaryotes (Petranovic and Nielsen, 2008; Foury, 1997).

The award of several Nobel prizes to research done in *S. cerevisiae* serves as a testament to the value of this microorganism in understanding our own biology. The most recent example is Yoshinori Ohsumi, who received the Nobel Prize of Physiology or Medicine in 2016 for the identification of the genes and mechanism involved in autophagy, an essential cellular process involved in protein and organelle degradation (Levine and Klionsky, 2017; Mizushima et al., 1998).

As another example, the 2009 Nobel Prize of Physiology or Medicine was granted to Elizabeth Blackburn, Carol Greider and Jack Szostak for their research on chromosomal protection and maintenance by telomerase enzymes (Varela and Blasco, 2010). Telomerase activity is a fundamental cellular function that permits eukaryotic cells to preserve chromosomal integrity after each genome duplication by maintaining the length of the telomeres (Flores et al., 2006). Deregulation of telomerase activity contributes to

the phenotype of diseases like cancer, highlighting the impact of this breakthrough (Trybek et al., 2020).

Likewise, Leland Hartwell, Timothy Hunt and Paul Nurse received the same award in 2001 for their studies on the regulation of the eukaryotic cell cycle (Watts, 2001). Leland Hartwell employed a series of *S. cerevisiae* temperature-sensitive mutant strains to identify the genes involved in the coordination of the eukaryotic cell cycle, including the regulator of the G1/S threshold *CDC28* (Hartwell, 2002). Additionally, Hartwell's group utilised this knowledge of cell cycle checkpoints and repair to identify which cellular defects granted sensitivity to a series of chemotherapeutic agents, thus translating knowledge obtained from yeast to human medicine (Simon et al., 2000).

These three example discoveries demonstrate that *S. cerevisiae* is a relatively simple and easy to manipulate host that has allowed scientists to acquire knowledge about the basic genetic and cellular functions that govern the life of higher organisms, including humans, while also shedding light on the genetic and molecular components of genetic diseases.

The versatility of *S. cerevisiae* as a model organism in research is not only due to possessing the same cellular machinery keeping most eukaryotic organisms alive, but also because of the wide array of tools available to genetically manipulate them, the availability of genome databases, and the existence of gene deletion libraries (Skrzypek et al., 2018; Duina et al., 2014; Winzeler et al., 1999). These tools allow researchers to answer biological questions by using multiple approaches, including disrupting genes of interest to study the consequences of their dysfunction, tagging gene products with specific markers to track their location within the cell or their interaction with other

molecules, or introducing one or multiple genes from other organisms to study the results of their expression in yeast.

### **5.2.2 Advantages of *S. cerevisiae* in the biosynthetic industry**

The success of *S. cerevisiae* in fermentation industries can be mainly attributed to its unique metabolism that prioritises glucose uptake and fermentation into ethanol over respiration and biomass accumulation, in both aerobic and anaerobic conditions, a phenomenon named the Crabtree effect (Pfeiffer and Morley, 2014). Curiously, a similar phenomenon was already reported by Otto Warburg and colleagues, who observed that cancer cells favour aerobic fermentation of glucose into lactic acid instead of respiration (Warburg et al., 1926). This metabolism is at the center of *S. cerevisiae*'s competitive strategy that revolves around the quick production and accumulation of ethanol, a toxic substance that is inhibitory to other microorganisms and to which *S. cerevisiae* is not only tolerant but can also utilise as a carbon source when fermentable sugars are depleted from the media by switching to a respiratory metabolism in a finely regulated process called the diauxic shift (Galdieri et al., 2010). This competitive advantage is also beneficial for the brewing process, as the inhibitory effect of ethanol aids in the elimination of microorganisms that may spoil the desired product.

Coupled with their innate ability to produce ethanol, *S. cerevisiae* industrial strains have been selected to tolerate the multiple stresses present in industrial environments. Some examples include temperature changes, high osmotic pressure caused by high concentrations of solutes in the feedstock, low pH (Narayanan et al., 2016; Fernández-Niño et al., 2015), and the toxic effects of ethanol and other substances produced during both the brewing of beverages and the production of bioethanol (Bleoanca and Bahrim, 2013; Walker and Basso, 2020). Additionally, *S. cerevisiae* cells are impervious to

bacteriophage contamination, a constant issue of bacterial fermentation processes that results in loss of productivity by destroying the bacterial cultures (Zahn and Halter, 2018). Industries that have reported losses by bacteriophage contamination include acetone-butanol-ethanol fermentation in *Clostridium spp.* (Jones et al., 2000), *Aerobacter spp.* vinegar fermentations (Sellmer et al., 1992), and dairy fermentation operations (Marcó et al., 2012).

These two traits have made *S. cerevisiae* into the best microorganism for ethanol production, but the benefits do not end there. By combining the power of yeast's genetic malleability and available tools with its industrial robustness, it is possible to engineer yeast strains to express the genes involved in the biosynthesis of multiple products of interest such as drugs, flavourants, chemical precursors, and biofuels in a new discipline termed synthetic biology (Walker and Pretorius, 2018; Galanie et al., 2015; Paddon and Keasling, 2014). Synthetic biology represents the next step in yeast biotechnology, further increasing its flexibility as a host for biosynthetic enterprises and allowing a new level of fine manipulation of each biosynthetic step, elevating yeast to the status of a model microbial factory.

## **5.3 Biofuels**

### **5.3.1 Biofuels as an emergent biotechnological need**

The discovery of crude oil in 1858 and its subsequent exploitation for the manufacture of a variety of synthetic organic materials and fossil fuels to produce the energy needed to power cities, industries, and transportation resulted in a technological revolution that shaped the global economy and politics due to the ever-increasing demand for these new oil-based commodities.

This technological revolution and the high global demand for oil and fuel has brought not only new benefits, but also new problems. The high worldwide demand for crude oil. Which reached 4484.5 million tonnes of oil per day on 2019 (BP, 2020), and the cyclical pattern of crude oil prices has resulted in political tensions between oil-producing countries and consumers, leading to international armed conflicts (Jaffe and Ellass, 2015; Colgan, 2013). Additionally, continuous combustion of fossil fuels has resulted in increased CO<sub>2</sub> emissions into the atmosphere, contributing to a process of global warming that can disturb the integrity of life on the planet (Letcher, 2019). Finally, because geological oil reserves are finite, their eventual depletion constitutes an economical and industrial challenge for a world that depends on oil for its industry and logistics (Miller and Sorrell, 2013). These problems have prompted the search for renewable alternatives to fossil fuels, and with that interest in mind, biotechnology might have the solutions the world is looking for.

Biofuels are liquid or gas chemical products manufactured using diverse forms of biomass that can be utilised as more sustainable alternatives to fossil fuels. Biofuels are produced by two general strategies: direct extraction and refinement of the biofuel from raw materials, or microbial fermentation of the organic feedstock into the desired product. Two contemporary examples of biofuels produced employing each general strategy are biodiesel and ethanol. Biodiesel is a lipid biofuel extracted directly from oil-rich biomass such as seed oils and oleaginous algae. Ethanol is fermented by *S. cerevisiae* cultures using sugar-rich plant extracts like corn, sugarcane, and beetroot as feedstock.

Because the biomass sources for biofuel production come from renewable sources including plant, algae, and animal biomass, biofuel production has more potential for sustainability than fossil fuels, as long as a balance between biomass production and conversion to biofuels is achieved. In addition, because vegetable and algae biomass used

for biofuel production is actively participating in CO<sub>2</sub> fixation, production of the feedstock contributes to the carbon cycle, unlike crude oil reserves that represent sequestered carbon sources that cannot actively fixate CO<sub>2</sub>. Finally, because biofuel production operations do not depend on existing geological reserves and can use a wide range of biomass sources as feedstock, it has the potential to alleviate the supply and demand tensions that exist in the crude oil market by facilitating the entry of new producers to satisfy the demand.

### **5.3.2 Classification of biofuels by generation**

Despite the many chemical species that can be considered biofuels and the different methods used for their manufacture, biofuels can be classified into four generations according to the type of biomass used as feedstock for their production and the potential for sustainability of each production strategy (Alalwan et al., 2019). Each generation introduces new possibilities and technical challenges that will be briefly discussed in this section.

#### **5.3.2.1 First Generation**

This group comprises biofuels produced using high-energy agricultural crops as raw materials and includes the contemporary commercial biofuel production models.

Contemporary bioethanol production belongs to this category. The two major bioethanol producers in the world, the United States and Brazil, ferment ethanol using corn and sugarcane as feedstocks, while other countries use grains, beetroot, or a combination of the above (Lamichhane et al., 2021). Biodiesel is another contemporary first-generation biofuel that is produced by transesterification of oils extracted from lipid-rich edible vegetable and animal biomass, usually palm oil, rapeseed, and soybeans (Mishra and Goswami, 2017).

This group of biofuels is the least sustainable because their production depends on large amounts of fertile land dedicated to growing the feedstock crops, conflicting with food production, negatively impacting ecosystems, and potentially countering the efforts to reduce greenhouse gas emissions (Crutzen et al., 2016). Thus, research has focused on finding other sources of biomass to produce more sustainable biofuels, leading to the development of advanced biofuels.

### **5.3.2.2 Second Generation**

In attempts to find more sustainable alternatives to crops for biofuel production, some research efforts have focused on finding methods to use raw materials low in simple sugars but high in cellulose that are often considered waste by-products of agricultural endeavors. This approach allows manufacturers to upcycle otherwise waste materials back into the production process, increasing the sustainability of biofuel production setups.

To be used as feedstock for biofuel production, lignocellulosic biomass must be pre-treated to expose cellulose, which is then hydrolyzed into monosaccharides that can be of use to the microorganisms involved in the fermentation process (Jönsson and Martín, 2016). Methane, also known as biogas, is an example of a second-generation biofuel produced by anaerobic fermentation of pre-treated lignocellulosic biomass (Principi et al., 2019).

While promising, the use of lignocellulose as the feedstock for bioethanol production presents a few challenges. One of them is that hydrolysis of lignocellulosic biomass releases different monosaccharides, mostly glucose and xylose. While *S. cerevisiae* readily uses and ferments glucose it is not able to ferment xylose, hence some areas of research have focused on engineering *S. cerevisiae* strains able to ferment both sugars

(Osiro et al., 2019; Patiño et al., 2019). Another challenge is that pre-treatment of lignocellulosic biomass releases a series of inhibiting compounds for microbes, including carboxylic acids, benzo-quinones, aromatic, and phenolic compounds (Jönsson and Martín, 2016). Strategies that can be used to alleviate this problem include selection of feedstock requiring less aggressive pre-treatments, detoxification steps, and selection or engineering of resistant microorganisms. Overcoming these challenges is of most importance for second-generation bioethanol production to be commercially competitive and more sustainable than first generation biofuels.

### **5.3.2.3 Third Generation**

Third generation biofuels use oleaginous microorganisms as sources of lipid-rich biomass, including microalgae, bacteria, and fungi (Leong et al., 2018). The main advantage of third generation cultures over plants for biomass production are that they do not require large areas of fertile land to grow and can be set in more space-efficient operations, thus avoiding conflicts with agricultural crop production.

Microalgae can be grouped by the carbon source used into autotrophs (photosynthetic algae), heterotrophs, and mixotrophs, which benefit from both types of carbon sources and have the highest biomass and lipid accumulation among all three (Bhatnagar et al., 2011). One of the challenges associated with third-generation biofuels is the high cost of carbon sources for microalgae biomass production. One approach to overcome this challenge is to seek microalgae that can use unfavorable carbon sources, such as toxic compounds in wastewaters (Adeniyi et al., 2018; Carbone et al., 2017) or hydrocarbon-containing field formation water (Das and Deka, 2019). This approach serves the double purpose of reducing culture costs and cleaning polluted waters, further demonstrating the potential of algae for a greener future.

In summary, third-generation biofuels have the potential not only to be more sustainable sources of lipid-rich biomass than plants, but also to assist in the remediation of polluted waters.

#### **5.3.2.4 Fourth Generation**

Production of fourth-generation biofuels involve the use of genetically engineered photosynthetic microorganisms with the goal of increasing carbon fixation efficiency, thus enhancing biomass accumulation and creating artificial carbon sinks that result in carbon negative biofuel production operations. The organisms employed in this type of biofuel production include macro and microalgae, and cyanobacteria. Because these microorganisms can grow in harsh culture conditions such as saltwater and wastewater, their culture does not require a high freshwater supply, thus reducing the competition over this precious resource (Abdullah et al., 2019).

Synthetic biology methods are accelerating the efforts of improving phototrophic microalgae for biofuel production through more precise genetic engineering. Improvements to production include increasing carbon fixation by clearing metabolic bottlenecks in the Calvin cycle, increasing photosynthetic efficiency by truncation of the light harvesting complex antenna, and reducing harvesting costs by inducing auto-flocculation of cells or stimulating secretion of lipid contents (Moravvej et al., 2019; Gomaa et al., 2016).

#### **5.4 Fusel alcohols as biofuels and chemical commodities**

The search for new sustainable biofuels has drawn the attention of scientists and industry to different metabolites produced by microorganisms. One such group of metabolites are fusel alcohols, composed of a series of short-chain alcohols produced by *S. cerevisiae* that include amyl alcohol, isoamyl alcohol, isobutanol and 1-butanol (Webb

and Ingraham, 1963). They are found in varying proportions as by-products of fermentation derived from the enzymatic breakdown of amino acids. When present in small quantities, they confer subtle aromas and flavour to alcoholic brews, contributing to the quality and sensorial identity of these products (Van der Schaft, 2015).

In 1907, Felix Ehrlich identified fusel alcohols as products of amino acid catabolism and proposed the biochemical bases of their biosynthesis (Ehrlich, 1907). Later studies by other biochemists described the individual reactions involved in this pathway and their enzymatic nature (Hazelwood et al., 2008). The metabolic pathway begins with transamination of amino acids, subsequent decarboxylation of the corresponding 2-oxo acid, which is finally reduced to an aldehyde. From this point, the aldehyde can be either oxidized to an acid or reduced to a fusel alcohol (Figure 5.1).

#### **5.4.1 Industrial uses and production of fusel alcohols**

The identification of the Ehrlich pathway allowed the design of culture conditions that stimulated the biosynthesis of these products. No longer were they a small fraction of yeast alcoholic fermentations, and their selective production was possible. Fusel alcohols have a variety of industrial uses such as solvents or precursors in the synthesis of a plethora of products, including perfumes, paint thinners and flavourants (Dürre, 2007; Van der Schaft, 2015). At the beginning of the 20<sup>th</sup> century, bulk production of fusel alcohols and other organic compounds was carried out by microbial fermentation. For instance, during World War I, stills were built in the United Kingdom and the United States of America to supply the demand for acetone, a chemical precursor required in the production of cordite for ammunition. These stills produced acetone and 1-butanol through the ABE (acetone-butanol-ethanol) pathway of *Clostridia* and continued to work after the war ended (Bud, 1993). Although promising, microbial fermentation of products

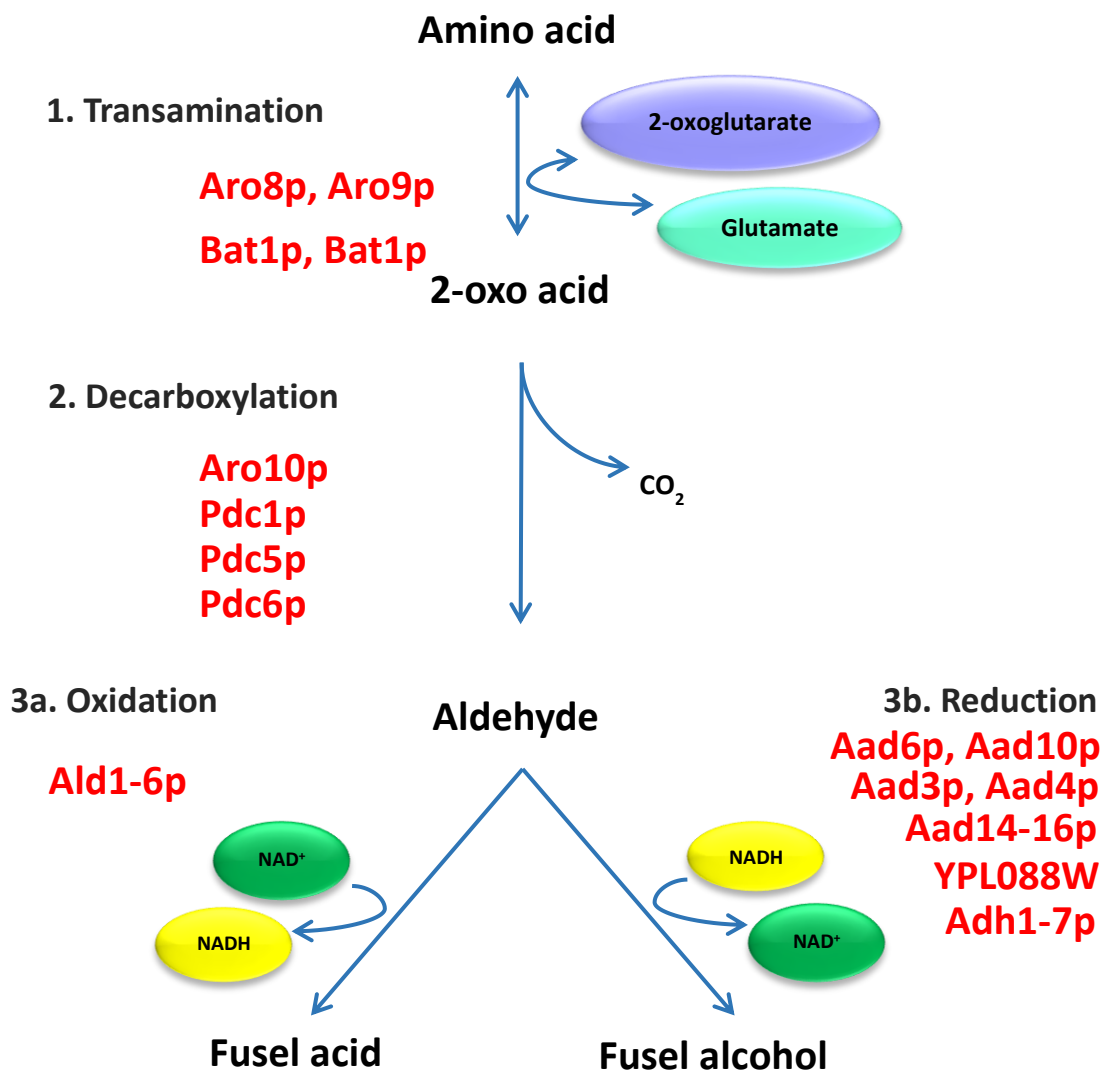


**Figure 5.1. The Ehrlich pathway.** Diagram shows the general steps involved in the conversion of an amino acid into its corresponding acid or alcohol. The enzymes involved in the pathway are aromatic aminotransferases (Aro), branched-chain amino acid transaminases (Bat), pyruvate decarboxylases (Pdc), aldehyde dehydrogenases (Ald), alcohol dehydrogenases (Adh), aryl-alcohol dehydrogenases (Aad). Abbreviated cofactors include oxidised nicotinamide adenine dinucleotide (NAD<sup>+</sup>), and reduced nicotinamide adenine dinucleotide (NADH).

of interest was quickly replaced by petrochemical production strategies, which have been used in mainstream industry ever since. Nonetheless, because of the rising economic and environmental factors associated with the fossil fuel industry, attention has turned once again to microbial biosynthesis in hopes of finding viable alternatives.

Due to the recent advances in molecular biology and genetic engineering (Nielsen, 2001; Hong and Nielsen, 2012), the design of microbial factories for the production of organic compounds has progressed rapidly, and the future of environment-friendly renewable biofuels may well provide part of the solution to fossil fuel depletion.

#### **5.4.2 Butanol as a biofuel**

Besides its uses as a chemical precursor in the production of other products, 1-butanol has recently emerged as a promising second-generation biofuel with physical and chemical properties that make it more suitable to use in the current infrastructure than the widely-produced and funded bioethanol. In order to assist the following discussion, some of the physical properties of 1-butanol, ethanol, and gasoline pertaining to their performance as fuels are summarised in Table 5.1.

First, 1-butanol has a higher specific energy than ethanol, with 36.1 MJ/kg versus 29.7 MJ/kg, which is more comparable to the energy content of gasoline at 46.5 MJ/kg (Haynes, 2014). This suggests that butanol behaves more closely to gasoline in respect to the amount of fuel required to produce work.

1-butanol's octane number of 96 (Galloni et al., 2016), a value related to a fuel's capacity to avoid premature ignition during compression in a spark-ignition engine, is comparable to the mid-range octane number of the commercially available gasolines (Table 5.1). On the other hand, ethanol has a higher-octane number of 107 (Galloni et al., 2016), surpassing even the highest-octane gasolines in the market. While this value

suggests that ethanol is better at preventing engine knocking, it does not mean that 1-butanol performs worse in the current engine technologies.

**Table 5.1. Fuel properties of gasoline, ethanol, and 1-butanol**

	Gasoline	Ethanol	1-butanol
Specific energy (MJ/kg)	46.5	29.7	36.1
Octane number	90-101	107	96
Flash point (°C)	-43	14	35
Autoignition temperature (°C)	246-280	365	343

Regarding to its ignition properties, butanol has a flash point of 35°C, higher than gasoline and ethanol, while possessing a high autoignition temperature of 343°C, close to ethanol's value of 365°C (Table 5.1). The higher flash point of 1-butanol might bring difficulties during ignition in a cold engine, but it also means that it is less prone to accidental ignition during handling (Demirbas, 2015). 1-butanol's high autoignition temperature also contributes to its properties as a safe fuel.

Finally, due to its higher hydrophobicity when compared to ethanol, 1-butanol can be used in pure form or blended with gasoline up to 85%, while being less hygroscopic, therefore less corrosive than ethanol and more suitable to use with the present combustion engines and piping infrastructure (Dürre, 2007).

## **5.5 Current strategies for 1-butanol biosynthesis**

### **5.5.1 Butanol biosynthesis through the ABE pathway in *Clostridium spp.***

As previously mentioned, the traditional strategy for 1-butanol production exploits the natural capacity of bacteria of the *Clostridium* genus, a group of gram-positive, obligate

anaerobes, to convert glucose into this alcohol through the ABE pathway (Zheng et al., 2009). 1-butanol synthesis in this way involves the condensation of two molecules of acetyl-CoA provided by glycolysis into acetoacetyl-CoA, and five consecutive reduction steps to yield 1-butanol (Jang et al, 2012; Patakova et al, 2019). Because acetyl-CoA is also used for the synthesis of ethanol and acetone, this process is also called solventogenesis. Figure 5.2 below shows a schematic of the ABE pathway.

Producing 1-butanol in the organisms that naturally synthesize it seems a logical strategy, and multiple efforts have been made to improve yields in *Clostridia* by overexpressing specific enzymes of the pathway in order to redirect metabolic flux into 1-butanol, resulting in yields of 11.4 g/l and 12.0 g/l in *C. acetobutylicum* and *C. tyrobutylicum*, respectively (Lee et al., 2009; Yu et al., 2015). Unfortunately, working with *Clostridia* presents a number of problems that may hinder further improvements in 1-butanol yields and its application in industry, such as oxygen and end-product toxicity, mixed fermentation products, slow growth, sporulation concomitant to solventogenesis, and lack of genetic tools (Zheng et al., 2009). This has led researchers to express the ABE pathway in more manageable and safe microorganisms to circumvent these problems.

*E. coli* and *S. cerevisiae* are popular hosts for the heterologous expression of the ABE pathway because of their rapid growth, easy cultivation and availability of tools for genetic manipulation. Because of their status as model organisms, their cellular physiology, metabolism, gene expression regulation and genome have been extensively studied, allowing the design of tools for genetic manipulation and synthetic biology that facilitate metabolic engineering in these species (Alberghina and Crulli, 2010).

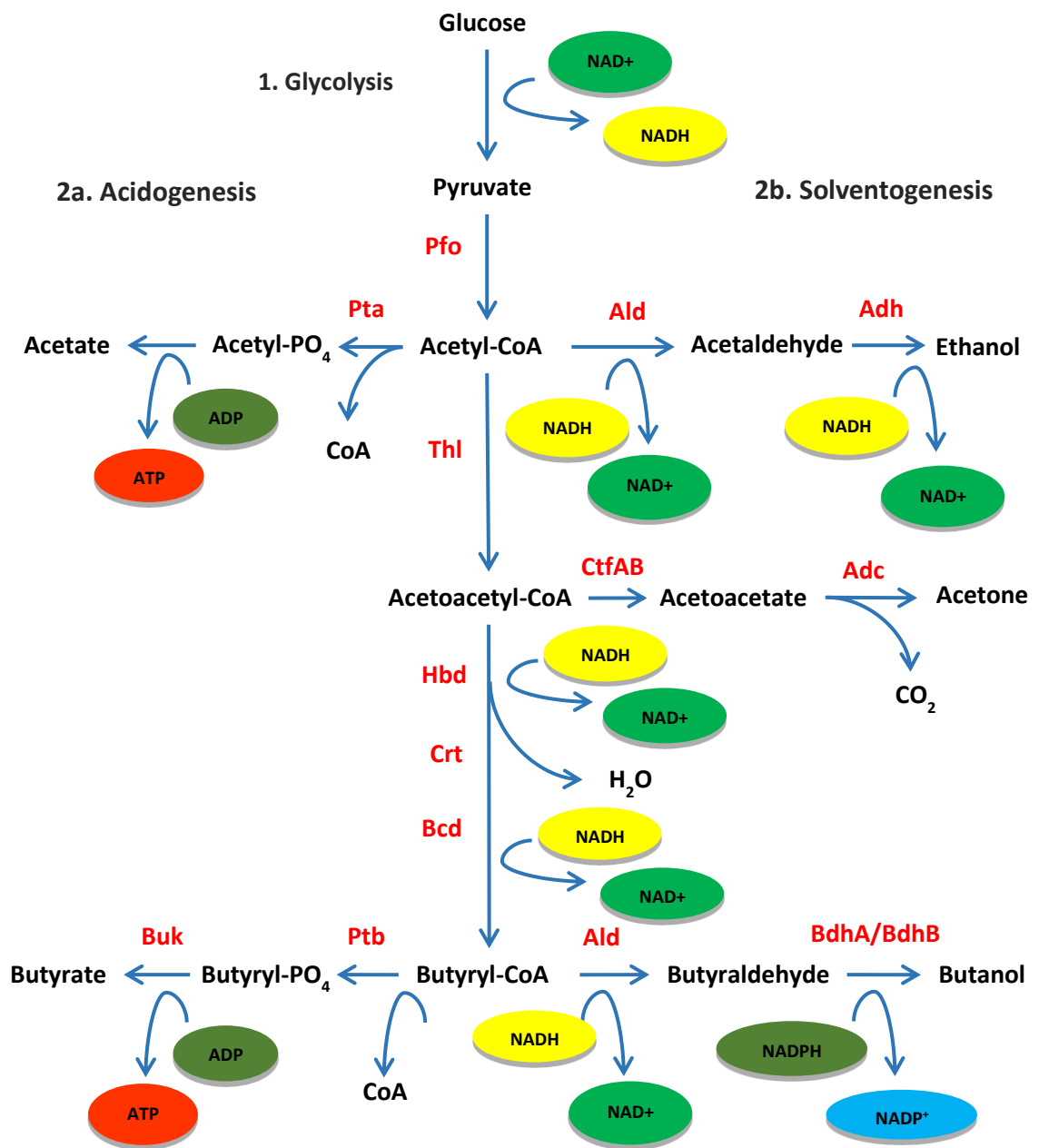


**Figure 5.2. The ABE fermentation pathway from Clostridia.** Diagram of the acetone-butanol-ethanol pathway, including the synthesis of acetyl-CoA from glycolysis. Enzymes involved: pyruvate-ferrodoxin oxidoreductase (Pfo), acetate kinase (Ack), phosphotransacetylase (Pta), CoA transferase (CoAt), Acetoacetyl-CoA:acetate CoA-transferase (CtfAB), acetoacetate decarboxylase (Adc), thiolase (Thl), butyrate kinase (Buk), phosphate acetyltransferase (Pta), phosphate butyryltransferase (Ptb), hydroxybutyryl-CoA dehydrogenase (Hbd), crotonase (Crt), acyl-CoA dehydrogenase (Bcd), aldehyde/ alcohol dehydrogenase (Adh), butanol dehydrogenases (BdhA, BdhB).

### **5.5.2 Expression of the ABE pathway in *E. coli* and *S. cerevisiae***

Initial attempts to express the core ABE pathway enzymes from *C acetobutylicum* in *E. coli* yielded low 1-butanol titers of 13.9 mg/l. Deletion of competing enzymes in the host genome (*ldhAp*, *adhEp* and *frdBCp*), coupled with higher NADH pools generated by an activated pyruvate dehydrogenase complex increased 1-butanol titers up to 373 mg/l, indicating that fine tuning of redox balance and acetyl-CoA pools is key to achieve higher yields (Atsumi et al., 2008). A novel strategy that reinforces this concept and has produced better results is the use of acetyl-CoA synthesis and NADH as driving forces, together with the introduction of an irreversible reduction step in the pathway. This strategy has proven to be effective by producing impressive 1-butanol titers of 15g/l to 30 g/l with end-product removal (Shen et al., 2011).

Compared to the bacterial alternatives, *S. cerevisiae* possesses some advantages for the industrial synthesis of 1-butanol, including a higher tolerance to the harsh conditions of industry, including high osmolarity and low pH (Nevoigt, 2008), and higher tolerance to alcohol toxicity (Fischer et al, 2008). Unfortunately, the first attempts at producing 1-butanol through the ABE pathway in this yeast yielded a strain that produced a titer of 2.5 mg/l (Steen et al, 2008), around 150-fold less than the results obtained with *E. coli* in the same year. This difference in yields has led researchers to investigate the driving forces behind butanol production by the ABE pathway in order to improve performance in *S. cerevisiae*.

### **5.5.3 Use of endogenous amino acid catabolic pathways for 1-butanol production in *S. cerevisiae***

A number of published studies have demonstrated that *S. cerevisiae* possesses the ability to produce 1-butanol through the degradation of amino acids to alcohols through

the Ehrlich pathway. One such study proposed that *S. cerevisiae* can produce 1-butanol from the catabolism of glycine (Branduardi et al, 2013). Indeed, yeast cultures grown in minimal media with 15 g/l glycine as the only nitrogen source accumulated up to 92 mg/l of 1-butanol, with 58 mg/l isobutanol as a byproduct. The pathway for 1-butanol production proposed by this study involves the deamination of glycine to glyoxylate by a putative glycine deaminase (Figure 5.3), which is then converted to 2-oxoalate through its condensation with butyryl-CoA by either Mls1p or Dal7p to yield 3-ethylmalate and its concomitant conversion to 2-oxoalate by the dehydrogenase activity of Leu2p. This 2-oxoalate is then decarboxylated to butanal by yeast pyruvate decarboxylases (PDCs), and this aldehyde is finally reduced to 1-butanol by yeast alcohol dehydrogenases (Branduardi et al., 2013).

Another study discovered that the deletion of *ADH1*, the major yeast alcohol dehydrogenase, induced the accumulation of 1-butanol in anaerobic cultures growing in rich media, achieving 1-butanol titers of 120 mg/l (Si et al., 2014). The authors proposed that deletion of this gene redirects metabolic flux from ethanol production to 1-butanol, likely to restore redox imbalances caused by this mutation. They also characterised the metabolic pathway responsible for 1-butanol production in their strains and concluded that it is a threonine catabolic process that uses similar steps to the Ehrlich pathway: L-threonine is transaminated to 2-oxobutyrate in the mitochondria, and then converted to 2-ethylmalate. Subsequent carboxylation and decarboxylation steps by cytosolic enzymes produce butyraldehyde, which is finally reduced to 1-butanol by alcohol dehydrogenases (Si et al, 2014).

Further improvements to the threonine-dependent 1-butanol production pathway were later published by the same group, producing a *S. cerevisiae* strain able to accumulate up to 835 mg/l of 1-butanol, approximately seven times more than their original *adh1Δ* strain

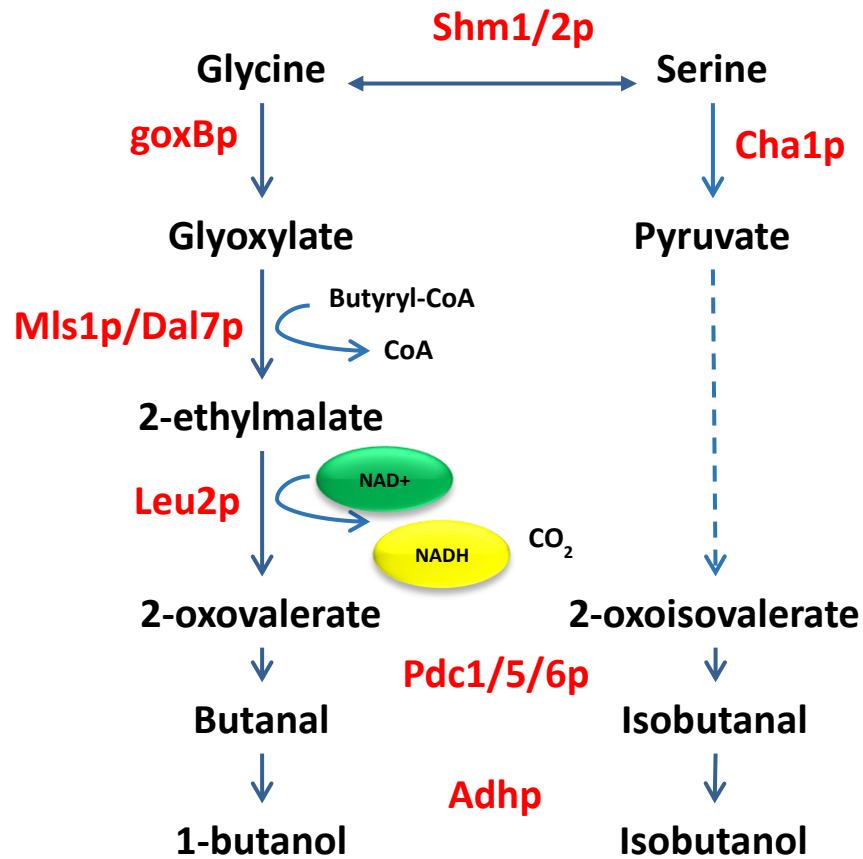


**Figure 5.3. Glycine-dependent 1-butanol biosynthetic pathway of *S. cerevisiae*.** Depiction of the putative glycine-dependent pathway for 1-butanol production. Enzymes involved: mitochondrial serine hydroxymethyltransferase (Shm), alcohol dehydrogenase (Adh) serine deaminase (Cha), malate synthase (Dal), *Bacillus subtilis* glycine oxidase (GoxB), beta-isopropylmalate dehydrogenase (Leu2), malate synthase (Mls), pyruvate decarboxylase (Pdc). Dashed line indicates multiple reactions.

(Shi et al, 2016). They achieved this by overexpressing key enzymes of the pathway in order to increase the availability of precursors, namely threonine and 2-oxobutyrate. They also relocated enzymes of threonine catabolism to the mitochondria in order to streamline the process and avoid competing cytosolic pathways.

A study published in 2015 by our laboratory constructed a butanol-producing strain of *S. cerevisiae* by combining the exogenous ABE pathway and the native yeast pathways activated by the deletion of *ADHI* (Swidah et al., 2015). Two additional genetic modifications were employed to further increase 1-butanol titers. First, acetaldehyde accumulated from the deletion of *ADHI* was channeled towards acetyl-CoA, the precursor of the ABE pathway, by constitutively overexpressing the *ALD6* and *ACS2* genes. Second, a butanol-resistant strain carrying a previously characterized mutant allele of *GCD1*, the  $\gamma$ -subunit of the yeast translation initiation factor eIFB2 (Ashe et al., 2001), was used as the host for 1-butanol production to test if translational resistance to butanol toxicity could further improve performance. The resulting strain was able to produce up to 300 mg/l of 1-butanol in anaerobic conditions, around seven times more than by deleting of *ADHI* alone (40 mg/l).

A follow-up to the previous study resulted in further insights into the contributions of the ABE pathway and the endogenous pathway to 1-butanol production in the constructed strain (Swidah et al., 2018). Interestingly, this study concluded that the threonine-dependent pathway was not responsible for the endogenous butanol production in their strains, as 1-butanol production was not hindered by the deletion of either *LEU1*, *LEU2* or *LEU4*, three genes involved in the aforementioned pathway. The study also demonstrated that the addition of glycine to the culture media of *adh1Δ* strains increased 1-butanol titers from 40 mg/l to 120 mg/l, suggesting that the glycine-dependent pathway is involved in 1-butanol accumulation.

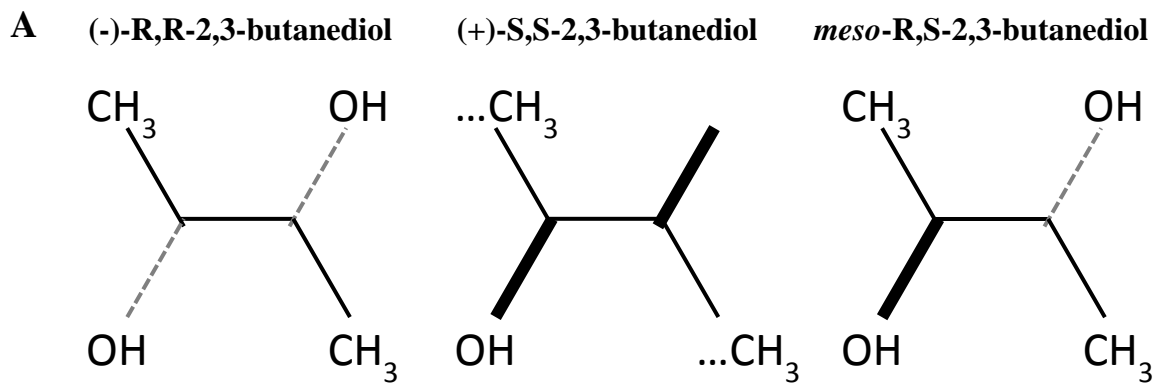
These studies hint at the existence of more than one endogenous biosynthetic pathway for 1-butanol production in *S. cerevisiae*. Thus, identifying these pathways and optimizing them for butanol production may lead us a few steps closer to constructing an industrially competitive *S. cerevisiae* strain.

## **5.6 2,3-butanediol as an alternative product of fermentation**

Besides ethanol and butanol, *S. cerevisiae* can naturally synthesize other chemicals of industrial interest. Butane-2,3-diol, more commonly known as 2,3-butanediol (2,3-BDO) is a minor byproduct of alcoholic fermentation in *S. cerevisiae* that has a number of industrial applications. 2,3-BDO is a 4 carbon odorless alcohol with a molecular mass of 90.12 g/mol that has three stereoisomers: D-(-)/-R,R-2,3-BDO, L-(+)/-S,S-2,3-BDO, and the optically inactive R,S-2,3-BDO (Figure 5.4 A) (Celińska and Grajek, 2009 ).

### **5.6.1 Industrial applications of 2,3-butanediol**

2,3-BDO is an example of a platform chemical: a compound that serves as the precursor for the synthesis of chemical products of interest. There are three main products that can be manufactured from 2,3-BDO. Methyl ethyl ketone (2-butanone) results from the dehydration of 2,3-BDO (Tran and Chambers, 1987) and it is used as a solvent for lacquers and resins (Villet, 1981), as well as glues and printing inks (National Center for Biotechnology Information [NCBI], 2020). Diacetyl (2,3-butanedione) is made by the dehydration of 2,3-BDO, and it is used as a flavourant in the food industry to confer a buttery flavour to products (Bartowsky and Henschke, 2004; Halligan, 2017) as well as serving as an antimicrobial additive (Jay, 1982). 1,3-butadiene is another product that results from the dehydration of 2,3-BDO (Liu et al., 2016), and it is used in the manufacturing of synthetic rubber polymers (Qi et al., 2019).



**B**

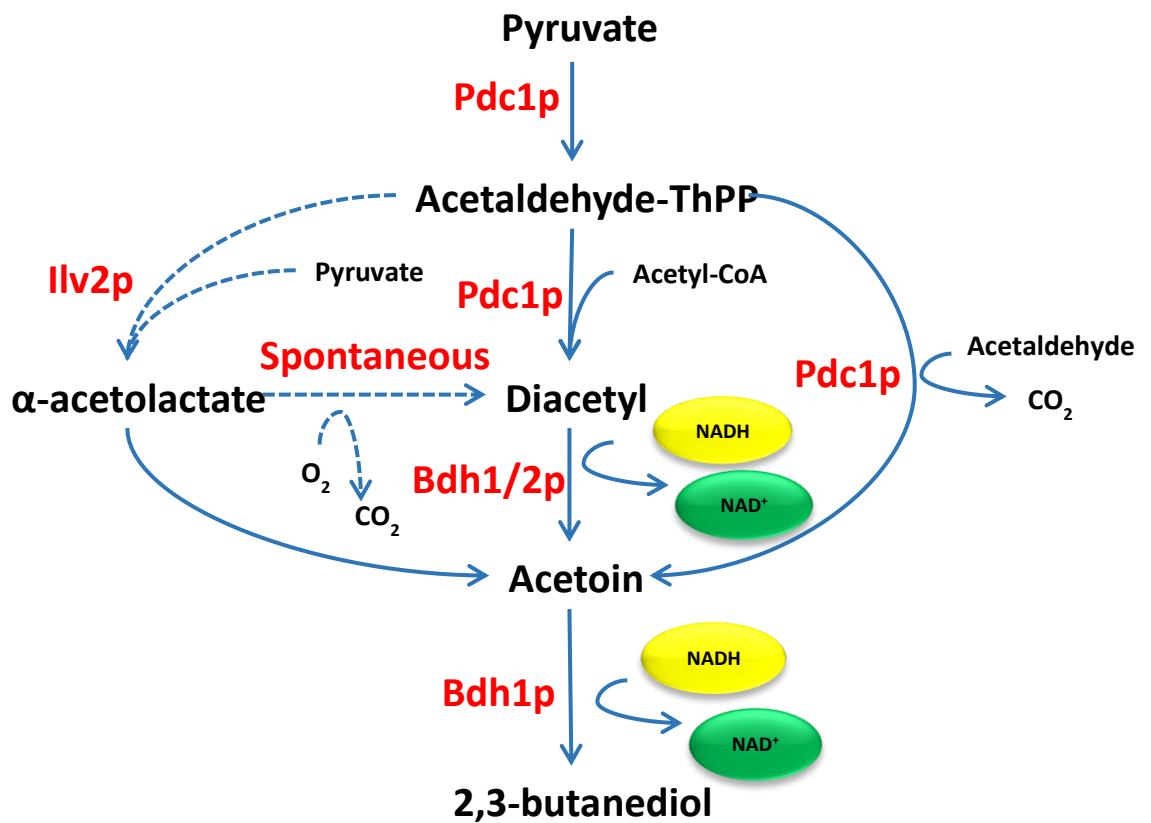


**Figure 5.4. 2,3-butanediol isomers and their biosynthesis in *S. cerevisiae*.** A) Structure of the three 2,3-butanediol isomers. B) Biochemical pathways leading to the synthesis of 2,3-butanediol in *S. cerevisiae*. Enzymes involved in each reaction are pyruvate decarboxylase (Pdc1p), butanediol dehydrogenase (Bdh1p and Bdh2p), acetolactate synthase (Ilv2p). Nicotineamide dinucleotide (NADH/NAD<sup>+</sup>) is the cofactor used by Bdh1p.

2,3-BDO itself has a number of potential applications in fuel technologies: its energy content of 27.2 MJ/mg is lower than butanol (36.1 MJ/kg), but it is similar to that of ethanol (29.7 MJ/kg) (Flickinger, 1980), indicating that it may perform at a similar level to the 2-carbon alcohol. Finally, due of its low freezing point of -60°C, S,S-2,3- BDO is a potential cryoprotectant agent for a number of applications including the clinical preservation of organs for transplants (Garg and Jain, 1995; Soltys et al., 2001).

### **5.6.2 2,3-butanediol biosynthesis in *S. cerevisiae***

2,3-BDO is produced in small quantities during alcoholic fermentation in *S. cerevisiae* by three known reaction pathways that convert pyruvate and acetaldehyde into either R- or S-acetoin (Figure 5.4 B). The final step involves the stereospecific reduction of acetoin isomers into R,R-2,3-BDO or R,S-2,3-BDO catalyzed by the NADH-dependent Bdh1p (González et al., 2000). Since this last reaction always yields a 2,3-BDO isomer corresponding to a specific acetoin isomer, it means that the activities of the pathways leading to acetoin formation should dictate how much of each R- or S- isoform is synthesized.

The three pathways that yield acetoin start with “active” acetaldehyde, which is an acetaldehyde-thiamine pyrohsophate (ThPP) complex that forms during decarboxylation of pyruvate by Pdc1p (Romano and Suzzi, 1996). Acetaldehyde-ThPP can react with three different molecules to yield acetoin (Figure 5.4 B): 1) pyruvate and acetaldehyde-ThPP can be converted into  $\alpha$ -acetolactate by Ilv2p, which can then be spontaneously decarboxylated into diacetyl in the presence of oxygen, or by an  $\alpha$ -acetolactate decarboxylase. Finally, diacetyl is reduced to acetoin by Bdh1p or Bdh2p. It is important to note that this pathway is highly inefficient in *S. cerevisiae* because Ilv2p localizes in the mitochondria where it catalyzes the first reaction involved in isoleucine and valine

biosynthesis (Falco et al., 1985). 2) Acetyl-CoA and acetaldehyde-ThPP can be condensed into diacetyl by the diacetyl synthetase enzyme, and then reduced to acetoin by diacetyl reductase (Romano and Suzzi, 1996). 3) Condensation of acetaldehyde-ThPP with free acetaldehyde by Pdc1p produces either R- or S- acetoin, bypassing diacetyl as an intermediate (Chen and Jordan, 1984).

### 5.6.3 Native bacterial 2,3-butanediol producers

Reports of experiments on microbial fermentation for the industrial-scale production of 2,3-BDO were reported as early as 1906, when Harden and Walpole used *Klebsiella pneumoniae* to produce it from glucose in anaerobic conditions (Harden and Walpole, 1906). Later in 1926, H. Donker reported 2,3-BDO production from *Bacillus polymyxa* in his doctoral dissertation (Donker, 1926). Pilot industrial-scale fermentations were later implemented during World War II due to the demand for 1,3-butadiene for rubber production (Blackwood et al., 1949; Ledingham and Neish, 1954), but like the contemporary 1-butanol fermentation attempts, they were abandoned after the availability of more economic petrochemical approaches. Then again, the current need for an alternative to petroleum-based chemical products and fuels has led to a renewed interest in microbial fermentation of 2,3-BDO.

Currently, among the most efficient bacterial 2,3-BDO producers known are members of the *Enterobacteriaceae* family, as well as *Bacillus polymyxa* which belongs to the *Paenibacillaceae* family (Celińska and Grajek, 2009). These bacteria synthesize 2,3-BDO by the same  $\alpha$ -acetolactate pathway present in *S. cerevisiae* (Figure 5.4 B), except they have enzymes that are able to catalyze these reactions more efficiently and are not separated by membrane-bound organelles as in the yeast acetolactate synthase Ilv2p. Unlike *S. cerevisiae*, bacterial 2,3-BDO producers have cytosolic  $\alpha$ -acetolactate (*alsS*)

synthase enzymes, and  $\alpha$ -acetolactate decarboxylase (*alsD*) which can readily convert the acid into acetoin instead of depending on its oxygen-dependent spontaneous decarboxylation (Jansen et al., 1984; Sablayrolles and Goma, 1984). Additionally, *B. polymyxa* and *Klebsiella oxytoca* can ferment 2,3-BDO from hexose and pentose sugars (Maddox, 1996), a flexible trait that can be exploited to use cellulosic waste products as feed to reduce the cost and increase the sustainability of industrial fermentations.

Despite their natural capacity for 2,3-BDO production, the aforementioned species are not the best hosts for industrial fermentation because of their pathogenic nature. Nonetheless, their study has led to the discovery of the genes responsible for efficient 2,3-BDO fermentation, which can then be expressed in model microorganisms to develop safe microbial 2,3-BDO factories.

#### **5.6.4 Metabolic engineering of *S. cerevisiae* for industrial production of 2,3-butanediol**

The current strategies employed to engineer *S. cerevisiae* for 2,3-BDO production involve improving  $\alpha$ -acetolactate catabolism and removing metabolic pathways competing for pyruvate. For example, one strategy employed by Jiazhang Lian and colleagues to improve the conversion of  $\alpha$ -acetolactate into diacetyl involved the construction of a non-mitochondrial *S. cerevisiae*  $\alpha$ -acetolactate synthase (*cytoILV2*), the heterologous expression of *alsD* from *Bacillus subtilis*, and overexpression of the host's *BDHI* to efficiently reduce acetoin to R,R-2,3-BDO (Lian et al., 2014). In order to remove competing pathways, they disrupted ethanol fermentation by deleting *PDC1*, *PDC5*, and *PDC6*, which resulted in slower growth on glucose. In order to correct this defect, they overexpressed *MTH1*, a negative regulator of glucose sensing, to alleviate the effects of glucose repression on cell growth (Blázquez et al., 1995; Moriya and Johnston, 2004).

The resulting strain produced 100 g/l R,R-2,3-BDO in a fed-batch anaerobic fermentation with 10 g/l glucose and galactose (Lian et al., 2014).

In a more recent publication, Ye-Gi Lee and Jin-Ho Seo made some additions to the fermentation strategy to further improve 2,3-BDO yields in a polyploid strain of *S. cerevisiae* (Lee and Seo, 2019). In addition to deleting the *PDC* genes, they also deleted *ADHI* to further impede ethanol fermentation. In order to correct the redox imbalance caused by these deletions, they overexpressed the *Lactococcus lactis* NADH oxidase *noxE*, an approach that was previously explored by the authors and another laboratory (Kim and Hahn, 2015; Bae et al., 2016). This strain was able to accumulate 132 g/l 2,3-BDO in a fed-batch fermentation using cassava hydrolysate as an inexpensive substrate.

These two examples show that *S. cerevisiae* is a flexible and capable host for 2,3-BDO fermentation with the potential to be used as a safe alternative to the native bacterial producers.

### **5.7 Yeast cellular responses to butanol stress**

One of the proposed strategies for increasing 1-butanol production in *S. cerevisiae* is improving its tolerance to the toxic effects of this alcohol. Although *S. cerevisiae* is one of the more resistant microbes used in bio-butanol research (Fischer et al, 2008), the cellular response to this fusel alcohol results in a decrease in cell growth and protein synthesis, thus impacting final product yields. As shown in the report by Swidah and colleagues in 2015, resistance to 1-butanol toxicity in *S. cerevisiae* leads to improvements in fusel alcohol production (Swidah et al., 2015). In order to design and propose solutions, the toxic effects of butanol and the response that yeast cells deploy against it must be characterized, and how they impact cell performance and survivability.

### **5.7.1 Butanol toxicity**

The biological effects of 1-butanol and other organic solvents can be related to their hydrophobicity, which is the ability to interact and mix with nonpolar compounds and mixtures like the lipid bilayer in biological membranes. The degree of hydrophobicity can be estimated using a number of solvent-water partition coefficients, the octanol-water coefficient is one of the more relatable to solvent toxicity (Isken and de Bont, 1998). Due to their hydrophobic nature, solvents can penetrate and accumulate in biological membranes, disrupting the lipid bilayer structure and causing an increase in membrane fluidity, compromising its function as a barrier between the cell and its environment, as well as between intracellular compartments and the cytoplasm. This disruption leads to leaking of solutes from organelles and loss of electrochemical gradients key for their function. For example, mitochondrial membrane permeability (MMP) leads to loss of the  $H^+$  gradient in the intermembrane matrix, hindering the function of ATP synthase and compromising cell energy production. Solvent accumulation in mitochondrial membranes might also disrupt regulation of apoptosis because MMP is thought to be the irreversible step leading to programmed cell death (Kroemer et al., 2007).

### **5.7.2 Cellular tolerance and responses to 1-butanol stress**

Tolerance mechanisms to exogenous solvents have been extensively studied in bacteria in the context of biofuel production and bioremediation, and some of them have been identified. These include expression of efflux pumps to remove the toxic substance, modification of lipid content in the plasma membrane to minimize structural disruption, activity of heat shock proteins (HSP) to prevent protein aggregation and a general transcriptional response of stress-related genes (Dunlop, 2011; Mukhopadhyay 2015). On the other hand, the solvent-tolerance mechanisms in *S. cerevisiae* have been mostly studied in the context of ethanol toxicity (Stanley et al., 2010). Because ethanol and

butanol are both alcohols, they probably have similar toxicity mechanisms and elicit similar responses on yeast, but the differences in their chemical structures seem to have an impact on their toxicity.

A study in 2013 generated a butanol tolerant strain of *S. cerevisiae* by exposing a series of batch cultures to increasing concentrations of 2-butanol up to 3% v/v. Proteomic analysis of the resulting strain revealed up-regulation of proteins involved in mitochondrial function (21 of the 34 up-regulated proteins), general stress response (Hsp42p) and glycerol synthesis (Hor2/Gpp2p). The authors suggested that the amount of up-regulated mitochondrial proteins could mean that this organelle has a central role in yeast butanol tolerance (Ghiaci et al., 2013).

One of the immediate cell responses to 1-butanol in yeast is the inhibition of global protein synthesis by blocking the activity of the guanine nucleotide exchange factor (GEF) eIF2B through its  $\gamma$  subunit Gcd1p, hence impeding the recycling of GTP-eIF2 required to form the GTP, eIF2, Met-tRNA<sub>i</sub><sup>Met</sup> ternary complex and limiting translation initiation (Ashe et al., 2001). It is important to note that this mechanism is independent of the phosphorylation of eIF2 $\alpha$  by Gcn2p observed in translation inhibition by amino acid starvation (Hinnebusch, 2000), suggesting that 1-butanol could serve as a metabolite that provides an alternative signal to poor nitrogen availability in the environment, allowing yeast cells to quickly change their translational programme.

A key point mutation of serine to proline in the residue 180 of Gcd1p has been reported to be associated with a butanol-resistant phenotype in *S. cerevisiae* (Taylor et al., 2010). This discovery opens the possibility of the engineering of resistant strains for industrial 1-butanol production. The hypothesis has been tested by the Ashe laboratory in a study that involved measuring 1-butanol production in semi-anaerobic fermentation in a

butanol-resistant W303-1A *S. cerevisiae* strain harboring a number of genetic modifications including 5 genes from the ABE pathway, deletion of *ADH1* and constitutive expression of *ALD6* and *ACS2*. This butanol-producing strain was able to yield up to 300 mg/ml 1-butanol, a value 1.5 to 2-fold higher than a sensitive strain harboring the same genetic modifications (Swidah et al., 2015). This study showed the importance of understanding resistance mechanisms, and how this resistance can improve yields of metabolites of interest.

### 5.7.3 Metabolic state and quorum-sensing

The study of the cell response to butanol toxicity has been carried out by exogenous addition of this alcohol, but it is important to remember that yeast cells can naturally produce 1-butanol through the Ehrlich pathway and the endogenous threonine catabolism pathway. If so, what is the impact of endogenous butanol yeast physiology?

Aliphatic and aromatic fusel alcohols are produced in yeasts during amino acid catabolism when nitrogen is limiting in the culture media (Chen and Fink, 2006), and it has been demonstrated that they can induce morphogenetic responses in yeast. Quorum-sensing is a regulatory mechanism discovered in bacteria that allows populations to change their behavior as a group in response to population density, resulting in the induction of processes including biofilm formation and morphogenetic responses related to virulence (Fuqua et al., 1994). A quorum-sensing mechanism mediated by farnesol was discovered in the human pathogen *Candida albicans*, a dimorphic fungus that grows as filaments of pseudohyphae at low populations or as yeast colonies at higher populations (Hornby et al., 2001). A similar response can be seen in *S. cerevisiae* where addition of fusel alcohols induces filamentation of yeast cells (Dickinson, 1996). Later studies demonstrated quorum-sensing mechanisms in *S. cerevisiae*, where endogenous

phenylethanol and tryptophol were able to induce filamentation of diploid cells and invasive growth of haploid cells in nitrogen-limiting conditions (Chen and Fink, 2006), supporting the hypothesis that aromatic and aliphatic alcohols serve as regulatory molecules that can activate cellular responses to changes in nutrient availability and cell density.

### **5.8 The pseudohyphal response in *Saccharomyces cerevisiae***

As briefly mentioned in the previous section, one of the most striking and complex responses to butanol stress observed in *S. cerevisiae* is a dimorphic transition from free budding yeasts to elongated chains of connected yeast cells called pseudohyphae in response to nutrient scarcity. This pseudohyphal growth is a complex morphogenetic adaptation traditionally associated with nutrient depletion in the environment, and it is thought to allow colonies of immobile cells to extend their reach into their environment and forage for nutrients when their local available resources are depleted.

This shift from free yeasts to pseudohyphal growth involves a series of cellular changes including elongation of cell bodies caused by a delay in the G2/M transition of the cell cycle (Sung-Hee et al., 1999), a change in the budding pattern from bipolar or axial in diploid and haploid cells respectively, to unipolar (Lorenz et al., 2000; Cullen and Sprague, 2002), and enhanced cell-cell and cell-substrate adhesion granted by increased expression of the cell wall flocculin *FLO11* (Wan-Sheng and Dranginis, 1998; Palecek et al., 2000). There are slight differences in how this response is induced between haploid and diploid cells and how they display the pseudohyphal phenotype in agar cultures. In diploids, pseudohyphal growth is characterized by chains of cells that extend along the surface of the agar and is induced by growing cells in a substrate low in nitrogen and high in carbon. On the other hand, haploid cells are known for their invasive growth

characterized by the extension of pseudohyphal chains into the agar when cells are grown in rich media.

Despite the aforementioned differences, filamentous growth in haploid and diploid cells of *S. cerevisiae* is regulated by the same nutrient sensors, signal transduction pathways, and effectors. Some of these signal transduction pathways are shared with other dimorphic yeast species such as the human pathogen *Candida albicans*, which undergoes the transition from yeast to fully hyphal in response to changes in temperature and chemical signals specific to human blood, driving tissue invasion and eventual systemic infection (Sudbery, 2011; Polvi et al., 2015).

### **5.8.1 Signaling pathways involved in yeast filamentation**

The ability to coordinate a complex morphogenetic response requires specialized cellular machinery that can sense the relevant stimuli and transduce the sensing event into signals able to interact and engage with intracellular effectors that respond to the stimulus. In *S. cerevisiae* there is not one, but at least four known signal transduction pathways that regulate filamentous growth in response to nutrient availability and other chemical signals. These pathways include the filamentous mitogen-activated protein kinase cascade (fMAPK), the rat sarcoma (RAS)/cAMP/ protein kinase A (PKA) pathway, AMP-dependent kinase Snf1p, and the target of rapamycin (TOR) pathway (Cullen and Sprague Jr., 2012).

### **5.8.2 Filamentous Mitogen-Activated Protein Kinase pathway**

MAPK pathways are a group of related transduction pathways conserved among eukaryotic organisms that consist of a series of three sequential serine-threonine protein kinases that mediate the key cellular response to numerous extracellular signals, including cell differentiation, stress responses, cell proliferation, and apoptosis (Widmann et al.,

1999; Morrison, 2012). There are five MAPK pathways described in *S. cerevisiae*, each involved in maintenance of cell wall integrity, the high osmolarity glycerol (HOG) response, haploid cell mating, and the filamentous response (Chen and Thorner, 2007; Molina et al., 2010). Although some of the pathways share a core set of enzymes: Cdc42 (RHO GTPase), Ste20p (MAP4K), Ste11p (MAP3K), and Ste7p (MAP2K), each of them is able to sense and modulate a different cellular response to specific stimuli. This specificity is achieved by the engagement of different plasma membrane receptors and cytoplasmic scaffold proteins for each pathway that recruit the required MAPK enzymes to the site of activation, resulting on the efficient and specific activation of the pathway-specific MAPK effectors. For instance, in the pheromone MAPK pathway and the HOG pathway, the scaffolding proteins Ste5p and Pbs2p recruit different members of the MAPK cascade, leading to the phosphorylation of the MAP kinases Kss1p/Fus3p and Hog1p, respectively.

The filamentous MAPK (fMAPK) pathway mediates pseudohyphal growth in response to glucose or nitrogen limitation in the environment sensed by three membrane proteins: Msb2p, Sho1p, and Mep2p (Figure 5.5). Msb2p is activated by the proteolytic cleavage of its inhibitory glycodomain by Yps1p (Vadaie et al., 2008), which then leads to Msb2p's association with the HOG-related osmosensor Sho1p (Cullen et al., 2004). Msb2p and Sho1p are known to interact with Cdc42p and Cdc24p, respectively. Thus, the active Msb2/Sho1p interaction brings the RHO GTPase/GDP-GTP exchange factor pair close together, localizing them to the source of the extracellular signal and committing the first enzymatic steps of the core MAPK pathway cascade to the filamentous response (Cullen et al., 2004; Vadaie et al., 2008).

Experimental data has also identified the plasma membrane ammonium transporter Mep2p as an inducer of the fMAPK pathway in low ammonium media (Lorentz and

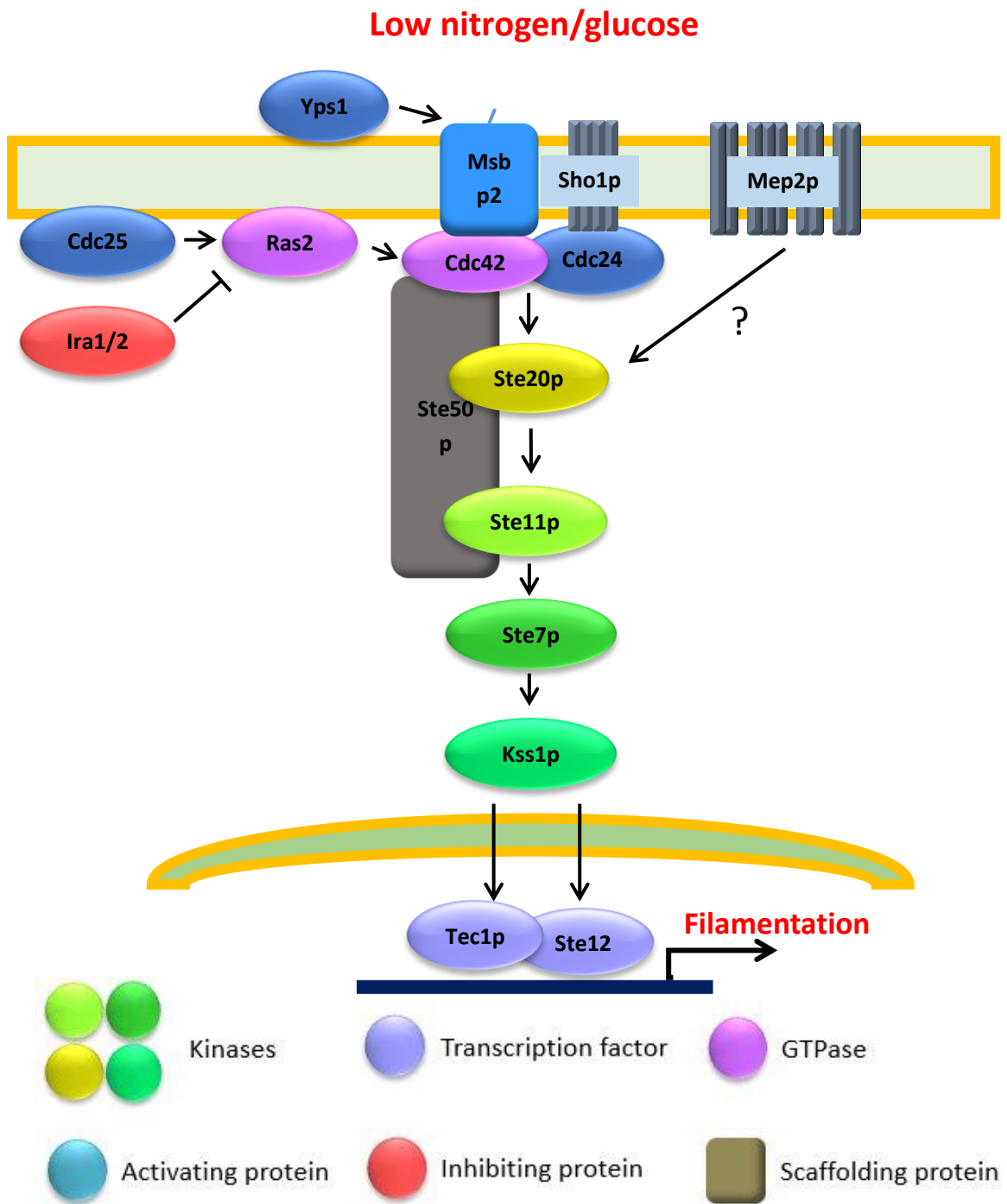


**Figure 5.5. Summary of the Filamentous MAPK pathway in *S. cerevisiae*.** Diagram depicts the proteins involved in nutrient sensing and activation of the filamentous Mitogen Activated Protein Kinase cascade, and the resulting activation of the Tec1p-Ste12p heterodimeric transcription factor.

Heitman, 1998; Rutherford et al., 2008; Brito et al., 2020). Although the mechanisms behind how the Mep2p-dependent signal is relayed to the downstream fMAPK cascade remain unknown, it is of no surprise that a membrane transporter would be involved in nitrogen sensing.

Additionally, the Ras2p GTPase is known to participate in the Cdc42p activation of the fMAPK pathway (Mösch et al., 1999). Ras2p participates in the RAS/cAMP/PKA pathway that regulates cell growth and differentiation in response to glucose, indicating a potential point for crosstalk between both pathways (Fink and Mösch et al., 1999; Chavel et al., 2010). Active Cdc42p is able to de-repress Ste20p, the first kinase in the cascade. Ste20p then readily phosphorylates the next kinase: Ste11p, thanks to the anchoring action of the adaptor protein Ste50p. Ste11p then phosphorylates Ste7p, which in turn activates the final kinase in the cascade: Kss1p. The activated MAPK then phosphorylates the transcription factors Ste12p and Tec1p, which together form an active heterodimer that is able to induce transcription of genes involved in the filamentous response, including the mucin *FLO11* and the cyclin *CLN1*.

### **5.8.3 RAS/cAMP/Protein Kinase A pathway**

The RAS/cAMP/PKA pathway is one of the main signaling pathways that coordinates cell function in response to glucose availability by using cAMP, synthesized by yeast adenylylate cyclase Cyr1p, as a second messenger to activate Protein Kinase A (Gancedo J., 2008). In *S. cerevisiae*, two glucose-responding GTPases activate Cyr1p: Gpa2p and Ras2p.

Gpa2p is the  $\alpha$ -subunit of the heterotrimeric G protein complex Gpa2p/Gpb1/2p/Gpg1p, a regulatory complex bound to the cytoplasmic side of the G-coupled receptor Gpr1p (Xue et al., 1998). When extracellular glucose is sensed by Gpr1p

(Thevelein and Voordeckers, 2009), a GDP-GTP exchange occurs in the  $\alpha$ -subunit Gpa2p, activating it and resulting in the dissociation of the  $\beta$  and  $\gamma$  subunits Gpb1p and Gpg1p, thus allowing GTP-bound Gpa2p to interact with and activate Cyr1p (Figure 5.6).

On the other hand, Ras2p is a monomeric GTPase that is thought to respond to intracellular glucose and active glycolysis, as revealed by its activation by the phosphorylation of glucose by yeast hexokinases and glucokinase (Colombo et al., 2004). The exact mechanisms of how glucose-6-phosphate induces Ras2p activation are not known, but it is clear that the active and inactive states of Ras2p are controlled by the opposite action of Ira1p/Ira2p and Cdc25/Sdc25. Ira1/Ira2p are GTPase activating proteins (GAP) that negatively regulate Ras2p by stimulating hydrolysis of its GTP into GDP, switching it into its inactive state (Tanaka et al., 1990). Cdc25 is Ras2p's guanine exchange factor (GEF) and is able to reactivate Ras2p by switching it into its GTP-bound state (Jones et al., 1991; Boy-Marcotte et al., 1996). Together, Gpa2p and Ras2p activate Cyr1p to produce an intracellular peak of cAMP (Gimeno et al., 1992). This second messenger induces the activation of PKA enzymes by binding to their regulatory subunit Bcy1p, allowing the release of the catalytic subunits Tpk1p, Tpk2p, and Tpk3p which in turn phosphorylate a number of target proteins to stimulate cell growth in the presence of glucose (Toda et al., 1987; Budovskaya et al., 2005).

Among the Tpk2p targets are two transcription factors involved in the expression of the pseudohyphal response: Flo8p and Slf1p. When phosphorylated by Tpk2p, Flo8p is able to induce the transcription of *FLO11* through the Flo8p/Mss11p heterodimer, leading to the enhanced cell-cell adhesion of the pseudohyphal response (Pan and Heitman, 1999; Kim et al, 2014).

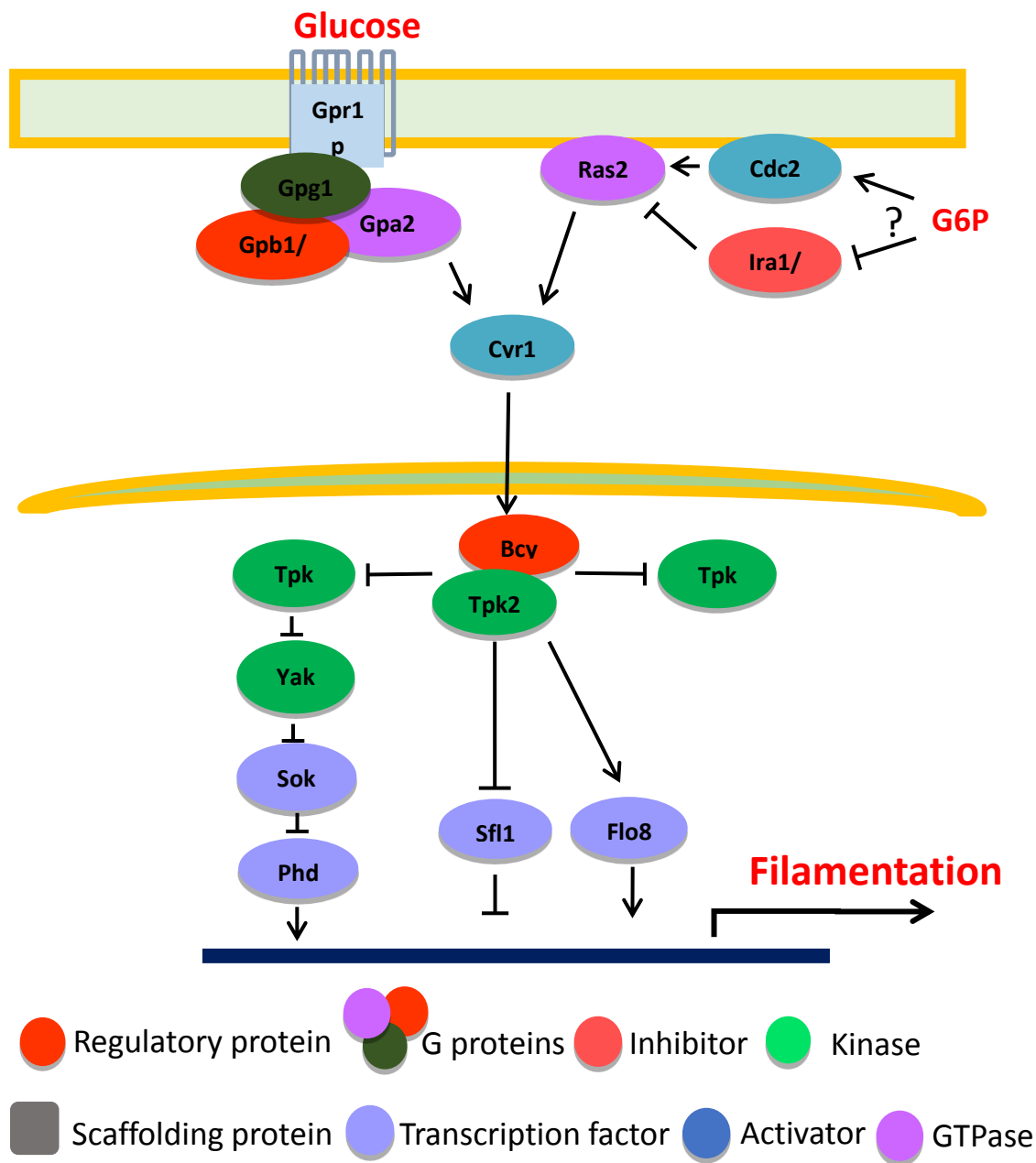


**Figure 5.6. Summary of the RAS/cAMP/Protein Kinase A pathway involved in yeast pseudohyphal growth.** Diagram shows the proteins involved in sugar sensing and activation of the RAS/cAMP/PKA signaling pathway resulting in the induction of the yeast filamentous response. G6P stands for glucose-6-phosphate.

During pseudohyphal growth of diploid strains of *S. cerevisiae*, the catalytic subunits of PKA have distinct roles in the induction of this morphogenetic response. Studies have revealed that Tpk2p acts as a positive regulator of the pseudohyphal response, while Tpk3p has no role, and Tpk1p acts as a negative regulator by blocking the action of Yak1p on Sok2p, an inhibitor of the transcription factor Phd1p (Pan and Heitman, 1999; Cullen and Sprague, 2012) (Figure 5.6).

Sfl1p is a transcriptional repressor of yeast pseudohyphal growth, whose interaction with the *FLO11* promoter is prevented when phosphorylated by Tpk2p (Robertson and Fink, 1998; Pan and Heitman, 2002). In summary, Flo8p and Sfl1p work as a duo of positive and negative regulators of *FLO11* whose active states are modulated by Tpk2p phosphorylation.

#### **5.8.4 SNF1/AMP-dependent Kinase pathway**

The AMP-dependent Kinase (AMPK), or SNF1 pathway in *S. cerevisiae*, modulates multiple cellular responses to glucose depletion, including the recovery from global translation inhibition (Ashe et al., 2000), the general stress response (Mayordomo et al., 2002), resistance to iron toxicity (Li et al., 2017), the expression of glucose-repressed genes (Hedbacker and Carlson, 2009), and both diploid pseudohyphal growth and haploid invasive growth (Cullen and Sprague, 2000; Kuchin et al., 2002).

The core kinase in the SNF1 pathway of *S. cerevisiae* is a heterotrimer composed of the serine/threonine kinase alpha subunit Snf1p and two regulatory subunits: the activating gamma subunit Snf4p, and a tethering beta subunit that can be either Sip1p, Sip2p, or Gal83p (Amodeo et al., 2010; Hardie, 2007) (Figure 5.7). Research has found evidence that the beta subunit defines the subcellular localization and specific functions of the SNF1 heterotrimer (Vincent et al., 2001). For instance, Gal83p is required for

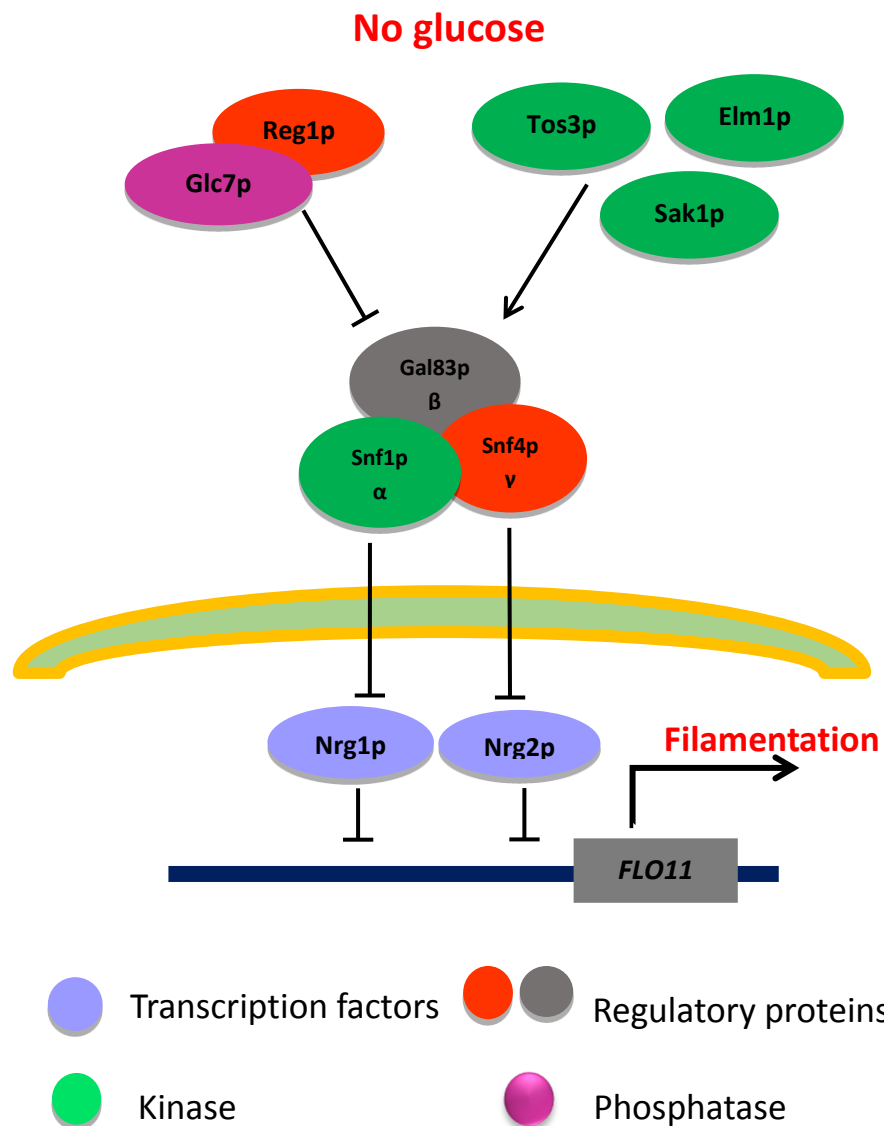


**Figure 5.7. Summary of the SNF1 pathway involvement in the yeast filamentous response.** The Glc7p/Reg1p heterodimer keeps Snf1p dephosphorylated when glucose is abundant. When glucose is depleted, Snf1p is phosphorylated by Elm1p, Sak1p, and Tos3p, resulting in downstream phosphorylation of Nrg1p and Nrg1p, two repressors of *FLO11* transcription.

growth in non-fermentable carbon sources (Schmidt and McCartney, 2000), while Sip2p is involved in cell lifespan during nutrient deprivation (Ashrafi et al., 2000). In particular, the beta subunits Gal83p and Sip2p are involved during induction of pseudohyphal genes by the SNF1 pathway by directing the complex towards Nrg1p and Nrg2p, two negative transcriptional regulators of *FLO11* (Kuchin et al., 2002; Vyas et al., 2005) (Figure 5.7).

Activity of the SNF1 complex is regulated by the phosphorylation state of threonine T210 in the activation loop domain of Snf1p (McCartney et al., 2016). When glucose is present, Snf1p is kept inhibited by the action of the PP1 phosphatase Glc7p, led by its regulatory partner Reg1p (Tu and Carlson, 1995). When glucose concentration falls, activation of Snf1p is achieved by two mechanisms: direct phosphorylation of T210 by SNF1-activating kinases Sak1p, Tos3p, and Elm1p (Nath et al., 2003; Hong et al., 2003), and increased resistance to Glc7p-dependent dephosphorylation due to ADP binding to Snf1p, resulting in conformational changes that restrict access of Glc7p to the activation loop (Rubenstein et al., 2007; Mayer et al., 2011). Active Snf1p is then able to phosphorylate a series of target proteins depending on its bound beta subunit. As mentioned above, Gal83p directs the complex towards Nrp1 and Nrp2p, relieving their suppressing effect on *FLO11* (Figure 5.7).

### **5.8.5 Target of Rapamycin (TOR) pathway**

TOR is a kinase signal transduction pathway widely conserved among eukaryotes that modulates cellular processes in response to amino acid and nitrogen presence, including cell growth, differentiation, ribosome biogenesis, and autophagy (González and Hall, 2017). The *S. cerevisiae* TOR pathway is characterised by two different protein complexes (TORC) formed by one of the main kinase isoforms Tor1p and Tor2p, and the proteins Lst8p and Kog1p. Of these complexes, only TORC1 is sensitive to rapamycin,

which inhibits its kinase activity by forming a complex with yeast prolyl isomerase Fpr1p and then binding to the complex (Loewith and Hall, 2011).

There is evidence that links TOR pathway function to the nutrient-dependent yeast pseudohyphal growth. A study by Cutler and colleagues found that rapamycin inhibits pseudohyphal growth and proposed a model that involves TOR-mediated phosphorylation of the regulatory protein Tap42p, which then forms a complex with the Sit4p phosphatase (Cutler et al., 2001). The association of Tap42p and Sit4p keeps the latter inactivated (Figure 5.8). As a result, Gcn2p, one of the targets of Sit4p, becomes active and phosphorylates eIF2 $\alpha$ , the regulator of global transcription initiation under nitrogen starvation. Concomitant expression of the transcriptional regulator encoded by *GCN4* results in the translation induction of a series of genes in response to amino acid starvation, including *FLO11*, thus leading to the filamentous response (Song and Kumar, 2012; Braus et al., 2003) (Figure 5.8).

### Amino acid starvation

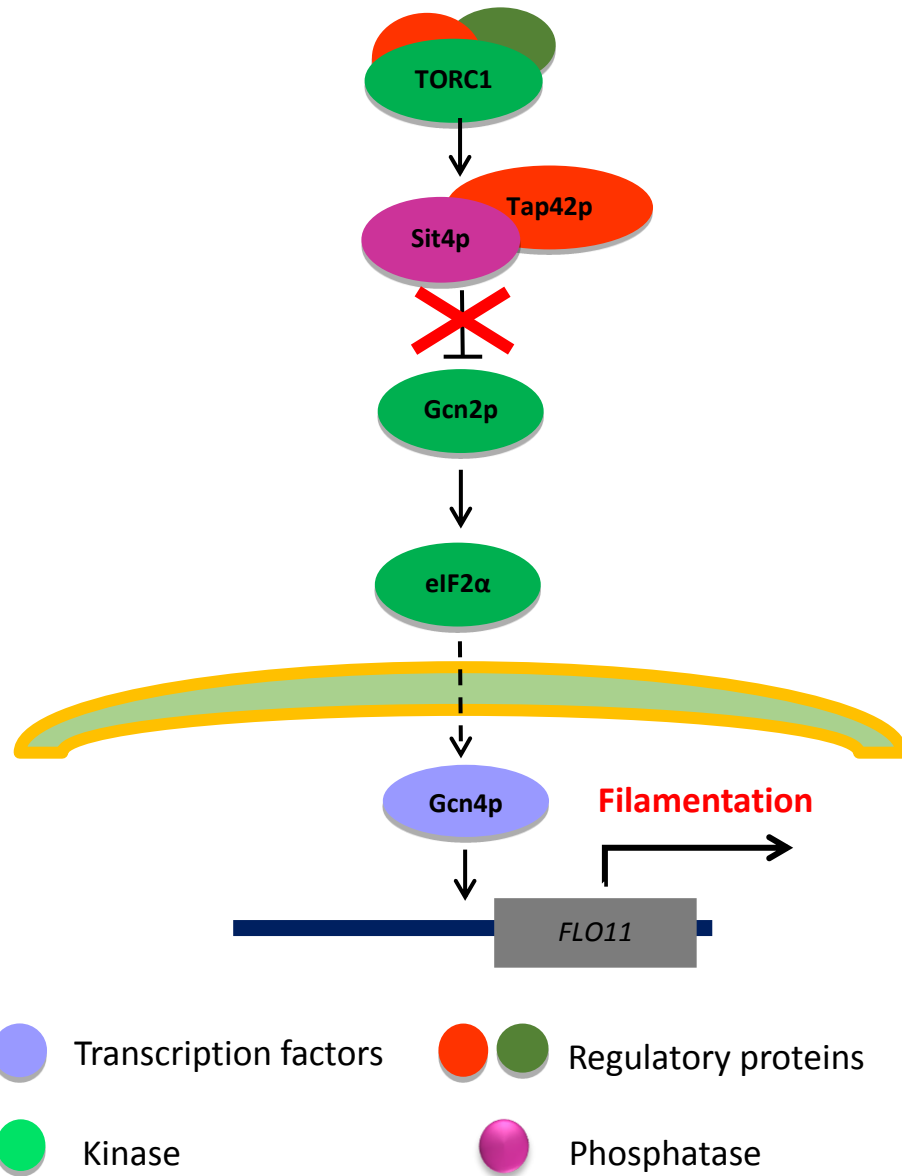


**Figure 5.8. Summary of the TOR signaling cascade leading to the filamentous response in *S. cerevisiae*.** Activation of TOR by amino acid starvation results in a phosphorylation cascade leading to the expression of the amino acid stress transcription factor Gcn4p, which in turn induces the transcription of *FLO11*.

### **5.8.6 Butanol-induced filamentation**

Interestingly, some studies suggest that the filamentous response induced by 1-butanol might be independent of the aforementioned nutrient-sensing pathways. A study evaluating alcohol-induced filamentation in *S. cerevisiae* strains showed that both 1-butanol and ethanol induced pseudohyphal growth in strains harboring null mutations in Gpa2p, Gpr1p and Mep2p, indicating that both alcohols can induce the activation of these pathways independent of the nutrient concentrations in the media (Lorenz et al., 2000). However, null mutations in downstream proteins of the fMAPK pathway (Ste7p, Ste11p, Ste12p, and Tec1p) prevented alcohol-induced filamentation, indicating that elements of this pathway are still required. The same study also identified mutations in mitochondrial genes (*CHD1*, *MSM1* and *MRP21*) that blocked butanol-induced filamentation, suggesting a possible role of mitochondria in the cellular response to this fusel alcohol (Lorentz et al., 2000).

If the traditional filamentous regulatory pathways are not required for butanol-induced filamentation, then which are the pathways involved in this specific response? Some authors have attempted to shed light into this question using proteomic and transcriptomic approaches to screen for genes or groups of genes that show differential expression under butanol treatment as outlined in the following sections.

### **5.8.7 Novel signaling pathways: the role of mitochondria**

There is a growing body of evidence that links mitochondria as signaling organelles in the fusel alcohol response of *S. cerevisiae*. First, research in 2004 found that filamentation induced by isoamyl alcohol was accompanied by an increase in the activity and number of mitochondria, compared to untreated cells (Kern, et al. 2004). Since this increase was immediate, the authors concluded that this phenomenon occurs by

conservation of organelles, rather than biogenesis. Later, other authors demonstrated that mitochondrial DNA integrity is required for yeast filamentation (Kang and Jiang, 2005), and identified several mitochondrial genes involved in filamentation through differential genome-wide analysis (Jin et al., 2008).

Further studies in mitochondrial function established a relationship between high mitochondrial transmembrane potential at the tip of the elongating yeast cells and their capacity to undergo filamentous growth when exposed to butanol (Starovoytova et al., 2013). Because loss of mitochondrial transmembrane potential induces activation of the mitochondrial retrograde (RTG) pathway (Miceli et al., 2012), the authors suggested that this pathway might have a role in filamentation. Indeed, Starovoytova and colleagues tested this hypothesis by individually deleting the key pathway genes *RTG1*, *RTG2* and *RTG3* in a series of W303 derived *S. cerevisiae* strains, which resulted in a decrease in butanol-induced cell elongation for any of the gene deletions.

Another study done by a different group reported similar results (González et al., 2017). Deletion of any of the three main RTG pathway genes resulted in reduced ethanol-induced filamentation in  $\Sigma$ 1278b *S. cerevisiae* strains. They also reported that deletion of one of the regulatory genes in any of the PKA (*RAS2*), AMPK (*TPK2*, *TPK2* and *TPK3*), Snf1p, and MAPK (*STE11*) did not prevent ethanol-mediated filamentation. Butanol-induced filamentation was also insensitive to the same gene deletions, suggesting the involvement of other regulatory pathways such as RTG.

## **5.9 Aims and objectives of the project**

So far, no studies have explored the filamentous stress response in butanol-producing *S. cerevisiae* strains. All of the published studies use exogenously added 1-butanol to induce filamentation (1% v/v), but there are no reports of pseudohyphal growth induced

by endogenous butanol. Characterizing the filamentation response to endogenous butanol can give us insight into the physiological mechanisms that allow yeast cells to adapt and tolerate increasing concentrations of biofuels. With this insight, new strategies for genetic engineering of tolerant strains can be designed and their performance on butanol production can be assessed.

Hence, the aim of this project will be to characterize in detail the phenotypical response of a filamentous strain of *S. cerevisiae* to endogenous 1-butanol and assess the ability of this filamentous strain to accumulate 1-butanol during anaerobic fermentations.

With the objective of developing high throughput tools to quickly screen for potential 1-butanol producing strains, the first group of experiments aimed to design and construct a set of fluorescent biosensors able to respond to the presence of 1-butanol in yeast cells.

In order to induce endogenous 1-butanol biosynthesis in the  $\Sigma$ 1278b filamentous strain, the *ADH1* gene was deleted and the resulting phenotype and physiological response to 1-butanol stress was assessed. 1-butanol accumulation during anaerobic fermentation was measured and compared to a non-filamentous strain of *S. cerevisiae*.

During the course of this project, attention was given to the potential role of acetaldehyde accumulation during endogenous 1-butanol production. Thus, a second objective of the project was to attempt to improve 1-butanol production by overexpressing *ALD6* and *ACS2* with the goal of reducing the levels of intracellular acetaldehyde.

The final objective of this project was to use RNA-seq methods to look at the transcriptomic response in the constructed 1-butanol-producing strains in search of potential genes behind the fermentation performances of each strain.

## 6. Materials and Methodology

### 6.1 Culture conditions

#### 6.1.1. *Saccharomyces cerevisiae* strains used and growth conditions

The *Saccharomyces cerevisiae* strains used in this project derive either from either the  $\Sigma$ 1278b or the W303-1A strain background, and are listed in Table 6.1. Cells were routinely cultured at 30°C with agitation at 180 rpm in a shalving incubator on yeast extract peptone dextrose (YPD) media (2% w/v Bacto Peptone, 2% w/v D-glucose, 1% w/v Yeast Extract and 0.167 mg/ml tryptophan), or on synthetic complete defined (SCD) media (0.17% w/v Yeast nitrogen base, 2% w/v D-glucose, 0.5% w/v ammonium sulphate, and supplemented with 0.02 mg/ml arginine, methionine, 0.06 mg/ml tyrosine, lysine and isoleucine, 0.05 mg/ml phenylalanine, 0.01 mg/ml glutamic and aspartic acid, 0.004 mg/ml serine, 0.0015 mg/ml valine and 0.002 mg/ml threonine, 0.2% w/v tryptophan, histidine-HCl, adenine sulphate, uracil, and 0.6% w/v leucine). For induction of *Cre* endonuclease activity, YP medium was prepared as stated, except D-glucose was replaced with 2% w/v D-galactose. When growing cells in solid media, agar was added to the mixture at 2% w/v. When preparing selection media for a strain carrying a specific auxotrophic marker or plasmid, the appropriate supplement was excluded from the media. Sporulation of diploid cells was carried out in solid media composed of 1% w/v potassium acetate, 0.1% w/v Yeast Extract, 0.05% w/v D-glucose, 0.2% w/v tryptophan, histidine-HCl, adenine sulphate, uracil, and 0.6% w/v leucine. All media was prepared in sterilised distilled water (SDW).

#### 6.1.2. Antibiotic-based selection media

25 mg/ml Antimycin A (Sigma) and 200 mg/ml nourseothricine stock solutions were stored at -20°C. Powdered Hygromycin B (Sigma) was stored at 4°C, and solutions were prepared with sterile distilled water. Hygromycin B (HygB), Antimycin A (AntA), and

**Table 6.1. *Saccharomyces cerevisiae* strains used in this study**

Strain name	Abbreviation	Genotype	Source
yMK7	Sa WT	<i>MATa, leu2Δ::hisG, his3Δ::hisG, trp1Δ::hisG, ura3-52</i>	Ashe lab.
yMK12	Sd WT	<i>MATa/MATα, leu2Δ::hisG/ leu2Δ::hisG, his3Δ::hisG/ his3Δ::hisG, trp1Δ::hisG/ trp1Δ::hisG, ura3-52/ ura3-52</i>	Ashe lab.
yMK13	Sa <i>ste7</i>	<i>MATα, leu2Δ::hisG, his3Δ::hisG, trp1Δ::hisG, ura3-52, ste7Δ::ura</i>	Ashe lab.
yMK14	Sd <i>ste7</i>	<i>MATa/MATα, leu2Δ::hisG/ leu2Δ::hisG, his3Δ::hisG/ his3Δ::hisG, trp1Δ::hisG/ trp1Δ::hisG, ura3-52/ ura3-52, ste7Δ::ura/ ste7Δ::ura</i>	Ashe lab.
yMK23	Wa WT	<i>MATa, ade2-1, his3-11, 15, leu2-3, 112, trp1-1, ura3-1, can1-100</i>	Ashe lab.
yMK50	Sst1	<i>MATa, sst1</i>	Ashe lab.
yMK50	Sst2	<i>MATα, sst2</i>	Ashe lab.
yMK467	Wa ADE	<i>MATa, ADE2, his3-11, 15, leu2-3, 112, trp1-1, ura3-1, can1-100, GCD1-P180</i>	Ashe lab.
yMK673	Sα WT	<i>MATα, leu2D::hisG, his3D::hisG, trp1D::hisG, ura3-52</i>	Ashe lab.
yMK880	W GCD-GFP	<i>MATa, ADE2, his3-11, 15, leu2-3, 112, TRP1, ura3-1, can1-100, GCD1-P180-GFP::G418</i>	Ashe lab.
yMK2227	W <i>adh1d</i> + 5g	<i>MATα GCD1-P180, ade2-1, his3-11,15, leu2-3,112, trp1-1, ura3-1::TDH3p-hbd-Flag2-CYC1t-LEU2, TDH3p-adhe2-Flag2-CYC1t-URA3, TDH3p-ERG10-Flag2-CYC1t-KanMX4,TDH3p-crt-Flag2-CYC1t-TRP1, TDH3p-ccr-Flag2-CYC1t-HIS3, adh1Δ::ADE2, TDH3p-ALD6-Flag2-CYC1t-TEF1p-ACS2-Flag2 ADH1t-hphNT1, adh1Δ::ADE2</i>	Swidah et al., 2015

yMK2633	W adh1d + A6A2	<i>MATa, ade2-1, his3-11, 15, leu2-3, 112, trp1-1, ura3-1, can1-100, GDC1-P180, adh1::ADE2</i> <i>ALD6.ACS2::hphNT1</i>	Ashe lab.
yMK2640	W adh1d	<i>MATa, adh1d::ADE2, his3-11, 15, leu2-3, 112, trp1-1, ura3-1, can1-100, GDC1-P180</i>	Ashe lab.
yMK3183	Sa adh1d	<i>MATa, leu2D::hisG, his3D::hisG, trp1D::hisG, ura3-52, adh1::loxLE-hphNT1-loxRE</i>	This study.
yMK3247	GAC1-GFP	<i>MATa, ADE2, his3-11, 15, leu2-3, 112, trp1-1, ura3-1, can1-100, GCD1-P180, GAC1-GFP, TRP1</i>	This study.
yMK3248	GLC7-GFP	<i>MATa, ADE21, his3-11, 15, leu2-3, 112, trp1-1, ura3-1, can1-100, GCD1-P180, GLC7-GFP, TRP1</i>	This study.
yMK3249	BDH2-GFP	<i>MATa, ADE2, his3-11, 15, leu2-3, 112, trp1-1, ura3-1, can1-100, GCD1-P180, BDH2-GFP, TRP1</i>	This study.
yMK3250	RTS3-GFP	<i>MATa, ADE2, his3-11, 15, leu2-3, 112, trp1-1, ura3-1, can1-100, GCD1-P180, RTS3-GFP, TRP1</i>	This study.
yMK3301	Sa adh1d HygB <sup>s</sup>	<i>MATa, leu2D::hisG, his3D::hisG, trp1D::hisG, ura3-52, adh1</i>	This study.
yMK3308	Sd adh1d	<i>MATa/MATα, leu2D::hisG/ leu2D::hisG, his3D::hisG/ his3D::hisG, trp1D::hisG/ trp1D::hisG, ura3-52/ ura3-52, adh1::loxLE-hphNT1-loxRE::adh1::loxLE-hphNT1-loxRE</i>	This study.
yMK3348	Sa adh1d + A6A2	<i>MATa, leu2D::hisG, his3D::hisG, trp1D::hisG, ura3-52, adh1, TDH3p-ALD6-Flag2-CYCt-TEF1p-ACS2-Flag2-ADH1t-hphNT1</i>	This study.
yMK3415	Wd WT	<i>MATa/MATα, ade2-1/ade2-1, his3-11, 15/ his3-11, 15, leu2-3, 112/ leu2-3, 112, trp1-1/ trp1-1, ura3-1/ ura3-1, can1-100/ can1-100, GDC1-P180/ GDC1-P180</i>	This study.
yMK3417	Wd adh1d	<i>MATa/MATα, adh1d::ADE2/ adh1d::ADE2, his3-11, 15/ his3-11, 15, leu2-3, 112/ leu2-3, 112, trp1-1/ trp1-1, ura3-1/ ura3-1, can1-100/ can1-100, GDC1-P180/ GDC1-P180</i>	This study.
yMK3421	SHQ1-GFP	<i>MATa, ADE2, his3-11, 15, leu2-3, 112, trp1-1, ura3-1, can1-100, GDC1-P180, SHQ1-GFP, TRP1</i>	This study.
yMK3436	NRP1-GFP	<i>MATa, ADE2, his3-11, 15, leu2-3, 112, trp1-1, ura3-1, can1-100, GDC1-P180, NRP1-GFP, TRP1</i>	This study.
yMK3452	Sa pdc1d	<i>MATa, leu2D::hisG, his3D::hisG, trp1D::hisG, ura3-52, pdc1::loxLE-hphNT1-loxRE</i>	This study.

yMK3454	Wa pdc1d	<i>MATa, ADE2, his3-11, 15, leu2-3, 112, trp1-1, ura3-1, can1-100, GDC1-P180, pdc1:: loxLE-hphNT1-loxRE</i>	This study.
yMK3461	Sd pdc1d	<i>MATa/MATa, leu2D::hisG/ leu2D::hisG, his3D::hisG/ his3D::hisG, trp1D::hisG/ trp1D::hisG, ura3-52/ ura3-52, pdc1:: loxLE-hphNT1-loxRE/ pdc1:: loxLE-hphNT1-loxRE</i>	This study.
yMK3556	Wa pdc5d	<i>MATa, ADE2, his3-11, 15, leu2-3, 112, trp1-1, ura3-1, can1-100, GDC1-P180, pdc5:: loxP-natNT2-loxP</i>	This study.
yMK3593	Sa pdc5d	<i>MATa, leu2D::hisG, his3D::hisG, trp1D::hisG, ura3-52, pdc5:: loxP-natNT2-loxP</i>	This study.
yMK3595	Sa pdc1,5d	<i>MATa, ADE2, his3-11, 15, leu2-3, 112, trp1-1, ura3-1, can1-100, GDC1-P180, pdc1:: loxLE-hphNT1-loxRE</i>	This study.
yMK3607	Wa pdc1,5d	<i>MATa, ADE2, his3-11, 15, leu2-3, 112, trp1-1, ura3-1, can1-100, GDC1-P180, pdc1:: loxLE-hphNT1-loxRE, pdc5:: loxP-natNT2-loxP</i>	This study.

nourseothricine were added to solid YPD at final concentrations of 300 µg/ml, 1 µg/ml, and 100 µg/ml respectively.

### 6.1.3. *Escherichia coli* strains used and growth conditions

DH5α background *E. coli* strains harboring the plasmids used in this project are listed in Table 6.2, and were grown at 37°C in a shaking incubator in Luria-Bertrani (LB) media (1% w/v Bacto Tryptone, 0.5% w/v Yeast extract and 2% w/v sodium chloride) supplemented with 0.1 mg/ml Ampicillin. When grown in solid media, agar was added at 2% w/v.

#### 6.1.4. Cell density in liquid cultures

Optical density (OD) was measured at 600 nm in a BioPhotometer plus (eppendorf) spectrophotometer, using the appropriate culture media as a blank. For heavily grown cultures samples were diluted 1:10 to give OD<sub>600</sub> values <1.0.

**Table 6.2. Plasmids used in this study**

Plasmid	Main features	Bacterial strain	Source
pAS54	<i>HO, URA3, CEN</i>	BMK116	Ashe lab.
pYM26	<i>yeGFP-STOP, klTRP1, AmpR</i>	BMK529	Janke et al. (2004).
pBMH-ALD6-ACS2-HYGR	<i>ALD6-Flag, ACS2-Flag, hphNT1, AmpR</i>	BMK671	Ashe lab.
pZC2	<i>loxP-natNT2-loxP</i>	BMK757	Carter and Delneri (2010).
pZC3	<i>loxLE-hphNT1-loxRE</i>	BMK834	Carter and Delneri (2010).
pSH47	<i>Cre, URA3</i>	BMK863	Ashe lab.

## 6.2. Nucleic acid manipulation and analysis

### 6.2.1. Purification of plasmid DNA from bacteria

Plasmid DNA was extracted from 5 ml of bacterial cultures grown overnight using a QIAprep<sup>®</sup> Spin MiniprepKit (QIAGEN). The extraction was performed according to the instructions provided by the manufacturer of the kit, and the purified plasmid DNA was stored at -20°C.

### **6.2.2. Extraction of genomic DNA from yeast cells**

Genomic DNA was extracted from 5 ml of yeast culture grown overnight by pelleting cells in a 4K15 centrifuge (Qiagen Sigma) at 4,000 rpm for 4 minutes. The supernatant was removed, and the pellet was resuspended in 1 ml EB solution (1 M sorbitol, 1 mM EDTA, 30  $\mu$ M dithiothreitol [DTT]) and centrifuged in a Heraeus Biofuge Pico microcentrifuge at 13,000 rpm for 4 minutes. The resulting supernatant was removed by pipetting, and the cell pellet was resuspended in 500  $\mu$ l EB solution containing 1mg/ml lyticase and incubated at 37°C to allow cell breakdown. After 1 hour, cell lysis was stopped by adding 55  $\mu$ l of a stop solution (3 M NaCl, 100 mM Tris pH 7.5 and 20 mM EDTA).

Nucleic acid was then extracted using a phenol:chloroform-based approach. 500  $\mu$ l of a 1:1 phenol:chloroform mixture was added to the cell lysate and mixed by vortexing. Then, the sample was centrifuged at 13,000 rpm for 2 minutes in a Centrifuge 5424 (Eppendorf), and the top aqueous phase was transferred to a new microcentrifuge tube. The above step was repeated, and 400  $\mu$ l of chloroform was added to the aqueous phase from the second extraction. The resulting aqueous phase was transferred to a new tube and 1 ml pure ethanol was added. Precipitated DNA was then collected by centrifugation at 13,000 rpm for 10 minutes. The supernatant was carefully removed by pipetting, and the pellet was left to dry in the fume hood for 30 minutes before resuspending in 20  $\mu$ l of sterile distilled water. Samples were stored in a freezer at -20°C.

### **6.2.3. Extraction of RNA from yeast cells**

Due to the delicate nature of RNA and the ubiquitous presence of RNases in the environment, bench areas and glassware were washed with a 1% w/v dodecyl sodium sulphate (SDS) solution in diethyl polycarbonate (DEPC)-treated water before working

with RNA. Ethanol, chloroform, and isopropanol are of molecular biology grade, and were diluted in Ultra Pure Distilled Water (Invitrogen), when necessary. Additionally, gloves and pipettes were routinely sprayed with 1% w/v SDS and RNase ZAP (Sigma Life Sciences).

RNA was extracted from yeast cells using the protocol recommended for TRIzol LS Reagent (Invitrogen). 45 ml of yeast cultures were pelleted by centrifuging in a 4K15 centrifuge (Qiagen Sigma) at 5,000 rpm for 3 minutes. The supernatant was tipped over, and the remaining liquid was carefully removed with a dry paper towel. Then, each cell pellet was resuspended in 750  $\mu$ l TRIzol reagent and transferred to a 1.5 ml screw cap tube containing approximately 400  $\mu$ l of acid-washed glass beads (425 to 600  $\mu$ m diameter, Sigma) and kept in ice for the rest of the procedure. The resuspended cells were lysed by shaking them three times for 40 seconds in a Mini Beadbeater-8 (Biospec Products) at 4°C, resting for 20 seconds between cycles. The lysed supernatants were transferred to a 1.5 ml tube, and 200  $\mu$ l chloroform was added before vigorously mixing the tubes by vortexing for 30 seconds. The tubes were left to settle at room temperature for 3 minutes before centrifuging them at 13,400 rpm for 15 minutes at 4°C in a 1-14 Centrifuge (Sigma). The top aqueous layer was then carefully transferred to another tube, where 1  $\mu$ l GlycoBlue Coprecipitant (Invitrogen) and 500  $\mu$ l isopropanol were added to precipitate the extracted RNA. Extracted samples were frozen at -80°C before continuing.

RNA extracts were thawed in ice, and centrifuged at 13,400 rpm for 15 minutes at 4°C. The resulting supernatant was removed by pipetting, and 1 ml of a 75% v/v ethanol solution was added to the extracts and mixed by briefly vortexing before centrifuging again under the same conditions for 10 minutes. The ethanol supernatant was removed by pipetting, and the RNA pellets were left to dry next to a Bunsen burner for 15 minutes.

The pellets were finally resuspended in 20  $\mu$ l Ultra Pure Water and frozen at  $-80^{\circ}\text{C}$  until needed.

#### **6.2.4. RNA sequencing**

Prepared RNA extracts were sent to the Genomic Technologies Core Facility of the University of Manchester for sequencing. Samples were sequenced using a HiSeq 4000 sequencer (Illumina).

The resulting data was analysed by a bioinformatician of the Bioinformatics Core Facility of the University of Manchester, who conducted the initial statistical analysis, quality control, and differential expression analysis of the dataset. RNA Quality Control was performed using FastQC v0.11.3, and mapping to multiple genomes for contaminant detection was done using FastqScreen v0.13.0 (Wingett and Andrews, 2018). Low-quality base trimming was done using BBDuk from BBMap v38.88 (Bushnell et al., 2017). Read mapping was done using the STAR v2.7.7a software (Dobin et al., 2013) using the *Saccharomyces cerevisiae* R64-1-1 (sacCer3) database as reference with Ensembl v102 annotation. STAR v2.7.7a was used for gene mapping and expression quantification. Differential expression analysis was carried out using DESeq2 v1.26.0 (Love et al., 2014) at  $\alpha = 0.05$ . Additionally, the *lfcShrink* function was used to generate more accurate  $\log_2$  fold-change estimates. Normalised counts were obtained using the *counts* function, where the raw counts were normalised using the median ratio method (Anders and Huber, 2010).

#### **6.2.5. Determination of DNA and RNA concentrations**

DNA and RNA concentration and purity were determined by measuring the absorbance at 260 and 280 nm of 1.5  $\mu$ l of a nucleic acid sample in a NanoDrop<sup>®</sup> ND-

8000 spectrophotometer, using the ND-8000 V1,0.3 software to calculate sample concentration, 260/280 ratio, and view absorbance curve.

### 6.2.6. DNA amplification by Polymerase Chain Reaction (PCR)

PCR reactions to amplify the *adh1* deletion cassette from the pZC3 plasmid and gene deletion or integration verifications were carried out using the Platinum Super PCR kit (Invitrogen), while GFP tagging cassettes were amplified from the pYM26 plasmid using Expand High Fidelity kit (Roche). All reaction cycles were performed in a T3 Biometra® thermocycler. The oligonucleotides used in this study are listed in Table 6.3.

**Table 6.3. Oligonucleotides used in this study**

Reference number (Ref)	Name	Purpose	Sequence (5'-3')
1	ADH DEL FW	Amplification of <i>ADH1</i> deletion cassette	TGCACAATATTTCAAGCTATACCAAGCA TACAATCAACTATCTCATATACACGTAC GCTGCAGGTCGAC
2	ADH1 DEL RV	Amplification of <i>ADH1</i> deletion cassette	TTTTTTATAACTTATTTAATAATAAAAAT CATAAATCATAAGAAATTCGCCACTATA GGGAGACCGGCAG
3	ADH1 VER FW	External verification of <i>ADH1</i> deletion	CGACAAAGACAGCACCAACA
4	ADH1 VER RV	External verification of <i>ADH1</i> deletion	CCGGTAGAGGTGTGGTCAAT
5	HYGB VER FW	Internal verification of <i>hphNT1</i> marker	GAAGGAGTTAGACAACCTGAAG
6	HYGB VER RV	Internal verification of <i>hphNT1</i> marker	TGTGAGAACTGTATCCTAGCAAG

7	PDC1 DEL FW	Amplification of <i>PDC1</i> deletion cassette	CAATTATTATTTTCTACTCATAACCTCAC GCAAATAACACAGTCCGTACGCTGCAG GTCGAC
8	PDC1 DEL RV	Amplification of <i>PDC1</i> deletion cassette	CGTTACATAAAAATGCTTATAAACTTTAA CTAATAATTAGAGATCACTATAGGGAGA CCGGCAG
9	PDC1 VER FW	External verification of <i>PDC1</i> deletion	CTCCTTGCAATCAGATTTGG
10	PDC1 VER RV	External verification of <i>PDC1</i> deletion	TCTTTCCATGGTAAGTGACA
11	PDC5 DEL FW	Amplification of <i>PDC5</i> deletion cassette	ATTACACTTATTTACATAATCAATCTCA AAGAGAACAACACAATCGTACGCTGCAG GTCGAC
12	PDC5 DEL RV	Amplification of <i>PDC5</i> deletion cassette	TCAAAAGTAAAAAATACACAAACGTTG AATCATGAGTTTTATGTCACTATAGGGA GACCGGCAG
13	PDC5 DEL VF	External verification of <i>PDC5</i> deletion	GTCCTTTCCTCTCTTTCTTA
14	PDC5 DEL VR	External verification of <i>PDC5</i> deletion	TAAATGGATTTGTAGATATT
15	PDC5 VF LONG	Elongated external verification of <i>PDC5</i> deletion	AGAAATTTTCATATGATGAGACTTG
16	PDC5 VF LONG	Elongated external verification of <i>PDC5</i> deletion	GATCATAGCTAAAGGTACAAAACCG
17	NAT VF	Internal verification of <i>natNT2</i> marker	GGTCAGGTTGCTTTCTCAGG
18	NAT VR	Internal verification of <i>natNT2</i> marker	TACGAGATGACCACGAA

19	BDH2 S2	Amplification of <i>BDH2</i> GFP tagging cassette	AGACCGCGGGATTAACACGAGAACGTGA GTACTCAATCACAATCAATCGATGAATT CGAGCTCG
20	BDH2 S3	Amplification of <i>BDH2</i> GFP tagging cassette	GAAAGACTACGAGAATCAATAAACGAG GCTAAACTGCGTCACACACGTACGCTGC AGGTCGAC
21	GAC1 S2	Amplification of <i>GAC1</i> GFP tagging cassette	AAGAATAAAATTAACAAATAGAAAAGTT GAATCTTTTAAACTCAATCGATGAATTC GAGCTCG
22	GAC1 S3	Amplification of <i>GAC1</i> GFP tagging cassette	TCATCTCCACCCATCCTTTCCCAAGAGGT TGATCGATGGCGACTTCGTACGCTGCAG GTCGAC
23	GLC7 S2	Amplification of <i>GLC7</i> GFP tagging cassette	AGTATTTTCCTTTTTAAACTTTGATTTAG GACGTGAATCTATTTAATCGATGAATTCG AGCTCG
24	GLC7 S3	Amplification of <i>GLC7</i> GFP tagging cassette	GCCCAAAAAGTCTACCAAGGCAAGCTG GGGGTAGAAAGAAAAACGTACGCTGC AGGTCGAC
25	RTS3 S2	Amplification of <i>RTS3</i> GFP tagging cassette	TATTTAGAGAACTCTGTTTTCTTATGTA TCTCGTTACAGCCTAATCGATGAATTCG AGCTCG
26	RTS3 S3	Amplification of <i>RTS3</i> GFP tagging cassette	AAGGCTGATCTCATGGCAAAGAGATTCC AAACTGGTTCATTGAAACGTACGCTGCA GGTCGAC
27	NRP1 S2	Amplification of <i>NRP1</i> GFP tagging cassette	CAATGTGGTTGTGAAATTTATTGACCTCG CCTGTTCCCTAACTAATCGATGAATTCGAG CTCG
28	NRP1 S3	Amplification of <i>NRP1</i> GFP tagging cassette	GTGATAATAGCGCTTTCGGTAATGGTTTT AATAGTTCAATACGTTGGCGTACGCTGC AGGTCGAC
29	SHQ1 S2	Amplification of <i>SHQ1</i> GFP tagging cassette	TCTATCTAATGCAGTAATCTACGCTAAAC ATTCAAATGATCTTCAATCGATGAATTCG AGCTCG
30	SHQ1 S3	Amplification of <i>SHQ1</i> GFP tagging cassette	ATTTTGGCAGAGTCTGAATACCGAGAGC AGCAGCAGAACCACAACGTACGCTGCA GGTCGAC

31	TRP1 VF	Verification of <i>TRP1</i> marker integration	CCTGTGGGAACTGGAACCTCTT
32	TRP1 VR	Verification of <i>TRP1</i> marker integration	CTATTCATCCAGCAGGCCTCTCAA
33	BDH2 GFP VF	Verification of <i>BDH2</i> GFP tag integration	ATAACGGGCAGAGTCAACAT
34	BDH2 GFP VR	Verification of <i>BDH2</i> GFP tag integration	CTTCTCTCCGTCGAAACGAA
35	GAC1 GFP VF	Verification of <i>GAC1</i> GFP tag integration	GAATTTCCCAAGCTTCTGAT
36	GAC1 GFP VR	Verification of <i>GAC1</i> GFP tag integration	CAACAGCGTAGATGCTTTTA
37	GLC7 GFP VF	Verification of <i>GLC7</i> GFP tag integration	GGAGTTGATTTGCAGGGCCC
38	GLC7 GFP VR	Verification of <i>GLC7</i> GFP tag integration	GCGGTTTGTGCACTAAAGGG
39	RTS3 GFP VF	Verification of <i>RTS3</i> GFP tag integration	CTCAGCACCAACAACAAACA
40	RTS3 GFP VR	Verification of <i>RTS3</i> GFP tag integration	GTAGTAGCTTGAAAAACGCC
41	NRP1 GFP VF	Verification of <i>NRP1</i> GFP tag integration	TTCAAAAGTGACAAAGCTAA
42	NRP1 GFP VR	Verification of <i>NRP1</i> GFP tag integration	AAGGTAGATCTGAAATGGGC

43	SHQ1 GFP VF	Verification of <i>SHQ1</i> GFP tag integration	AAATGAGAAAAGAGCAAGAG
44	SHQ1 GFP VR	Verification of <i>SHQ1</i> GFP tag integration	CCAAATGCAGATATAAGAAC
45	ALD6 ACS2 VER P1 FW	Verification of <i>ALD6/ACS2</i> integration	GAAAACGGAAGAGGAGTAGGG
46	ALD6 ACS2 VER P2 RV	Verification of <i>ALD6/ACS2</i> integration	CGTCGAAACTAAGTTCTTGG
47	ALD6 ACS2 VER P3 FW	Verification of <i>ALD6/ACS2</i> integration	GTTATGTTTATCGGCACTTGG
48	ALD6 ACS2 VER P4 RV	Verification of <i>ALD6/ACS2</i> integration	CGAGGATACGGAGAGAGGTATG

Reactions using the Platinum Super PCR kit were carried out by mixing 1 µl template DNA (pure or diluted up to 1:1000) or distilled water, 2 µl of each 10 µM oligonucleotide and 45 µl Platinum Super PCR mix for a reaction volume of 50 µl. The thermocycler programme used was:

**1.-Initial denaturation:** 95°C for 1 minute

**2.-Denaturation:** 95°C for 1 minute

**3.-Annealing:** 54°C for 1 minute

**4.-Amplification:** 72°C for 2 minutes (steps 2 to 4 are repeated 25 times)

**5.-Final amplification:** 72°C for 10 minutes

Reactions using the Expand<sup>TM</sup> High Fidelity kit (Sigma-Aldrich) with a reaction mix containing 1x Expand High Fidelity buffer with 1.5 mM MgCl<sub>2</sub>, 200 μM deoxynucleotide triphosphates (dNTPs), 2.6 U Enzyme Mix, with 10 μl template DNA at 1:100 dilution in a final volume of 50 μl. 1 μl of each oligonucleotide at 10 μM was added on “hot start” to the tube once the initial denaturation step of the reaction reached at least 90°C. The thermocycler programme used was:

**1.-Initial denaturation:** 95°C for 3 minutes

**2.-Denaturation:** 95°C for 15 seconds

**3.-Annealing:** 55°C for 39 seconds

**4.-Amplification:** 68°C for 4 minutes (steps 2 to 4 repeated 30 times)

**5.-Final amplification:** 68°C for 5 minutes

### **6.2.7. Agarose gel electrophoresis**

PCR products and digested plasmids were analyzed by agarose gel electrophoresis. Samples were mixed with Orange G loading dye (2 mg/ml Orange G, 10 mM EDTA, 25% v/v Ficoll) at a ratio of 1 μl loading dye per 5 μl sample before loading into the gel, together with 5 μl of Hyper Ladder<sup>TM</sup> (Bioline) 1kb molecular weight marker in order to estimate the size of the sample DNA bands. Agarose gels were prepared at 1% w/v molecular grade agarose (Bioline) in TAE buffer (40 mM Tris-base, 20 mM acetic acid, 1 mM EDTA pH 8.0), supplemented with 0.1 μl/ml SafeView Nucleic Acid Stain (NBS Biologicals). Samples were separated at 90 V for 45 minutes. DNA fragments in the

agarose gel were visualized and photographed with an UVIDOC HD6 (Clever Scientific) transilluminator.

Analysis of RNA extracts by agarose gel electrophoresis required that the electrophoresis tank, gel case, and comb were soaked in 1% w/v SDS before use. The 1% w/v agarose gel was made with TBE buffer (90 mM Tris-base, 90 mM boric acid, 2 mM EDTA pH 8.0) prepared in DEPC-treated distilled water, supplemented with 0.5 µg/ml ethidium bromide (10 mg/ml solution, Sigma). Samples were diluted to 0.2 µg/µl in a 1:1 mixture of 2X RNA Loading Dye (Thermo Scientific) and DEPC-treated water and denatured at 70°C for 10 minutes before loading. RNA samples were separated at 70V for 90 minutes at 4°C.

#### **6.2.8. Digestion of plasmid DNA with restriction enzymes**

In order to verify the identity of extracted plasmid DNA, 5 µl of the extracted DNA was digested with 1 µl of each restriction enzyme used (High Fidelity, New England BioLabs®), in 1X CutSmart® buffer (New England BioLabs®), topped to a final volume of 20 µl with sterile distilled water. The reactions were carried out at 37°C for 1 hour, and digestion fragments were separated by agarose gel electrophoresis, or stored at -20°C.

#### **6.2.9. Transformation of yeast cells with plasmid DNA or PCR product**

A modified version of the high efficiency lithium acetate transformation protocol from (Schiestl and Gietz, 1989) was used in this project.

A 5 ml or 20 ml liquid culture media was prepared from a single colony of the strain to be transformed and grown overnight. The equivalent of a 25 ml OD<sub>600</sub> 0.15 culture was prepared from the overnight culture and incubated for 3 to 4 hours, or until OD<sub>600</sub> ~ 0.6. The culture was then transferred to a 50 ml sterile centrifuge tube and centrifuged in a

4K15 centrifuge (Qiagen Sigma) at 4,000 rpm for 5 minutes. The supernatant was then removed, and the cell pellet was resuspended in 12.5 ml sterile distilled water and centrifuged again. The resulting pellet was resuspended in 1 ml 100 mM lithium acetate, transferred to a 1.5 ml centrifuge tube and centrifuged in a Heraeus Biofuge Pico microcentrifuge at 13,000 rpm for 15 seconds. Then, the supernatant was removed by pipetting, and the cell pellet was resuspended in 250  $\mu$ l 100 mM lithium acetate.

50  $\mu$ l of the resuspended yeast cells were transferred to new 1.5 ml tubes, where reagents of the 'transformation mix' were added in the following order: 266.6  $\mu$ l 50% v/v PEG, 40  $\mu$ l 1M lithium acetate, 12.5  $\mu$ l 10 mg/ml salmon sperm carrier DNA (boiled for 5 minutes and then chilled in ice to denature), 25  $\mu$ l or 2  $\mu$ l sterile distilled water for transformation with PCR product, plasmid DNA, respectively (sterile distilled water was used instead for negative controls). The mix was then topped to 400  $\mu$ l with sterile distilled water, mixed by vortex for 1 minute and incubated in a rotating incubator (Labnet International, Inc.) at 30°C for 1 hour. The cells were then incubated in a water bath at 42°C for 20 minutes. Cells transformed with plasmid DNA were then centrifuged at 4000 rpm for 3 minutes to remove the transformation mix, resuspended in 200  $\mu$ l sterile distilled water and spread onto the corresponding solid selection media. Cells transformed with PCR product were transferred to 3 ml YPD and left on the bench overnight. The next day cells were washed as described above and 200  $\mu$ l of the suspension spread onto the corresponding selection media. Plates were then incubated at 30°C until yeast colonies were visible.

### **6.3. Characterisation of yeast strains**

#### **6.3.1. Photomicroscopy**

Single-cell pictures were taken in a Nikon Eclipse E600 (Nikon) optic microscope with a 100x/0.5-1.3 Oil Iris objective. Images were captured with a Ds-Qi1Mc monochrome digital camera (Nikon) and processed with the NIS-elements F software (Nikon).

For single-cell fluorescent microscopy, the above microscope was used together with a Nikon Intensilight C-HGF1 light source and equipped with a green fluorescent protein (GFP) filter.

#### **6.3.2. Stereomicroscopy**

Yeast colonies were visualized in a Leica MZ10F stereomicroscope at 10x magnification. Images were captured with a coupled Leica DFC420C camera, and pictures were saved and edited using the Leica Application Suite v.4.0.0. software.

#### **6.3.3. Growth curves in liquid culture**

120 ml cultures of log-phase yeast cells were grown overnight until an  $OD_{600}$  of 0.15 to 0.2. Then the culture was split into three 40 ml cultures, and different amounts of 1-butanol were added to achieve final concentrations of 0 (control), 1, and 2% v/v, and flasks were incubated at 30°C. Every hour after the incubation started, 1 ml aliquots of each culture were taken to measure  $OD_{600}$  throughout the experiment.

The results were plotted as  $OD_{600}$  versus time (hours), and the data was fitted to the following two parameter exponential curve using the software SigmaPlot 11.0:

$$N_t = N_0 * e^{G*t}$$

Where  $N_t$  is OD<sub>600</sub> at a specific time (t),  $N_0$  is the OD<sub>600</sub> at t=0, and G is growth rate (h<sup>-1</sup>).

Doubling time for each curve was then calculated as follows:

$$\text{Doubling time (h)} = \ln(2) / G$$

#### **6.3.4. Cell viability assays**

60 ml cultures of log-phase yeast cells were grown overnight until an OD<sub>600</sub> of 0.4 to 0.6, and then split into three 20 ml flasks. 1-butanol was added to achieve final concentrations of 0, 1 and 2% v/v, and the flasks were then put in incubation at 30°C. At 1 and 2 hours after incubation started, 100 µl aliquots were taken from each of the cultures and serially diluted to 1:1,000 in SDW, vigorously mixing by vortex for 20 to 40 seconds between each dilution. Finally, 100 µl aliquots of each 1:1,000 dilution were streaked in a YPD agar plate in triplicate, and grown at 30°C for 24 to 48 hours to allow colony formation. Colonies were then counted manually, and average and standard deviation for each treatment was then calculated.

#### **6.3.5. Agar invasion assay**

The agar invasion assay of yeast cultures on solid media was based on a published method (Cullen, 2015). YPD agar plates were prepared by patching yeast cells from single colonies and left to grow at 30°C for 3 days. Plates were then scanned in an EPSON PERFECTION V750 PRO scanner before washing away surface cells with a stream of distilled water. Plates were scanned again after washing to reveal invasive cells.

## **6.4. Protein analysis**

### **6.4.1. Preparation of whole cell protein extracts**

Whole cell protein extracts were prepared from 50 ml liquid cultures in exponential phase ( $OD_{600}$  between 0.4 and 0.7) by first centrifuging the culture at 4,000 rpm for 5 minutes in a 4K15 centrifuge (Qiagen Sigma) to collect the cell pellet. The supernatant was removed, and the cell pellet was resuspended in 1 ml of Buffer A (30 mM HEPES pH 7.5, 100 mM potassium acetate, 2mM magnesium acetate, 1 mM phenylmethanesulfonyl fluoride [PMSF]) supplemented with a fresh cOmplete Protease Inhibitor Cocktail tablet (Roche, 1 tablet per 10 ml of buffer), and transferred to an ice-cold 1.5 ml tube.

The cell pellet was then centrifuged at 13,000 rpm for 3 minutes at 4°C in a 1-14 Centrifuge (Sigma) and the resulting supernatant was removed. The cell pellet was resuspended in 100  $\mu$ l of ice-cold Buffer A, and approximately 60  $\mu$ l of acid-washed glass beads (425 to 600  $\mu$ m diameter, Sigma) were added to aid in cell lysis. Cells were lysed by vortexing them in six cycles of 40 seconds, resting them for 20 seconds in ice between cycles. Finally, the resulting extracts were centrifuged at 13,000 rpm for 3 minutes at 4°C, collected into fresh 1.5 ml tubes and stored at -20°C until needed.

### **6.4.2. Determination of protein concentration**

Protein concentration of whole cell extracts was estimated by measuring the absorbance at 280 nm of a 1.5  $\mu$ l aliquot in a NanoDrop® ND-8000 spectrophotometer, using the ND-8000 V1,0.3 software to calculate sample concentration, and view absorbance curve.

#### **6.4.3. Polyacrylamide gel electrophoresis (PAGE)**

Protein extracts were diluted 10 mg/ml in 100 µl distilled water, and 50 µl of this dilution was mixed with 15 µl NuPAGE LDS Sample Buffer 4X (Novex), and 6 µl Bolt Sample Reducing Agent 10X (Novex), and then denatured at 95 °C for 5 minutes before loading.

15 µl of protein extract in loading buffer was loaded into a Bolt 4-12% Bis-Tris Plus gel (Invitrogen), mounted in an X Cell SureLock electrophoretic cell (Novex) filled with NuPAGE MOPS SDS Running Buffer (Novex) diluted in ultra pure water (Milli-Q® Synthesis, Millipore). Additionally, 5 µl of either Spectra Multicolor Broad Range (ThermoFisher Scientific) or Precision Plus All Blue (Bio-Rad) protein ladder was loaded together with the samples to assess sample proteins band size. Protein samples were first separated at 100 V for 10 minutes, and then at 170 V for 50 minutes at room temperature.

#### **6.4.4. Western Blot**

The gel containing the separated proteins was removed from their plastic casing and transferred to a stack of filter paper soaked in NuPAGE transfer buffer (Novex) supplemented with 20 % v/v methanol (Fisher Chemical). A pre-soaked Amersham Protran 0.45 µm NC nitrocellulose blotting membrane (GE Health care Life Sciences) was then mounted over the gel and covered with more soaked filter paper. The stack was then mounted in a X Cell II Blot Module (Novex), filled with transfer buffer and the proteins were electro transferred from the gel into the membrane at 30 V for 90 minutes at room temperature.

After the transfer, the nitrocellulose membrane was briefly stained with Ponceau S solution (0.1% w/v Ponceau red in 1% v/v acetic acid) to verify the presence of protein bands in the membrane, and then washed with tris-buffered saline buffer supplemented with Tween 20 (TBS-Tween) (50 mM Tris-HCl pH 7.4, 150 mM NaCl, 0.1% v/v Tween 20) on a rocking platform until the stain was removed.

The membrane was left to block overnight at 4°C on a rocking platform, submerged in a blocking buffer containing 5% w/v skim milk (Sigma-Aldrich) in TBS-Tween. After blocking, the membrane was incubated with the appropriate primary antibody diluted in blocking buffer for 1 hour on a rocking platform at room temperature. The antibodies used in this project are listed in table 6.4 below.

**Table 6.4. Antibodies used in this project**

Primary Antibodies		Secondary Antibodies		
Name	Dilution	Name	Dilution	Source
$\alpha$ -GFP (rabbit)	1:5,000	$\alpha$ -Rabbit	1:10,000	Li-Cor
$\alpha$ -Flag (mouse)	1:10,000	$\alpha$ -Mouse	1:10,000	Li-Cor
$\alpha$ -Pgk1p (mouse)	1:5,000	$\alpha$ -Mouse	1:10,000	Li-Cor
$\alpha$ -Tif1p (rabbit)	1:10,000	$\alpha$ -Rabbit	1:10,000	Li-Cor

The membrane was removed from the buffer and washed with TBS-Tween three times on a rocking platform for 5 minutes each. The membrane was then incubated with secondary antibody diluted in blocking buffer for 1 hour on a rocking platform for 1 hour. The blot was removed from the buffer and washed again three times with TBS-Tween

before revealing the bands in an Odyssey-Fc (Li-Cor) using the Image Studio v. 5.2.5 software (Li-Cor).

## **6.5. Anaerobic fermentation and metabolite detection by gas chromatography**

### **6.5.1. Preparation of gas chromatography standards and glassware**

All glassware used for the preparation of gas chromatography (GC) standards and the glass vials for aerobic and semi-anaerobic fermentations were washed thoroughly with tap water, then washed three times with distilled water, and finally washed three times with ultra pure water (Milli-Q<sup>®</sup> Synthesis, Millipore). Clean glassware was then dried overnight in an oven at 60°C. 20 ml of each GC standard mix was prepared in volumetric flasks and aliquoted into amber GC vials to be stored at -20°C until used. The composition of each GC standard mix is described below:

**C1:** 1.0% v/v ethanol, 100 ppm 1-butanol, 100 ppm isobutanol.

**C2:** 0.1% v/v ethanol, 500 ppm 1-butanol, 100 ppm isobutanol.

**C3:** 0.1% v/v ethanol, 100 ppm 1-butanol, 1000 ppm R,R-2,3-butanediol, 1000 ppm R,S-2,3-butanediol.

**C4:** 0.1% v/v ethanol, 0.1% v/v acetaldehyde, 0.1% v/v glycerol, 1000 ppm R,R-2,3-butanediol, 1000 ppm R,S-2,3-butanediol.

**C5:** 1% v/v ethanol, 100 ppm 1-butanol, 0.1% v/v acetaldehyde.

### **6.5.2. Semi-anaerobic fermentation and butanol measurement procedures**

Fermentation vessels were prepared by aliquoting 45 ml of freshly prepared YPD media into 50 ml serum type reaction vials (Supelco), sealed with rubber stoppers and aluminum crimps (Supelco), and autoclaved at 115°C for 30 minutes.

Precultures were prepared by inoculating single colonies of the desired strains into 25 ml YPD in flasks and growing them until saturation. The strains were then inoculated into 45 ml of sterile YPD in the glass vials to a starting OD<sub>600</sub> of 0.1, unless specified. A 1ml sample was taken from the vials with a sterile syringe to measure OD<sub>600</sub>. Strains were then grown at 30°C in a static incubator for 16 days. On days 2, 4, 7, 9, 11, and 14, 3 ml samples were taken with a sterile syringe. 1 ml of this sample was used to measure OD<sub>600</sub> of the cell culture, and the rest was passed through a 0.22 µm Millex<sup>®</sup> filter (Millipore) into glass gas chromatography vials and stored at -20°C until needed.

Chemical separation and detection of analytes was done using an Agilent 6850A gas chromatography system with an Agilent 4513A automatic sample injector (Agilent technologies Ltd, Stockport, UK). Instrument control and data collection was managed by the GC ChemStation B.04.03[52] software (Agilent Tehcnologies). Hydrogen gas for the detector was supplied by a H2PEM-100 hydrogen generator (Parker Balston). 0.4 µl of each filtered sample was injected in a 20:1 split at an inlet temperature of 230°C. Samples were separated in a DB-WAX (30 m length, 0.25 mm diameter, 0.25 mm film thickness, Agilent technologies Ltd) polar capillary column, using helium as a carrier gas at 15.0 psi with a constant flow of 32.3 ml/min. Column temperature was increased from 40°C to 220°C over 15 minutes. Analyte concentration was calculated relative to the signals of chemical standards C1, C2, or C3.

## **6.6. Detection of GFP fluorescence in yeast cells**

### **6.6.1. Qualitative detection of fluorescence in agar cultures using a laser scanner**

Fluorescence of yeast cells grown in solid media was detected in a Sapphire Biomolecular Imager (Azure biosystems), using the Sapphire Capture v.1.7.0319.0

(Azure biosystems) software for image capture and analysis. Wavelength of the scanning laser was 520 nm, and pictures were taken at a pixel size of 500  $\mu\text{m}$ .

### **6.6.2. Microplate assay for the measurement of GFP fluorescence in liquid cultures**

Measurement of GFP fluorescence in yeast cells was done by pelleting 10 ml aliquots of cultures growing in SCD by centrifuging them at 4,000 rpm for 5 minutes. The supernatant was removed and the pellet washed in 10 ml of sterile distilled water, and centrifuged one more time in the same conditions. The supernatant was removed again, and the cells were resuspended in enough water to result in an OD<sub>600</sub> of 10. Then, 100  $\mu\text{l}$  of the cell suspension were pipetted into a clear 96-well microplate (Greiner Bio-One) and fluorescence was measured in a Synergy HT (Bio-Tek) microplate reader, using the Gen5 v. 2.09 software for equipment control and data collection. The excitation and emission wavelengths used were 485/20 nm and 530/25 nm, respectively.

### **6.7. Statistical analysis**

Statistical significance between experimental groups was calculated by Welch's t test using the GraphPad Prism 8.1.2 software (GraphPad Software, Inc.). A p-value less than 0.05 was considered statistically significant.

Adjusted p-values of the differential expression of transcripts in the RNA-seq dataset were obtained by correcting the p-values obtained in the Wald test using the Benjamini and Hochberg method in the DESeq2 v1.26.0 package.

Venn's diagrams were made using the Venny v2.1 web browser tool (Oliveros, 2015).

## 6.8. Gene Ontology Enrichment analysis

The web tool PANTHER Version 16.0 (Mi et al., 2020) was used for Gene Ontology (GO) enrichment analysis of RNA-seq results. While grouping genes according to expression changes between conditions, genes with a  $\log_2$  Fold Change equal to 1 or higher were considered differentially upregulated, while values equal to -1 or lower were considered differentially downregulated. Custom reference lists (*Saccharomyces cerevisiae*) were made for each analysis using the complete list of sequenced transcripts in each strain that had a valid calculated adjusted p-value. The annotation data set used for the enrichment analyses was GO biological process complete, and the Bonferroni correction for multiple testing was used to correct the results, including only enriched terms with calculated p-values lesser than 0.05. When presenting results, only the highest term in any given hierarchy was included to reduce the number of redundant categories.

## **7. Development of butanol-responding fluorescent biosensors for *S. cerevisiae* strains**

### **7.1 Introduction**

One strategy to expand the search for genes that have the potential to facilitate higher 1-butanol accumulation is the screening of multiple randomly generated mutants, deletion libraries, or cell populations generated by directed evolution techniques to look for favourable phenotypes (Mans et al., 2018; Tapia et al., 2012). Unfortunately, the anaerobic fermentation and gas chromatography analysis methods used in this project are not appropriate for high throughput screenings, thus, a more appropriate technique to assess butanol accumulation would enable genome wide assessments of the genetic requirements for butanol synthesis.

Biosensors are molecules that can detect the presence of a specific substance by using a biological or biochemical element that interacts with the desired analyte, coupled with a signal-transducing element that can generate a signal proportional to the concentration of the detected analyte (Naresh and Lee, 2021; Liu et al, 2015). In metabolic engineering, biosensors are widely used in high-throughput identification of stress-resistant or high-producing strains of specific metabolites, usually resulting from directed evolution methods. For instance, one study used an *ARO9*-based aromatic amino acid biosensor to screen for *S. cerevisiae* mutants produced with adaptive laboratory evolution techniques that were able to produce high titers of muconic acid through the shikimate pathway (Leavitt et al., 2017). Similarly, a more recent study employed a transcription factor-based fluorescent biosensor to aid in the directed evolution of the methanol dehydrogenase enzyme from *Lysinibacillus xylanilyticus* (Le et al., 2021).

Among biosensors, one class involves combining a responsive genetic element to drive the transcription of a reporter gene such as a fluorescent protein (Ding et al., 2021; Mahr and Frunzke, 2016). Such a biosensor is an attractive possible method to generate a 1-butanol biosensor in *S. cerevisiae* for a number of reasons. Firstly, due to the wide availability of genetic modification tools and procedures, there are several options available to enable construction of such a biosensor. These include the use of a plasmid system or genomically integrating reporter cassettes (Hahne and Ostermann, 2021; D'Ambrosio and Jensen, 2017), the generation of fusion proteins with fluorescent proteins (Kim et al, 2020; Rosado et al., 2008) or the use of responsive promoters directly driving the expression of a reporter (Hanko et al., 2018; Shi et al., 2018). In addition, should the system prove sufficiently sensitive it might be possible that this strategy can be employed for *in vivo* detection of the desired molecule in high throughput screenings of potential producers or mutant collections using simple plate assays to measure the fluorescence of individual yeast colonies (Feilmeier et al., 2000; Siemering et al., 1996) or fluorescence-assisted cell sorting techniques (Tu et al., 2020; Williams et al., 2017; Binder et al., 2012).

One of the key challenges underlying the above strategy is the identification of genetic elements or proteins that respond or interact specifically with the selected analyte in a dose-dependent manner. To this end, transcriptomic and proteomic profiling of cells exposed to the metabolite of interest can yield valuable data on potential candidate genes that might respond to the metabolite to enable construction of sensitive and specific gene expression-based biosensors. Indeed, a previous transcriptomic strategy to identify genes responsive to 1-butanol enabled construction of two plasmid-based biosensors that were able to discern between the 1-butanol titers of two butanol-producing strains after 96 hours of anaerobic fermentation (Shi et al., 2017). The design strategy behind these

biosensors was to use the promoter regions of *NRPI* and *SHQ1*, two genes identified as butanol-responding in their transcriptomic screening, to drive the expression of the fluorescent reporter mCherry.

Therefore, in order to assist with the identification of strain variants that can improve butanol production in *S. cerevisiae*, a strategy was developed for the construction and verification of fluorescent biosensors for the detection of 1-butanol in yeast cells.

## **7.2 General strategy for biosensor construction**

Despite the results of the study by Shi and colleagues, it presents a few limitations in its candidate gene screening and biosensor design. For instance, their screening does not take into account post transcriptional effects that may impact expression of the fluorescent biosensor such as the general translation initiation inhibition caused by fusel alcohol stress (Ashe et al., 2001). Additionally, the response time of their *NRPI* and *SHQ1* mCherry biosensors is at least 20 hours, while a faster response time would be more desirable in screening applications. Hence, identification of new candidate genes for the construction of 1-butanol biosensors was based on a more appropriate study.

To this end, the selection of candidate genes for the construction of 1-butanol biosensors was based on a study previously published in our laboratory that explored the global translational and transcriptional response of yeast cells to acute 1-butanol stress (Smirnova et al., 2005). This report identified a series of mRNAs that were both highly expressed and remained ribosome-associated despite the inhibition of global translation initiation observed during fusel alcohol stress. From this study, four transcriptionally and translationally upregulated genes were selected as candidates to be used as 1-butanol biosensors: *GAC1*, *GLC7*, *BDH2*, and *RTS3*. Their open reading frame (ORF) number and known function are summarised in Table 7.1.

**Table 7.1. Candidate genes for the construction of *in-vivo* 1-butanol biosensors**

Name	ORF	Function	Oligonucleotides used in the amplification
<i>GAC1</i>	YOR178C	Regulatory subunit of yeast protein phosphatase 1 (PP1).	GAC1 S2, GAC1 S3
<i>GLC7</i>	YER133W	Catalytic subunit of yeast protein phosphatase 1 (PP1).	GLC7 S2, GLC7 S3
<i>RTS3</i>	YGR161C	Putative component of the protein phosphatase 2A complex.	RTS3 S2, RTS3 S3
<i>BDH2</i>	YAL061W	Putative alcohol dehydrogenase similar to <i>BDH1</i> .	BDH2 S2, BDH2 S3

Instead of the plasmid biosensors constructed in studies mentioned above, it was decided in this project that gene fusions of GFP (green fluorescent protein) with each candidate gene would be attempted. This method has the advantage of generating a stable, single-copy gene construct that does not require any selection media to maintain its presence in the cell. In addition, the only change is the addition of a c-terminal tag to a specific protein which can be tolerated by a majority of yeast proteins (Senejani et al., 2007; Chang et al., 2005), although it is formally possible that the resulting fusion proteins may have their functions hindered.

### 7.3 Construction and insertion verification of GFP-based biosensor strains

After selecting the candidates, gene fusions with GFP were constructed using insertion cassettes directed towards the codon upstream of the termination codon in each candidate gene (Figure 7.1 A). The cassettes were amplified by PCR from the pYM26 plasmid

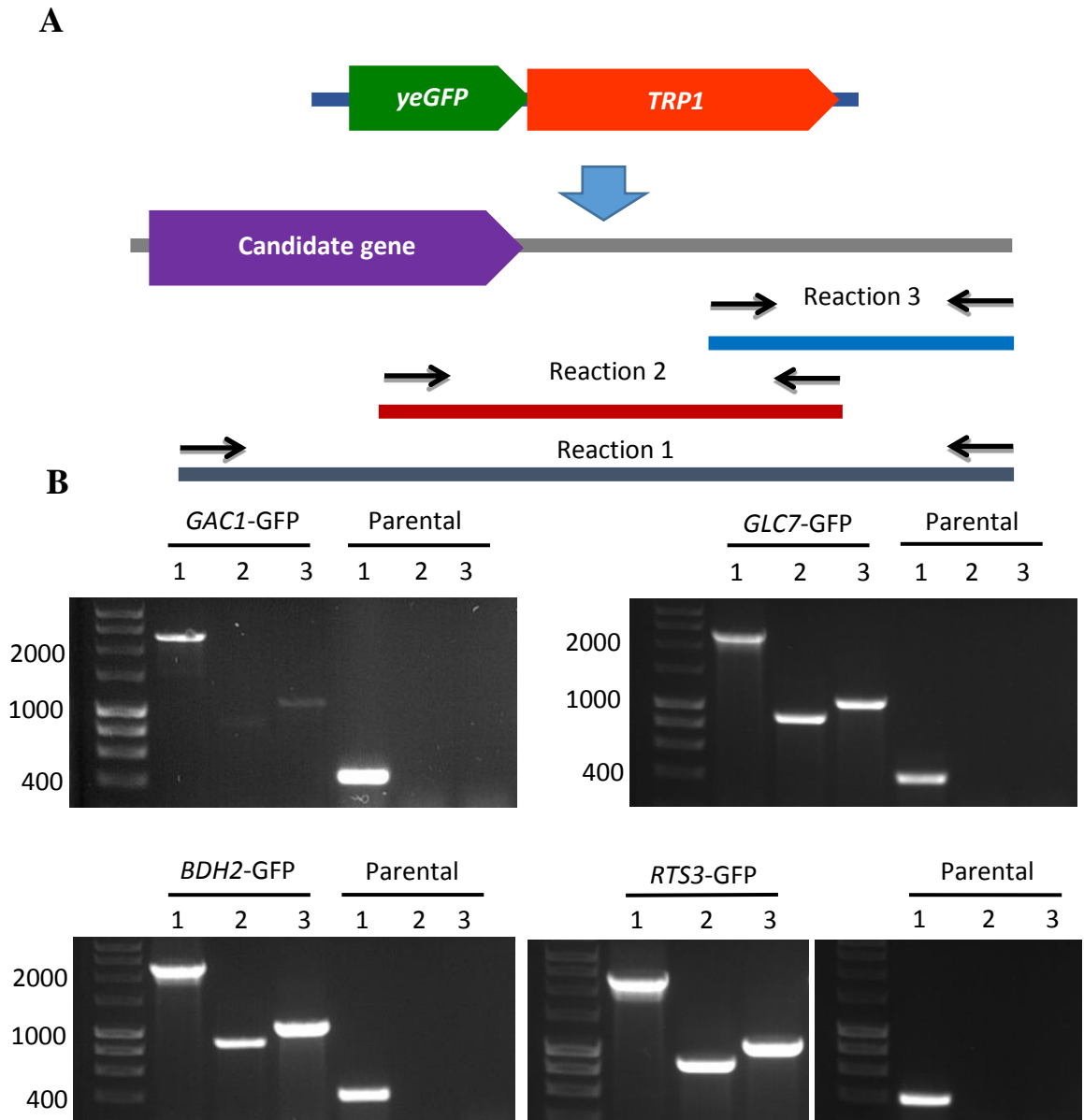


**Figure 7.1. General strategy for the construction of potential butanol-responding biosensor strains and verification of c-terminal GFP integration.** A) Schematic representation of the c-terminal integration of GFP into the selected candidate gene loci and the verification strategy assessing the PCR products 1, 2 and 3 for each gene. B) Images of 1% w/v agarose gels displaying the PCR verification of the C-terminal insertion of GFP in the locus of *GAC1*, *GLC7*, *BDH2* and *RTS3* in a W303 haploid strain. For each gel 1kb HyperLadder DNA markers are shown (left lane) and key marker sizes are labelled in bp.

(Janke et al., 2004) using the designed oligonucleotide pairs listed in Table 6.3 to generate a cassette carrying the GFP tag and the downstream *TRP1* marker gene. A W303-1A derived strain (yMK467) where the *ade2-1* marker has been rescued to give *ADE2*, such that the resulting strain has significantly reduced autofluorescence was used in the study (Zenklusen et al., 2016; Weisman et al., 1987). Cells were transformed with each insertion cassette and transformants were selected on media lacking tryptophan. Correct c-terminal tagging of each candidate gene was then verified by preparing genomic DNA from potential transformants and using a set of three diagnostic PCR reactions directed towards the c-terminal region of each gene, and the internal *TRP1* gene of the integration cassette (Figure 7.1 A). The oligonucleotides used for each of the three verification reactions and the expected products for a successful integration are summarised in Table 7.2. Products of 2280, 850, and 1000 bp were obtained in each of the reactions (Figure 7.1 B).

**Table 3.7. Oligonucleotides used for the verification of GFP tagging of candidate genes**

Reaction	Oligonucleotides used	Expected band size (bp)
1	GC*VF + CG VR	2280
2	CG VF + TRP1 VR	850
3	TRP1 VF + CG VR	1000

\*GG corresponds to the oligonucleotides specific to each target gene: *GAC1*, *GLC7*, *BDH2*, and *RTS3*.

Agarose gel electrophoresis of the PCR products from each verification reaction indicates that the GFP cassette was appropriately integrated at the *GAC1*, *GLC7*, *BDH2*, and *RTS3* loci, as evidenced by the amplification. Reaction 1 was the only reaction that

yielded a product for the parental strain, as the primers for reaction 2 and 3 were directed to the inserted sequence. For the parental strain product 1 is significantly smaller than the product obtained for the test strains: a small band of approximately 400 bp was obtained as opposed to a band of ~2.3kb (Figure 7.1 B).

Thus, four potential GFP biosensor strains have been constructed from genes that are upregulated under butanol stress. As a brief test of the presence of GFP and the ability of each biosensor strain to respond to butanol, cells growing in exponential phase in SCD media were stressed with 1% v/v 1-butanol for 1 and 4 hours to test for induction of the target gene-GFP fusion proteins. Observation of the biosensor strains by fluorescent microscopy revealed that the *GAC1-GFP* and *BDH2-GFP* biosensors strains displayed little to no fluorescence under any of the conditions, while the *GLC7-GFP* and *RTS3-GFP* strains showed evidence of fluorescence (Figure 7.2, figure 7.3). The *GLC7-GFP* cells exhibit clear fluorescence particularly in the nucleus and at the incipient bud sites (Cannon, 2010), however little evidence for butanol-dependent induction was found. In contrast, the *RTS3-GFP* strain only showed evidence of fluorescence after butanol stress making this a promising candidate as a butanol sensor strain however, further experiments will be required in order to verify the effectiveness of all of the strains at responding to the presence of 1-butanol in the cell.

#### **7.4 Qualitative assessment of GFP fluorescence using a biomolecular imager**

A simple method that can be adapted to detect GFP fluorescence in yeast colonies grown on solid media is the use of a UV transilluminator or a similar scanning device to excite and detect fluorescence. This method has been used by many researchers, to accurately quantify GFP in polyacrylamide gels (Few et al., 2009), and to visualise GFP-expressing microorganisms grown on agar plates (Feilmeier et al., 2000; Tresse et al.,

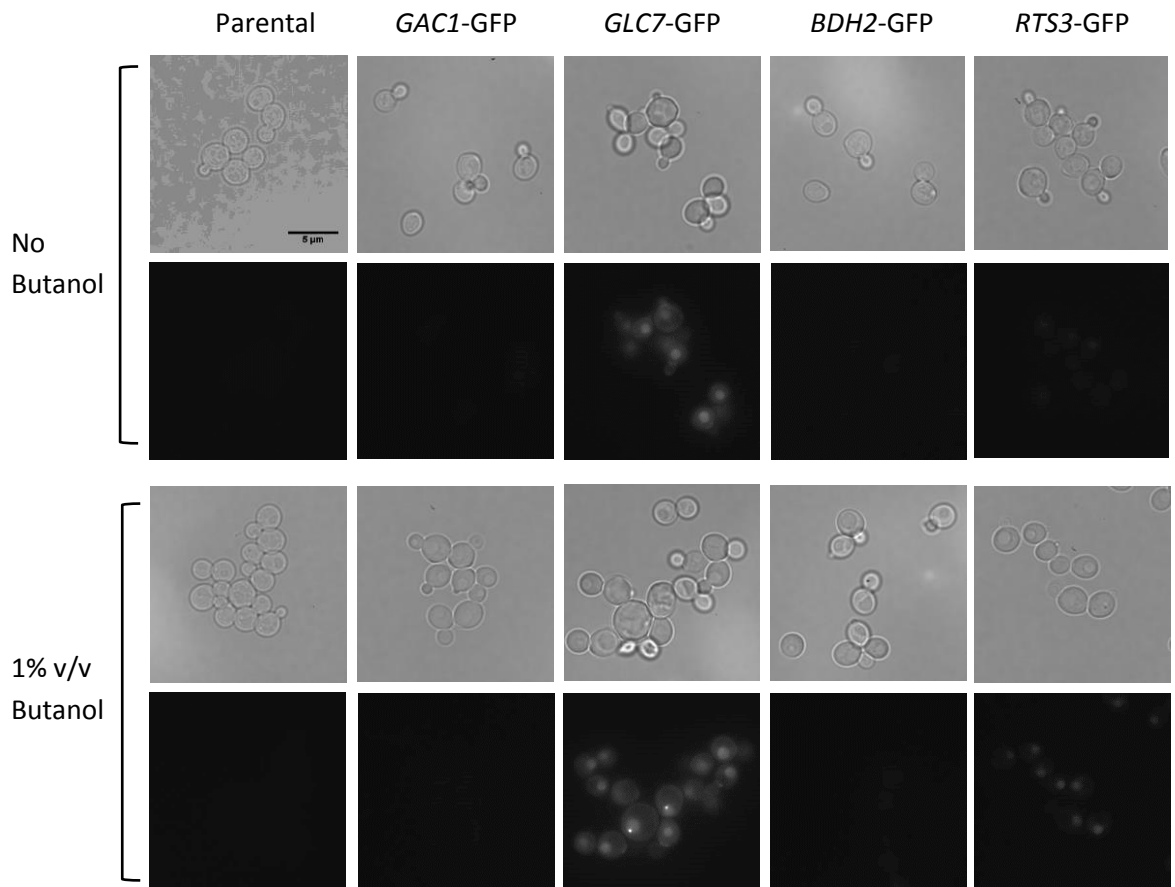


**Figure 7.2. Detection of the presence of GFP fusion proteins in living cells by fluorescence microscopy after a 1-hour 1-butanol stress.** Fluorescent microscopy of the verified biosensor yeast strains grown to exponential phase in SCD media, and treated with 1% (v/v) 1-butanol for 1 hour. Magnification is 100x and scale bar is 5  $\mu$ m in length.

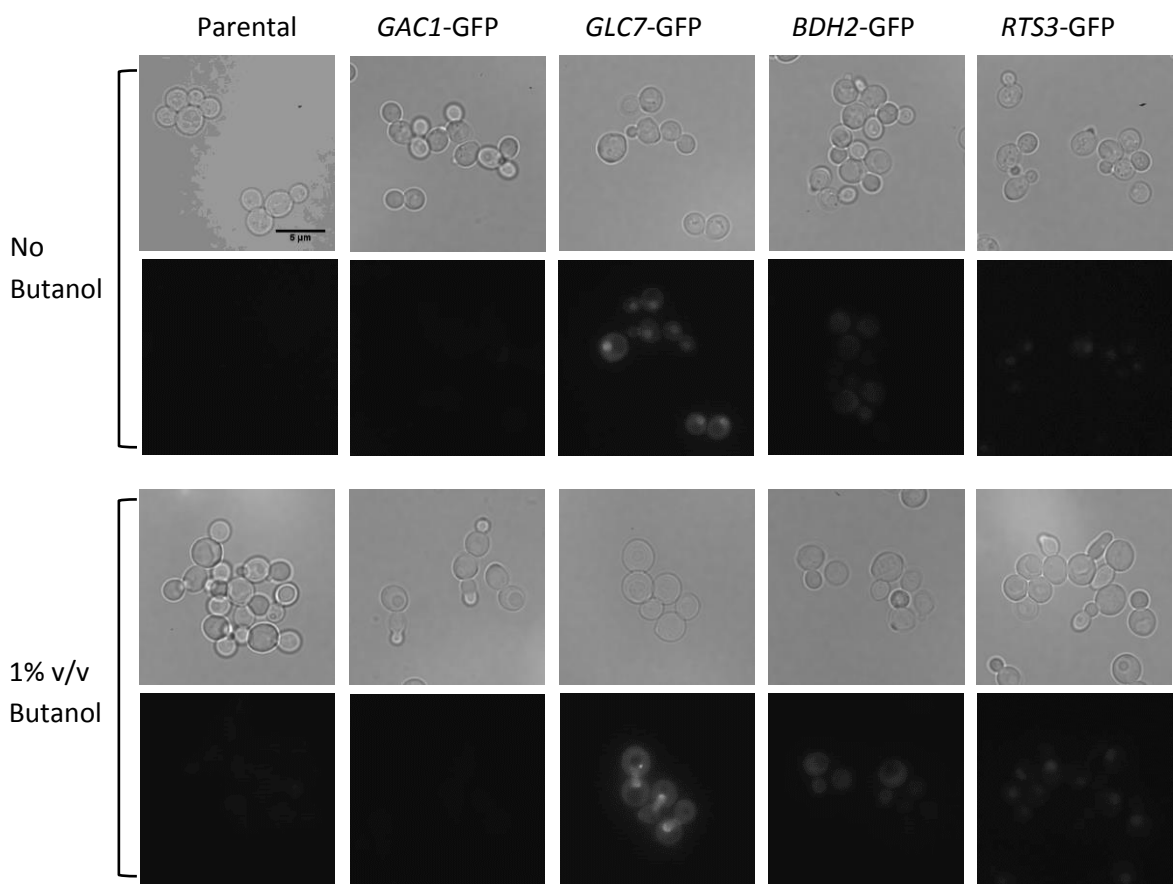


**Figure 7.3. Detection of the presence of GFP fusion proteins in living cells by fluorescence microscopy after a 4-hour 1-butanol stress.** Fluorescent microscopy of the verified biosensor strains grown to exponential phase in SCD media, and treated with 1% (v/v) 1-butanol for 4 hours. Magnification is 100x and scale bar is 5  $\mu\text{m}$  in length.

1998; Siemerling et al., 1996). Because the agar plate format and the speed of the assay facilitate the testing of multiple biosensor strains, it could eventually be used as a qualitative screening method for butanol-producing strains. Thus, fluorescence from the constructed biosensor strains will be measured using a qualitative agar plate assay.

Cells were prepared by making serial dilutions from liquid cultures of each of the four potential butanol biosensor strains (*GAC1*-GFP, *GLC7*-GFP, *BDH2*-GFP, *RTS3*-GFP), and the parent strain growing in logarithmic phase. Each dilution was then spotted onto two SCD agar plates, one of which was supplemented with 1% v/v 1-butanol, and the plates were scanned to monitor colony growth, and scanned with a 520 nm laser to visualise GFP fluorescence.

All of the potential biosensor strains exhibited more fluorescence than the parental strain, while no biosensor strain in particular stood out as more fluorescent (Figure 7.4). Fluorescence intensity seems at its highest on day 3 of growth on the SCD plate, while biosensor strains on the 1% 1-butanol plate do not exhibit fluorescence over the signal of the parental strain. This result is at odds with the previously examined fluorescent microscopy data, which showed that *GLC7*-GFP had a more intense fluorescent pattern than the other biosensor strains (Figures 7.2 and 7.3).

It is also interesting to note that all of the biosensor strains were more sensitive to 1-butanol stress than the parental strain. The four potential butanol biosensor genes were selected because their expression was induced under acute butanol stress. This implies that the corresponding gene products probably have a role in the stress response to this fusel alcohol. The introduction of a GFP fusion to these genes always carries the risk of interfering with their ability to interact with other proteins, an important property of

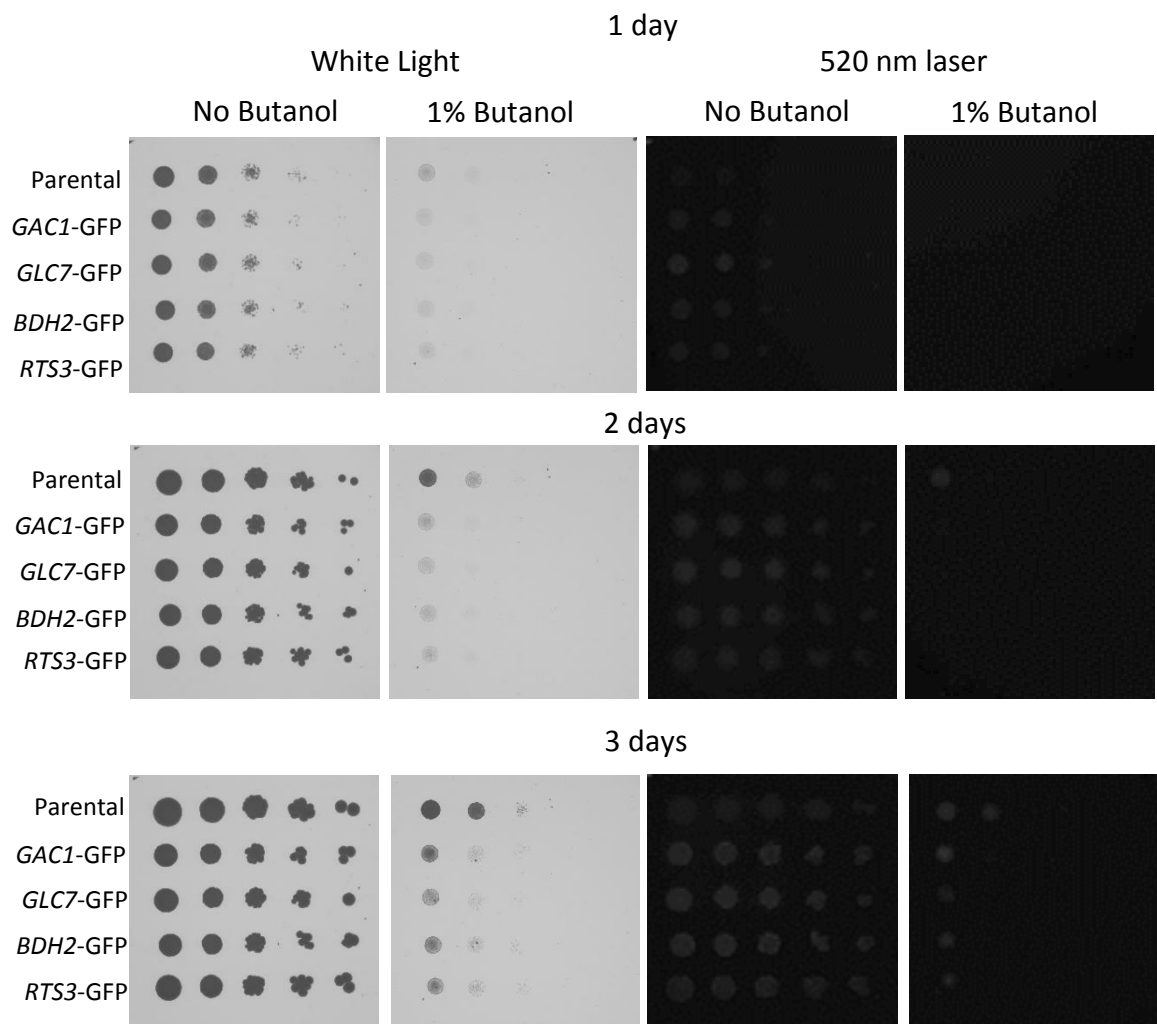


**Figure 7.4. Detection of the fluorescent response of the potential biosensor strains in solid media under 1% butanol stress.** Strains growing in logarithmic phase were spotted as 1:10 serial dilutions in solid SCD and solid SCD supplemented with 1% v/v 1-butanol. On days 1, 2, and 3 after cells were spotted, plates were scanned and photographed under a 520 nm laser using a Sapphire Biomolecular Imager (Azure biosystems).

*GAC1* and *GLC7*, two proteins that together function as a type-1 protein phosphatase (Williams-Hart et al., 2002).

Together, these results suggest that the biosensor strains are not able to respond with increased fluorescence to 1-butanol stress in the agar plate assay. This could be due to an effective inability of the strains to induce and maintain expression of the fluorescent fusion proteins, or due to the limitations of the assay. Additional experiments will be required to produce more precise measurements of the intensity of the biosensor strains' fluorescence response to 1-butanol stress.

### **7.5 Microplate assay for quantifying GFP fluorescence in biosensor strains**

The use of a microplate reader to measure fluorescence from a reporter in living cells is a method that has been used by researchers to obtain information about the degree of expression of a biosensor when exposed to its target analyte (Shi et al., 2017; Bui et al., 2016; Bermejo et al., 2011). The main advantage of using this method instead of colony-based screening is a more precise detection of fluorescence emitted by the biosensors, with the potential to discern between different titers of intracellular butanol, depending on the dynamic range of the biosensor. On the other hand, a colony-based assay has much higher throughput than a microplate assay.

After considering the above advantages and disadvantages, it was decided that the next step in evaluating their ability to respond to 1-butanol was to set up a quantitative microplate assay.

### **7.6 Time-course fluorescence in the *GLC7*-GFP biosensor strain**

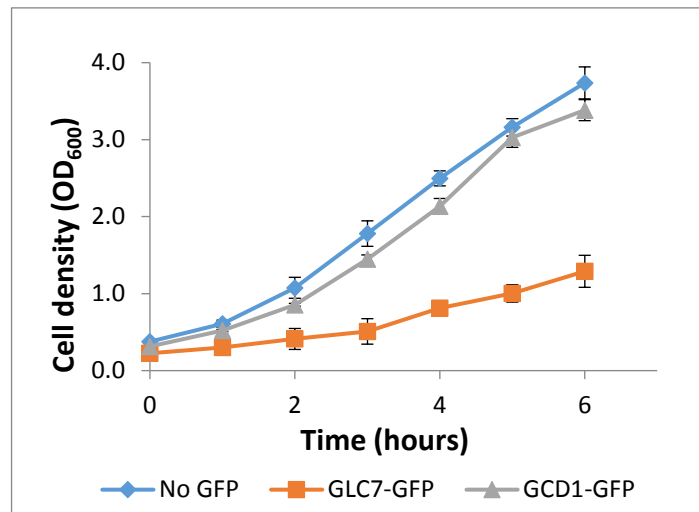
An initial experiment was conducted to test the fluorescence levels over a time-course using growing cells with the goal of finding optimal cell numbers and growth points for

future experiments. The *GLC7*-GFP strain was used in this experiment since this strain appeared to give the most intense fluorescence in previous analyses. Additionally, a *GCD1*-GFP strain was included as a positive control for GFP activity: GFP-tagged Gcd1p localises to a defined cytosolic body that has been termed the eIF2B body or 2B body (Campbell et al., 2005). The W303-1A parent strain was used as a negative control that lacks GFP.

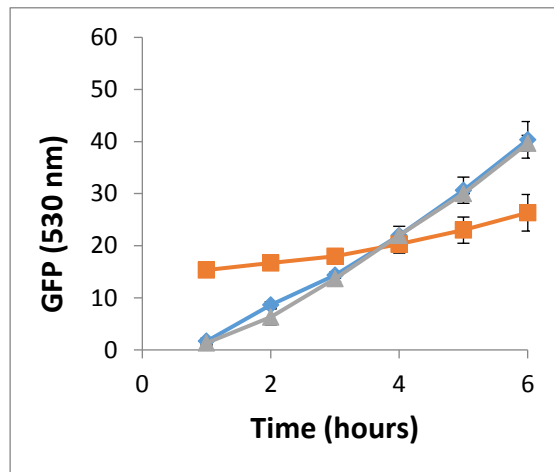
100  $\mu$ l from liquid SCD cultures grown to exponential phase was sampled every hour over 6 hours to assess fluorescence at 530 nm. Simultaneously, 1 ml samples were taken to measure cell density by spectrophotometry. From the analysis, there appears little evidence for any specific fluorescence in the GFP-tagged strains relative to the background parent strain (Figure 7.5 B). Even for the positive control, fluorescence above background was only evident when the cell density was taken into account (Figure 7.5 C). The high fluorescence values observed for the negative control could mean that metabolites are produced that emit fluorescence in the GFP range and populate the media increasing as yeast proliferate. Indeed, previous studies have shown that riboflavin shares a similar excitation/ emission profile to GFP (Demuyser et al., 2020; Maslanka et al., 2018; Marx et al., 2008)

If the accumulation of such metabolites explains the fluorescence increase over time for the parent strain then it is possible that measuring fluorescence at earlier points in exponential growth will result in more specific fluorescent signal from the GFP-tagged protein. However in this case, cells will need to be concentrated to allow sufficient signal to be obtained.

A



B



C

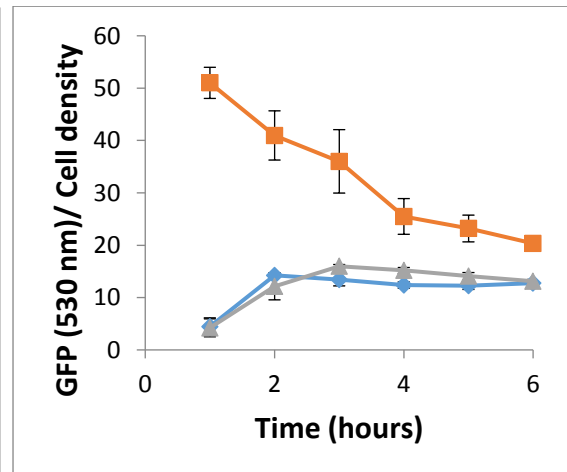


**Figure 7.5. Time-course measurement of fluorescence in the *GLC7-GFP* biosensor strain relative to controls.** A) Growth curve of the *GLC7-GFP* strain, a *GCD1-GFP* strain, and the W303-1A parental strain grown in liquid SCD. Cell density was measured as absorbance at 600 nm. B) Time-course measurement of GFP fluorescence of the same cell cultures. Excitation and emission wavelengths were 485 nm and 530 nm, respectively. C) Ratio of GFP fluorescence over cell density for the time-course experiment. In all three plots, points correspond to mean ( $\pm$ SD) of three biological replicates.

### 7.6.1 Evaluation of fluorescence from set concentrations of biosensor strains

As described above, early preliminary attempts at using the microplate reader to detect fluorescence from living cells showed little evidence of increased fluorescence relative to negative control strains (Figure 7.5). One possible strategy that can be employed to increase the signal is to concentrate the cells to a predetermined density before measuring fluorescence. This method might ensure that sufficient cells are present to give a signal over background, especially at early points of a culture's growth before potential fluorescent metabolites accumulate.

To prepare the samples, 10 ml aliquots of SCD cultures were collected from *GAC1-GFP*, *GLC7-GFP*, *BDH2-GFP*, *RTS3-GFP* and control strains grown to early exponential phase. The cell density for each culture was determined, then cells were pelleted and a volume of supernatant was removed such that after resuspension final cell densities of 5.0, 10.0, and 20.0 OD<sub>600</sub>/ml were obtained. Finally, the fluorescence at 530 nm for 100 µl of each sample was measured in the microplate reader.

Overall, evidence was obtained that the plate reader assay was able to detect fluorescence over and above that obtained for the non-GFP control strain (Figure 7.6). The only strain where robust signal was obtained at each cell concentration was the *GLC7-GFP* strain. For the other strains, while the mean fluorescence was always higher in the GFP-tagged strain than the parent, this only reached statistical significance at certain concentrations.

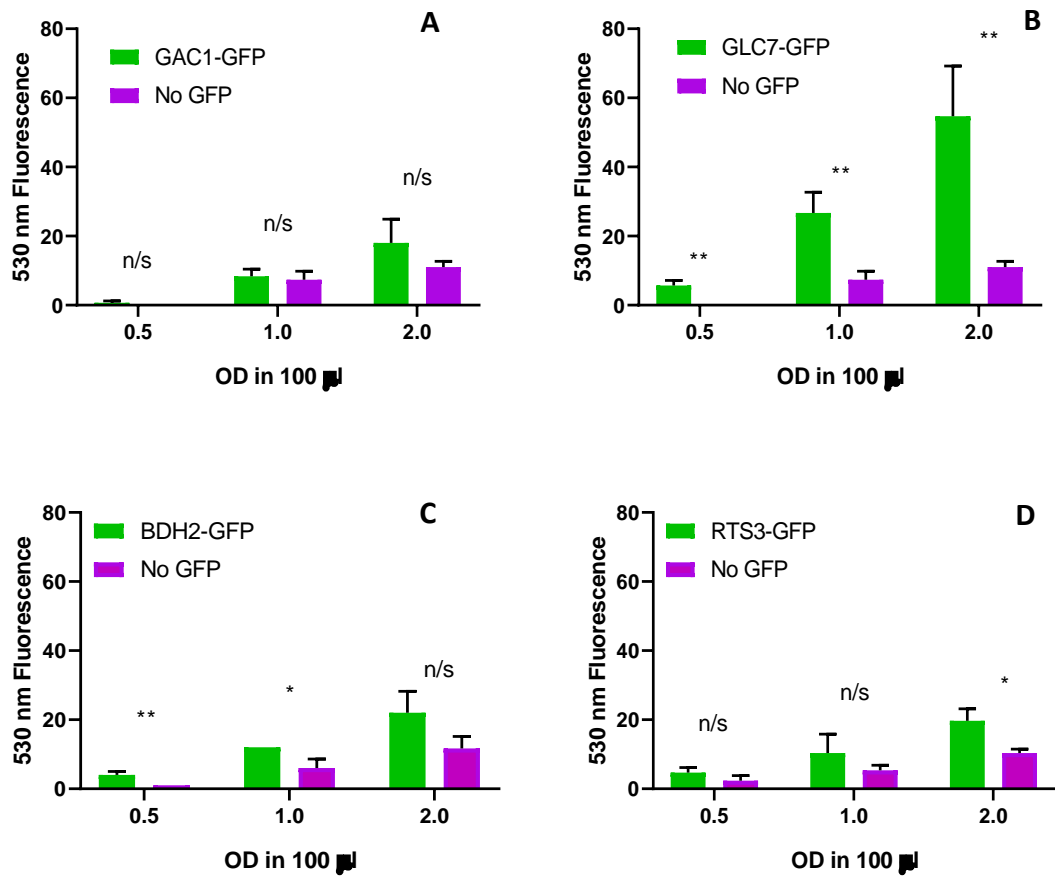


**Figure 7.6. Concentrating cells to overcome background strain fluorescence in the fluorescence microplate assay.** Fluorescence at 530 nm for early exponential cultures of A) *GAC1-GFP*, B) *GLC7-GFP*, C) *BDH2-GFP*, and D) *RTS3-GFP* biosensor strains compared to a parent strain. Cell cultures were concentrated by centrifuging to obtain final concentrations of 0.5, 1.0, and 2.0 OD<sub>600</sub>/100 µl. The mean ( $\pm$ SD) is plotted for three biological replicates. An unpaired t-test was used to calculate statistical significance, where n/s indicates no significance, \* indicates a p-value < 0.05, and \*\* indicates a p-value < 0.01.

These results for the *GLC7-GFP* strain correlate well with the previous qualitative assessments of this strain's high fluorescence (Figures 7.2 and 7.3). In addition, by using cell densities of over 1.0 increases in fluorescence over background could be detected for most of the potential biosensor strains with the exception of *GAC1-GFP*. This again correlates well with the qualitative assays where little evidence for Gac1-GFP expression was found (Figures 7.2 and 7.3).

Overall, these data suggest that concentrating cells can be used as a strategy to overcome background problems associated with yeast cell or media autofluorescence in a plate reader assay.

#### **7.6.2 Fluorescence intensity of biosensor strains does not increase when exposed to 1-butanol for 4 hours**

Considering the above results, it was decided that concentrating early exponential cultures to an  $OD_{600}$  of 1.0 would likely allow any increases in fluorescence upon addition of butanol to the cultures to be readily detected. Biosensor strain cultures were therefore prepared as above, except they were split into two flasks, one of which was treated with 1-butanol to a 1% v/v final concentration and the other left untreated. After 4 hours at 30°C, 10 ml aliquots were collected to measure fluorescence from each biosensor strain in the microplate reader. The 4-hour time point was used since previous 'omics data for these GFP-tagged target genes suggested that both their transcription and translation would be induced by short term (10 min) butanol treatment and a more protracted time would give time for GFP maturation (Balleza et al., 2018; Shashkova et al., 2018; Iizuka et al., 2011).

In keeping with previous results (Figures 7.2, 7.3, 7.4 and 7.5), the *GLC7-GFP* strain was the only strain where significant fluorescence was observed above that observed for the parental non-GFP strain. Exposure of this strain to 1-butanol, however, did not cause a significant increase in the measured fluorescence (Figure 7.7). Equally, the addition of 1-butanol did not induce significant levels of fluorescence for the other three GFP- tagged strains leading to the conclusion that the potential biosensors were unable to respond to a 4-hour 1% v/v butanol stimulus.

### **7.7 Western Blot reveals strong expression of the Glc7p-GFP fusion protein**

A key question that must be addressed given the lack of response observed above for the potential biosensor strains is whether the fluorescent fusion proteins are even expressed in the tagged strains. In order to assess the expression level of the fusion proteins, a western blot analysis was conducted for each of the biosensor strains, as well as for the parental non-GFP strain and the *GCD1-GFP* strain. Whole cell protein extracts were prepared from early exponential cells: either untreated or after exposure to 1% 1-butanol for 4 hours. The protein samples were separated by SDS-PAGE electrophoresis and transferred to a nitrocellulose membrane before immunoblotting with an anti-GFP antibody (Table 6.4).

The Western Blot revealed a pattern of expression that correlated well with previous results, as among all biosensor strains, only the Glc7p-GFP fusion protein was robustly detected by the antibodies in both the treated and untreated extracts (Figure 7.8). The position of the Glc7p-GFP protein band approximates to the expected protein size, (Table 7.3). The rest of the biosensor protein bands are faint, implying minimal presence of each fusion protein.

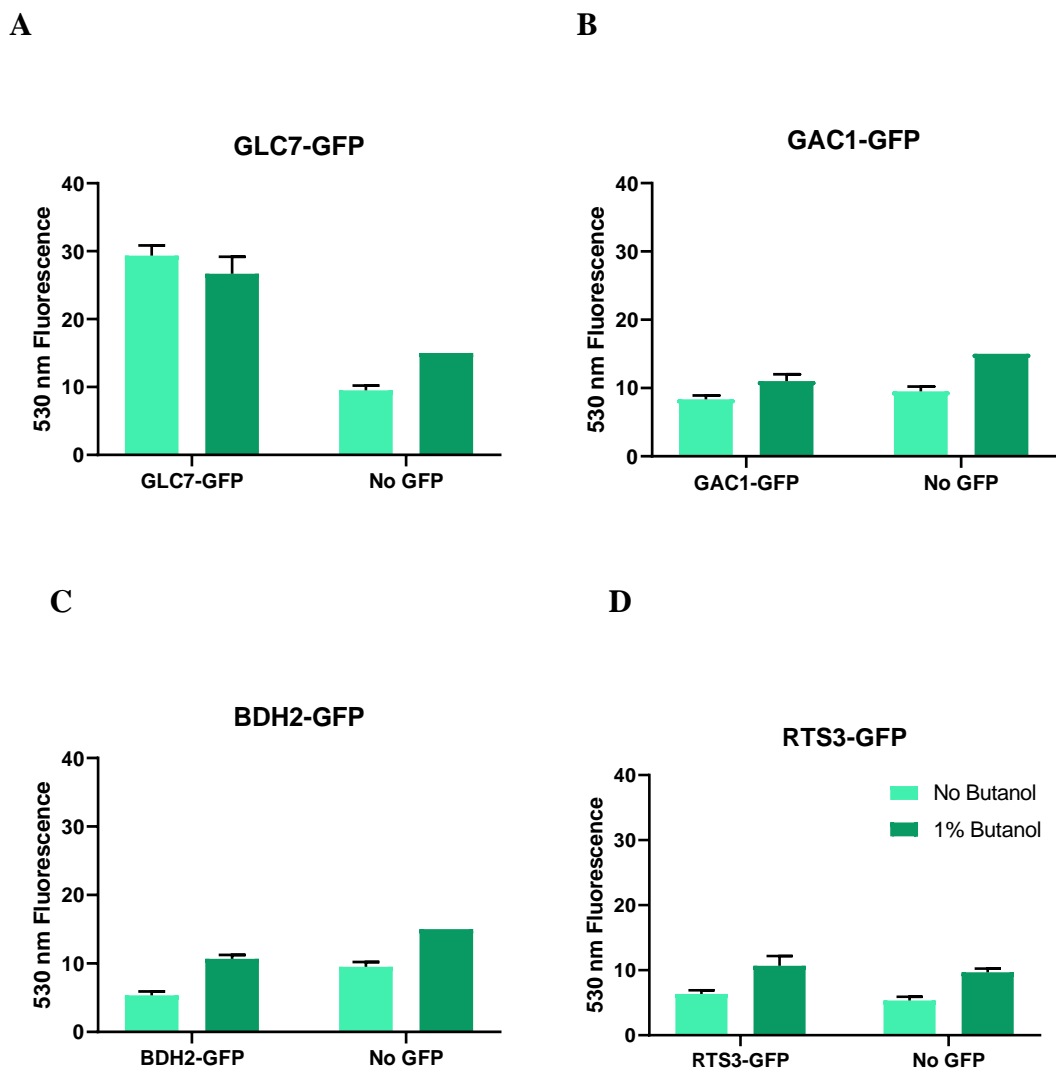


**Figure 7.7. Fluorescence of biosensor strains after a 4-hour 1% butanol stress.** Fluorescence at 530 nm of biosensor strains A) *GAC1-GFP*, B) *GLC7-GFP*, C) *BDH2-GFP*, and D) *RTS3-GFP* after 4 hours of exposure to 1% v/v 1-butanol in liquid YPD culture. Mean values ( $\pm$ SD) are plotted from three biological replicates.

**Table 7.3. Expected size of GFP fusion proteins and loading control used in Western Blot**

Protein	Weight (kDa)
Gcd1p-GFP	92
Gac1p-GFP	116
Glc7p-GFP	63
Bdh2p-GFP	73
Rts3p-GFP	56
Nrp1-GFP	106
Shq1p-GFP	86
Pgk1p	45

The results obtained in this protein detection experiment fall in line with previous results, and together they imply that the lack of fluorescence detected in the biosensor strains using the UV-based assay and the microplate assay may simply reflect poor expression for the fusion proteins.

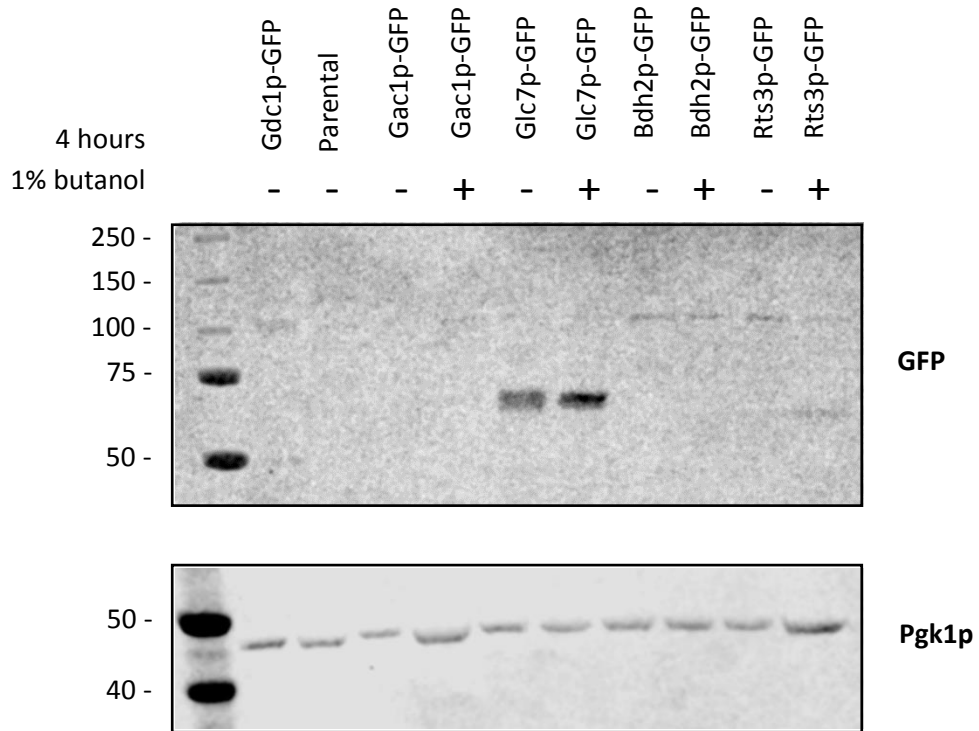


**Figure 7.8. Evaluation of GFP fusion protein expression in the constructed biosensor strains.** Western blot using protein extracts prepared from cells either exposed to 1% v/v or no 1-butanol for 4 hours prior to harvesting. Blots were probed with anti-GFP antibodies to evaluate GFP fusion protein levels in each of the biosensor strains, their parental strain, and a *GCDI*-GFP positive control strain (upper panel). An anti-Pgk1p antibody was used to generate a loading control (lower panel). Numbered dashes on the left correspond to molecular weight marker sizes in kiloDaltons.

## 7.8 Construction of *SHQ1* and *NRP1* GFP biosensor strains

Previous work has evaluated *SHQ1* and *NRP1* gene promoters driving mCherry from plasmids as potential 1-butanol biosensors (Shi et al., 2017). Using these constructs, a doubling in fluorescence was observed after 20 hours of exposure to 1-butanol (Shi et al., 2017). The initial evaluation of these biosensors suggested that they may not be suitable for a colony-based assay such as that envisaged at the outset of this program of work, since the increase in fluorescence is minor and occurs over a protracted period. However, given that the potential biosensors designed above failed to deliver a significant increase in fluorescence, a decision was made to generate strains using the *SHQ1* and *NRP1* genes as a fallback option.

Therefore, the *NRP1* and *SHQ1* genes were tagged with GFP to test their performance as 1-butanol biosensors in our yeast strain. The GFP tagging cassette amplification, strain transformation, and GFP insertion verification by PCR was done in the same manner as with the previous biosensor strains (Section 7.2) using the appropriate oligonucleotides listed in Table 6.3. The three verification reactions yielded the expected DNA products of approximately 2280, 850, and 1000 bp, for both the *NRP1-GFP* and *SHQ1-GFP* transformants, indicating that insertion of the fluorescent protein gene was successful (Figure 7.9 A).

In order to streamline verification experiments and the following fluorescence measurement experiments, expression of the Nrp1p-GFP and Shq1p-GFP fusion proteins in the presence or absence of 1% 1-butanol was first assessed by western blotting using the procedure described in Section 3.5. The Shq1p-GFP protein was found to be present both in the presence or absence of 1% v/v 1-butanol, as evidenced by the band around the expected

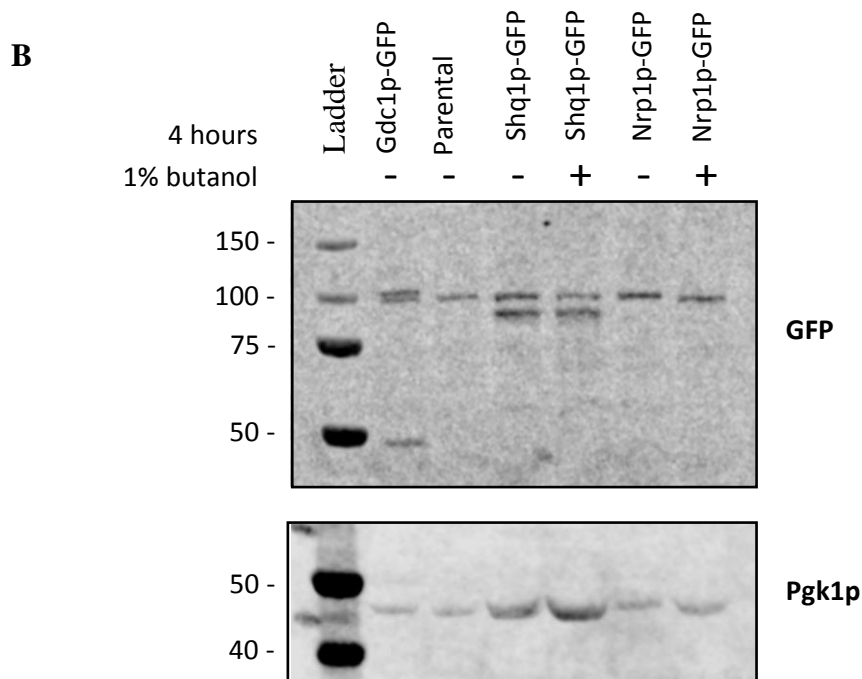
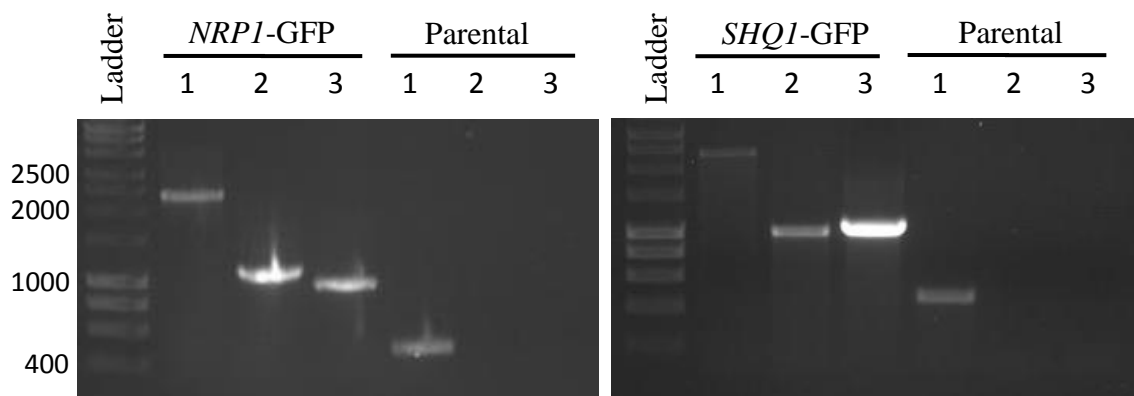


**Figure 7.9 Verification of GFP tagging of *NRPI* and *SHQ1* genes and expression of fusion protein.** A) 1% w/v agarose gel shows the products of the three PCR for the verification of the c-terminal tagging of *NRPI* and *SHQ1* with GFP in a W303-1A *ADE2* haploid strain. Ladder used was HyperLadder 1kb (Bioline). B) Western blot shows expression of the GFP fusion proteins in both biosensor strains. Cells were exposed to 1% or no 1-butanol for 4 hours before harvesting the extracts. Pgk1p was used as the loading control for the experiment. Numbered bands correspond to the Spectra Multicolor Broad Range protein ladder (ThermoFisher Scientific).

86 kDa size (Figure 7.9 B). On the other hand, the Nrp1p-GFP protein was not easy to distinguish, since its expected size of 106 kDa overlaps with a non-specific band (Figure 7.9 B), that was also present on the previous Western Blot (Figure 7.8).

This means that it is difficult to confirm that Nrp1p-GFP fusion protein is expressed in this experiment. Given more time, a different source of anti-GFP antibody could have been used to find a reagent that does not generate non-specific bands in the 100kDa range.

### **7.9 The *SHQ1* and *NRP1* biosensor strains had no changes in fluorescence after 1-butanol stress**

The newly generated *SHQ1-GFP* and *NRP1-GFP* strains were tested for their ability to fluoresce under 1 and 4 hours of 1% butanol stress by fluorescent microscopy, in the same manner described for the rest of the constructed strains (Figure 7.2). The fluorescent microscopy pictures revealed that none of the strains were able to produce fluorescence under any of the tested conditions (Figure 7.10), suggesting that they might not be properly responding to 1-butanol stress.

A qualitative agar plate assay was set up as described previously (Section 7.4). This revealed that both the *NRP1-GFP* and *SHQ1-GFP* biosensor strains exhibit minimal fluorescence when compared to the non-fluorescent parental strain over the course of the experiment, whether in the presence or absence of 1-butanol (Figure 7.11).

Curiously, this assay also showed that the *SHQ1-GFP* biosensor strain was sensitive to 1-butanol stress, as evidenced by the lack of growth of each spot. *SHQ1* is an essential gene that encodes a chaperone protein required for the assembly and stability of H/ACA ribonucleoproteins, complexes involved in the pseudouridylation of ribosomal RNA and

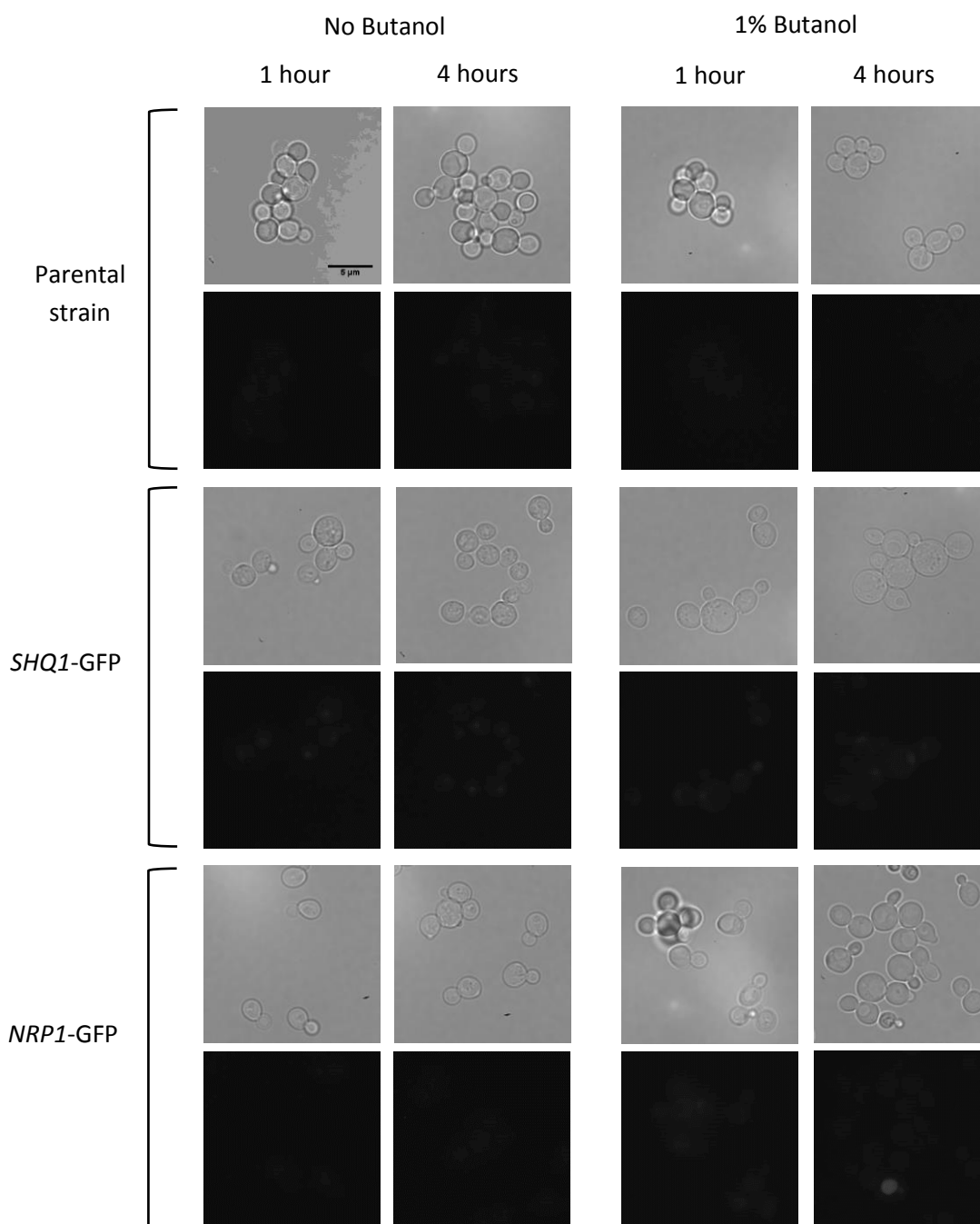


**Figure 7.10. Detection of the presence of Nrp1p-GFP and Shq1p-GFP fusion proteins in living cells by fluorescence microscopy.** Fluorescent microscopy of the verified biosensor strains treated with 1% (v/v) 1-butanol for 1 hour. Excitation and emission wavelengths used were 470 nm and 525 nm, respectively. Magnification is 100x and scale bar is 5  $\mu$ m in length.

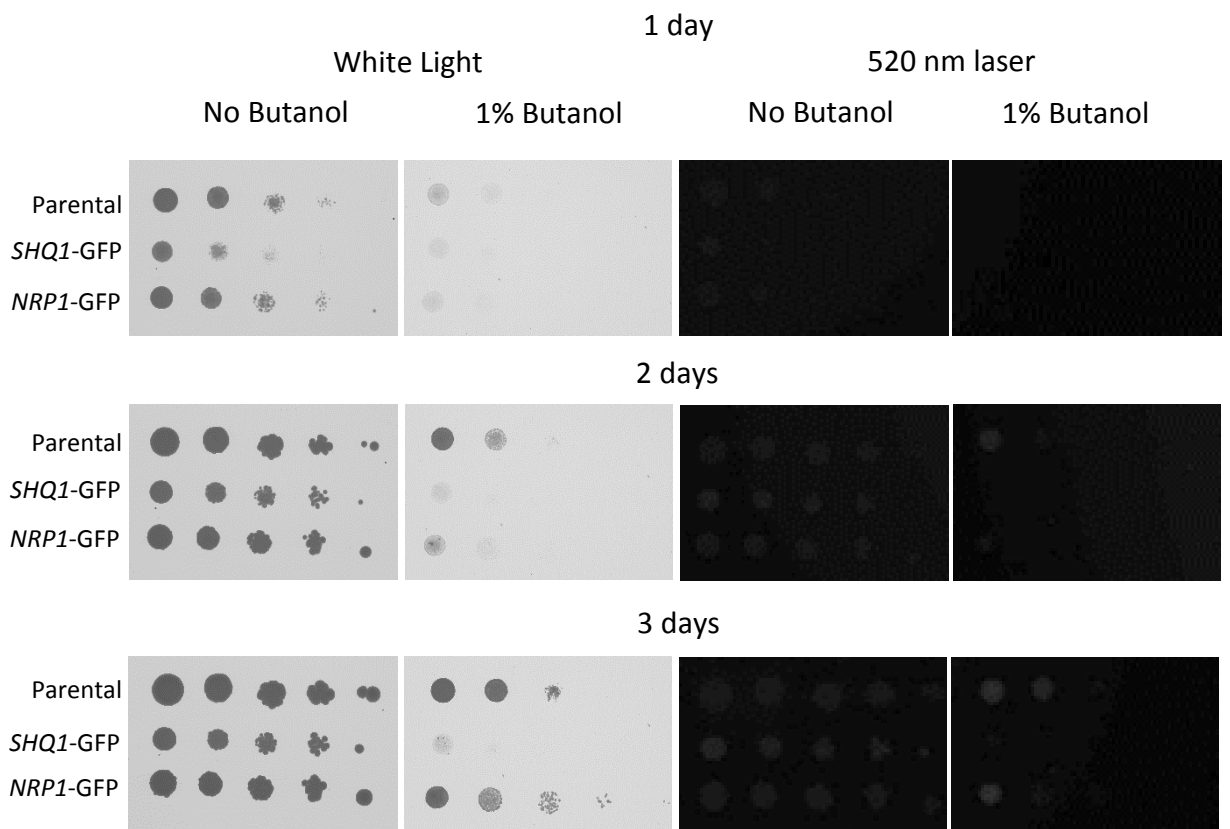


**Figure 7.11. Detection of the fluorescent response of the *NRP1* and *SHQ1* biosensor strains in solid media under 1% butanol stress.** Strains growing in logarithmic phase were spotted as 1:10 serial dilutions in solid SCD and solid SCD supplemented with 1% v/v 1-butanol. On days 1, 2, and 3 after cells were spotted, plates were scanned and photographed under a 520 nm laser using a Sapphire Biomolecular Imager (Azure biosystems).

small nuclear RNA (Kiss et al., 2010; Grozdanov et al., 2009). Perhaps the c-terminal fusion of GFP to Shq1p results in impaired chaperone function, ultimately affecting the adequate assembly of ribosomes and reducing cellular fitness.

In order to obtain a more precise measurement of the fluorescent response of the *SHQ1-GFP* and *NRP1-GFP* strains to 1-butanol stress, a 4-hour 1% v/v butanol stress was assessed using the plate assay described in Section 7.4 above. Frustratingly, neither strain produced fluorescence at 530 nm above that measured for the non-tagged strain (Figures 7.12 A and B). This set of experiments demonstrate that despite the successful integration of GFP to the *SHQ1* and *NRP1* loci, and the western blot revealing an appropriately sized band when an anti-GFP antibody was used (at least for Shq1p), no significant fluorescent signal was produced by either strain in any of the tested conditions using a plate reader assay.

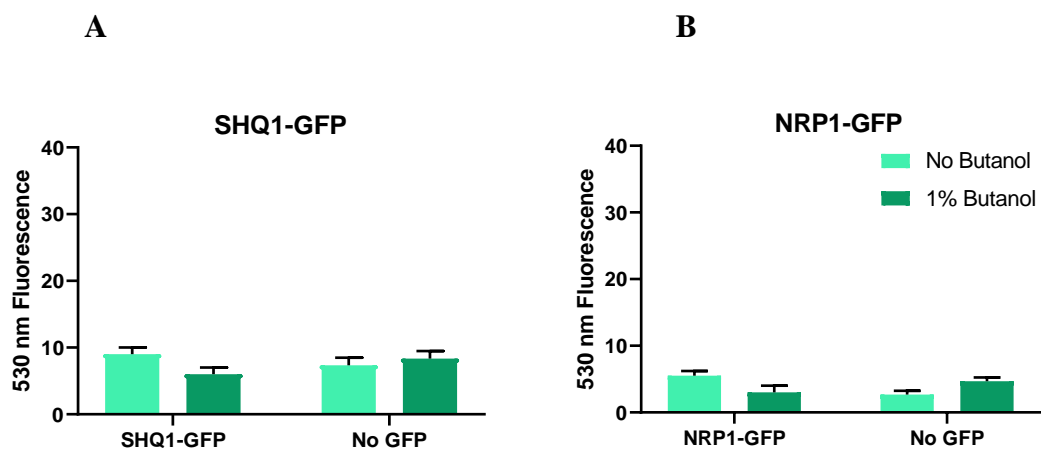


**Figure 7.12. The *SHQ1* and *NRP1* biosensors do not increase in fluorescence after 1% butanol treatment.** Fluorescence at 530 nm of biosensor strains A) *SHQ1*-GFP, and B) *NRP1*-GFP after 4 hours of exposure to 1% v/v 1-butanol in liquid YPD culture. Bars correspond to mean ( $\pm$ SD) of three biological replicates.

## 7.10 Discussion

The aim of this set of experiments was to develop biosensors able to respond to different concentrations of 1-butanol in *S. cerevisiae* to aid in the identification of better butanol-producing strains. To achieve this, potential biosensor strains were constructed by introducing GFP at the C-terminal location of six genes reported to be upregulated under 1-butanol stress: *GAC1*, *GLC7*, *BDH2*, *RTS3*, *SHQ1*, and *NRP1* (Smirnova et al., 2005; Shi et al., 2017). Fluorescence of the biosensor strains in response to 1% v/v 1-butanol stress was evaluated using qualitative and quantitative assays, and fusion protein expression was detected by immunoblotting.

Overall, the experiments showed that there was no significant increase in fluorescence for any of the tested biosensor strains when exposed to 1% v/v 1-butanol. While the Glc7p-GFP biosensor strain showed about three times the fluorescence of the other biosensor strains in all the tested conditions, it was not able to respond to the 1% v/v 1-butanol stress applied in the qualitative and quantitative assays, thus rendering it unusable for future 1-butanol-sensing assays. Glc7p's high stability (Nigavekar et al., 2002) and key role as the only PP1 phosphatase in *S. cerevisiae* (Cannon, 2010) correlate well with the high and sustained fluorescence levels observed in the *GLC7*-GFP biosensor strain in both qualitative and quantitative assays, further supporting the idea that this protein was not an adequate candidate for the regulatory element of a 1-butanol biosensor.

Immunoblot analysis of protein extracts of each of the biosensor strains subjected to a 4-hour 1-butanol stress reflected the same pattern observed in the microplate assays, indicating that the low fluorescence and inability to respond 1-butanol stress seen in the strains is likely due to a failure to induce and sustain increased protein expression.

The *GAC1*, *GLC7*, *BDH2*, and *RTS3* genes were selected from a list of transcriptionally and translationally upregulated genes after 1% v/v 1-butanol stress from a study published by our laboratory (Smirnova et al., 2005). The goal of that study was to identify transcripts that are maintained with actively translating ribosomes after short-term exposure to 1-butanol and amino acid starvation, two stresses known to globally inhibit translation. Because the study focused on short-term stresses, there is the possibility that the expression changes observed after the 10-minute stress period are not sustained for longer periods, such as the 4 hours used in the microplate assay, and 24 to 72 hours in the agar plate assay. Since 1-butanol begins to accumulate on day 2 of anaerobic fermentations, and peak concentrations can be estimated around day nine (see Figure 8.7), it is highly important to make sure that the constructed biosensors are able to respond and sustain a signal during longer periods of exposure to this metabolite.

After obtaining the above results for the candidate biosensors, a new pair of GFP fusions were made using *NRP1* and *SHQ1* as butanol-responding genes. These two genes were identified in a screen for genes upregulated after a 2.5-hour 1% 1-butanol stress performed in a more recent study (Shi et al., 2017). Furthermore, the results indicated that the promoters of both genes were able to drive mCherry expression after a longer 20-hour 1-butanol stress in a dose-dependent manner. This makes *NRP1* and *SHQ1* two promising candidates for the goals of this project, although they were only found to increase two-fold (Shi et al., 2017) which may not be sufficient for colony screening.

Thus, a GFP gene tag was introduced at the C-terminal loci of *NRP1* and *SHQ1* in a W303-1A *ADE2* strain in the same manner as previously described. When fusion protein expression and GFP fluorescence of the new biosensor strains was assessed during a 4-hour 1% 1-butanol stress, the data showed no increase in the presence of the fusion proteins or in the level of fluorescence after treatment. It appears that the strains fail to

induce synthesis of the fusion proteins accounting for the lack of a fluorescent response in the plate reader assay.

This result comes as a surprise due to the promising evidence in favour of the viability of *NRPI* and *SHQI* as butanol-responding genes. One possible cause of the observed discrepancies in biosensor performance is the nature of the fluorescent construct itself. Biosensor modules are often constructed by assembling the promoter region of the chosen candidate gene(s) and the reporter element in a plasmid vector for transformation into the host cells. This was the strategy used in the previous study for the construction of the *NRPI* and *SHQI* mCherry biosensor (Shi et al., 2017), as well as in other successful yeast biosensors (Williams et al., 2017). Perhaps the use of GFP fusion proteins had an impact on target gene stability or subcellular location, hindering their ability to sustain a fluorescent response to 1-butanol. Alternatively, perhaps the use of just a fluorescent protein cassette as in previous studies leads to more consistent accumulation of protein throughout the cell and somehow this gives greater overall detectable fluorescence. In addition, the previous study used mCherry not eGFP. eGFP was used in this thesis because past experience in the laboratory as well as a range of other studies suggests that the fluorescence intensity of mCherry is weak relative to eGFP (Cranfill et al., 2016; Heppert et al., 2016). However, it is possible that in the ~610nm range where mCherry emits (Shi et al., 2017), the level of background fluorescence in yeast or yeast media is reduced making the plate reader assay a more viable option.

In order to test if the fusion protein approach and/or the fluorescent protein was the cause of the non-responsive biosensors, new constructs would have to be made by assembling the promoter region and a fluorescent protein in a plasmid vector in a similar manner to the ones reported in the literature (Shi et al., 2017). Special attention has to be given to *SHQI* and *NRPI*, as both promoters should be able to drive expression of the reporter

gene when exposed to 1% 1-butanol. Another possible approach would be to use reverse transcription quantitative real-time PCR (rt-qPCR) analysis to confirm the induction of the genes in question in response to 1-butanol at the transcript level, then the appropriate constructs could be developed subsequently.

While practical, promoter-based biosensors depend on the specificity of the genetic response to the analyte in order to function. One of the challenges of designing promoter-based biosensors for 1-butanol detection is that because the toxic effects of this molecule affect multiple cellular structures, the cellular stress response to this alcohol involves the transcription of a wide array of genes (González-Ramos et al., 2013; Sardi et al., 2018). In addition, the toxic effects of 1-butanol are similar to those of other alcohols and so the construction of a biosensor of this kind that is *specific* for 1-butanol was always going to be a challenge. Indeed, it is likely that any gene induced by 1-butanol would also be induced by a range of other alcohols and possibly even ethanol. So, while metabolite-specific gene expression responses have proved invaluable in genetic screens to uncover a host of stress responses and pathways (Dacquay and McMillen, 2021; Zhang and Shi, 2021) in the case of a butanol biosensor perhaps a different approach is called for.

One such strategy is the use of specific ligand-binding proteins fused to fluorescent reporter proteins in a way that the conformational change caused by binding results in a measurable alteration in fluorescence. This approach has been used in many different studies to successfully construct *in vivo* biosensors for a series of small molecules of biological interest, such as ATP (Lobas et al., 2019), NADP<sup>+</sup>/NADPH ratios (Sallin et al., 2018), Ca<sup>2+</sup> (Nagai et al., 2001), and neurotransmitters such as dopamine (Patriarchi et al., 2018). Besides their increased specificity, this type of biosensor is able to respond much more rapidly than transcription-based biosensors thanks to the relative simplicity

of their activation mechanism, displaying response times in the order of seconds rather than hours.

If the conformational change biosensor strategy is to be explored, significant challenges associated with their design have to be addressed, such as identifying proteins able to interact specifically with 1-butanol and not with other alcohols. It is likely the search for such butanol binding proteins would have to extend to organisms other than *S. cerevisiae*, perhaps to *Clostridia*, or other native 1-butanol producers. Then the expression of these proteins in *S. cerevisiae* would need to be carefully evaluated. In addition, the precise junction for the fusion between GFP and the butanol binding protein would require careful optimization, since the biophysical folding profile of the fluorescent fusion is likely to be complex and a change in fluorescence upon 1-butanol binding is a requirement.

## 8. Construction and characterization of *adh1Δ* mutants in a filamentous strain of *Saccharomyces cerevisiae*

### 8.1 Introduction

*S. cerevisiae* naturally produces high quantities of ethanol, hence is the host organism for the industrial production of this biofuel. The search for better biofuels has led researchers to look into *S. cerevisiae* for the production of 1-butanol, a biofuel and chemical precursor that is traditionally fermented from *Clostridia* species through a process called solventogenesis (Lee et al., 2009).

As mentioned previously, using *S. cerevisiae* to host the ABE pathway can circumvent some of the disadvantages of fermenting butanol in *Clostridia* such as the co-production of acetone and ethanol, strict anaerobiosis requirements, concomitant sporulation of cultures and bacteriophage contamination, and industrial scalability problems (Zheng et al., 2009). Additionally, *S. cerevisiae* has high tolerance to industrial stresses and its genetic malleability provides a sandbox for metabolic engineering. Unfortunately, 1-butanol titers from *S. cerevisiae* expressing the ABE pathway alone are much lower when compared to *Clostridia* with 2.5 mg/l in *S. cerevisiae* compared to 12 g/l in *C. acetobutylicum* (Steen et al., 2008; Yu et al., 2015), thus developing strategies to increase metabolic flow towards butanol production is of high importance to create a competent yeast butanol-producing strain.

One such strategy involved increasing the availability of acetyl CoA by deleting *ADHI* to provide more substrate for the ABE pathway in yeast (Si et al., 2014). This not only increased the yield of the ABE pathway, but it also activated an endogenous butanol-producing pathway in yeast. Literature evidence suggests that this endogenous pathway is dependent on amino acid catabolism, more specifically of glycine and threonine

(Branduardi et al., 2013; Si et al., 2014; Swidah et al., 2018), but the exact mechanism that links deletion of *ADHI* and induction of butanol production has not been elucidated.

Because the induction of this endogenous pathway can be achieved by deleting only one gene (*ADHI*), this strategy could be employed to screen for better butanol producers in different genetic backgrounds or mutant libraries of *S. cerevisiae*, in particular the ones that can adapt to the presence of butanol in different manners. The  $\Sigma$ 1278b background can respond to butanol stress by changing its mode of growth from yeast to pseudohyphal (Lorenz et al., 2000), a complex morphogenetic adaptation that involves the induction and interaction of at least five signaling pathways: fMAPK, RAS/PKA, TOR, the AMPK Snf1p, and RTG (Cullen and Sprague., 2012; González et al., 2017), which work in concert to sense the nutrient state of the cell, as well as the presence of molecules associated to population density, such as ethanol, and respond by activating transcription factors that regulate the expression of effector genes, resulting in changes in budding pattern, cell adhesion, cell polarity and shape, that result in the formation of pseudohyphae under nutrient-limiting conditions. One of the major effectors of this signaling network is the cell wall protein *FLO11*, a flocculin involved in cell-cell adhesion that is tightly regulated at transcription level and whose involvement in the formation of pseudohyphae and biofilms (Fidalgo et al., 2006).

Since the proposed butanol-producing pathway involves amino acid catabolism, then butanol could represent a quorum-sensing metabolite that signal yeast populations to switch to pseudohyphal growth to scavenge for nutrients or avoid the presence of toxic metabolites in the microenvironment or coordinate the formation of resistant biofilms to increase their tolerance to a stressful environment. Because of this close relationship between endogenous butanol production and the filamentous adaptive responses, it would be valuable to study the effect of endogenous butanol on a filamentous strain, as well as

the ability of this strain to accumulate butanol. In order to achieve this, the first step is to delete *ADHI* in a yeast strain of the  $\Sigma$ 1278b background and characterize its phenotype.

## 8.2 Deletion of *ADHI* in a haploid filamentous strain of *S. cerevisiae*

The *ADHI* gene was deleted using a gene-disrupting cassette bearing the hygromycin B resistance marker *hphNT1* (*HygB<sup>R</sup>*) (Carter and Delneri, 2010). The cassette was amplified from the pZC3 plasmid (Table 6.2) by PCR using the oligonucleotides ADH DEL FW and ADH DEL RV (Table 6.3), which have 45 nucleotide sequences that are complementary to the flanking regions of the *ADHI* locus in the yeast genome (Figure 8.1 A). The disrupting cassette was then introduced into a haploid  $\Sigma$ 1278b strain using a standard yeast transformation method and transformants were selected on Hygromycin B containing agar plates.

Transformants were reselected on hygromycin B, then genomic DNA was prepared and insertion of the disruption cassette at the *ADHI* locus was then verified using a PCR strategy (Figure 8.1 A) composed of three PCR reactions that target different regions of the disrupted gene. The expected bands and oligonucleotides used in each of the three reactions are summarised in Table 8.1.

**Table 8.1. Oligonucleotides used for the verification of the deletion of *ADHI***

Reaction	Oligonucleotides used	Expected band size (bp)
1	ADH1 VER FW + ADH1 VER RV	2237
2	ADH1 VER FW + HYGB VER RV	752
3	HYGB VER FW + ADH1 VER RV	479

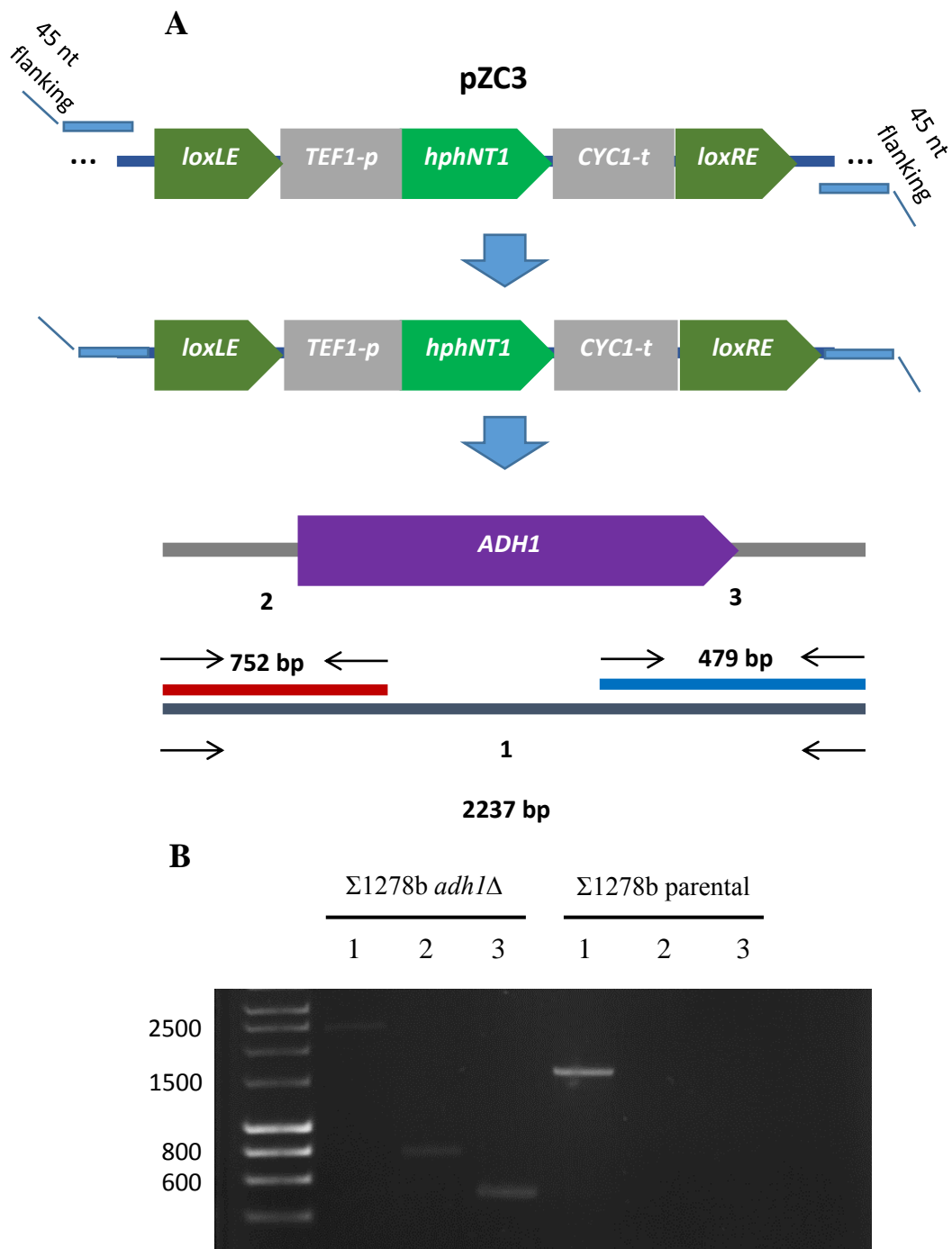


**Figure 8.1. Strategy for the deletion of *ADH1* in a haploid  $\Sigma 1278b$  strain of *S. cerevisiae*.** A) Schematic representation of the amplification of the *ADH1* disruption cassette, integration into the target region and PCR design and expected product sizes for a successful integration. B) 1% (w/v) agarose gel displays the verification PCR for the deletion of *ADH1* in a haploid filamentous strain, compared to its corresponding parental strain.

Agarose gel electrophoresis of the PCR reactions from the *adh1Δ* strain and the parental strain displayed the bands of the expected sizes for each reaction, indicating that the integration of the *HygB<sup>R</sup>* gene at the *ADH1* gene locus had been successful in the new Sa *adh1Δ* strain.

### 8.3 Construction of a diploid *adh1Δ* filamentous strain

Considering that haploid and diploid cells of the  $\Sigma$ 1278b background have some phenotypical differences, such as their mode of filamentation when growing on agar plates which is superficial in diploids and invasive in haploids, a diploid *adh1Δ* strain of the  $\Sigma$ 1278b background was constructed in order to study how this mutation affects the phenotype of both haploid and diploid strains. This was achieved by transforming the Sa *adh1Δ* strain with the pAS54 plasmid (Table 6.2) that carries a functional copy of the HO endonuclease. This enzyme is normally absent in laboratory strains to prevent haploids from switching mating-types and concomitant formation of diploids (Haber J., 2012). Introducing HO in a plasmid allows a window of opportunity for mate-switching in the laboratory. After potential diploids are formed, the cells can be then grown out of the plasmid selection media, encouraging loss of the plasmid, and removing HO from the new yeast cells.

After the selection of potential diploid strains, a simple mating type testing assay was conducted. In this assay the mating factor  $\alpha$  and  $\alpha$ -sensitive strains Sst1 and Sst2 (Table 6.1) are spread as a lawn on a standard yeast agar plate. Haploid strains are patched onto these lawns and if the haploid strains secrete the appropriate mating factors, a zone of growth inhibition or halo develops around them. In contrast, diploid strains do not secrete mating factors, thus they do not form an inhibition halo. Similar to a diploid control strain, a selected potential  $\Sigma$ 1278b *adh1Δ* diploid strain was tested during this assay and no halo

was observed (Figure 8.2 A). In contrast, haploid control strains were able produce characteristic inhibition halos; a narrow halo on the *MATa* testing lawn and a broad halo on the *MAT $\alpha$*  testing lawn. As an additional assay to test the construction of a diploid strain, the  $\Sigma$ 1278b *adh1 $\Delta$*  diploid strain was grown in liquid sporulation media for 7 days. Formation of asca containing spores was visualised by light microscopy, producing additional evidence for the diploid nature of this strain (Figure 8.2 B).

Appropriate disruption of the *ADHI* locus was then evaluated in the  $\Sigma$ 1278b *adh1 $\Delta$*  diploid strain following the same procedure used for verification on the haploid *adh1 $\Delta$*  strain. The agarose gel shows that the set of reactions resulted in the same band pattern as the haploid strain, indicating that the diploid strain carries the same *ADHI* deletion than the haploid strain (Figure 8.2 C).

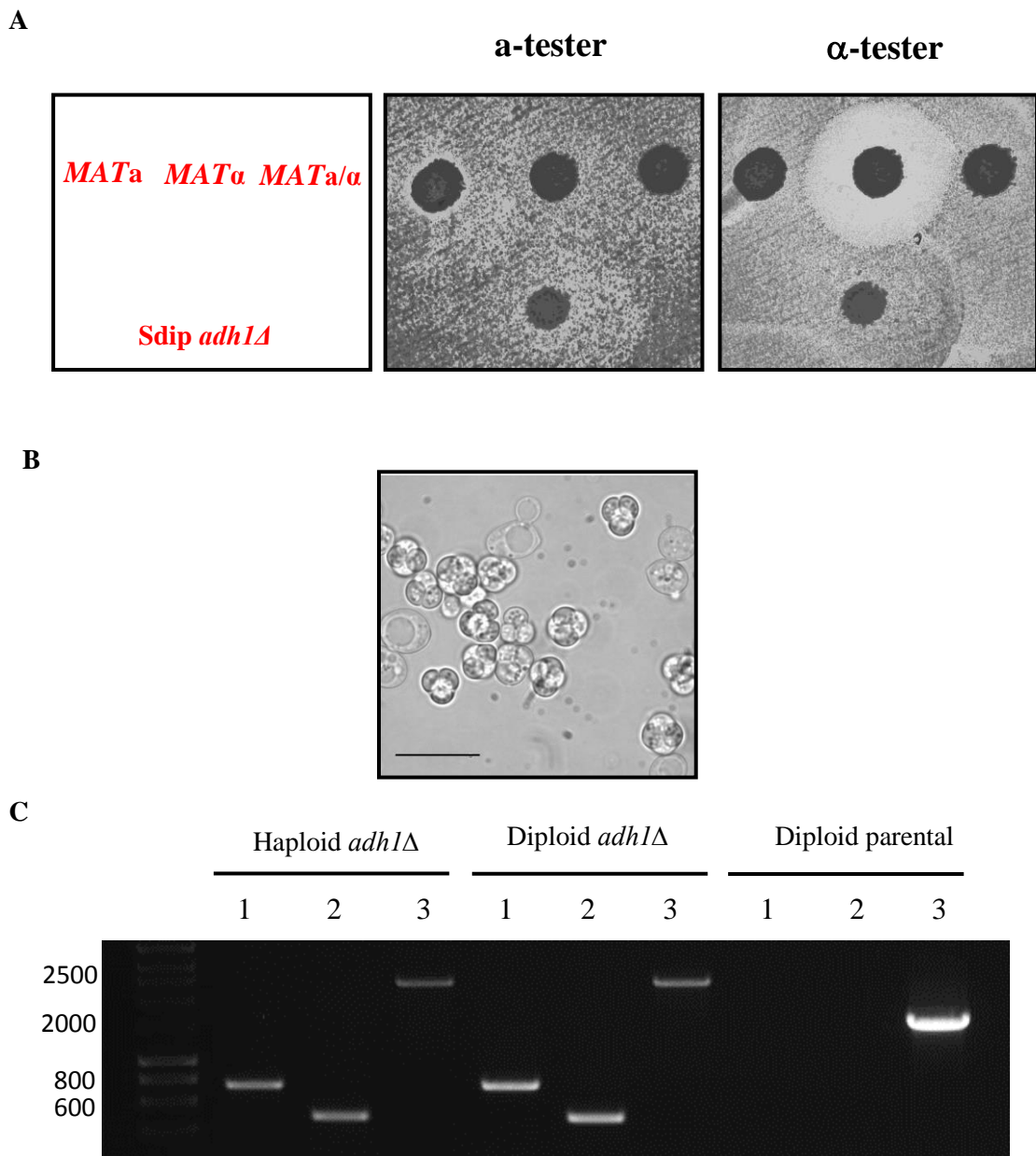


**Figure 8.2. Construction and verification of a diploid *adh1Δ* strain in the  $\Sigma$ 1278b background.** A) Phenotypical mate type test on an *adh1Δ* filamentous strain transformed with an HO-bearing plasmid. Cells were spotted onto solid YPD containing a lawn of each tester strain and left to grow for 2 days before taking pictures. B) Tetrads of diploid *adh1Δ* cells grown in sporulation media for 7 days. Scale bar is 10  $\mu$ m. C) 1% w/v agarose gel displaying the PCR verification of the deletion of *ADHI* in the diploid strain, compared to its parental strain.

#### 8.4 Drug sensitivity further verifies the deletion of *ADHI*

A drug sensitivity experiment was performed to phenotypically assess the loss of *ADHI* and the presence of the *HygB<sup>R</sup>* selection marker in the constructed *adh1Δ* haploid and diploid strains. It is expected that deletion of *ADHI* would cause a decrease in overall cell growth as fermentation of glucose is reduced and a redox imbalance is created due to an inability of cells to recycle  $\text{NAD}^+$  generated earlier in the glycolytic pathway by the reduction of acetaldehyde into ethanol. This deficiency causes cells to depend on oxidative phosphorylation for ATP synthesis, and as a result, *adh1Δ* strains should not be able to grow on media containing Antimycin A, as this drug inhibits electron transport in the inner mitochondria membrane, compromising oxidative phosphorylation (Rieske, 1967). Additionally, transformed cells should also be resistant to Hygromycin B, as the *HygB<sup>R</sup>* marker confers resistance to this drug. A summary of the expected results for the parental strain and the *adh1Δ* strain is shown in Figure 8.3 A.

Serial dilution analysis on various plates for the haploid and diploid *adh1Δ* filamentous strains as well as their corresponding wild-types, show the expected profile (Figure 8.3 B). More specifically, the *adh1Δ* strains are slow-growing on rich glucose media, grow well on hygromycin B plates and do not grow on Antimycin A. The sum of these data shows that the *ADHI* gene has been successfully deleted in both haploid and diploid yeast filamentous strains.

A

Strain	YPD	YPD + Antimycin A	YPD + Hygromycin B
WT	++	++	-
<i>adh1Δ</i>	+	-	+

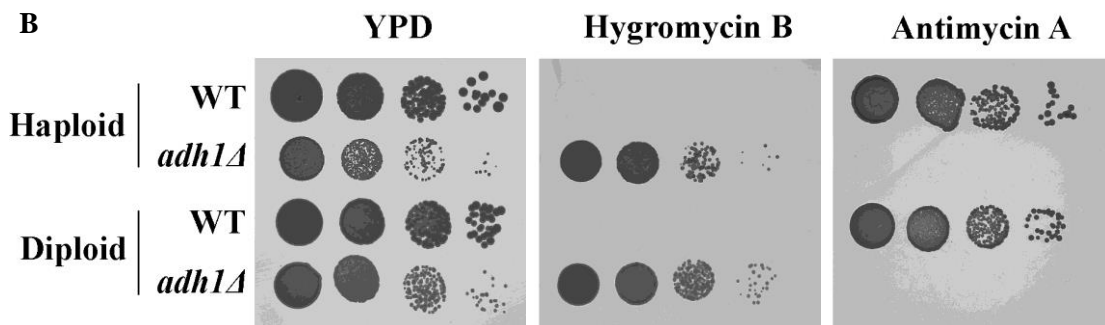


**Figure 8.3. Phenotypical verification of the deletion of *ADHI* in haploid and diploid strains by drug sensitivity.** A) Expected growth of each strain on each testing media. ++ indicates fast growth, + indicates slow growth, - indicates no growth. B) Drug sensitivity assay for parental and *adh1Δ* filamentous strains. Serial dilutions of stationary liquid cultures of each tested strain were spotted on the indicated media and left to grow at 30°C for 2 days.

## 8.5 Phenotypical characterization of the *adh1Δ* filamentous strains

To better understand the physiological consequences of the deletion of *ADHI* in yeast strains of the  $\Sigma$ 1278b background and their response to 1-butanol stress, the constructed haploid and diploid mutant strains were tested for colony morphology, induction of pseudohyphal growth, agar invasion, cell growth rate and cell viability. For all these experiments, the *adh1Δ* haploid and diploid strains were compared to their respective wild-type strains, as well as *ste7Δ* strains of the  $\Sigma$ 1278b background that were available in the lab's strain collection (Table 6.1). As some of the characterization involves assessing the ability of the *adh1Δ* strains to undergo filamentous growth, the *ste7Δ* strain was used as a negative control because loss of *STE7* disrupts the signaling cascade of the fMAPK pathway involved in the filamentous response, mating and cell-cell adhesion, thus resulting in a strain deficient in filamentous phenotypes (Madhani et al., 1997).

## 8.6 Loss of *ADHI* causes changes in colony morphology in haploids

One of the adaptative responses to nutritional stress seen in wild and some industrial strains is the formation of colonies with complex patterns of bands, ridges and wrinkles, as opposed to many laboratory strains that retain their smooth surface (Granek and Magwene, 2010). This response is known to occur due to *FLO11*-dependent pseudohyphal growth and cell aggregation, and represents the formation of biofilms that increase the survivability of yeast populations in stressful conditions (Fidalgo et al., 2006). Because the deletion of *ADHI* is expected to cause metabolic changes that lead to butanol production in yeast cells, possible changes in colony morphology of the *adh1Δ* mutants were studied.

In order to assess colony morphology changes, cells were streaked from solid YPD colonies into fresh solid rich media and left to grow for 6 days before photographing

colonies. Deletion of *ADHI* causes a change in surface features in the haploid strain, particularly the appearance of complex ridges and wrinkles (Figure 8.4). Although the WT haploid colonies display a pattern of radial, shallow ridges forming around a central mound, these structures are not as developed as the ones seen in the *adh1Δ* strain. The *ste7Δ* haploid strain presents smooth colonies that lack any of the features present in the other two strains, indicating that the *STE7*-depending MAPK signaling pathway is required for complex colony morphology in the  $\Sigma$ 1278b background (Figure 8.4). Together, these observations suggest that deletion of *ADHI* induces the formation of complex wrinkled structures on haploid colonies. This result is striking, as *ADHI* has a core metabolic role as the main alcohol dehydrogenase that drives fermentation, and as such does not participate directly in any of the signaling pathways or nutrient sensors involved in the filamentous response, suggesting that the induction of the ruffled colony phenotype may occur due to the metabolites that arise from the cell adapting to a truncated fermentative pathway.

Curiously, all of the assessed diploid strains show smooth colonies in the experiment (Figure 8.4). This exact behavior has been reported in a publication that assessed colony morphology in four yeast backgrounds, including  $\Sigma$ 1278b (Granek and Magwene, 2010). This difference in colony morphology can be explained by the ploidy-dependent expression pattern of *FLO11*, which was described in 1999 and found to decrease with ploidy, explaining the observed differences in the filamentous phenotypes of haploid and diploid strains of the same background (Lo and Dranginis, 1996; Galitski et al., 1999).

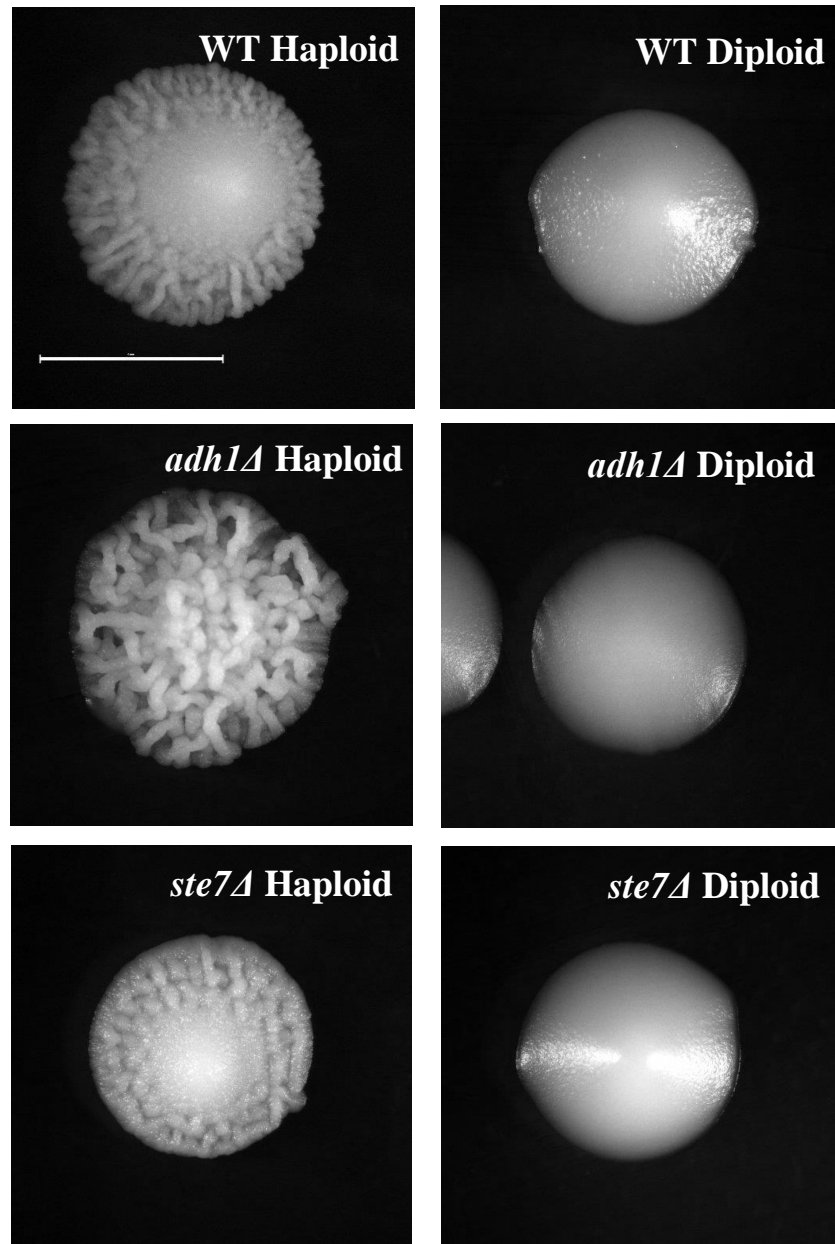


**Figure 8.4. Deletion of *ADH1* leads to changes in colony morphology of a  $\Sigma$ 1278b haploid strain.** Colony morphology of haploid and diploid versions of the parental, *adh1Δ*, and *ste7Δ* strains of the  $\Sigma$ 1278b background, was assessed by growing them at 30°C on YPD agar plates and photographing colonies after 6 days of incubation. Pictures were taken in a Leica L2 (Leica microsystems) stereomicroscope at 10x magnification. Colonies shown are representative of the morphology of single colonies. Scale bar is 1 mm in length.

## 8.7 Butanol-induced pseudohyphal growth and agar invasion are present in *adh1Δ* strains

Since deletion of *ADHI* is expected to activate endogenous butanol production in yeast and this alcohol is known for inducing pseudohyphal growth in strains of the  $\Sigma$ 1278b background, the ability to produce pseudohyphae in the *adh1Δ* strains was tested by growing exponential cultures in liquid rich media for 24 hours in absence or presence of 1% v/v butanol. Parental haploid and diploid cells were able to produce pseudohyphae under 1% v/v butanol, as evidenced by the elongated cells and the unipolarised budding of new cells from the tip of mother cells (Figure 8.5 A) (Cullen and Sprague Jr, 2002). The *adh1Δ* haploid and diploid strains displayed similar behavior, showing evidence for elongated cells and unipolar budding (pointed by arrows in the figure) even in absence of butanol, suggesting that some part of the pseudohyphal response may be induced by the deletion of *ADHI* in the filamentous strain. As a contrast, *ste7Δ* strains deficient in pseudohyphal growth do not display elongation or unipolar budding in any of the tested conditions (Figure 8.5 A).

Another example of filamentous growth in yeast is haploid invasive growth, an adaptive response observed in haploids that is triggered by nutrient deprivation and depends on pseudohyphal growth to occur (Cullen and Sprague, 2000). In order to complement the previous assessment of pseudohyphal growth in response to butanol treatment, the ability of the *adh1Δ* strains to invade a solid substrate was tested using a simple agar-based assay. Test strains are grown in solid YPD for 5 days then imaged

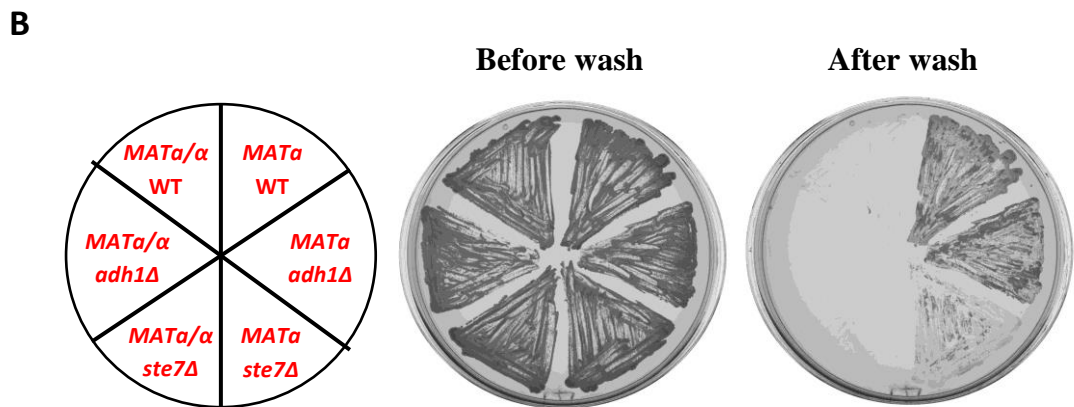
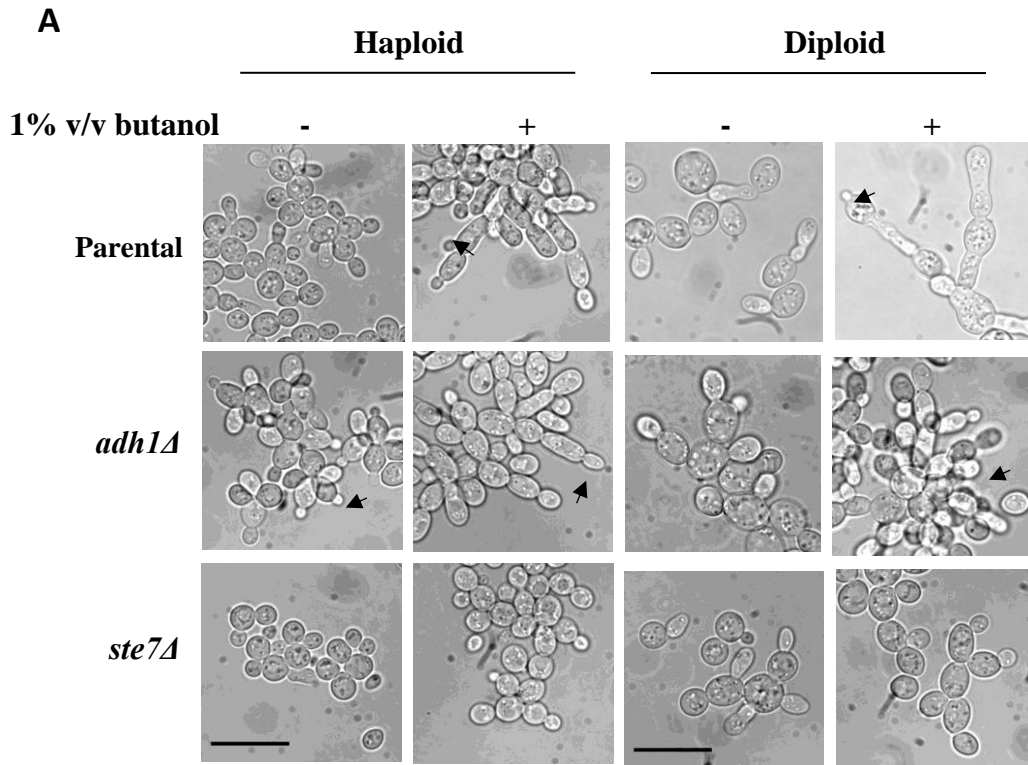


**Figure 8.5 Pseudohyphal growth and agar invasion of *adh1Δ* filamentous strains.** A) Images at 100x magnification show different *S. cerevisiae* strains grown for 24 hours in liquid YPD at the indicated concentrations of 1-butanol added during exponential growth. Arrows indicate where budding occurs at the tip of yeast cells. Scale Bar is 10  $\mu$ m in length. B) Agar invasion assay of  $\Sigma$ 1278b *adh1Δ* strains. Cells were grown at 30°C in a YPD agar plate for 3 days and then left to grow at room temperature for 2 more days before assessing agar invasion. Pictures show the YPD plate before and after washing away surface cells with a stream of distilled water to display invasion of agar by haploid cells.

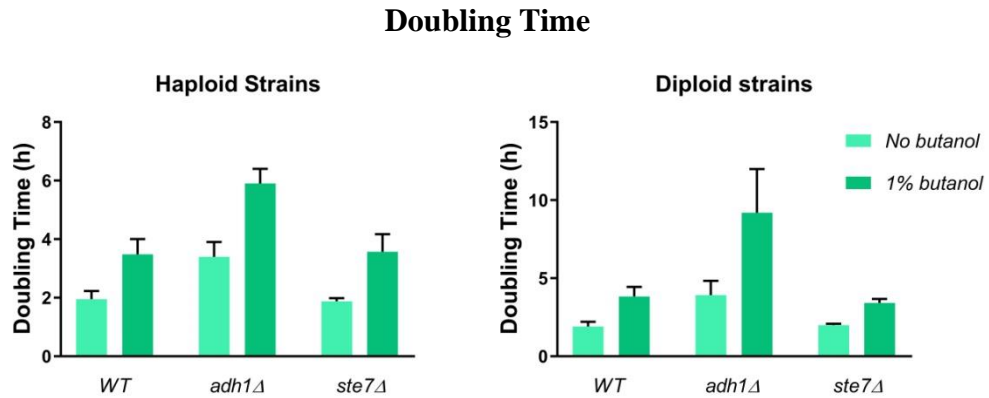
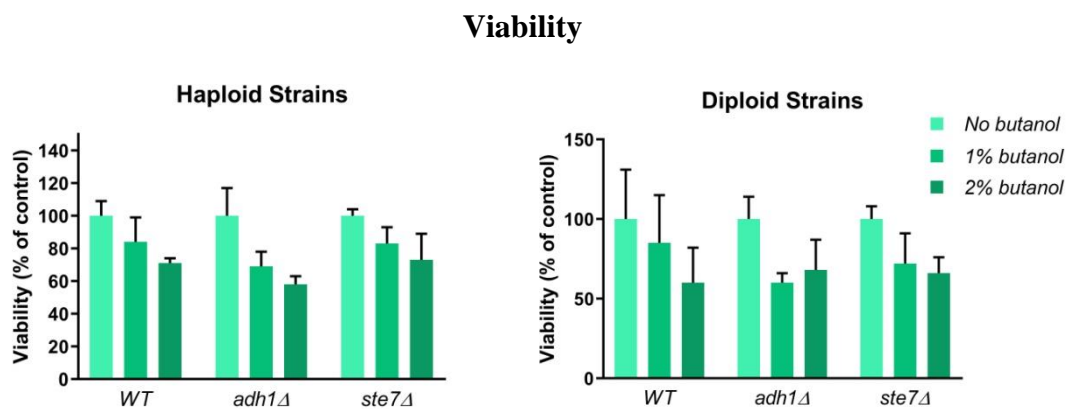
before and after washing the surface cells with a stream of water. Haploid parental and *adh1Δ* strains exhibit invasive growth, as cells remain in the agar after the surface cells have been washed away (Figure 8.5 B).

As discussed above, expression of *FLO11*, a key effector of the filamentous phenotype is drastically reduced on diploid cells (Galitski et al., 1999), which correlates with the absence of invasive growth in all of the tested diploid strains (Figure 8.5 B). Interestingly, invasive growth was not completely abolished in the haploid *ste7Δ* strain, indicating that other signaling pathways may be compensating for the loss of function of the MAPK pathway in this strain.

### **8.8 *adh1Δ* strains exhibit slow growth and similar sensitivity to butanol stress to their wild-type**

Deletion of the major alcohol dehydrogenase prevents the final step in glucose fermentation, causing a number of metabolic issues such as an inability to easily regenerate NAD<sup>+</sup> and potential accumulation of toxic metabolic intermediates like acetaldehyde and pyruvate. Because these imbalances may have an overall impact on fitness, growth rate and viability of the *adh1Δ* strains were assessed under optimal and 1-butanol stress conditions.

First, growth rate was calculated as the doubling time, which corresponds to the time required for a cell culture to double in number of cells, of the filamentous strains growing in exponential phase in YPD in absence or presence of 1% v/v butanol. This value was calculated using the appropriate formula in section 6.3.3. The doubling time under 2% v/v butanol could not be calculated, as none of the strains entered an exponential phase when grown with this amount of butanol (data not shown). The deletion of *ADHI* in either the haploid or diploid background caused an increase in doubling time- for instance a 1.8-

**A****B**

**Figure 8.6 Deletion of *ADH1* causes slow growth but does not affect cell viability on butanol stress.** A) Doubling time of  $\Sigma$ 1278b strains of *S. cerevisiae* grown in liquid YPD with or without 1% v/v 1-butanol for 8 hours in exponential phase. Bars indicate average and standard deviation of multiple independent experiments. B) Viability of  $\Sigma$ 1278b strains after 1 hour exposure to the indicated butanol concentrations. Results are expressed as average percentage of viable colonies, respect to an untreated control for each strain, plus standard deviation (n =3).

fold increase in rich media alone, and 1.7–fold when stressed with 1% v/v 1-butanol were observed (Figure 8.6 A). The fact that the impact of butanol on growth rate is similar regardless of ploidy or presence of *ADHI* suggests that deletion of this gene does not alter sensitivity to externally added butanol, at least in regard to cell growth.

As with previous experiments, a *ste7Δ* strain was also tested to see if disruption of pseudohyphal growth has an effect on cell growth under 1-butanol stress. Doubling times appear to closely match the parental strain indicating that loss of pseudohyphal growth has little effects on growth rate (Figure 8.6 A).

In order to test the impact of butanol on cell viability for the haploid and diploid *adh1Δ* strains relative to their wild-type, cells in the exponential growth phase were treated with 1% or 2% v/v 1-butanol for 1 hour, diluted and spread on solid YPD and grown until colonies appeared. Then, viability of each strain was then calculated as the number of colonies on each treated plate related to an untreated control. While the treatments lead to some reduction in viability (1% v/v butanol treatment reduces viability to ~80-85%, whereas 2% v/v reduces to ~70-75%), there is no major differences based on ploidy or the deletion of the *ADHI* gene in the level of cell viability after exposure to high butanol concentrations (Figure 8.6 B). In fact, compared to many treatments that are known to inhibit growth and/or impact upon membrane structure, viability is remarkably stable.

### **8.9 The filamentous *adh1Δ* strain accumulates more butanol than its non-filamentous counterpart**

The main purpose for deleting *ADHI* in the filamentous  $\Sigma$ 1278b background of yeast strains was to compare the capacity of this strain to accumulate butanol with similar strains in the W303-1A background (Swidah et al., 2015). This represents the starting

point towards assessing if the filamentous phenotype confers any advantages on butanol production, as pseudohyphal growth is induced by this alcohol, among other stimuli.

Parental and *adh1Δ* strains of the  $\Sigma$ 1278b and W303-1A backgrounds were therefore tested for butanol and ethanol accumulation by gas chromatography of filtered samples collected over a 14-day period from yeast cultures grown in semi-anaerobic conditions, as described in section 6.5. As expected, none of the parental strains were able to accumulate butanol over the course of the experiment, while both *adh1Δ* strains did accumulate up to  $114 \pm 19$  mg/l in the  $\Sigma$ 1278b background, and  $70 \pm 22$  mg/l in the W303-1A background (Figure 8.7A). The difference in butanol yield between both strains was statistically significant from day 7 onwards.

In order to verify if this higher yield is due to greater biomass present in the cultures of the filamentous strain, butanol measurements were normalized to cell density. After normalization, the peak butanol values obtained on day 11 for the  $\Sigma$ 1278b and W303-1A strains were  $480 \pm 190$ , and  $243 \pm 138$  mg/l/OD<sub>600</sub>, respectively (Figure 8.7 B and C). In this case, the difference is no longer statistically significant essentially due to high variability in the measurement of the cell density.

This experiment also served to observe the disruption of ethanol biosynthesis and accumulation caused by the deletion of *ADHI* in both strains. Both filamentous and non-filamentous parental strains were able to produce up to  $\sim 8$  g/l, while the *adh1Δ* strains only accumulated  $\sim 2.5$  g/l (Figure 8.7 D). It is important to note here that despite the loss of *ADHI*, the mutant strains are still able to accumulate ethanol albeit at lower concentrations, suggesting that other *ADH* enzymes may be compensating for the loss of the major enzyme. Perhaps, the difference observed in butanol accumulation in both *adh1Δ* strains may be related to the presence of different or more abundant alternative

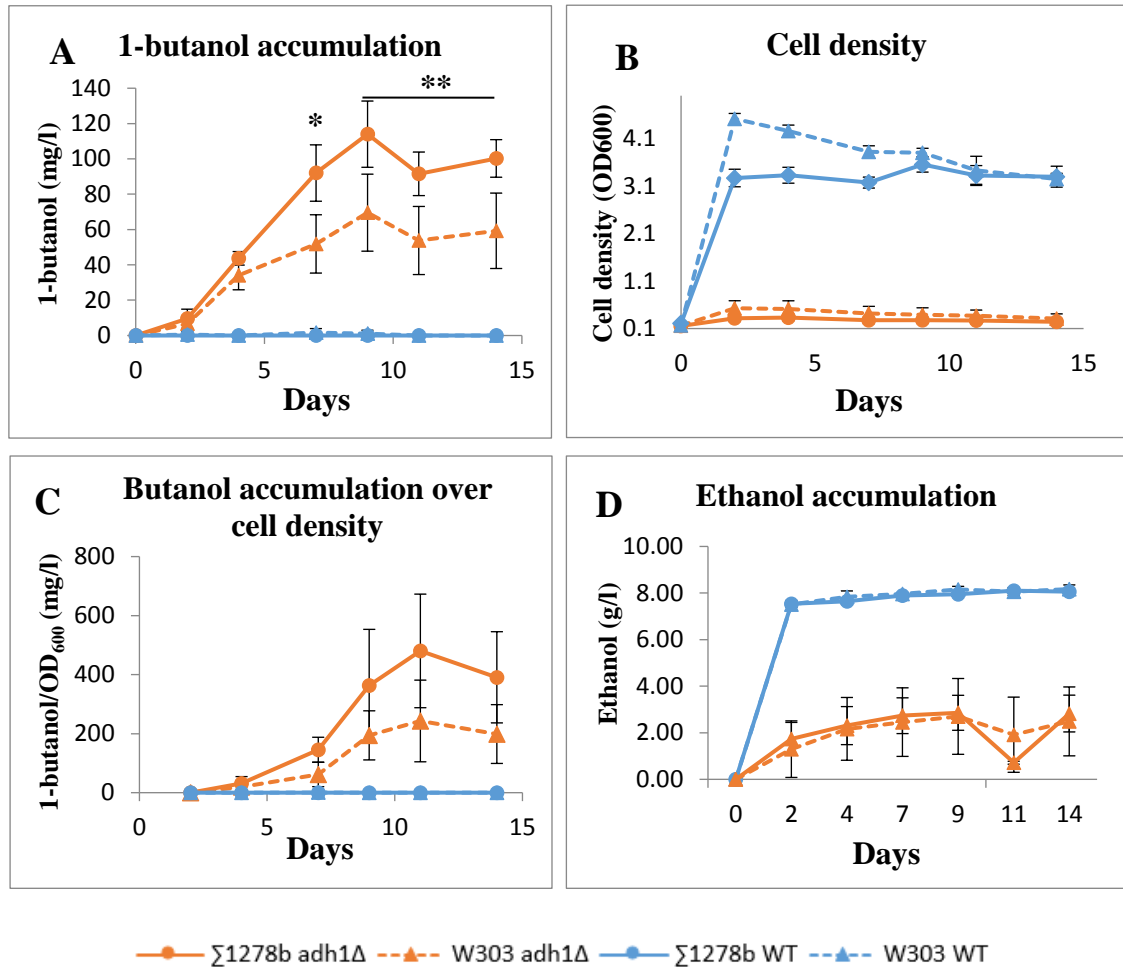


**Figure 8.7 Deletion of *ADHI* reduces ethanol accumulation and induces butanol production in haploid filamentous strains of *S. cerevisiae*.** Concentration of A) 1-butanol and B) ethanol in a 14-day semi-anaerobic fermentation experiment of four *S. cerevisiae* strains was measured by gas chromatography. C) Cell density of the cultures was measured by spectrophotometry at 600 nm, and D) 1-butanol concentration per unit of cell density was calculated from the measured data. Plot points correspond to mean ( $\pm$ SD) of 5 biological replicates. Asterisks indicate statistical significance, \* p-value < 0.05 and \*\* p-value < 0.01.

*ADH* enzymes, as the final step in the proposed endogenous pathways for butanol biosynthesis can also be catalysed by these enzymes (Branduardi et al, 2013; Shi et al, 2016; Swidah et al, 2018).

## 8.10 Discussion

It has been reported in the literature that deletion of *ADHI* results in the activation of an endogenous 1-butanol biosynthetic pathway in *S. cerevisiae* that depends on amino-acid catabolism (Si et al., 2016; Branduardi et al., 2013).

One attractive cellular trait to look for when searching for potential robust 1-butanol-producing yeast strains is the resistance to fusel alcohol toxicity, as higher tolerance is often associated with better yields (Swidah et al., 2015; Taylor et al., 2010). The yeast filamentous response is an adaptive mechanism induced by nitrogen starvation, and results in cells forming elongated chains that reach onto the growth medium to forage for new nutrient sources (Chen and Fink, 2006; Dickinson, 1996). This response can also be induced by exposure to fusel alcohols, including 1-butanol, and it has been proposed that because they are the product of amino-acid catabolism, they serve as a secondary signal for poor nitrogen availability (Lorenz et al., 2000).

Because of this relationship between the production of fusel alcohols and the induction of the filamentous response, the core goal of this chapter was to assess 1-butanol production, as well as characterise some of the phenotypical features of a filamentous  $\Sigma 1278b$  strain of *S. cerevisiae* able to produce 1-butanol via the endogenous pathways in order to delve into the potential benefits of this strain for 1-butanol production.

In order to induce endogenous butanol production, the *ADHI* gene was deleted in a haploid strain of  $\Sigma 1278b$ , and then a diploid version was made by HO-dependent mate-

type switching and crossing of haploids. Selected transformants were then verified by PCR and a drug sensitivity assay, confirming the success of the transformation procedure.

Characterisation of the phenotype of the mutant strains led to the identification of a number of physiological consequences of the deletion of *ADHI*. First, the mutants exhibited a decrease in growth rate, which could be explained by the metabolic imbalances caused by the truncation of glycolysis, such as slower regeneration of NAD<sup>+</sup> and accumulation of toxic intermediates like acetaldehyde. Curiously, the sensitivity of the *adh1Δ* strains to the growth-inhibiting effects of butanol was similar to the wild-type, indicating that the mutation does not compromise the strain's ability to tolerate butanol toxicity. Deletion of *ADHI* did not hamper butanol-induced pseudohyphal growth or haploid invasive growth, but it caused the appearance of ruffled colonies in the haploid strain, suggesting that the metabolic changes caused by the deletion of this enzyme may lead to the induction of morphologic changes at population level. Finally, the haploid *adh1Δ* filamentous strain managed to accumulate more butanol than its non-filamentous counterpart in semi-anaerobic fermentation, suggesting that it may represent a more favorable strain to achieve higher production levels.

One of the more remarkable results of this chapter is the appearance of ruffled colonies in the *adh1Δ* haploid filamentous strain. As mentioned previously, complex colonies arise under nutrient-limiting conditions and depend on *FLO11*-driven pseudohyphal growth to properly develop (Fidalgo et al., 2006; Reynolds and Fink, 2001), leading to the formation of resistant biofilms that increase the survival of the yeast population to a wide array of environmental stresses (Vachová et al., 2012).

A similar effect was described in a study involving in the human pathogen *Candida albicans*, in which deletion or inhibition of *ADHI* activity enhanced biofilm formation

(Mukherjee et al., 2006). The study concluded that *ADHI* may inhibit *C. albicans* biofilms formation through ethanol-specific mechanisms, thus the decrease in ethanol production through its deletion may be the trigger to induce biofilm formation in this pathogenic yeast.

Although ethanol accumulation was diminished in this study's  $\Sigma 1278b$  *adh1Δ* strain, it was not completely abolished, thus other metabolites may be involved in the induction of complex colonies in the filamentous strain. One such metabolite is acetaldehyde, a toxic chemical which accumulates in the cytoplasm when *ADHI* is deleted (Si et al., 2014) that may contribute to the slow growth of the strain and changes in colony morphology. While 1-butanol and acetaldehyde are two metabolites that accumulate in the filamentous *adh1Δ* strain, it is possible that other fusel alcohols may contribute to the formation of complex colonies in this mutant, thus measuring the presence of other fusel alcohols in samples of complex colonies may yield further information about the pro-filamentation environment present in the  $\Sigma 1278b$  *adh1Δ* haploid strain.

Another approach to explore the role of signaling metabolites on 1-butanol production and colony morphology in the  $\Sigma 1278b$  *adh1Δ* strain could involve reducing acetaldehyde accumulation. This strategy may yield some insight into the mechanisms behind the activation of the endogenous butanol-production pathway, as pyruvate and 3p-glycerate are upstream glycolytic intermediates that are fed into the threonine-based and glycine-based pathways proposed in the literature (Swidah et al., 2018) and will be explored in the following chapter.

## 9. Exploring the role of acetaldehyde as a key metabolite in endogenous butanol production

### 9.1 Introduction

Chapter 8 previously demonstrated that deletion of *ADHI* in a haploid  $\Sigma$ 1278b strain resulted in higher 1-butanol production than the same mutant in the W303-1A background. Deletion of *ADHI* also resulted in slower cell growth, which may have a negative impact on further 1-butanol production. One of the direct consequences of deleting *ADHI* is the accumulation of intracellular acetaldehyde, a highly toxic metabolite that might contribute to the observed decrease in cell growth (Stanley et al, 1993; Ingram and Buttko, 1984). The research described in this chapter therefore focuses on the role of acetaldehyde in the endogenous butanol production pathway.

Acetaldehyde is a 2-carbon aldehyde that results from the decarboxylation of pyruvate by Pdc1p and represents the commitment step for glycolysis-derived pyruvate fermentation (Schaaff et al., 1989). During yeast fermentative metabolism, most of the acetaldehyde is reduced to ethanol by Adh1p, but other fates include the synthesis of acetyl-CoA by Ald6p and Acs2p, and fermentation into 2,3-butanediol by Pdc1p and Bdh1p (Figure 9.1).

When glucose is exhausted from the culture media, *S. cerevisiae* switches its metabolism from fermentative to respiratory by inducing the expression of previously glucose-repressed genes, a shift mediated by the PKA and AMPK signaling pathways (Simpson-Lavy and Kupiec, 2019). One of the key changes is the expression of *ADH2*, an alcohol dehydrogenase isozyme that favors the oxidation of ethanol back to acetaldehyde (Ganzhorn et al, 1987; Russel and Smith, 1982). The latter is then reincorporated into yeast metabolism by feeding into the tricarboxylic acid cycle (TCA).

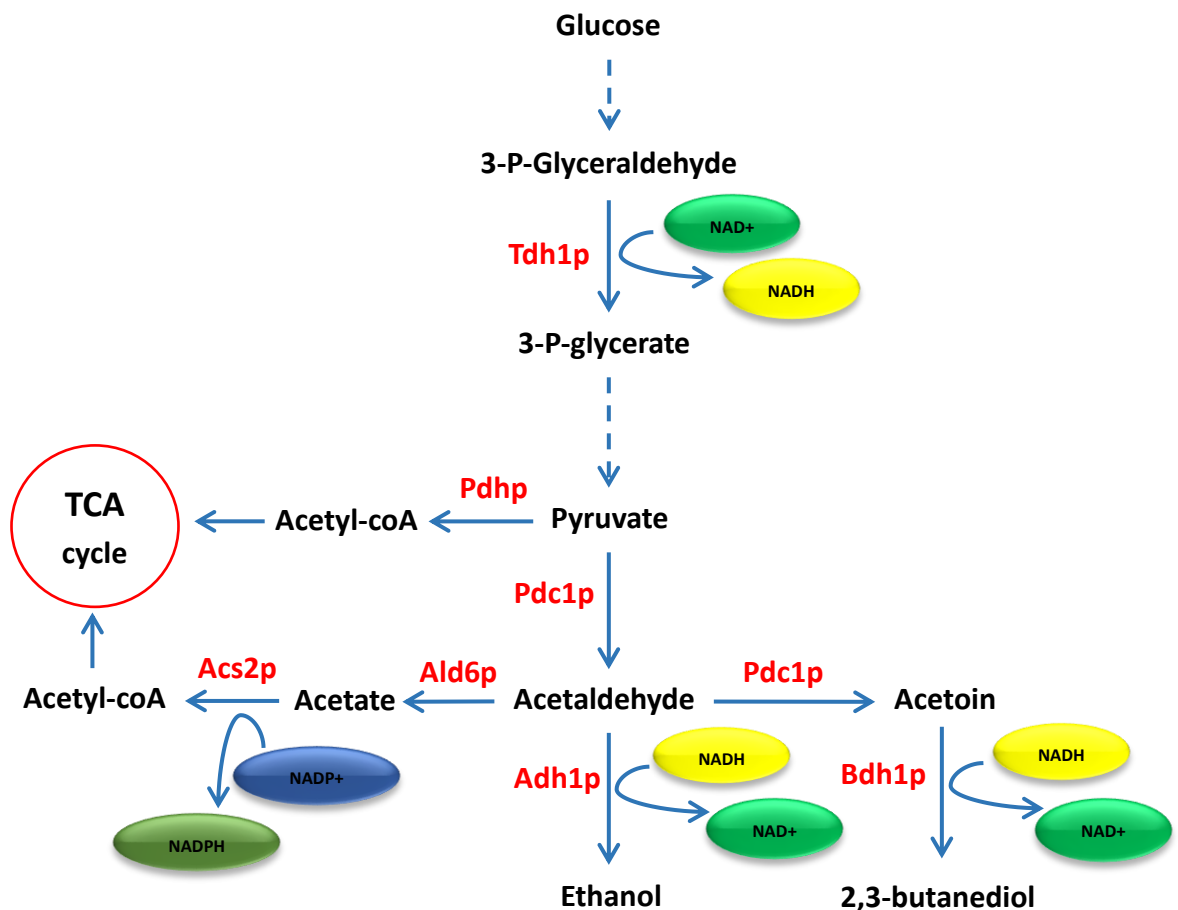


**Figure 9.1. Metabolic fates of acetaldehyde in *S. cerevisiae*.** Dashed lines indicate multiple reaction steps. Enzymes involved in glycolysis and acetaldehyde metabolism: triose-phosphate dehydrogenase (Tdh1p), pyruvate decarboxylase (Pdc1p), pyruvate dehydrogenase (Pdh) aldehyde dehydrogenase (Ald6p), acetyl CoA synthetase (Acs2p), alcohol dehydrogenase (Adh1p), 2,3-butanediol dehydrogenase (Bdh1p). Redox steps are associated to cofactors nicotine adenine dinucleotide (NADH) and nicotine adenine diphosphonucleotide (NADPH). Tricarboxylic acid cycle (TCA).

When *ADHI* is deleted, the metabolic flow of glycolysis and fermentation is interrupted, causing accumulation of acetaldehyde (decarboxylation of pyruvate is an irreversible reaction) and an imbalance in the NADH/NAD<sup>+</sup> ratio that results from the loss of the acetaldehyde reduction step that oxidizes NADH back to NAD<sup>+</sup>, which is required for the oxidation of 3-P-glyceraldehyde to 3-P-glycerate during glycolysis (Figure 9.1). Because acetaldehyde diffuses poorly across biological membranes (Stanley and Pamment, 1992), it can quickly accumulate in the cytoplasm and exert its inhibitory effects on a wide range of cellular processes, including cell growth and protein synthesis (Jones, 1990). Yeast cells respond to acetaldehyde stress by inducing the expression of *HSP* genes and *ALD* genes regulated by the general stress response transcription factors Msn2p and Msn4p (Aranda, 2003). Expression of Ald6p during stress contributes by reducing acetaldehyde into acetate, thus permitting the synthesis of acetyl-CoA by Acs2p and providing precursors for the TCA cycle when glucose is depleted and respiratory metabolism is activated (Figure 9.1).

Overexpression of the genetic products of *ALD6* and *ACS2* is a strategy that has been used to improve butanol production in yeast strains bearing the exogenous ABE pathway, as these enzymes increase the availability of cytosolic acetyl-CoA, which is the precursor for 1-butanol production through the ABE pathway (Krivoruchko et al., 2013; Swidah et al., 2015). Although these reports did not detect reductions in acetaldehyde levels after overexpression of *ALD6* and *ACS2*, the strategy could still be viable to attempt to detoxify acetaldehyde accumulation in an *adh1Δ* strain.

The first objective of this series of experiments was therefore to express the *ALD6* and *ACS2* genes in the haploid  $\Sigma$ 1278b *adh1Δ* strain and assess the impact of this addition on

butanol, ethanol and acetaldehyde accumulation in semi-anaerobic fermentation, as well as other effects on cell physiology such as growth rate, pseudohyphal growth, and colony morphology.

## 9.2 Removal of the Hygromycin B resistance marker in the $\Sigma$ 1278b *adh1Δ* strain

In order to constitutively express *ALD6* and *ACS2* in the  $\Sigma$ 1278b *adh1Δ* strain, an integration cassette previously described in Swidah et al., 2015 was used. In this expression cassette (contained in the pSH47 plasmid, Table 2.2), *ALD6* and *ACS2* are expressed under the control of the constitutive *TDH3* and *TEF1* promoters, respectively. Additionally, each gene has a C-terminal FLAG tag to facilitate immuno-detection of the protein products (Figure 9.3 A). These cassettes can be integrated into the yeast genome via homologous recombination using two 200 bp flanking regions that are homologous to the *TRP1* locus. Finally, the integration cassette also contains the *hphNT1* (*HygB<sup>R</sup>*) selection marker, allowing hygromycin-B selection of transformants. The construct can be excised from the plasmid by digesting it with BspQI, generating a double-stranded DNA-cassette with no linker sequences.

Because *HygB<sup>R</sup>* was already used as the selection marker for the *ADH1* deletion in the  $\Sigma$ 1278b strain, the marker had to be first removed in this strain before integrating the *ALD6/ACS2* cassette. The disruption cassette used to delete *ADH1* contains two *lox* sites flanking the integrated sequence which allow the removal of the *HygB<sup>R</sup>* marker by the *Cre* endonuclease (Figure 9.2 A). *Cre* was expressed in the haploid  $\Sigma$  *adh1Δ* strain by transforming it with the pSH47 plasmid (Table 6.2), and its endonuclease activity was induced by growing cells overnight in YPG (YP + 2% w/v galactose) liquid media.

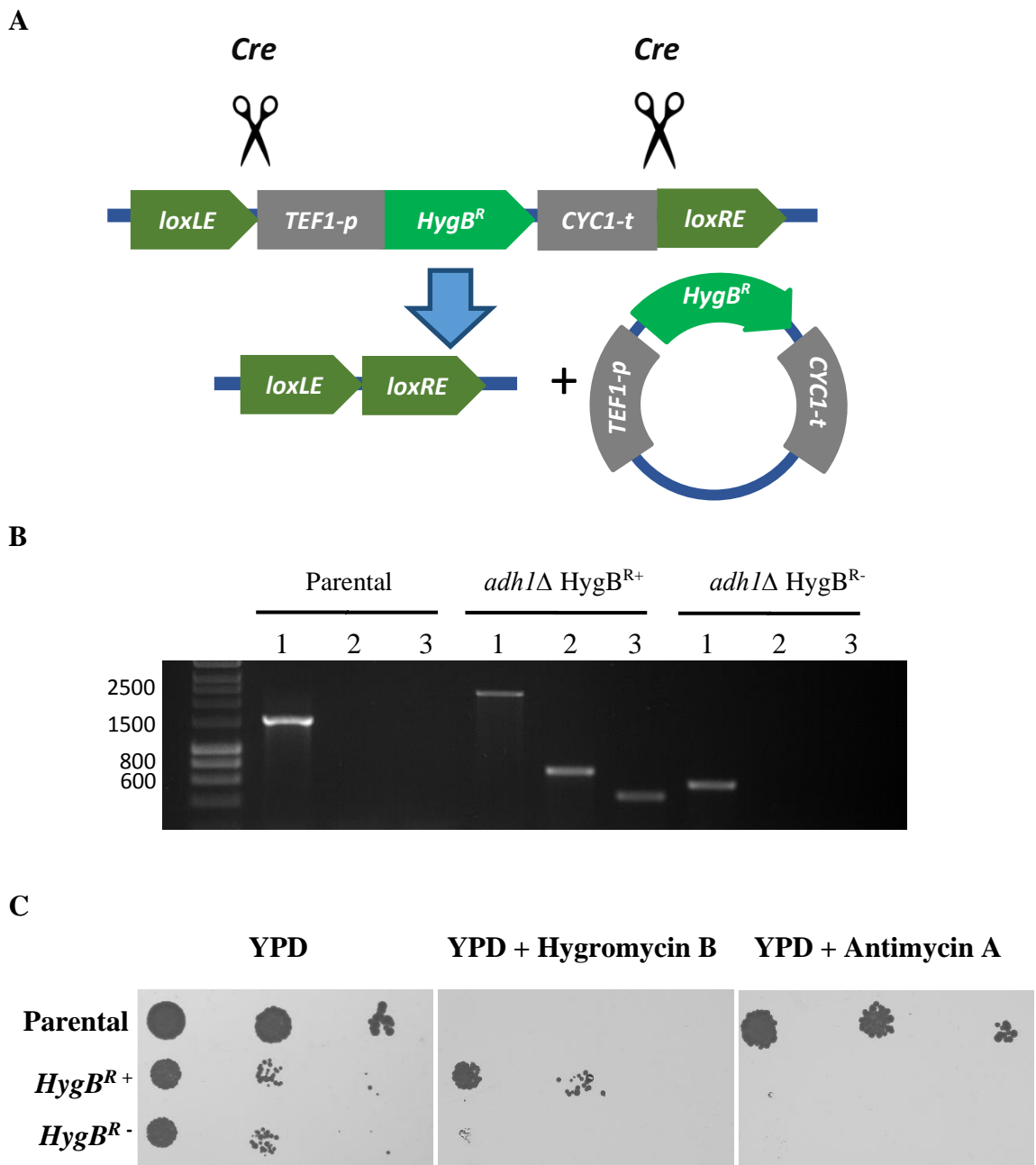


**Figure 9.2. The Hygromycin B resistance selection marker was removed from the filamentous *adh1Δ* strain.** A) Schematic representation of the excision of the *Hyg*<sup>B<sup>R</sup></sup> marker in the haploid *adh1Δ* strain by *Cre* endonuclease. B) 1% w/v agarose gel shows the PCR products that verify the removal of the *Hyg*<sup>B<sup>R</sup></sup> marker in the haploid *adh1Δ*. DNA ladder corresponds to HyperLadder 1kb (Invitrogen). C) Drug sensitivity assay further verifies the removal of the *Hyg*<sup>B<sup>R</sup></sup> marker by drug sensitivity. Stationary phase cells were spotted on solid YPD supplemented with the indicated antibiotics and left to grow at 30°C for 2 days.

Verification of the removal of the *HygB<sup>R</sup>* marker in candidate colonies was performed with the same PCR and drug-based assays used previously to verify *ADHI* deletion described in sections 8.3 and 8.4. Agarose gel electrophoresis of DNA extracted from a candidate colony shows that reaction 1, which spans the flanking regions of the *TRP1* locus, yielded a product of approximately 500 bp, while reactions 2 and 3, corresponding to internal sequences of the *HygB<sup>R</sup>* gene, yielded no PCR product. This result indicates that the internal *HygB<sup>R</sup>* sequences were not present and that only the genomic regions flanking the *TRP1* locus were present in the *Cre*-treated strain (Figure 9.2 B). Additionally, both the parental and *adh1Δ HygB<sup>R+</sup>* strains PCR products are displayed to further indicate the difference in product size for each reaction.

As an additional assay to test the removal of the *HygB<sup>R</sup>* marker from the haploid  $\Sigma$ 1278 *adh1Δ* strain, a drug sensitivity assay was performed to assess the sensitivity of the generated strain to Hygromycin B. The assay demonstrated that the *adh1Δ HygB<sup>R-</sup>* strain was unable to grow in either antimycin A or hygromycin B, further confirming the loss of the selection marker and its dependence on respiratory metabolism (Figure 9.2 C).

Together, these results show that the *HygB<sup>R</sup>* marker was successfully excised from the haploid  $\Sigma$ 1278 *adh1Δ*, resulting in a strain ready to be transformed with the *ALD6/ACS2* overexpression cassette.

### **9.3 Insertion of the *ALD6/ACS2* cassette in the $\Sigma$ 1278 *adh1Δ* strain**

To begin with, the *ALD6/ACS2* overexpression cassette was released from the pBMH-ALD6-ACS2-HYGR plasmid (Table 6.2) by digesting a bacterial plasmid DNA extract with the BspQI restriction enzyme at 37°C for 1 hour.

The resulting DNA fragment was then transformed into the  $\Sigma$ 1278 *adh1Δ HygB<sup>R</sup>* strain and potential transformants were selected on media containing Hygromycin B. Genomic

DNA was extracted from candidate transformants to verify insertion of the *ALD6/ACS2* cassette at the *TRP1* locus using a PCR strategy. A set of two reactions each spanning one of the flanking regions and the internal cassette sequence were used to verify the insertion of the cassette, producing PCR fragments of 905 and 1187 bp, respectively (Figure 9.3 A).

Agarose gel electrophoresis confirmed that the PCR product matched the expected pattern of a successful integration (Figure 9.3 B). The bands of an *ALD6/ACS2* overexpressing strain previously constructed in the laboratory in the W303-1A background (Table 6.1) are shown as a positive control for integration. Although faint, the bands of the control strain match the expected pattern.

In addition to the verification PCR, a Western Blot based approach was used to check the expression of Ald6p and Acs2p in the transformed  $\Sigma 1278$  *adh1Δ* strain. Whole cell protein extracts were made from liquid cultures grown to exponential phase in YPD, and then separated using SDS-PAGE. Immunoblotting with anti-FLAG antibodies revealed bands of approximately 70 and 100 kDa in the extracts of the  $\Sigma 1278$ b A6A2 (*ALD6/ACS2*) strain, corresponding to the expected sizes for the FLAG-tagged Acs2p and Ald6p (Figure 9.3 C). Two isolates of a W303-1A strain overexpressing *ALD6* and *ACS2* previously constructed in the lab, together with a strain bearing the ABE pathway genes as well as *ALD6* and *ACS2* were used as positive controls for the presence of the Ald6p and Acs2p FLAG-tagged proteins, all showing the expected bands at 70 and 100 kDa. The  $\Sigma 1278$ b parental strain has no band at 70 kDa, but there is a faint band heavier than the 100 kDa mark (Figure 9.3 C).

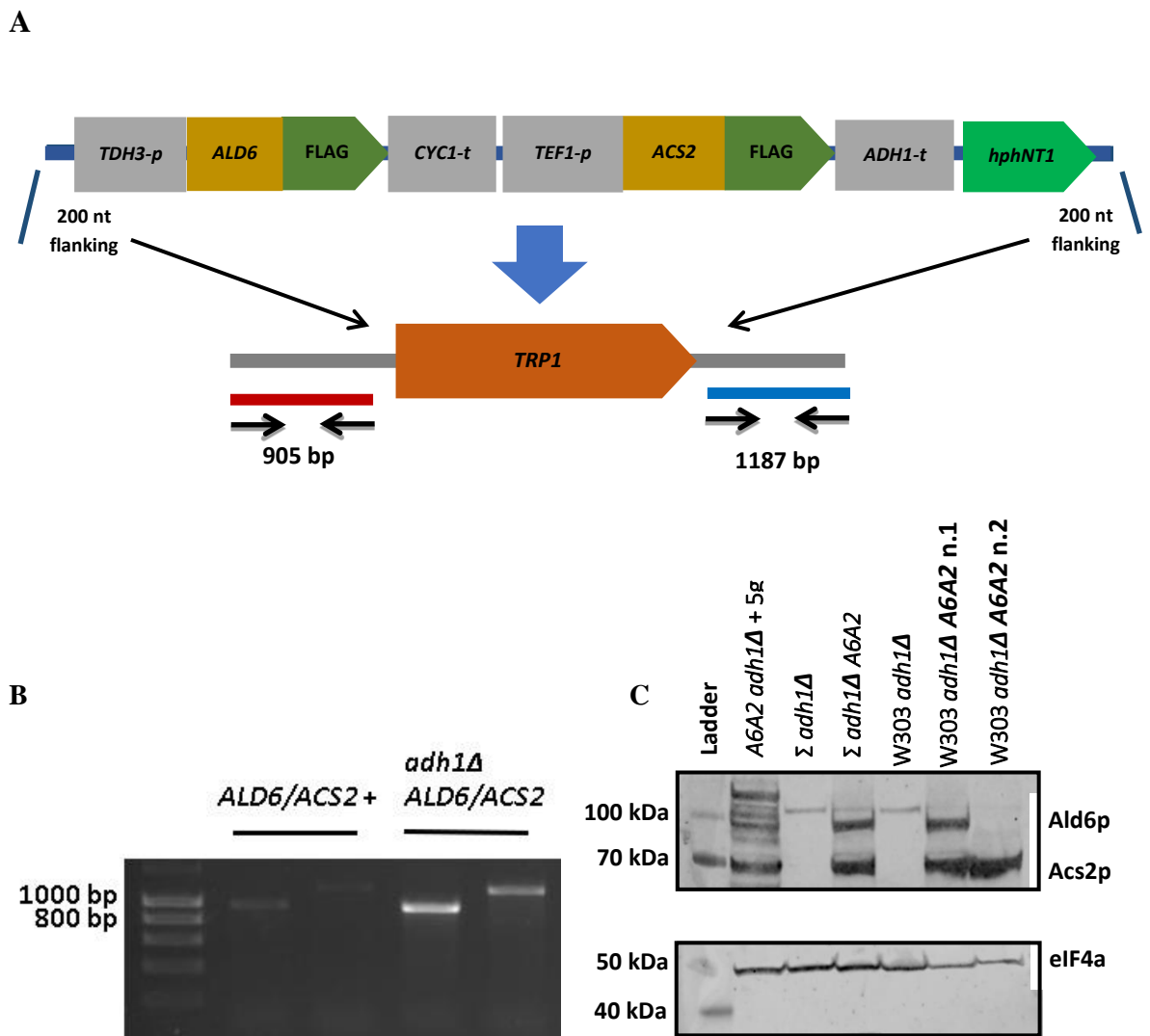


**Figure 9.3. Insertion and verification of Flag-tagged *ALD6* and *ACS2* genes in the *adh1Δ* filamentous strain.** A) Schematic representation of the insertion of the *ALD6/ACS2* expression cassette in the *S. cerevisiae TRP1* locus and expected product sizes of the confirmation PCR. B) Verification PCR displaying the expected bands of a transformed *adh1Δ* filamentous strain, with a W303-1A positive control. HyperLadder 1kb was used as a DNA size standard. C) Western Blot of protein extracts of strains harboring the *ALD6/ACS2* cassette, and their parental strains. Tif1p was used as a loading control. Numbered bands correspond to the protein ladder standard.

This set of experiments indicates that the constructed  $\Sigma 1278b$  A6A2 strain has the integrated cassette at the *TRP1* locus, and that the tagged gene products are being expressed in growing cells of this new strain.

#### **9.4 Expression of *ALD6* and *ACS2* reduces the ruffled colony phenotype in the *adh1Δ* filamentous strain**

Previously, it was observed that the deletion of *ADH1* in the haploid  $\Sigma 1278$  strain caused the formation of ruffled colonies that displayed pronounced surface wrinkles and were visually distinct to that of the WT (Figure 8.4). One possibility is that it might be caused by the accumulation of acetaldehyde in the mutant strain. To test this idea,  $\Sigma 1278b$  A6A2 colonies were streaked from solid YPD onto fresh YPD media and grown for 6 days to examine whether the expression of *ALD6* and *ACS2* affected colony morphology.

Colonies of the  $\Sigma 1278b$  A6A2 strain did not display the ruffled phenotype, unlike the *adh1Δ* strain with the Hygromycin B resistance marker present (*adh1Δ HygB<sup>R+</sup>*) or the  $\Sigma$  *adh1Δ* lacking the selection marker (*adh1Δ HygB<sup>R-</sup>*) (Figure 9.4). This result suggests that overexpression of *ALD6* and *ACS2* in the cell may be reducing the presence of a metabolite causing the induction of the ruffled phenotype, most likely acetaldehyde. In order to verify changes in metabolite accumulation in this new strain that may correlate with the phenotype change, an anaerobic fermentation experiment was performed.

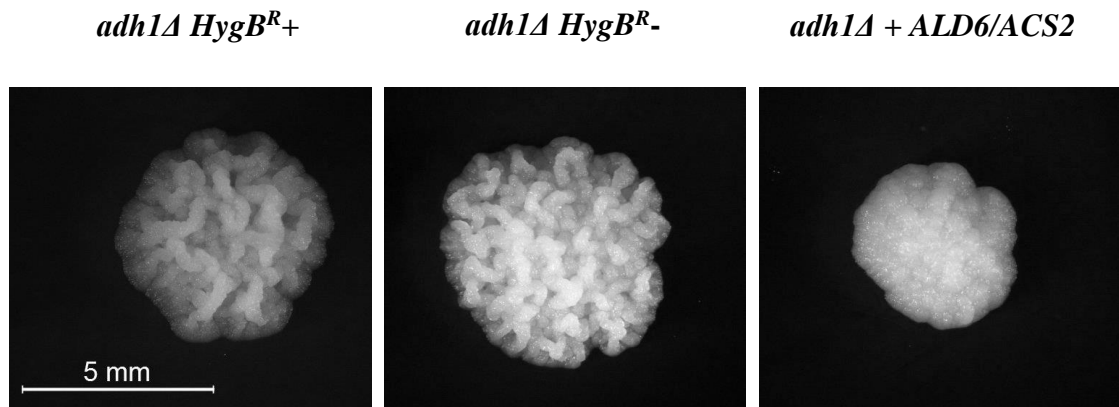


**Figure 9.4. Overexpression of *ALD6* and *ACS2* in a  $\Sigma$ 1278b *adh1Δ* strain disrupts its ruffled colony phenotype.** Colony morphology of  $\Sigma$ 1278b *adh1Δ* strains with, and without the Hygromycin B resistance marker, as well as an *adh1Δ* mutant overexpressing *ALD6* and *ACS2*. Cells in stationary phase were spotted on solid YPD and grown at 30°C for 7 days. Pictures were taken in a Leica L2 (Leica microsystems) stereomicroscope at 10x magnification. Colonies shown are representative of the morphology of single colonies. Scale bar is 5 mm in length.

## 9.5 Expression of *ALD6* and *ACS2* reduces 1-butanol and acetaldehyde accumulation in an *adh1Δ* strain

The aim of expressing the *ALD6* and *ACS2* genes in the filamentous *adh1Δ* strain was to test if overexpression of these enzymes could reduce acetaldehyde accumulation, and whether this has any effect on endogenous butanol production. Acetaldehyde, butanol and ethanol accumulation were measured in the *adh1Δ* and *A6A2* strains of the  $\Sigma$ 1278b and W303-1A backgrounds by gas chromatography using samples collected over a 14-day period from yeast cultures grown in semi-anaerobic conditions.

Acetaldehyde accumulation in the W303-1A *adh1Δ* strain started rising on day 2, reaching  $0.58 \pm 0.09$  g/l, then decreasing on day 4 and peaking again on day 7 at  $1.00 \pm 0.09$  g/l, and finally stabilizing around  $0.52 \pm 0.06$  g/l starting from day 11 onwards (Figure 9.5 A). The W303-1A *ALD6/ACS2* showed a similar behavior on day 2, accumulating  $0.66 \pm 0.06$  g/l of acetaldehyde, but from day 4 onwards acetaldehyde concentration started decreasing until no acetaldehyde was detected starting from day 7 (Figure 9.5 A), indicating that the overexpression of *ALD6* and *ACS2* was able to reduce acetaldehyde accumulation in the W303-1A *adh1Δ* strain.

Interestingly, the overexpression of *ALD6* and *ACS2* also affected butanol accumulation in the W303-1A strain. While butanol concentration in the parental strain rose until it reached a stable concentration of  $40.29 \pm 10.35$  mg/l on day 7, little, if any, butanol was detected in the *A6A2* strain (Figure 9.5 B). These results suggest a relationship between acetaldehyde accumulation in the W303-1A *adh1Δ* strain and its ability to synthesize butanol by the endogenous pathway.

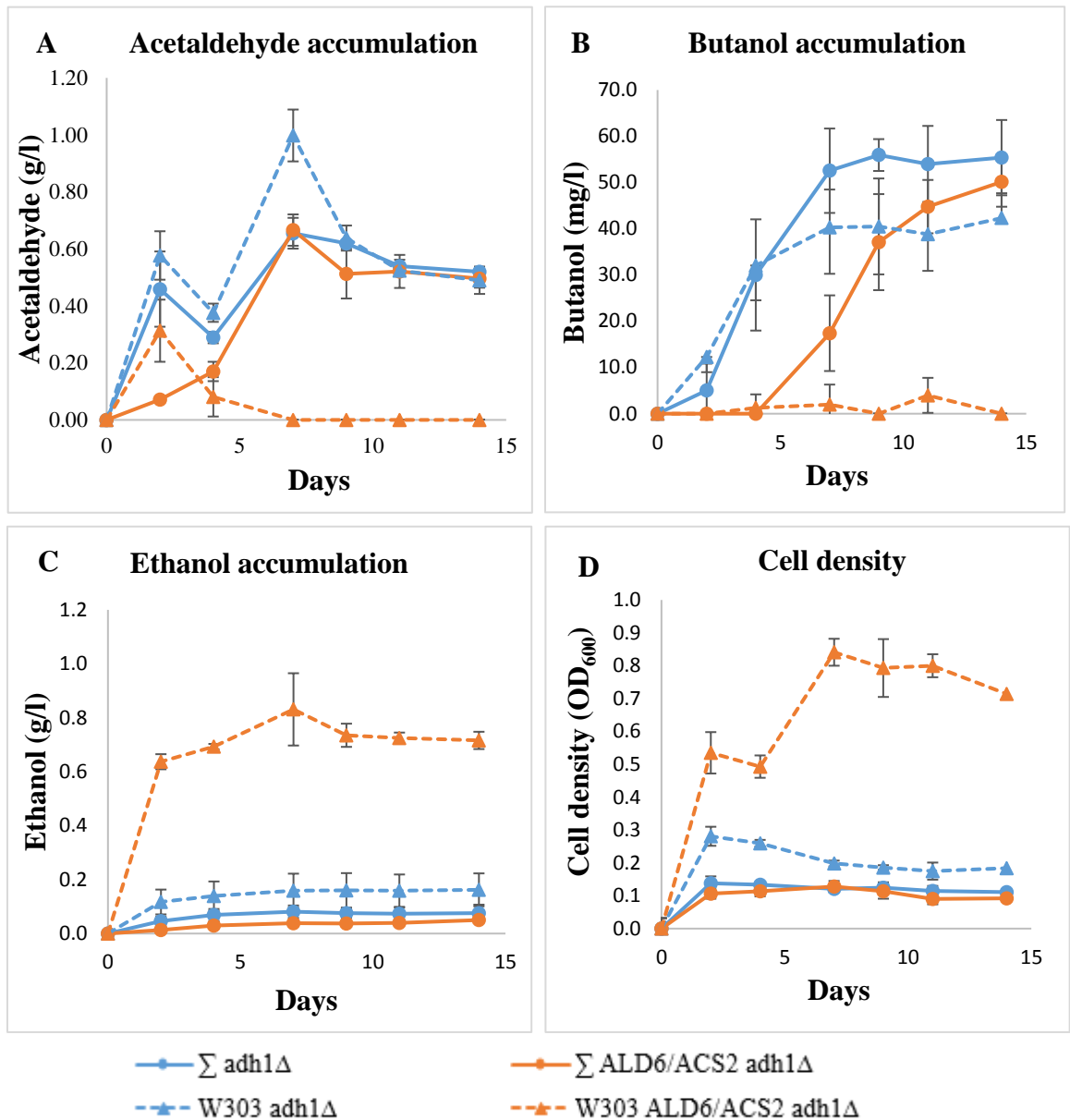


**Figure 9.5 Insertion of the *ALD6* and *ACS2* genes abolishes 1-butanol and acetaldehyde accumulation in the non-filamentous *adh1Δ* strain.** Concentration of A) acetaldehyde, B) 1-butanol and C) ethanol in a 14-day semi-anaerobic fermentation experiment was measured by gas chromatography. D) Cell density of the cultures was measured by spectrophotometry at 600 nm. Plot points correspond to mean ( $\pm$ SD) of 5 biological replicates.

In contrast, both acetaldehyde and butanol accumulation were less affected by the introduction of the *ALD6/ACS2* cassette in the  $\Sigma 1278b$  strain. The  $\Sigma 1278b$  *adh1Δ* strain accumulated acetaldehyde in a fashion similar to its W303-1A counterpart, reaching a small peak on day 2 of  $0.46 \pm 0.13$  g/l, then a higher peak on day 7 of  $0.66 \pm 0.05$  g/l and finally stabilizing at  $0.54 \pm 0.02$  g/l on day 11 (Figure 9.5 A).

Acetaldehyde accumulation in the  $\Sigma 1278b$  A6A2 strain was much lower on day 2, reaching only  $0.07 \pm 0.01$  g/l, but unlike the W303-1A strain, it rose until it reached  $0.67 \pm 0.06$  g/l on day 7 before stabilizing at  $0.52 \pm 0.06$  g/l on day 11 (Figure 9.5 A).

As stated above, butanol concentrations were also affected by the expression of *ALD6* and *ACS2* in the  $\Sigma 1278b$  *adh1Δ* strain. While the parental strain started accumulating  $5 \pm 12$  mg/l of butanol on day 2, the first signs of butanol in the  $\Sigma 1278b$  A6A2 strain were detected on day 7 ( $17 \pm 10$  mg/l) (Figure 9.5 B). It is important to notice that butanol concentration in the *adh1Δ* strain stopped rising on day 9, while butanol concentration in the A6A2 strain continued rising until day 14, when concentrations in both  $\Sigma 1278b$  strains reached ~50 mg/l.

These findings indicate that acetaldehyde accumulation is differentially affected by overexpression of *ALD6* and *ACS2* in the  $\Sigma 1278b$  and W303-1A strains, and that butanol production depends, to some degree, on acetaldehyde accumulation. Further experiments will be required to identify the factors that cause this difference between the strains, and to determine what is the role of acetaldehyde in endogenous butanol production.

Another difference with the W303-1A A6A2 strain compared with the other tested strains is that it accumulates more ethanol. While both *adh1Δ* strains and the  $\Sigma 1278b$  A6A2 only accumulate up to ~0.08 g/l of ethanol starting from day 2, the W303-1A A6A2 strain accumulates up to  $0.83 \pm 0.13$  g/l ethanol on day 7, approximately one order of

magnitude higher than the rest of the strains (Figure 9.5 C). This high ethanol yield is matched by an increase in culture growth, as evidenced by its peak cell density of  $0.841 \pm 0.03$  on day 7, nearly eight-fold of the peak cell density of  $0.138 \pm 0.01$  registered for the *adh1Δ* strain (Figure 9.5 D). In contrast, expression of *ALD6* and *ACS2* in the  $\Sigma 1278b$  *adh1Δ* strain did not improve cell growth, as cell density from both  $\Sigma 1278b$  strains remained around  $OD_{600}$  0.1 for the whole experiment.

These results suggest that expression of *ALD6* and *ACS2* was able to rescue fermentative metabolism in the W3031-1A *adh1Δ* strain. This reactivation of ethanol production may be the responsible for the loss of butanol production in this strain, as acetaldehyde accumulation seems to be necessary for it to occur.

#### **9.6 Overexpression of *ALD6* and *ACS2* in *adh1Δ* strains reduces R,R-2,3-butanediol accumulation.**

As well the conversion of acetaldehyde to acetyl-CoA mediated by Ald6p and Acs2p, an alternative metabolic fate for acetaldehyde in the *adh1Δ* strains is its conversion to 2,3-BDO catalyzed by Pdc1p and Bdh1p. In the last step of this process, reduction of acetoin to 2,3-BDO oxidizes NADH back to  $NAD^+$ , relieving the redox imbalance caused by the deletion of *ADHI* (Figure 9.1). Although beneficial to the cell, the accumulation of 2,3-BDO in *adh1Δ* strains removes acetaldehyde from entering a putative endogenous butanol-producing pathway. Hence, in order to relate the presence of 2,3-BDO isomers to the differences in butanol and acetaldehyde accumulation observed in the *adh1Δ* and *A6A2* strains, the concentration of R,R-2,3-BDO and R,S-2,3-BDO were measured on day 14 of the semi-anaerobic fermentation experiment described above.

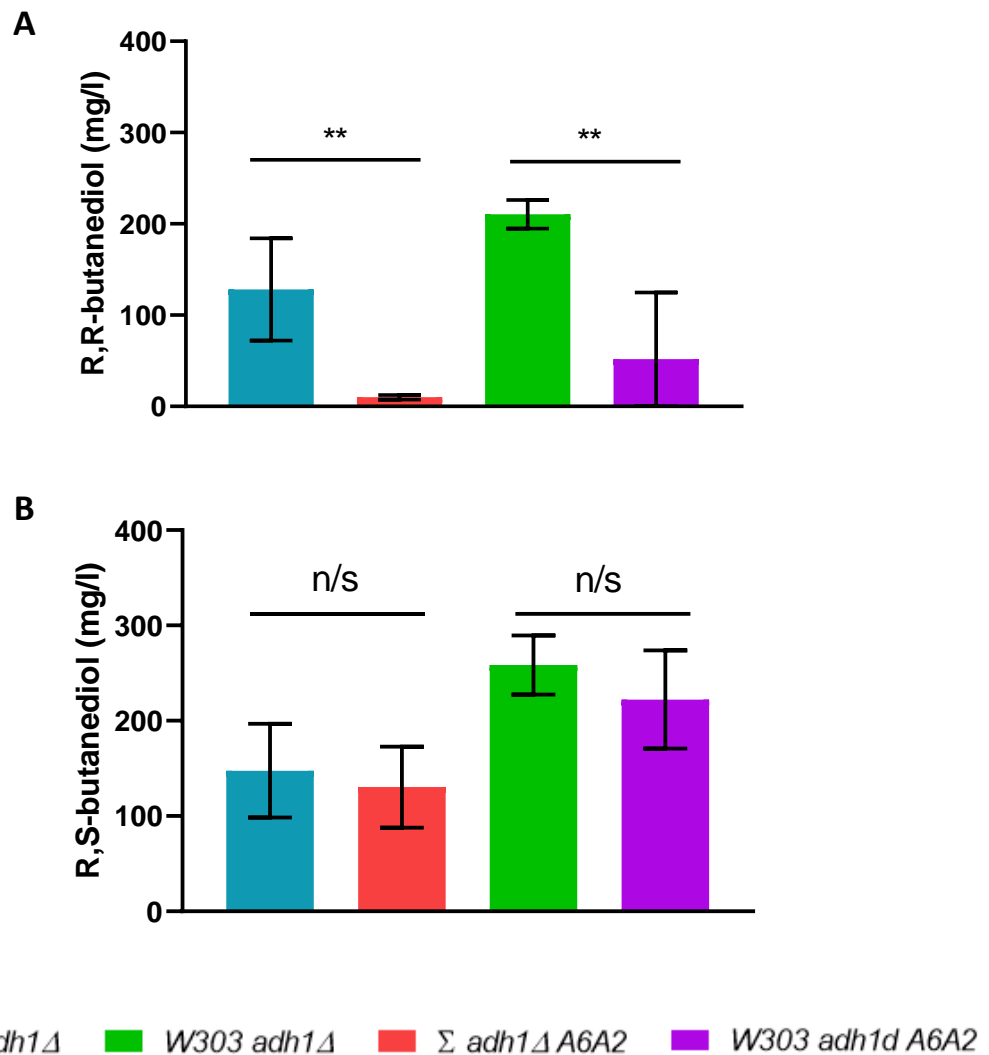


**Figure 9.6 Overexpression of *ALD6* and *ACS2* reduces accumulation of R,R-butenediol in the *adh1Δ* strains.** Concentration of A) R,R-butenediol and B) R,S-butenediol on day 14 of a semi-anaerobic fermentation experiment measured by gas chromatography. Plot points correspond to mean ( $\pm$ SD) of 5 biological replicates. Asterisks indicate statistical significance from Welch's t-test. \*\* means p-value < 0.05 and n/s means non-significant.

R,R-2,3-BDO concentrations on day 14 were  $128 \pm 56$  mg/l in the  $\Sigma 1278b$  *adh1Δ* strain and  $210 \pm 16$  mg/l in the W303 *adh1Δ* (Figure 9.6 A). This difference in R,R-2,3-BDO concentration between the strains was statistically significant, suggesting that the W303-1A strain accumulates more of this alcohol. A similar difference was observed for R,S-2,3-BDO accumulation, as measured concentrations for this isomer on day 14 were  $148 \pm 49$  mg/l and  $259 \pm 31$  mg/l, similar in magnitude to the difference observed for R,R-2,3-BDO and also statistically significant (Figure 9.6 B). These readings show that the W303 strain accumulates more 2,3-BDO isomers than the  $\Sigma 1278b$  strain after 14 days of semi-anaerobic fermentation.

When *ALD6* and *ACS2* were overexpressed to the *adh1Δ* strains there was a significant decrease in R,R-2,3-BDO produced by both strains on day 14. In the  $\Sigma 1278b$  strain R,R-2,3-BDO concentration drops to  $10 \pm 3$  mg/l, while in the W303 strain they reach  $52 \pm 74$  mg/l (Figure 9.6 A). On the other hand, R,S-2,3-BDO concentrations decrease only slightly, with measured values of  $130 \pm 43$  mg/l and  $222 \pm 52$  mg/l for the filamentous and non-filamentous strain, respectively (Figure 9.6 B). Given the fact that R-acetoin, the precursor for R,R-2,3-BDO, can be synthesized by *PDC1* using two molecules of acetaldehyde, or acetaldehyde and pyruvate (Bornemann et al., 1993), and that acetaldehyde accumulation is reduced to zero in the W303 A6A2 strain, these results suggest that the overexpression of *ALD6* and *ACS2* in the W303 *adh1Δ* strain indirectly reduces R,R-2,3-BDO by depleting cytosolic acetaldehyde.

It is interesting that R,R-2,3-BDO accumulation is also reduced in the  $\Sigma 1278b$  A6A2 strain despite acetaldehyde concentrations matching that of its parental strain on day 14 of anaerobic fermentation (Figure 9.5 A). This indicates that in this strain, the decrease in R,R-2,3-BDO cannot be attributed to acetaldehyde depletion. Thus, there must be other

differences between both A6A2 strains that should explain this effect on 2,3-BDO accumulation, such as differences in enzyme expression or activity.

### **9.7 Investigating the potential of yeast pyruvate decarboxylase enzymes as alternative switches for endogenous butanol production**

Another approach to investigate the potential role of acetaldehyde in endogenous butanol production and colony morphology involves the deletion of other glycolytic genes to attempt to mimic the effects of *ADHI* deletion. One potential target for this approach is to hinder the decarboxylation of pyruvate to acetaldehyde by deleting the yeast pyruvate decarboxylase genes *PDC1*, *PDC5*, and *PDC6*. This strategy would allow us to discern if butanol accumulation and formation of complex colonies in the filamentous strain are acetaldehyde-dependent or if disruption of glycolysis at a different step is enough to induce these changes.

One important note regarding this strategy is that expression of *PDC5* is induced when *PDC1* is absent (Eberhardt et al., 1999), compensating the attempt to hinder cellular pyruvate dehydrogenase activity. A *pdc1Δ, pdc5Δ* double deletion strain should have its pyruvate decarboxylase activity impaired (Hohmann, 1991), serving as a better candidate to test any effects on 1-butanol accumulation. While *PDC6* is not normally expressed, it has been reported to be highly expressed under sulfur-limiting conditions (Boer et al., 2003), thus at this stage it would be the last candidate for deletion. Additionally, it is best to avoid the need to test a *PDC* triple deletion strain, as it results in slow growth in medium containing glucose (Hohmann, 1991; Flikweert et al., 1996), forcing the need to change the carbon source in the fermentation medium from glucose to ethanol and glycerol.

Thus, the next section of this project will deal with testing if disruption of pyruvate decarboxylation by first deleting the major pyruvate decarboxylase *PDC1* and *PDC5* results in butanol accumulation in *S. cerevisiae*.

### 9.8 Deletion of *PDC1* in haploid $\Sigma$ 1278b and W303 strains and construction of a diploid *pdc1* $\Delta$ strain

Deletion of *PDC1* in haploid  $\Sigma$ 1278 and W303 haploid strains was carried out using the same strategy employed for the deletion of *ADHI* (See section 8.2). A disruption cassette was amplified by PCR from the pZC3 plasmid (Carter and Delneri, 2010) using oligonucleotides designed to direct the cassette towards the *PDC1* ORF (Table 6.3). Parental  $\Sigma$ 1278b and W303 haploid strains were then transformed with the cassette and selected on solid YPD supplemented with 300  $\mu$ g/ml Hygromycin B.

Genomic DNA was extracted from potential transformants and insertion of the HygB<sup>R</sup> selection marker in the *PDC1* locus was verified using a set of three PCR reactions directed towards the flanking regions of the *PDC1* locus and the internal HygB<sup>R</sup> marker. The selected oligonucleotide pairs used in each reaction and their expected product size in a successful deletion are summarised in table 9.1.

**Table 9.1. Oligonucleotides used for the verification of the deletion of *PDC1***

Reaction	Oligonucleotides used	Expected band size (bp)
1	PDC1 VER FW + HYGB VER RV	545
2	PDC1 VER RV + HYGB VER FW	400
3	PDC1 VER FW + PDC1 VER RV	2164

A 1% w/v agarose gel shows that each of the three reactions performed in one of the potential transformants from both the  $\Sigma$ 1278b and W303 backgrounds resulted in product bands of the expected sizes, indicating that the deletion of *PDC1* was successful in both instances (Figure 9.7 A). In contrast, each of the parental strains compared to their respective parental strains only had a product in reaction 3, demonstrating the absence of the *HygB<sup>R</sup>* selection marker and the presence of the *PDC1* gene.

Additionally, a diploid  $\Sigma$ 1278b *pdc1Δ* was made by transforming the corresponding haploid *pdc1Δ* strain with the HO endonuclease-containing plasmid pAS54 (Table 6.2) in the same way as with the *adh1Δ* strain (See section 7.3). After transformation, cells were grown in plasmid selection media until colonies formed, and then transferred to rich media to encourage loss of the plasmid and removing HO from the new yeast cells.

In addition to the above PCR verification, a drug resistance assay was used to confirm the replacement of the *PDC1* gene with the *HygB<sup>R</sup>* selection marker. In the same manner as with the *adh1Δ* strains, serial dilutions of each of the constructed *pdc1Δ* strains were spotted on solid YPD media containing Hygromycin B in order to verify their ability to grow in presence of this antibiotic. Both the haploid and diploid *pdc1Δ* strains were able to grow in the presence of the antibiotic, as evidenced by the growth of colonies across serial dilutions (Figure 9.7 B).

Finally, a mate-testing assay was used to verify the identity of the constructed haploid and diploid *pdc1Δ* strains. The haploid *pdc1Δ* strain produced a halo only in the a-tester plate, revealing that it secretes the same *MATa* mating factor of its parental strain (Figure 9.7 C). On the other hand, the absence of a halo in either tester plate seen in the diploid *pdc1Δ* strain suggests that it does not secrete any mating factors, thus verifying its diploid status (Figure 9.7 C).

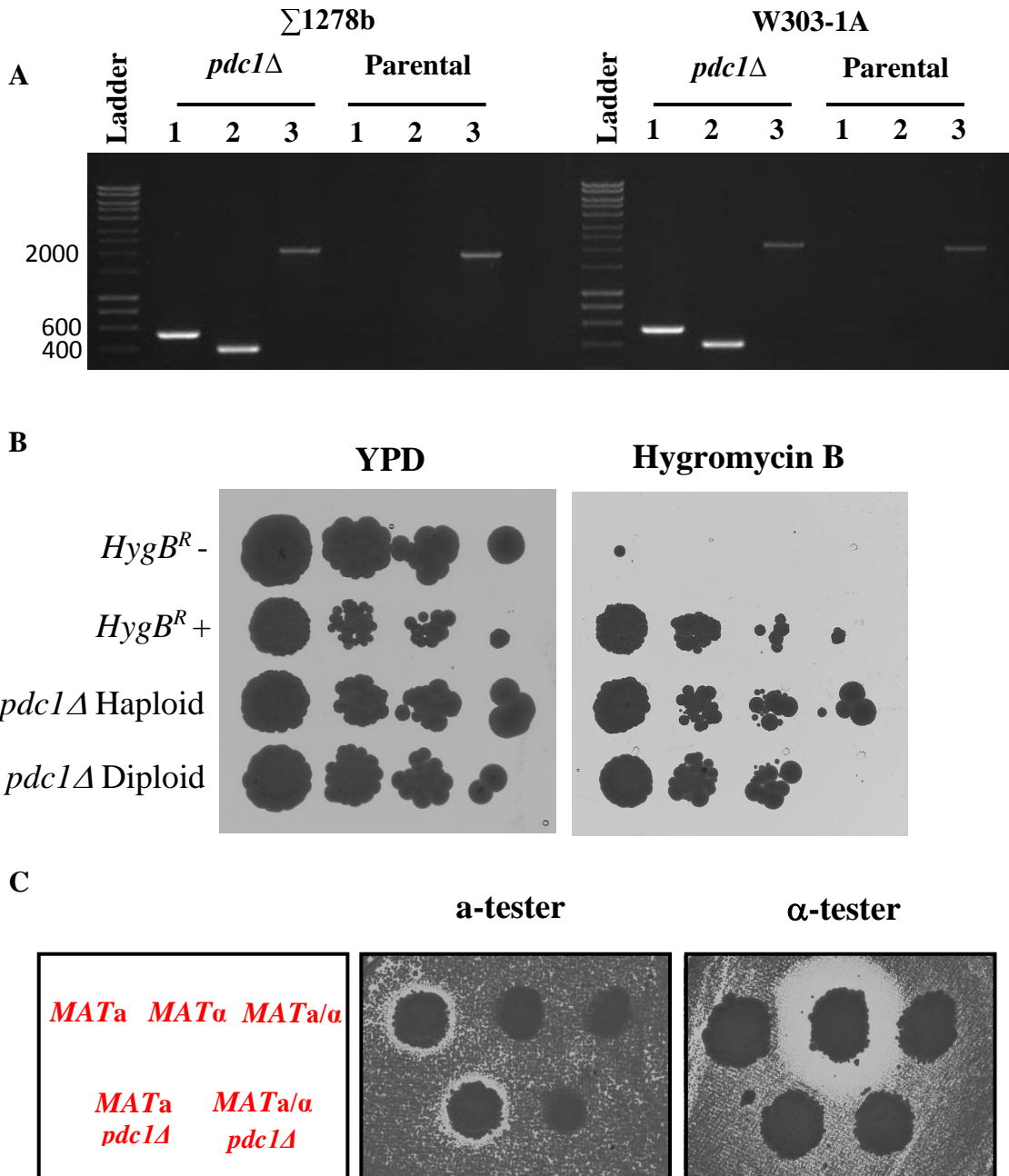


**Figure 9.7. Verification of *PDC1* deletion and mate testing of haploid and diploid  $\Sigma 1278b$  strains.** A) 1% (w/w) agarose gel electrophoresis shows the products of the three *PDC1* deletion verification reactions in both  $\Sigma 1278b$  and W303-1A strains. DNA ladder used was HyperLadder 1kb. B) Drug sensitivity assay for haploid and diploid *pdc1Δ* filamentous strains. Serial dilutions of stationary liquid cultures of each tested strain were spotted on the indicated media and left to grow at 30°C for 2 days. C) Phenotypic mate type test on a  $\Sigma 1278b$  *pdc1Δ* strain transformed with an HO-bearing plasmid. Cells were spotted onto solid YPD containing a lawn of each tester strain and left to grow for 2 days before taking pictures.

Together, these three experiments confirm the construction of haploid *pdclΔ* strains in the  $\Sigma$ 1278b and W303-1A backgrounds, as well as an isogenic *pdclΔ* diploid strain in the  $\Sigma$ 1278b background. These three strains will be used to study the impact of this deletion on 1-butanol accumulation in both genetic backgrounds, and its effect on the filamentous phenotypes of the  $\Sigma$ 1278b strains.

### **9.9 Deletion of *PDC1* alone does not induce 1-butanol accumulation in either $\Sigma$ 1278b or W303-1A strains.**

The next step after verifying the construction of the new *pdclΔ* was to test if these strains were able to accumulate 1-butanol like the *adh1Δ* mutants, in which disruption of alcoholic fermentation resulted in accumulation of acetaldehyde and production of 1-butanol in anaerobic conditions. To test this hypothesis, a 14-day anaerobic fermentation experiment in liquid YPD media was conducted to measure ethanol, acetaldehyde, and butanol accumulation in the *pdclΔ* and *adh1Δ* haploid strains of the  $\Sigma$ 1278b and W303-1A backgrounds, compared to their respective parental strains.

Gas chromatography detection of volatile analytes during the 14 days of anaerobic fermentation revealed that butanol accumulation in both *pdclΔ* strains was similar to their respective parental strains. The  $\Sigma$ 1278b and W303-1A mutant strains produced a maximum of  $3 \pm 0$  mg/l and  $4 \pm 1$  mg/l of 1-butanol on day 11, respectively, while the corresponding *adh1Δ* strains accumulated up to  $117 \pm 21$  mg/l and  $82 \pm 21$  mg/l of 1-butanol on day 14 (Figure 9.8 A).

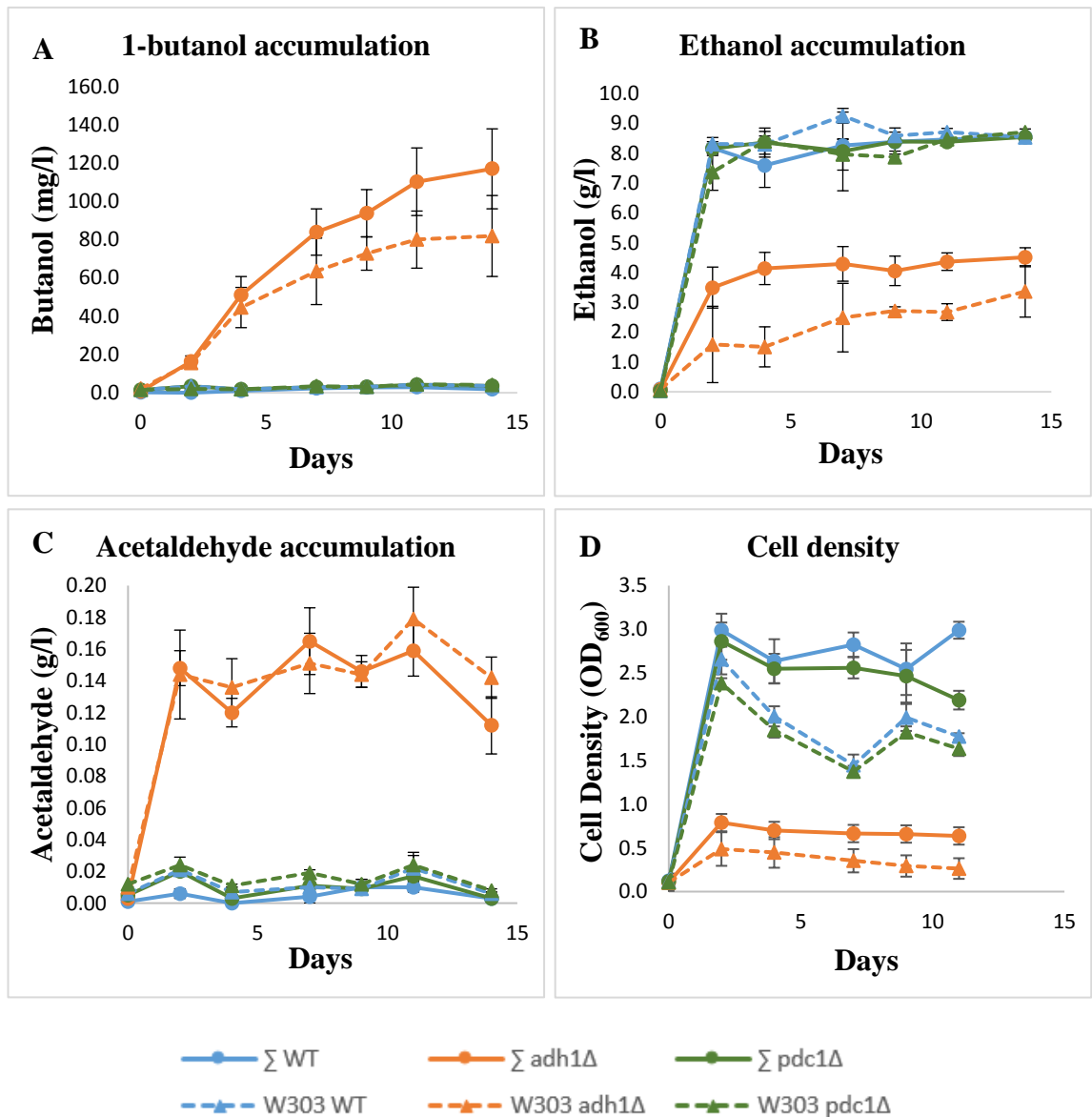


**Figure 9.8. Deletion of *PDC1* does not have an impact on ethanol, butanol or acetaldehyde accumulation in *S. cerevisiae*.** Concentration of A) 1-butanol, B) ethanol and C) acetaldehyde produced by eight *S. cerevisiae* strains grown semi-anaerobically in liquid YPD for 14 days was measured by gas chromatography. D) Cell density of the cultures was measured by spectrophotometry at 600 nm. Plot points correspond to mean ( $\pm$ SD) of 5 biological replicates.

As expected from the previous observation, ethanol production in the *pdclΔ* strains closely matched ethanol accumulation in the parental strains, reaching values of  $\approx 8.5$  g/l on day 14, unlike the  $\Sigma 1278b$  and W303-1A *adh1Δ* strains, which only managed to produce up to  $4.5 \pm 0.3$  g/l and  $3.4 \pm 0.9$  g/l, respectively (Figure 9.8 B).

In line with the observed levels of ethanol, acetaldehyde did not accumulate in the *pdclΔ* strains to the same levels as in the *adh1Δ* strains. The maximum acetaldehyde concentration measured in the *pdclΔ* strains was  $0.02 \pm 0.01$  mg/l on day 11, similar to the W303-1A parental strain which measured  $0.02 \pm 0.02$  mg/l on the same day (Figure 9.8 C). On the other hand, the highest value in the *adh1Δ* strains was  $0.179 \pm 0.02$  mg/l on day 11, about 9 orders of magnitude higher than the *pdclΔ* strains (Figure 9.8 C).

Finally, the high levels of ethanol produced by the *adh1Δ* strains also correlated with healthy cell growth under anaerobic conditions as evidenced by the cell density measurements taken during the experiment. For instance, the cell density peak of the  $\Sigma 1278b$  parental and *pdclΔ* strains was on day 2 with  $3.0 \pm 0.2$  and  $2.9 \pm 0.2$ , while their respective *adh1Δ* peaked at  $0.8 \pm 0.1$  on the same day (Figure 9.8 D). A similar trend was observed for the W303-1A strains, in which peak cell density for the parental and *pdclΔ* strains was  $2.7 \pm 0.2$  and  $2.4 \pm 0.1$  on day 2, compared to the measly peak of  $0.5 \pm 0.2$  for the *adh1Δ* strain.

This set of results shows that deletion of *pdclΔ* was unable to disrupt ethanol production and induce endogenous 1-butanol production in any of the tested yeast strain backgrounds.

## 9.10 Construction and analysis 1-butanol accumulation in of *pdc1,5Δ* yeast strains

Given that none of the constructed *pdc1Δ* strains accumulated butanol or had their ethanol accumulation disrupted, it is likely that *PDC5* and *PDC6* can efficiently compensating for the loss of *PDC1*. Thus, in an attempt to produce a stronger disruption of the decarboxylation of pyruvate, *pdc1,5Δ* strains in the  $\Sigma$ 1278b and W303-1A were constructed and tested for metabolite accumulation during anaerobic fermentation.

Deletion of *PDC5* was performed using a gene disruption cassette directed to the flanking regions of the *PDC5* locus. The cassette was amplified by PCR from the pZC2 plasmid (Carter and Delneri, 2010) using the appropriate oligonucleotide pair (Table 6.3) to produce a cassette that replaces *PDC5* with the *natNT2* selection marker. Cells were transformed with each insertion cassette and transformants were selected on rich media supplemented with 100  $\mu$ g/ml nourseotricine.

Replacement of the *PDC5* ORF with the *natNT2* marker was then verified by extracting genomic DNA from potential transformants and using a series of PCR reactions directed towards the flanking regions of the *PDC5* locus, and the internal *natNT2* marker. The oligonucleotides used for each of the three verification reactions and the expected products for a successful integration are summarised in Table 9.2.

Due to difficulties experienced during the construction of a successful *pdc1,5Δ* strain in the W303-1A background, a different transformation and verification strategy was employed. The *pdc1Δ* W303-1A strain was transformed with the PCR product from the Reaction 3 of the *PDC5* deletion verification in a verified *pdc5Δ* W303-1A transformant.

**Table 9.2. Oligonucleotides used for the verification of the deletion of *PDC5***

Reaction	Oligonucleotides used	Expected band size (bp)
1	PDC5 VF + NAT VR	854
2	PDC5 VR + NAT VF	481
3	PDC5 VF + PDC5 VR	1750

This PCR product spans the entire *PDC5* ORF, extending a few base pairs longer than the other cassette. The *pd5Δ* W303-1A strain was then transformed with this cassette and potential transformants were verified by PCR using a new set of oligonucleotides, resulting in different expected PCR product sizes for each of the reactions (Table 9.3).

**Table 9.3. Oligonucleotides used for the verification of the deletion of *PDC5* in the *pd5Δ* W303-1A strain**

Reaction	Oligonucleotides used	Expected band size (bp)
1	PDC5 VF LONG + NAT VR	916
2	PDC5 VR LONG + NAT VF	581
3	PDC5 VF LONG + PDC5 VR LONG	1926

Agarose gel electrophoresis showed that the deletion of *PDC5* was successful in the  $\Sigma$ 1278b and W303-1A backgrounds, as seen by the three bands of the expected sizes (Figure 9.10). Although faint, the reaction 2 bands of 481 kb are present in both *pd5Δ* strains.

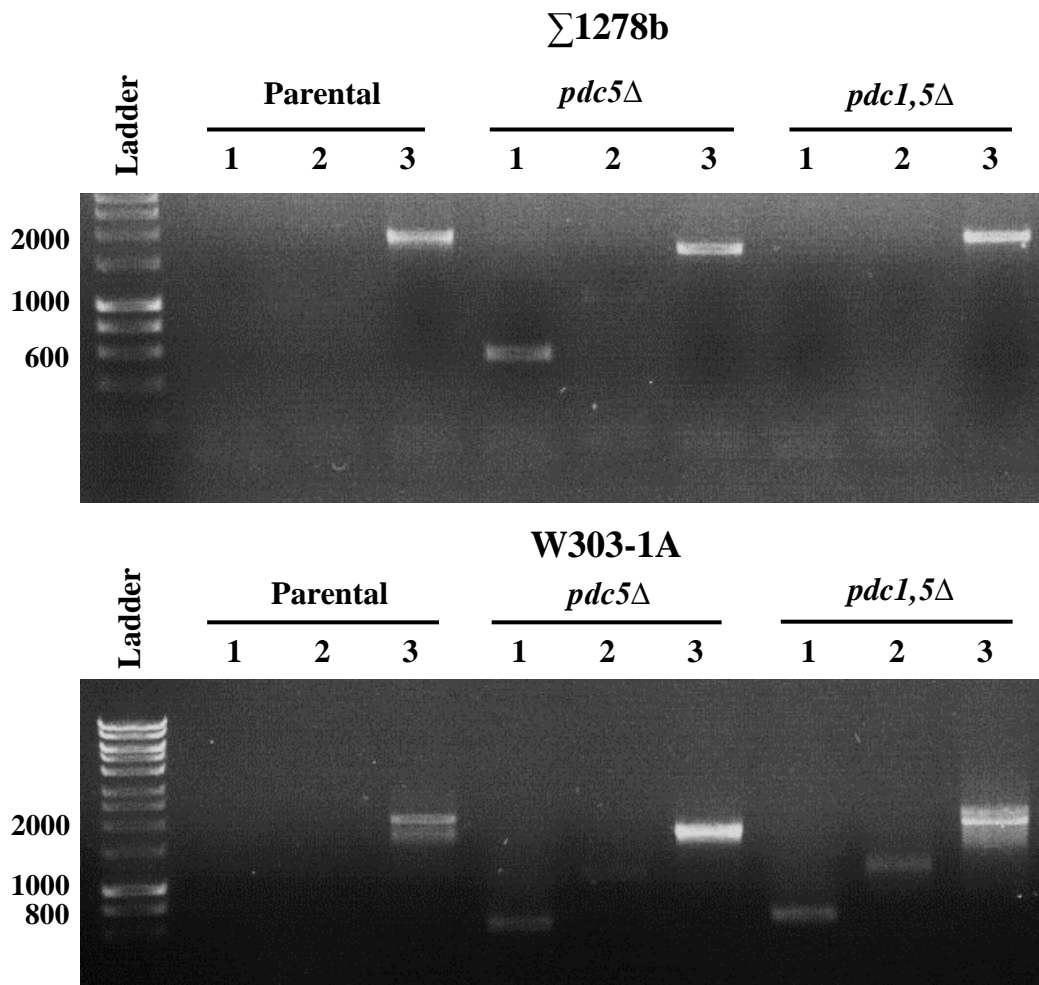


**Figure 9.10. Verification of *PDC5* deletion in  $\Sigma$ 1278b and W303-1A haploid strains.** 1% w/w agarose gel electrophoresis shows the products of the three *PDC5* deletion verification reactions performed in parental, *pdc5Δ*, and *pdc1,5Δ* strains constructed in the  $\Sigma$ 1278b and W303-1A genetic backgrounds. DNA ladder used was HyperLadder 1kb.

On the other hand, the agarose gel revealed that the construction of a *pdcl,5Δ* strain was successful only in the W303-1A background, as the reaction bands 1 and 2 are not present for the  $\Sigma$ 1278b strain (Figure 9.10). Despite this, it was deemed important to proceed with measuring 1-butanol production in the newly constructed strains.

### **9.11 Double deletion of *PDC1* and *PDC5* was not able to induce 1-butanol accumulation in either $\Sigma$ 1278b or W303-1A strains.**

Following the construction of *pdc5Δ* and *pdcl,5Δ* mutants in the  $\Sigma$ 1278b and W303-1A strains, an anaerobic fermentation experiment was conducted to test the ability of these new strains to produce 1-butanol compared to the previously constructed *adh1Δ* strains.

The fermentation setup, sampling, and gas chromatography analysis of the collected samples was carried out as stated previously (See section 6.9), and included the *adh1Δ*, *pdclΔ*, *pdc5Δ*, and *pdcl,5Δ* strains constructed in the  $\Sigma$ 1278b and W303-1A backgrounds.

Analysis of the collected samples by gas chromatography showed that all of the *pdclΔ*, *pdc5Δ*, and *pdcl,5Δ* strains accumulated negligible amounts of 1-butanol, while the *adh1Δ*  $\Sigma$ 1278b and W303-1A mutants produced up to  $117 \pm 21$  mg/l and  $82 \pm 21$  mg/l on day 14, respectively (Figure 9.11 A). Ethanol accumulation in each of the *pdclΔ*, *pdc5Δ*, and *pdcl,5Δ* strains was higher than their respective *adh1Δ* mutants, sustaining concentrations of  $\sim 4.0$  g/l from day 4 onwards while the *adh1Δ* strains only accumulated up to  $\sim 2.0$  g/l (Figure 9.11 B). Interestingly, the *pdcl,5Δ*  $\Sigma$ 1278b strain displayed an ethanol concentration of  $0.86 \pm 0.68$  g/l on day 2, much closer to the *adh1Δ* than its W303-1A counterpart. Despite this observation, ethanol accumulation in this strain reached

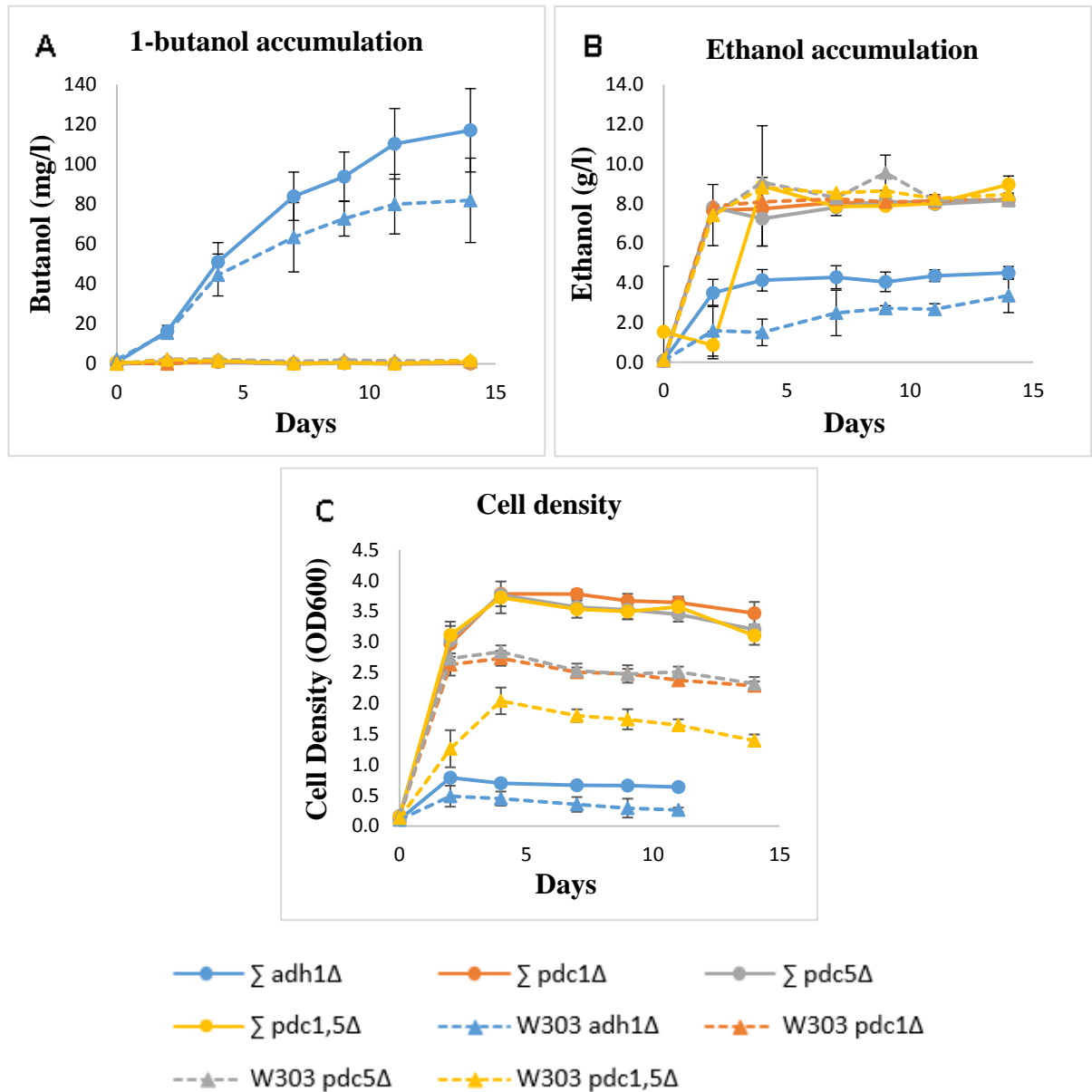


**Figure 9.11. Deletion of *PDC1*, *PDC5*, or *PDC1/5* does not result in 1-butanol production in *S. cerevisiae*.** Concentration of A) 1-butanol and B) ethanol produced by eight *S. cerevisiae* strains during a 14-day semi-anaerobic fermentation was measured by gas chromatography. D) Cell density of the cultures at each point was determined by spectrophotometry at 600 nm. Plot points correspond to mean ( $\pm$ SD) of 4 biological replicates.

values similar to the other PDC deletion strains, suggesting that the ethanol production deficiency observed was likely supplemented by PDC6.

The results of this experiment indicate that neither individual deletion of *PDC1* or *PDC5*, as well as the double deletion, were able to induce 1-butanol production in *S. cerevisiae*.

## 9.12 Discussion

The deletion of *ADH1* in *S. cerevisiae* results in the disruption of the fermentative metabolism of glucose, causing metabolic and redox imbalances that result the accumulation of 1-butanol and acetaldehyde (Si et al., 2014). Due to the high toxicity of the latter, the *ALD6* and *ACS2* genes were overexpressed in *adh1Δ*  $\Sigma$ 1278b and W303-1A strains in order to try to mitigate acetaldehyde accumulation by stimulating its conversion to acetyl-CoA. Then, endogenous 1-butanol production of these strains was assessed by gas chromatography.

Interestingly, overexpression of *ALD6* and *ACS2* resulted in a decrease in both acetaldehyde and 1-butanol in a background-dependent manner. Whilst the  $\Sigma$ 1278b strain displayed impaired accumulation of both metabolites, the W303-1A strain lost the ability to produce both butanol and acetaldehyde. R,R-butanediol accumulation was also decreased in *adh1Δ* strains overexpressing *ALD6* and *ACS2*, but unlike acetaldehyde, this decrease was similar between both strains. Finally, overexpression of *ALD6* and *ACS2* in the *adh1Δ*  $\Sigma$ 1278b strain was found to result in loss of the complex colony phenotype previously observed in this mutant.

While these results hinted at a potential role for acetaldehyde accumulation in the induction of 1-butanol in *S. cerevisiae* and the appearance of complex colonies in the  $\Sigma$ 1278b strain, additional experiments were conducted to explore alternative factors that

may yield similar phenotypes. Thus, deletions of *PDC1*, *PDC5*, and *PDC1,5* were constructed in each strain background to test if disruption of pyruvate decarboxylation, a mutation that does not result in acetaldehyde accumulation, could mimic the phenotypes observed in *adh1Δ* strains.

When tested for 1-butanol production, none of the *PDC* deletion strains were able to generate significant amounts of the fusel alcohol. This suggests that either these deletions were not enough to disrupt fermentative metabolism or that acetaldehyde accumulation resulting from the deletion of *ADHI* is required for the activation of 1-butanol production in our strains.

While it could be argued that a *PDC1,5,6* triple deletion would be necessary for an effective disruption of alcoholic fermentation due to enzymatic redundancy, such a strain may display deficient 1-butanol biosynthesis due to the central role of these enzymes in the reduction of  $\alpha$ -ketovalerate to butyraldehyde (Branduardi et al., 2013; Romagnoli et al., 2012). On the other hand, the deletion of *ADHI* is at a pivotal point for the activation of endogenous 1-butanol production because it sufficiently disrupts ethanol production without disrupting potential butyraldehyde reduction ability due to the presence of multiple yeast *ADH* enzymes (de Smidt et al., 2008).

One hypothesis that may explain this phenomenon is that as a response to the redox imbalances caused by the loss of *ADHI* function in the cell, the expression of other alcohol dehydrogenase genes is induced in an effort to compensate for the loss of NADH oxidase activity required to continue with glycolysis. While this hypothesis could be tested experimentally by performing multiple deletions of the NADH-requiring alcohol dehydrogenase genes in an *adh1Δ* strain and assessing 1-butanol production in each deletion strain, it could prove challenging to identify a single enzyme responsible for

butryaldehyde reduction due to enzymatic redundancy. For instance, a study published by Dickinson and colleagues that employed a similar approach to evaluate the formation of fusel alcohols in *S. cerevisiae* concluded that any one NADH-dependent yeast alcohol dehydrogenases (*ADH1-5*, and *SFA1*) were sufficient to sustain complex alcohol biosynthesis in *S. cerevisiae* (Dickinson et al., 2003).

The above arguments, in addition to the observations made in *ALD6/ACS2*-overexpressing strains from this project hint at a central role for acetaldehyde accumulation in the induction of endogenous 1-butanol production. One obvious question arising from this idea is what the mechanism through which acetaldehyde accumulation results in 1-butanol biosynthesis is.

As briefly mentioned above, one explanation could be that the metabolic and stress responses to acetaldehyde toxicity result in the expression of enzymes involved in amino acid catabolism. A study in 2003 reported that the yeast acetaldehyde stress response involved the expression of aldehyde dehydrogenase genes (*ALD*) induced by the Hsf1p and Msn4/2p general stress response transcription factors (Aranda and del Olmo, 2003). *ALD* enzymes oxidise acetaldehyde to acetic acid, which is in turn converted to acetyl-CoA by acetyl-CoA synthase enzymes (*ACS*) and fed into the tricarboxylic acid cycle (Figure 9.1).

Interestingly, the results obtained in this project showed that overexpression of *ALD6* and *ACS2* resulted in impaired 1-butanol and acetaldehyde accumulation in the W303-1A and  $\Sigma$ 1278b strains, indicating that *ALD* activity actually has a detrimental effect on 1-butanol biosynthesis in the tested strains.

Due to the number of pathways that handle acetaldehyde, the cellular mechanisms that arise to compensate the redox imbalance caused by *ADH1* deletion, and the lack of

knowledge on the exact enzymes involved in 1-butanol production, it would prove challenging to continue with a rational approach to address this question. Hence, the use of a high-throughput strategy to find candidate genes involved in the observed 1-butanol production in the tested strains will be explored in the following chapter of this work.

## 10. Transcriptomic analysis approach to the identification of potential genes involved in the endogenous production of 1-butanol in *S. cerevisiae*

### 10.1 Introduction

The experiments conducted in the previous chapter of this project were aimed towards elucidating the role of acetaldehyde accumulation and the deletion of *ADHI* in the induction of 1-butanol production in *S. cerevisiae*. While the results hinted at key role for the reduction of acetaldehyde to ethanol in activating this metabolic switch, no further insight was obtained about how the deletion of *ADHI* results in 1-butanol accumulation, nor about the mechanisms underlying the difference in levels obtained between the  $\Sigma$ 1278b and W303-1A strain backgrounds.

As previously stated in the general introduction, the current hypotheses in the literature that attempt to explain the endogenous production of 1-butanol in *S. cerevisiae* point at amino acid catabolism as the metabolic source of this and other fusel alcohols (Hazelwood et al., 2008). While two independent hypotheses propose that either a glycine-dependent or a threonine-dependent metabolic pathway is responsible for 1-butanol accumulation (Branduardi et al., 2013; Si et al., 2014), it is potentially more complicated than either scenario with the possibility that redundant as well as uncharacterised enzymes are involved (Swidah et al., 2018).

One avenue to explore the observed differences in different mutants and strain backgrounds is to assess the transcriptome in these different contexts.

Therefore, the aim of the work in this chapter was to assess the transcriptomic landscape of the *adh1* $\Delta$ , *adh1* $\Delta$  *ALD6/ACS2*, and *pdcl* $\Delta$  mutants constructed in the  $\Sigma$ 1278b and W303-1A strains of *S. cerevisiae* during anaerobic fermentation. The goal being to provide potential answers to two core questions: what are the mechanisms behind

the observed differences in 1-butanol production between the  $\Sigma$ 1278b and W303-1A strains? What are the changes that result in 1-butanol production in the *adh1* $\Delta$  and *ALD6/ACS2 adh1* $\Delta$  strains?

## 10.2 Preparation of RNA extracts from anaerobic cultures

The first step required to produce a transcriptomic analysis is the extraction and purification of RNA from the selected strains. To this end, anaerobic fermentation cultures of parental, *adh1* $\Delta$ , *adh1* $\Delta$  *ALD6/ACS2*, and *pdcl* $\Delta$  strains of the  $\Sigma$ 1278b and W303-1A backgrounds were set up in biological triplicates. On day 9 of the fermentation, an early point where 1-butanol is being produced (See figure 8.7), cell pellets were collected, and total RNA was extracted.

## 10.3 Sequencing and Quality Control analyses of *S. cerevisiae* RNA samples

As a routine part of RNA-seq experiments performed by the UoM Core Facility, quality control (QC) analyses are undertaken in order to assure data integrity and quality before further analysis (Conesa et al., 2016).

To this end, a series of QC analyses were performed using FastQC. This includes the number of reads per sample, a contamination screen mapping reads to multiple organism databases, and a principal component analysis (PCA) of the sample.

The average number of reads per sample was  $40.5 \pm 12.8$  million, with the highest RNA sample was DL37 (W303-1A WT) at 65.5 million reads and the lowest sample was DL32 ( $\Sigma$ 1278b *ALD/ACS2 adh1* $\Delta$ ) at 18.2 million reads (Figure 10.1 A). One of the first steps in data quality control is identifying samples that may not have enough sequencing depth to provide data to quantify the less abundant RNAs. The ENCODE consortium suggests a minimum of 20 million unique mapped reads for the precise quantification of

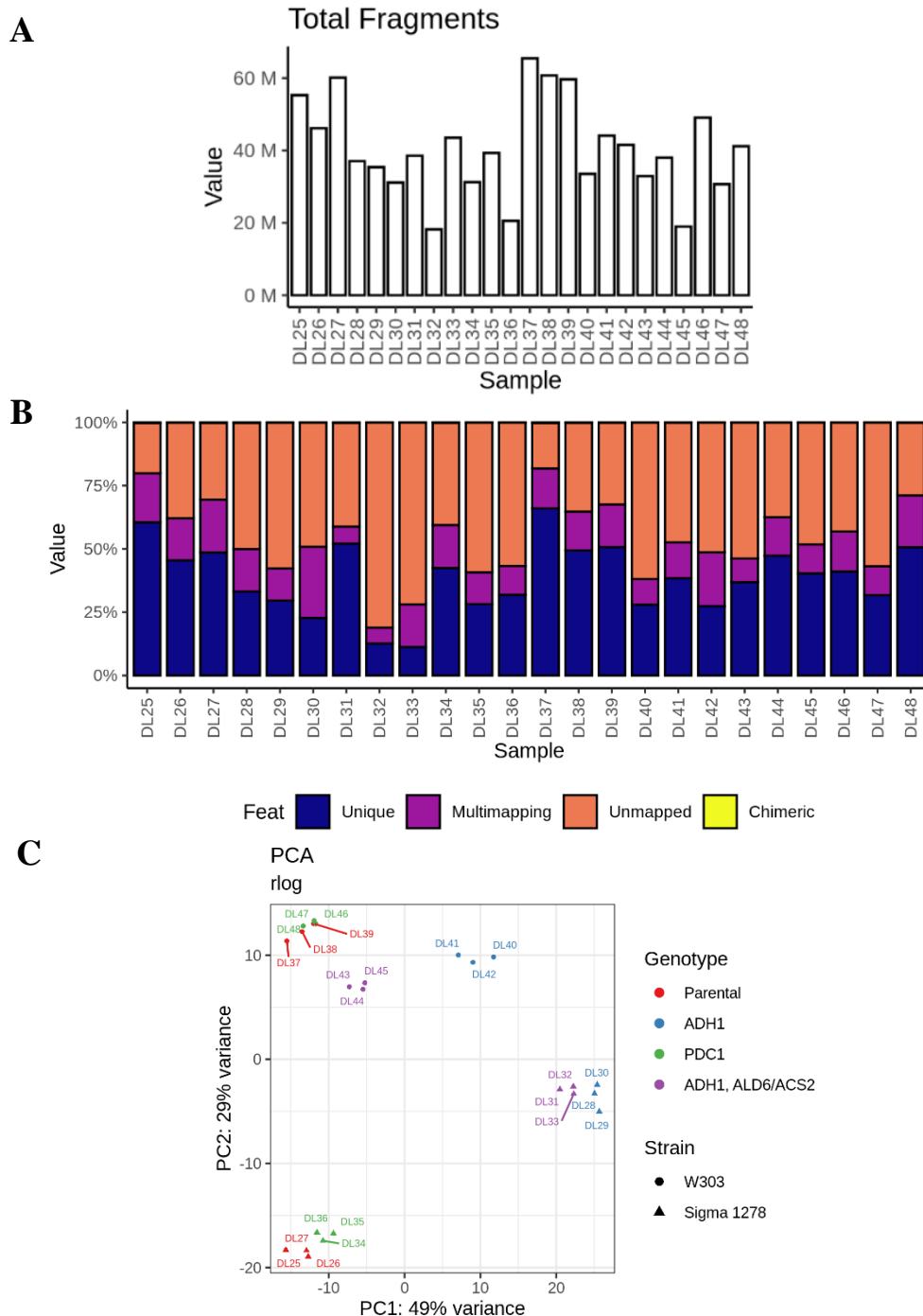


**Figure 10.1. Quality Control reports reveal contaminated RNA samples and grouping of samples by strain and genetic background.** A) Total number of reads per RNA sample, expressed as million reads. B) FastQC screen mapping of sequences to *S. cerevisiae* and other organisms' databases shows percentage sequences assigned to unique, multimapped, and unmapped sequences. C) Principal component analysis (PCA) of RNA samples from each biological replicate grown in anaerobic fermentation for 9 days. Sample labeling:  $\Sigma$  WT DL25-27,  $\Sigma$  *adh1* $\Delta$  DL28-30,  $\Sigma$  *A6A2 adh1* $\Delta$  DL31-33,  $\Sigma$  *cdc1* $\Delta$  DL34-36, W303 WT DL37-39, W303 *adh1* $\Delta$  DL40-42, W303 *A6A2 adh1* $\Delta$  DL43-45, W303 *cdc1* $\Delta$  DL46-48.

genes in human cell samples (ENCODE, 2011), but the yeast transcriptome is significantly less complex than human cells with lower gene numbers and reduced level of alternative splicing. Hence, published transcriptomic analyses for differential expression in *S. cerevisiae* have used as little as 11 million reads (Shekhawat et al., 2019).

While the total number of reads of each sample might seem sufficient for downstream analyses, it does not consider the possibility of sample contamination with extraneous RNAs. The presence of contaminant RNAs has a negative impact on sequencing depth by decreasing the number of effective *S. cerevisiae* mapped reads from the total number of reads.

The presence of potential contaminant RNAs was evaluated by mapping to a series of genome databases including model organisms using the STAR software. The resulting reads were plotted as unique, multi-mapped, unmapped, and chimeric, as percentages of the total reads for each sample. While the analysis showed that many of the samples had a percentage of uniquely mapped reads lesser than 50%, likely due to contamination with human RNA from sample handling during extraction (Figure 10.1 B), it does not necessarily indicate low-quality samples if there are enough *S. cerevisiae* gene reads to perform an analysis.

The third QC analysis performed in the anaerobic fermentation dataset was a principal component analysis (PCA) with the objective of observing the similarity across biological replicates.

The PCA plot showed that biological replicates clustered together, supporting their quality as accurate representations of each strain (Figure 10.1 C). Additionally, other clustering effects can be observed among some of the sequenced strains. For instance, there is an overlap between the parental and the *pdcl* $\Delta$  samples of both the  $\Sigma$ 1278b and

W303-1A background, suggesting that the deletion of *PDC1* had little impact on the transcriptome of each strain (Figure 10.1 C). Another overlap can be seen between the  $\Sigma$ 1278b *adh1* $\Delta$  and *ALD6/ACS2 adh1* $\Delta$  samples, again suggesting a close relationship between both transcriptomes (Figure 10.1 C).

These clustering effects reflect some of the previous observations made on the 1-butanol accumulation profiles of each strain under anaerobic fermentation, with the 1-butanol-producing strains (*adh1* $\Delta$  and *ALD6/ACS2 adh1* $\Delta$ ) positioned away from the non-producing strains (Parental and *pdc1* $\Delta$ ). Another interesting similarity is that the samples from the W303-1A *ALD6/ACS2 adh1* $\Delta$  strain, which in a previous experiment was unable to accumulate 1-butanol (Figure 9.5), are located closer to the parental strain than any of the 1-butanol-accumulating strains, further supporting a relationship between transcriptome and 1-butanol production.

Together, these initial tests show that samples clustered well among not only biological replicates, but also in respect to previous observations on 1-butanol production. Thus, the dataset was approved to proceed with the differential expression analysis.

#### **10.4 Differential expression analysis of RNA-seq data**

After quality control tests were completed on the sequenced RNA samples, the next step taken was to assess the differential expression of transcripts between the strains using the *DESeq2* package, with the objective of identifying individual transcripts or groups of transcripts that could be potentially related to the differences in 1-butanol production between the  $\Sigma$ 1278b and W303-1A strains and the activation of 1-butanol biosynthesis in the *adh1* $\Delta$  strains.

To this end, the ratio of the normalized counts of mutant-to-parental strains ( $\log_2$  fold-change) was calculated for each transcript in order to quantify their differential expression.

The differential expression datasets of each mutant strain of the  $\Sigma$ 1278b and W303-1A background were then interrogated further to identify potential transcripts of interests.

#### **10.4.1 Deletion of *PDC1* results in little transcriptomic change in either the $\Sigma$ 1278b or W303-1A backgrounds**

The first pair of strains studied in this manner were the *pdc1* $\Delta$  mutants of each background. The *pdc1* $\Delta$  mutant does not produce 1-butanol even though it might be anticipated that a *PDC1* deletion would have a similar consequence on cellular metabolism as an *ADH1* deletion. So, the *pdc1* $\Delta$  strains essentially serve as a non-butanol-producing control strain. With the aim of having a general view of the number of both exclusive and overlapping differentially expressed transcripts between each strain, a Venn diagram was plotted using transcripts with greater or less than  $\log_2$  fold-change = 1.0, with an adjusted p-value less than 0.05. The resulting diagrams showed that the deletion of *pdc1* $\Delta$  resulted in very few transcriptomic changes relative to the parental strains. From a total of 7127 annotated genes, 84 genes were found differentially expressed in the  $\Sigma$ 1278b *pdc1* $\Delta$  strain, and only 3 genes in the W303-A *pdc1* $\Delta$  strain (Figure 10.2 A). The diagram also revealed that the deletion of *pdc1* $\Delta$  resulted in substantially more downregulated genes than upregulated genes in the  $\Sigma$ 1278b background. So overall, this mutant strain elicits a stronger transcriptomic change in the  $\Sigma$ 1278b background and in the most part transcript levels are reduced in the mutant.

While Venn diagrams are a practical way to visualise the number of shared and exclusive differentially expressed genes (DEGs) of each background, they do not yield information on the degree of differential expression of each gene. In order to present this, a scatter plot of the  $\log_2$ (fold-change) of every gene in the W303-A strain (x-axis) and

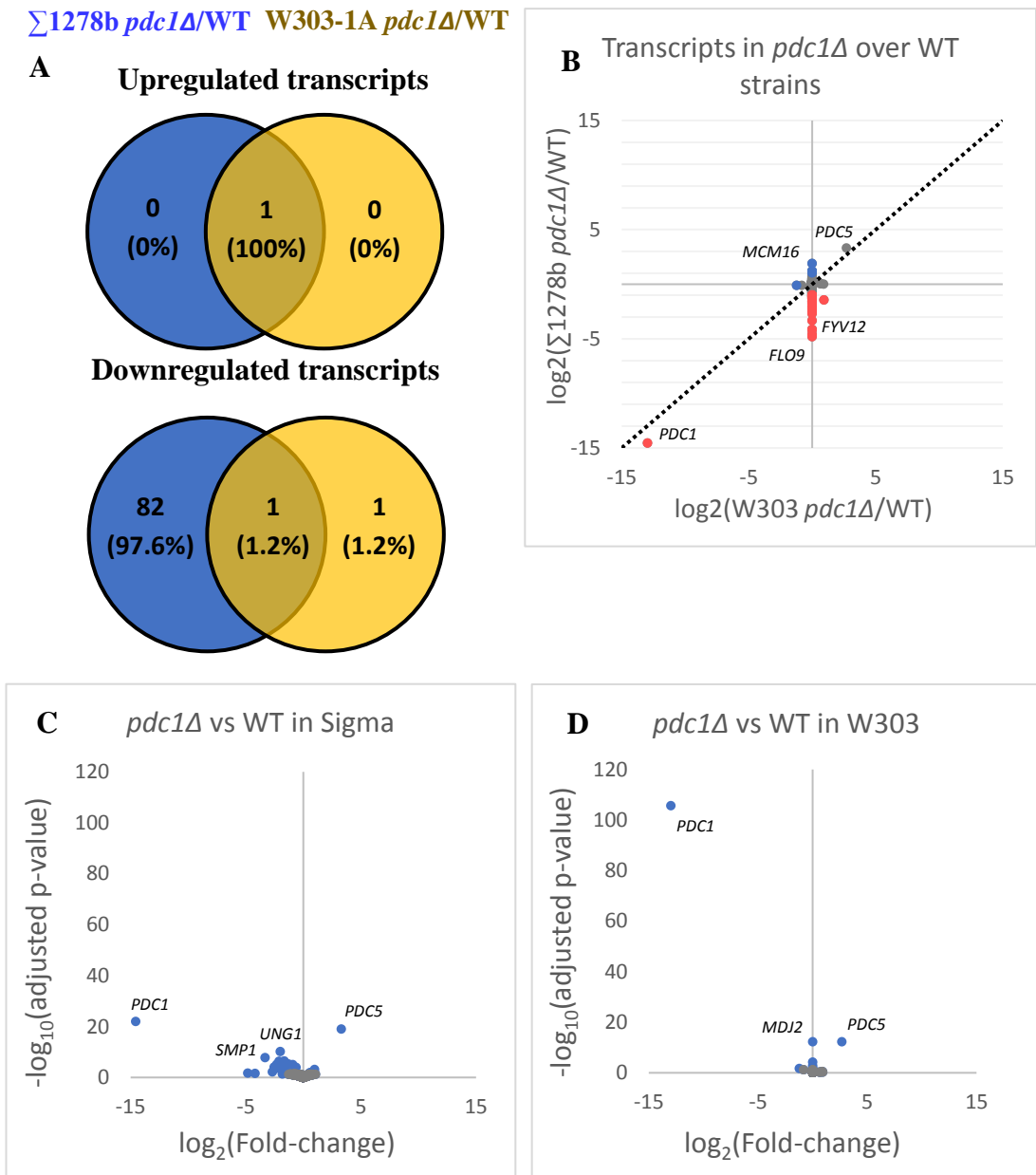


**Figure 10.2. Transcriptional profile of the *pdcl1* $\Delta$  strains in the  $\Sigma 1278b$  and W303-1A backgrounds.** A) Venn diagrams represent the number of individual and overlapping differentially expressed transcripts in *pdcl1* $\Delta$  strains of the  $\Sigma 1278b$  and W303-1A backgrounds. B) Fold-change of transcript levels in the *pdcl1* $\Delta$  W303-1A strain was plotted against fold-change of transcripts in the *pdcl1* $\Delta$   $\Sigma 1278b$  strain. Dotted line represents transcripts showing identical differential expression between each background. Points in blue and red indicate transcripts found over and under a threshold of 1.0 around the diagonal line, respectively. C) and D) Volcano plots of Fold-change and adjusted p-value of transcript levels between the *pdcl1* $\Delta$  and parental strains in the  $\Sigma 1278b$  and W303-1A backgrounds, respectively. Genes with the highest  $-\log_{10}(\text{adjusted p-value})$  are highlighted. Data points coloured blue have an adjusted p-value lesser than 0.05.

$\Sigma$ 1278b strain (y-axis) was produced (Figure 10.2 B). Each point in the plot represents the ratio of differential expression between the  $\Sigma$ 1278b and W303-A strains, with a theoretical line of gene transcripts with a ratio of 1.0 representing transcripts with identical levels between the two strains (dotted line in the plot). Genes positioned above and below cut-off points of 1.0 and -1.0 around this line were coloured blue and red, respectively, and were considered to have different levels of expression between each background.

As expected, the *PDC1* gene was easily identified as highly downregulated in both backgrounds serving as a control for the quality of the sequencing process, given that this gene is deleted in both backgrounds. On the opposite quadrant, *PDC5* was seen to be upregulated in both strains. This may provide part of the rationale for the limited transcriptional impact of the *PDC1* mutant and is in keeping with the literature where *PDC1* deletion causes an induction of the *PDC5* promoter (Eberhardt et al., 1999).

The volcano plot is a third type of plot that displays information about both the degree of differential expression and the statistical strength of the elements of an RNA-seq dataset by plotting  $\log_2(\text{fold-change})$  against  $-\log_{10}(\text{adjusted p-value})$  of each gene.

Once again, the changes in the *PDC1* and *PDC5* transcript levels stand out (Figure 10.2 C and D).

These data from the *pdcl1* $\Delta$  strains provide independent verification of the strain identity and provide validation for the overall scheme of differential transcript level analysis across the whole experiment.

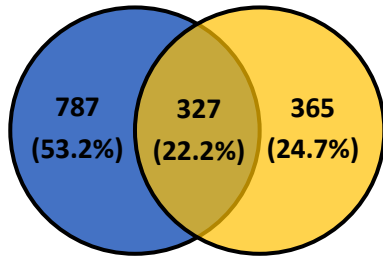
#### 10.4.2 Transcriptomic profile of *adh1*Δ strains of the Σ1278b and W303-1A backgrounds

Preliminary differential expression analyses of the *adh1*Δ strains showed that this deletion causes a clearer and broader transcriptomic response in both backgrounds than the deletion of *PDC1*. For instance, 1600 gene transcripts were differentially expressed in the *adh1*Δ Σ1278b strain (787 up, 813 down), and in the *adh1*Δ W303-1A 809 gene transcripts were significantly affected (365 up, 444 down) (Figure 10.3 A). Approximately one quarter of the total gene transcripts were overlapping between the Σ1278b and W303-1A strains, while the Σ1278b strain had nearly twice as many exclusive DEGs compared with the W303-1A strain, indicating that the deletion of *ADHI* results in more background-specific transcriptomic changes in the Σ1278b strain than in the W303-1A strain.

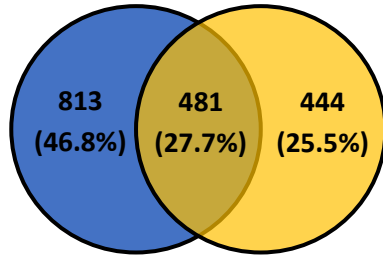
When the differential gene expression data for *adh1*Δ strain relative to the parental strains were plotted as either a scatter plot or volcano plot, it is immediately evident that larger transcriptomic differences are apparent for the *adh1*Δ strains than the previously noted for the *pdc1*Δ strains (Figure 10.3 B, C and D). The fact that *ADHI* is an outlier on both plots again serves as validation for the efficacy of the sequencing data, as this would be expected since this gene is deleted. Another outlier which in this case is higher in the *adh1*Δ W303-1A strain is *HMRA1*. The *HMRA1* gene encodes a transcription co-repressor that is generally only expressed in cells of the *MATa* mating type. However, the W303-1A strains used in this experiment were of the *MATα* mating type, and *HMRA1* is only expressed in *MATa* cells (Herskowitz, 1989), so it is unclear why this gene is upregulated. A deeper look into the differential expression of the mating type genes *HMRA1*, *HMRA2*, *ALPHA1*, and *ALPHA2* in the Σ1278b strains in respect to the W303-

$\Sigma$ 1278b *adh1* $\Delta$ /WT W303-1A *adh1* $\Delta$ /WT

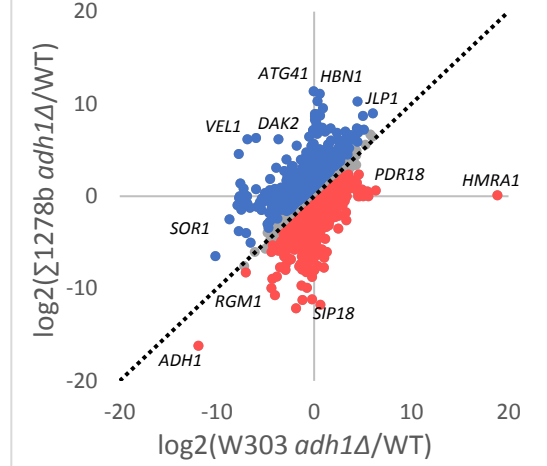
**A** Upregulated transcripts



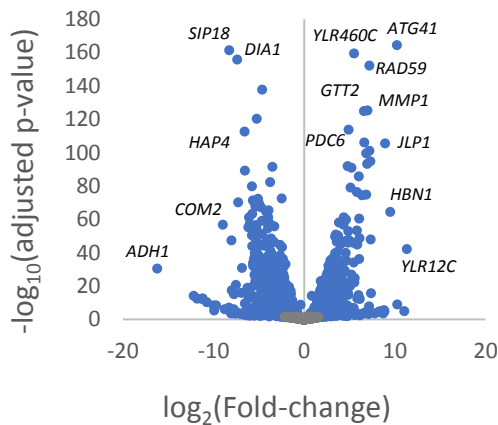
Downregulated transcripts



**B** Transcripts in *adh1* $\Delta$  over WT strains



**C** *adh1* $\Delta$  vs WT in Sigma



**D** *adh1* $\Delta$  vs WT in W303

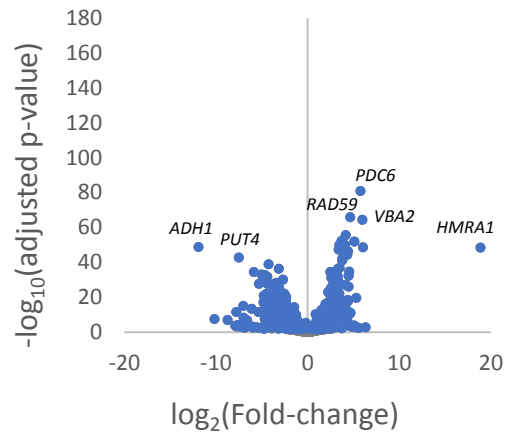


**Figure 10.3. Transcriptional profile of the *adh1* $\Delta$  strains in the  $\Sigma$ 1278b and W303-1A backgrounds.** A) Venn diagrams represent the number of individual and overlapping differentially expressed transcripts in *adh1* $\Delta$  strains of the  $\Sigma$ 1278b and W303-1A backgrounds. B) Fold-change of transcript levels in the *adh1* $\Delta$  W303-1A strain was plotted against fold-change of transcripts in the *adh1* $\Delta$   $\Sigma$ 1278b strain. Dotted line represents transcripts showing identical differential expression between each background. Points in blue and red indicate transcripts found over and under a threshold of 1.0 around the diagonal line, respectively. C) and D) Volcano plots of Fold-change and adjusted p-value of transcript levels between the *adh1* $\Delta$  and parental strains in the  $\Sigma$ 1278b and W303-1A backgrounds, respectively. Genes with the highest  $-\log_{10}(\text{adjusted p-value})$  are highlighted. Data points coloured blue have an adjusted p-value lesser than 0.05.

1A strains revealed that differential expression of *HMRA1* was high in the wild-type and *adh1Δ* strains, but it drastically decreased in the *adh1Δ* and *ALD6/ACS2 adh1Δ* mutants (Figure 10.4). This observed strain-dependent expression of the *HMRA1* gene transcript is an unexpected result that suggests that the deletion of *ADHI* may cause disruption of the physiological expression of this mate-type gene. In order to address this question, a simple mate-type assay could be used to assess the mate-type phenotype of each strain and verify if the *adh1Δ* and *ALD6/ACS2 adh1Δ* mutants behave either as *MATa* or *MATα*.

The scatter and volcano plots also revealed a number of genes with background-specific differential expression. Identifying these genes could yield new clues about the genetics behind the observed differences in 1-butanol production between each strain.

Some of the gene transcripts found induced in the  $\Sigma$ 1278b version of the strain *adh1Δ* were *ATG41*, *HBN1*, *VBA5*, *DAK2*, *VEL1*, and YLR012C (Figure 10.3 B). Many of the highlighted genes do not have a precisely known function but have been found involved in multiple cellular stress responses. For instance, *ATG41* encodes a protein of unknown function required for autophagy which is upregulated when yeast cells shift to non-fermentable carbon sources (Yaoe et al., 2015). Other stress response genes are *DAK2*, encoding a dihydroxyacyl-CoA lyase involved in the saline stress response (Molin et al., 2003), and *VEL1*, a gene encoding a protein of unknown function induced under zinc deficiency (Higgins et al., 2020).

On the other hand, fewer transcripts were differentially expressed in the W303-1A *adh1Δ* strain. Among them, *PDR18* is an ATP-binding cassette membrane transporter that confers ethanol tolerance and is involved in multidrug resistance and controlling the sterol content of the plasma membrane (Teixeira et al., 2012; Cabrito et al., 2011).

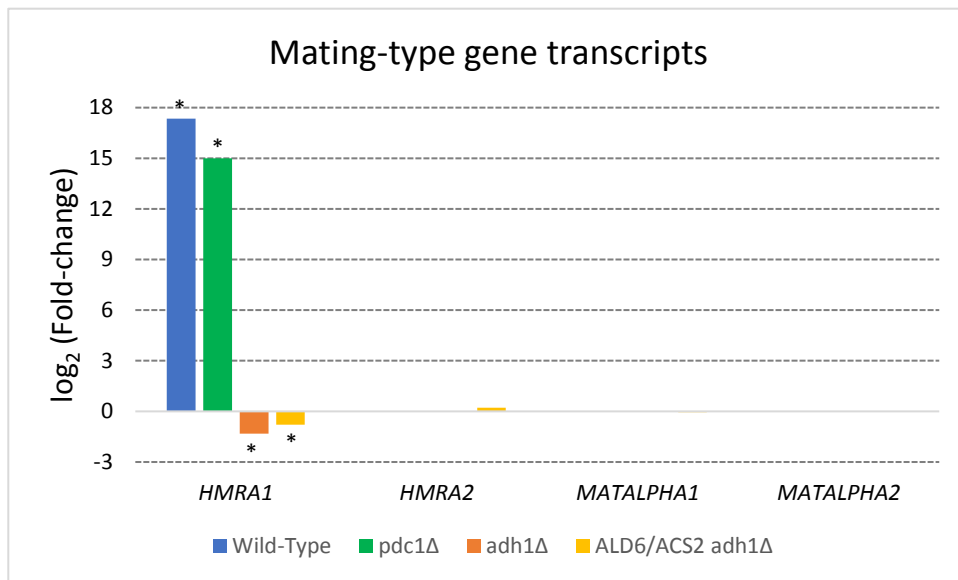


**Figure 10.4. Expression of *HMRA1* is decreased in the  $\Sigma$ 1278b *adh1*Δ and *ALD6/ACS2 adh1*Δ strains.** Differential expression of mating-type genes in each  $\Sigma$ 1278b strain over their respective W303-1A version, plotted as of  $\log_2$  of the fold-change. Asterisks (\*) over each bar indicate a DEG with an adjusted p-value less than 0.05.

The volcano plots of the *adh1*Δ strains revealed further DEGs of interest (Figure 10.3 C and D). For the *adh1*Δ Σ1278b strain *GTT2*, *MMP1*, *YLR460C*, and *YLR12C* gene transcripts were increased. The *GTT2* gene encodes a glutathione S-transferase involved in cell detoxification of xenobiotics by conjugating them with glutathione (Collinson and Grant, 2003; Choi et al., 1998). *MMP1* is a S-methylmethionine membrane transporter that allows yeast cells to uptake this compound for their metabolism (Roullion et al., 1999). Finally, *YLR460C* is a member of the quinone oxidoreductase family (Santos et al., 2009), and *YLR12C* is an unknown protein.

Therefore, across both strain backgrounds deletion of *ADHI* leads to alterations in transcripts involved in various stress responses, although the precise nature of these alterations varies with the strain background. This reinforces the notion that the deletion of *ADHI* results in a stressful cellular environment, and that the transcriptional response enabling survival under chronic stress conditions is strain-dependent.

#### **10.4.3 Differentially expressed genes in the *ALD6/ACS2 adh1*Δ mutants of the Σ1278b and W303-1A backgrounds**

Identification of DEGs when *ALD6* and *ACS2* are overexpressed in each *adh1*Δ strain could yield information on the genes behind the differences in 1-butanol accumulation between each background. As a reminder, for the *ALD6/ACS2 adh1*Δ Σ1278b strain a slowdown in 1-butanol accumulation was observed, while for the W303-1A strain 1-butanol production was completely abolished (See Figure 8.8). To this end, the following differential gene analysis compared DEGs between each *ALD6/ACS2 adh1*Δ strain over the parental strains.

Venn diagrams show that a total of 1296 genes were differentially expressed in the *ALD6/ACS2 adh1*Δ Σ1278b strain (916 up, 380 down), while in the W303-1A a total of

1331 gene transcripts were differentially expressed (854 up, 477 down) (Figure 10.5 A). Once again, the  $\Sigma$ 1278b strain had approximately twice as many exclusive DEGs compared with the W303-1A strain, but the proportion of shared DEGs increased to 29% of all gene transcripts, suggesting that the transcriptional response is more similar between the *ALD6/ACS2 adh1* $\Delta$  strains than between the *adh1* $\Delta$  strains.

Differential expression data of each *ALD6/ACS2 adh1* $\Delta$  strain was plotted on a scatter plot and two individual volcano plots, revealing transcriptomic responses similar in scale to that of the *adh1* $\Delta$  strains (Figure 10.5 B, C and D). Consistent with the above data, the scatter plot showed a cluster of transcripts at the middle with DEGs reaching along each of the axis up to approximately 10-fold up or downregulation, once again suggestive of divergent transcriptomic profiles between the  $\Sigma$ 1278b and W303-1A backgrounds (Figure 10.5 B). While the presence of *ADHI* as an outlier in the scatter plot is once again evidence for the validity of the strains, *ALD6* nor *ACS2* appear as highly expressed gene transcripts, a result that might appear as at odds with the identity of the strains. The transformation cassette used to overexpress *ALD6* and *ACS2* in the strains harboured codon-optimised versions of each gene which are not annotated in the mapping software, hence the absence of induced gene transcripts for *ALD6* and *ACS2* in the RNA-seq dataset.

Among the most significant gene transcripts induced in the *ALD6/ACS2 adh1* $\Delta$   $\Sigma$ 1278b are *ANS1*, *FLO1*, *VBA5*, and *VEL1* (Figure 10.5 B). Their gene products are involved in different cellular processes with few functions in common. *ANS1* encodes a putative vacuolar GPI-anchored protein potentially involved in some stress responses (de Groot et al., 2003). The *FLO1* gene encodes one of the yeast flocculins that allow cell-cell anchoring of cell walls, contributing to the flocculant phenotype characteristic of the

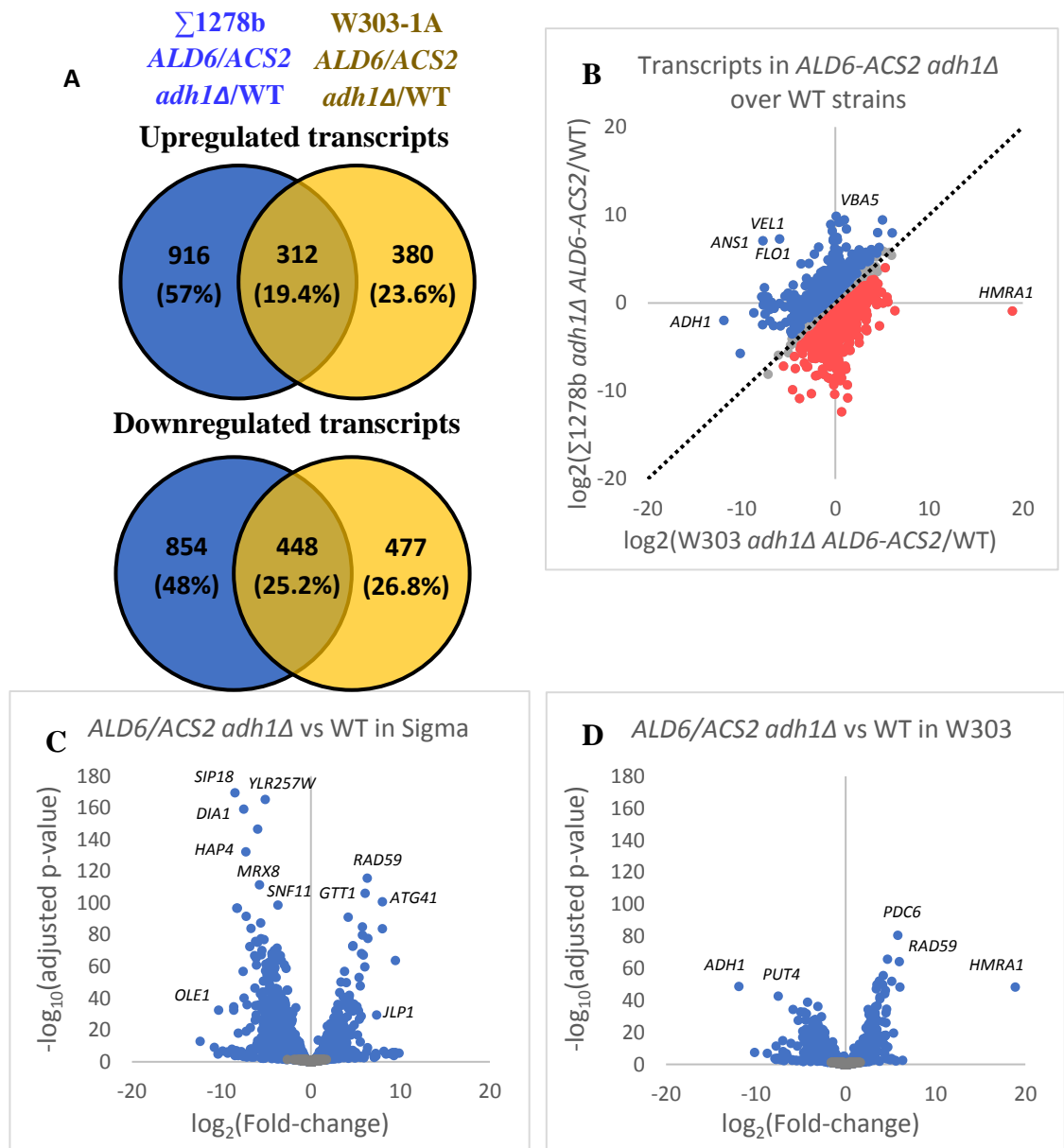


**Figure 10.5. Transcriptional profile of the *ALD6/ACS2 adh1Δ* strains in the  $\Sigma 1278b$  and W303-1A backgrounds.** A) Venn diagrams represent the number of individual and overlapping differentially expressed transcripts in *ALD6/ACS2 adh1Δ* strains of the  $\Sigma 1278b$  and W303-1A backgrounds. B) Fold-change of transcript levels in the *ALD6/ACS2 adh1Δ* W303-1A strain was plotted against fold-change of transcripts in the *ALD6/ACS2 adh1Δ*  $\Sigma 1278b$  strain. Dotted line represents transcripts showing identical differential expression between each background. Points in blue and red indicate transcripts found over and under a threshold of 1.0 around the diagonal line, respectively. C) and D) Volcano plots of Fold-change and adjusted p-value of transcript levels between the *ALD6/ACS2 adh1Δ* and parental strains in the  $\Sigma 1278b$  and W303-1A backgrounds, respectively. Genes with the highest  $-\log_{10}(\text{adjusted p-value})$  are highlighted. Data points coloured blue have an adjusted p-value lesser than 0.05.

$\Sigma$ 1278b background (Bidard et al., 1995). *VEL1* is a gene of unknown function that is induced by zinc deficiency (Higgins et al., 2003).

Besides the previously identified *HMRA1* gene, no particular transcripts were identified as clear outliers of high expression in the *ALD6/ACS2 adh1 $\Delta$*  W303-1A strain from the scatter plot alone (Figure 10.5 B).

Volcano plots revealed further gene transcripts of potential interest in each *ALD6/ACS2 adh1 $\Delta$*  strain (Figure 10.5 C and D). Some of the DEGs with the highest induction in the  $\Sigma$ 1278b strain were *RAD59*, *GTT1*, *ATG41*, and *JLP1*; while among the highlighted downregulated gene transcripts were *DIA1*, *OLE1*, *MRX8*, *HAP4*, *SIP18*, and *YLR257W*.

Two of the induced gene transcripts, *GTT1* and *JLP1* are involved in yeast sulfur metabolism and are induced under sulfur-limited conditions. *GTT1* encodes one of the two yeast glutathione-S-transferases that catalyses the conjugation of glutathione to xenobiotics and other toxic compounds to facilitate their removal from the cell (Jakoby, 1985), while *JLP1* encodes a sulfonate/2-oxoglutarate dioxygenase that allows yeast cells to use sulfonates as sulfur sources (Hogan et al., 1999). On the other hand, *ATG41* and *RAD59* are involved in different cellular stress responses. *ATG41* is required for autophagosome formation during autophagy and its expression is known to be induced when yeasts shift to a non-fermentable carbon source (Yao et al., 2015; Kuhn et al., 2001). *RAD59* participates in DNA double-strand break repair, thus granting yeast cells resistance to DNA-damaging agents like ionizing radiation (Pannunzio et al., 2012; Davis and Symington, 2001).

Three of the highlighted downregulated DEGs in the  $\Sigma$ 1278b strain were related to either respiratory or mitochondrial function. *OLE1* is the only mitochondrial Acyl-CoA desaturase, essential for cellular biosynthesis of unsaturated fatty acids (Martin et al.,

2007). *MRX8* is a non-essential gene whose product associates with mitochondrial ribosomes (Kehrein et al., 2015). *HAP4* encodes one of the subunits of the glucose-repressed CCAAT-binding complex, a transcriptional regulator that participates in the diauxic shift (Zampar et al., 2013; Forsberg and Guarente, 1989). *YLR257W* produces an unknown protein induced during the DNA damage response (Tkach et al., 2012).

*DIA1* and *SIP18*, the last two highlighted downregulated genes are associated with cellular stress responses. While *DIA1* is involved in yeast invasive and pseudohyphal growth (Palecek et al., 2000), *SIP18* encodes a hydrophillin involved with tolerance to dissection (Dang and Hinch, 2011).

The volcano plot also revealed a number of transcriptionally induced and repressed genes in the *ALD6/ACS2 adh1Δ* W303-1A strain (Figure 10.5 D). Among the upregulated gene transcripts, *HMRA1*, *RAD59*, and *PDC6* were present, while among the downregulated gene transcripts, only *PUT4* was highlighted besides *ADH1*.

*RAD59* was previously identified in the induced DEGs of the *ALD6/ACS2 adh1Δ*  $\Sigma$ 1278b strain, indicating that both genetic backgrounds induce this DNA damage response gene during anaerobic growth, while *PDC6* encodes an isoform of pyruvate decarboxylase that is expressed under sulfur-limiting conditions (Boer et al., 2003; Hohmann, 1991).

*PUT4* was highlighted as a downregulated DEG in the *ALD6/ACS2 adh1Δ* W303-1A strain. This high affinity L-proline membrane transporter (Vandenbol et al., 1989) was also downregulated in all other strains, indicating that transcriptional repression of this transporter is a general effect of the culture conditions.

#### 10.4.4 Transcriptomic effect of the overexpression of *ALD6* and *ACS2* in the *adh1Δ* strains

While the above comparisons revealed the differences and similarities between the transcriptomes of each *ALD6/ACS2 adh1Δ* mutants in respect to the parental strains, a similar comparison can be made between the *ALD6/ACS2 adh1Δ* strains and their corresponding *adh1Δ* mutants. This second analysis could prove valuable by revealing new differentially expressed transcripts and present transcriptional changes from a different perspective.

Venn diagrams showed that a total of 663 genes were differentially expressed in the *ALD6/ACS2 adh1Δ*  $\Sigma$ 1278b strain (342 up, 321 down), while the *adh1Δ* W303-1A had a total of 706 DEGs (393 up, 313 down) (Figure 10.6 A). There was less overlap in the gene transcripts between the *ALD6/ACS2 adh1Δ* strains of each background, with less than a fifth of the DEGs overlapping between the backgrounds. This indicates that the overexpression of *ALD6* and *ACS2* results in more divergent transcriptomes, which in part reflects some of the phenotypic differences observed in each strain.

Consistent with the above data, scatter plot and volcano plots revealed divergent transcriptomic profiles between the  $\Sigma$ 1278b and W303-1A backgrounds and highlighted a number of transcripts differentially expressed in each background, as evidenced by the data points grouped by each x and y-axis in the plot (Figure 10.6 B).

Some of the highlighted induced gene transcripts in the scatter plot and volcano plot of the *ALD6/ACS2 adh1Δ*  $\Sigma$ 1278b strain included *CTM1*, *JLP2*, *PES4*, *YNL146W*, *YJL027C*, and *YNR064C* (Figure 10.6 B and C). Three of the highlighted genes, *YNL146W*, *YJL027C*, and *JLP2* encode proteins with no known function, while *CTM1*,

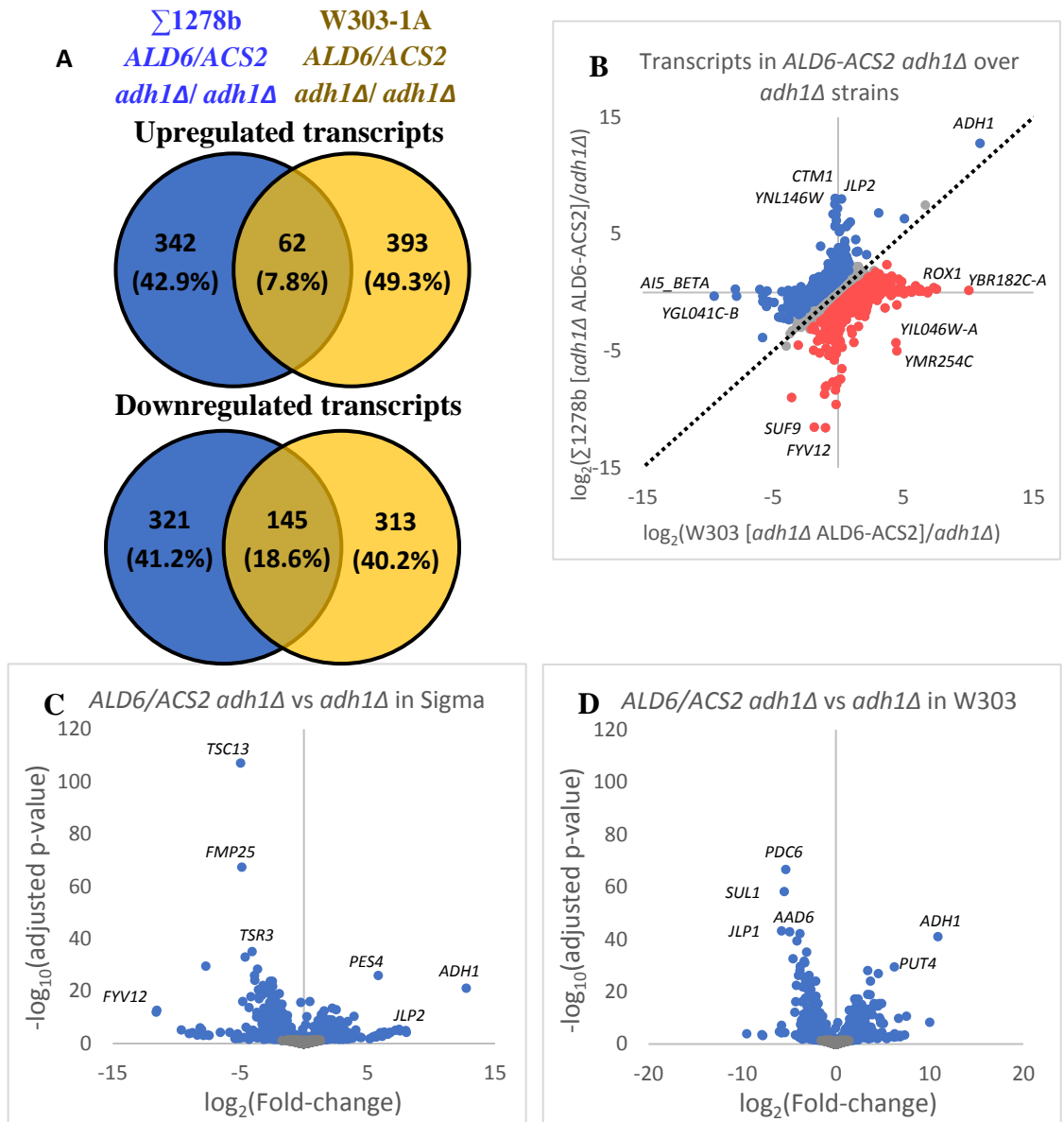


**Figure 10.6. Transcriptional changes caused by the overexpression of *ALD6* and *ACS2* in the *adh1Δ* strains of the  $\Sigma 1278b$  and W303-1A backgrounds.** A) Venn diagrams represent the number of individual and overlapping differentially expressed transcripts in *ALD6/ACS2 adh1Δ* strains of the  $\Sigma 1278b$  and W303-1A backgrounds. B) Fold-change of transcript levels in the *ALD6/ACS2 adh1Δ* W303-1A strain was plotted against fold-change of transcripts in the *ALD6/ACS2 adh1Δ*  $\Sigma 1278b$  strain. Dotted line represents transcripts showing identical differential expression between each background. Points in blue and red indicate transcripts found over and under a threshold of 1.0 around the diagonal line, respectively. C) and D) Volcano plots of Fold-change and adjusted p-value of transcript levels between the *ALD6/ACS2 adh1Δ* and parental strains in the  $\Sigma 1278b$  and W303-1A backgrounds, respectively. Genes with the highest  $-\log_{10}(\text{adjusted p-value})$  are highlighted. Data points coloured blue have an adjusted p-value lesser than 0.05.

*PES4*, and *YNR064C* encode a cytochrome c lysine methyl transferase, a poly(A) binding protein, and an epoxide hydrolase, respectively (Elfström and Widersten, 2005; Polevoda et al., 2000).

Among the repressed DEGs in the same strain, there were three more genes of unknown function: *FYV12*, *YIL046W-A*, and *YMR254C*. The rest of the highlighted gene transcripts, *FMP25*, *SUF9*, *TSC13*, and *TSR3*, are associated with fundamental cellular processes. The *FMP25* gene product is required for assembly of the respiratory complex III (Mathieu et al., 2011), while *TSR3* is involved in pre-processing of the 20S rRNA to yield mature 18S rRNA (Li et al., 2009). *TSC13* encodes an essential yeast enoyl reductase required for long fatty acid elongation (Kohlwein et al., 2001). Finally, *SUF9* encodes the proline tRNA (Winey et al., 1989).

Induced DEGs that can be highlighted from the scatter plot and volcano plot of the *ALD6/ACS2 adh1Δ* W303-1A strain included *ROX1*, *PUT4*, and the gene of unknown function *YBR182C-A* (Figures 10.6 B and D). *PUT4* was found downregulated in the previous comparison with the parental strain, indicating that transcript repression in the *adh1Δ* W303-1A strain is partially reverted when *ALD6* and *ACS2* are overexpressed. *ROX1* is a transcriptional repressor of hypoxia-induced genes during aerobic growth (Liu and Barrientos, 2013), suggesting that this strain behaves as in aerobic conditions despite being grown in anaerobic cultures.

Repressed gene transcripts in the *ALD6/ACS2 adh1Δ* W303-1A strain included *AAD6*, *PDC6*, *SUL1*, as well as *YGL041C-B*, which encodes a protein of unknown function (Figures 10.6 C and D). *AAD6* is a putative aryl alcohol dehydrogenase that responds to oxidative stress and has no role in fusel alcohol biosynthesis (Dickinson et al., 2003; Delneri et al., 1999). Downregulation of the *SUL1* high affinity sulfate transporter in this

strain may indicate a reduced cellular need for sulfur (Cherest et al., 1997). This notion is supported by the observed decrease in the gene transcript of *PDC6*, which was previously found upregulated in the *adh1*Δ W303-1A strain.

These transcriptomic comparisons hint at a transcriptomic response to oxidative stress and sulfur deprivation in the *adh1*Δ strains that appears to be relieved when *ALD6* and *ACS2* are overexpressed in the W303-1A background. This shift in the transcriptome could be part of the mechanisms behind the abolishment of 1-butanol and acetaldehyde accumulation in this strain (Figure 9.8). However, in order to obtain a better measure of the expression patterns in each strain, further differential expression analyses are required.

### **10.5 Gene enrichment analysis reveals trends in differentially expressed genes between the *adh1*Δ and *ALD6/ACS2 adh1*Δ strains**

GO enrichment analysis is a method used to identify overrepresented functional categories (GO terms) in a specific dataset, such as the list of upregulated genes in an *adh1*Δ strain growing in anaerobic conditions. Computational tools like the Gene Ontology Resource and the PANTHER classification system can aid in the identification of functional trends in DEGs according to their molecular function, role in a biological process, or as part of cellular components.

Thus, in order to identify functional groups of transcripts that may be involved in the observed differences in 1-butanol production between the *adh1*Δ, *pdcl*Δ, and *ALD6/ACS2 adh1*Δ strains of each background, a gene enrichment analysis was performed on each list of significantly upregulated and downregulated genes, respect to the parental strains. Additionally, due to the differences in 1-butanol accumulation between the  $\Sigma$ 1278b and W303-1A *ALD6/ACS2 adh1*Δ strains, two sets of significant

DEGs for each *ALD6/ACS2 adh1Δ* strain, with respect to their corresponding parental *adh1Δ* strains were included in order to identify trends in transcriptomic changes that could unveil the nature of the observed differences.

Because gene enrichment analysis of the *pdh1Δ* strains resulted in no enriched categories, likely due to the low number of DEGs in these mutants, they were excluded from the following analyses.

### **10.5.1 Aerobic respiration is downregulated in the *adh1Δ* strains, while overexpression of *ALD6* and *ACS2* partially rescues this downregulation**

The aerobic respiration GO term was found enriched in the list of downregulated genes of the *adh1Δ*  $\Sigma$ 1278b strain with 45 downregulated genes, while a 44 DEGs found downregulated in the *ALD6/ACS2 adh1Δ*  $\Sigma$ 1278b strain were also enriched for the same GO term, respect to the parental strain (Figure 10.7). Genes in this category included members of the mitochondrial electron transport chain such as *QCR* genes of the cytochrome bc1 complex, *COX* genes belonging to the cytochrome c complex, and ATP synthase subunits *ATP5* and *ATP2* (Figure 10.8 A). Additionally, all three malate dehydrogenase gene isoforms *MDH1*, *MDH2*, and *MDH3* were downregulated in the *adh1Δ* strains, which have roles in the tricarboxylic acid (TCA) cycle, gluconeogenesis, and glyoxylate cycle, respectively (Steffan and McAlister-Henn, 1992; Minard and McAlister-Henn, 1991). Other TCA cycle genes were also significantly downregulated, such as the  $\alpha$ -ketoglutarate complex genes *KGD1* and *KGD2*, isocitrate dehydrogenase genes *IDH1* and *IDH2*, succinate dehydrogenase genes *SDH1*, *SDH4*, and *SDH9*, and aconitate hydratases *ACO1* and *ACO2* (Figure 10.8 A).

Genes assigned to the aerobic respiration GO term were manually identified in the *adh1Δ* W303-1A and *ALD6/ACS2 adh1Δ* W303-1A differential expression data sets and

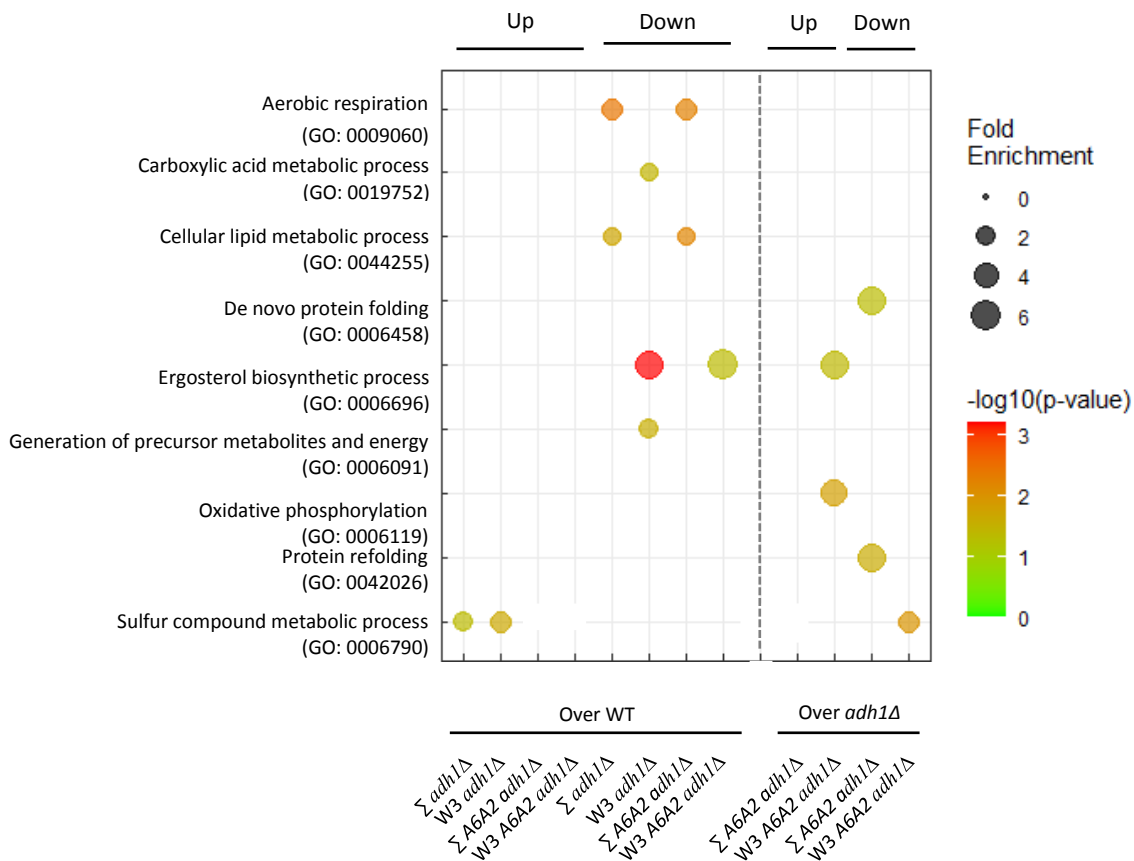


**Figure 10.7. Gene Ontology enrichment analysis of differentially expressed genes between mutants and their parental strains across  $\Sigma 1278b$  and W303 strains.** Bubble plots show fold-enrichment and p-value of each Gene Ontology term assigned to sets of differentially expressed transcripts ( $\log_2$  fold-change higher than 1.0 or lower than -1.0) in each mutant strain of both the  $\Sigma 1278b$  and W303-A backgrounds. PANTHER's GO biological process complete was used as the annotation data set, and data was corrected using the Bonferroni correction for multiple testing.

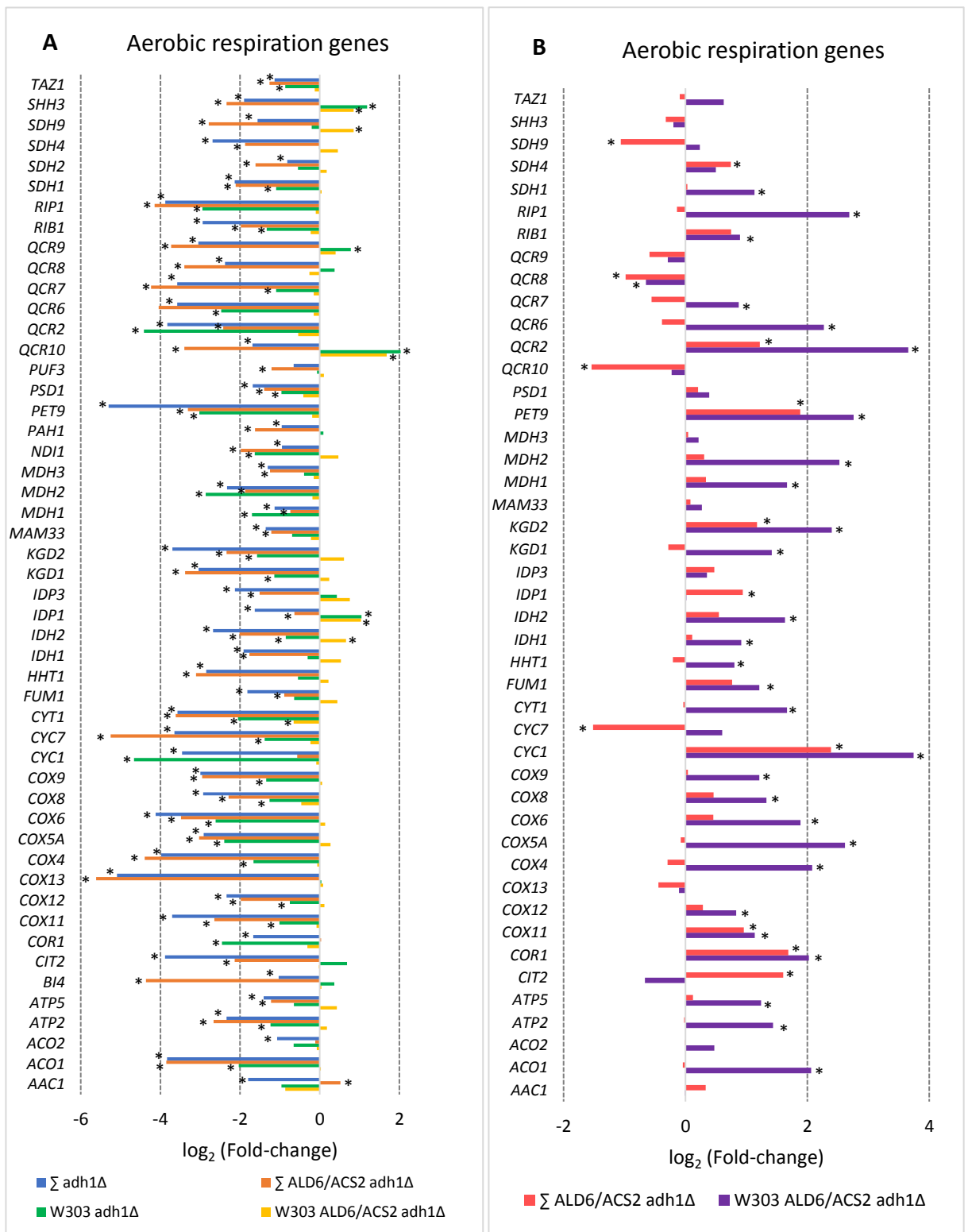


**Figure 10.8. Downregulation of aerobic respiration in the *adh1* $\Delta$  strains is reversed in the W303-1A strain when *ALD6* and *ACS2* are overexpressed.** A) Bar plot of  $\log_2$  of the fold-change in expression of aerobic respiration genes of the *adh1* $\Delta$  and *ALD6/ACS2 adh1* $\Delta$  strains, over their parental strains of the  $\Sigma 1278b$  and W303-1A backgrounds. B) Bar plot of fold-change expression of genes in the *ALD6/ACS2 adh1* $\Delta$  strains, over their respective *adh1* $\Delta$  strains. Asterisks (\*) over each bar indicate a DEG with an adjusted p-value less than 0.05.

included in the bar plot below. Most of the genes in the category were also downregulated in the *adh1*Δ W303-1A strains, but to a lesser extent than in the  $\Sigma$ 1278b strain (Figure 10.8 A). A few genes, such as *IDP1*, *QCR10*, and *SHH3* were instead upregulated in the *adh1*Δ W303-1A strain. On the other hand, the *ALD6/ACS2 adh1*Δ W303-1A displayed fewer DEGs than any other strain, and the degree of expression was overall lesser, and in some genes upregulated (Figure 10.8 A).

This effect can be seen more clearly when directly comparing gene expression between the *ALD6/ACS2 adh1*Δ and *adh1*Δ strains, where multiple genes of the W303-1A strain were displayed increased expression relative to the *adh1*Δ strain (Figure 10.8 B). This effect was less pronounced for the  $\Sigma$ 1278b strain, suggesting that the overexpression of *ALD6* and *ACS2* had a lesser impact on the downregulation of respiratory genes in this background.

The above data implies that respiratory metabolism is downregulated in both *adh1*Δ strains, relative to their parental strains, when grown for 9 days in anaerobic conditions, while overexpression of *ALD6* and *ACS2* in each strain resulted in a partial reversal of this downregulation, with a stronger effect seen in the W303-1A strain. These trends in gene expression somewhat parallel the differences in 1-butanol and acetaldehyde accumulation in each strain, where the *adh1*Δ  $\Sigma$ 1278b strain produced slightly more 1-butanol than the W303-1A and overexpression of *ALD6* and *ACS2* resulted in a complete loss of 1-butanol and acetaldehyde accumulation only in the W303-1A background.

Whether changes in respiratory gene expression is a cause or a consequence of the decrease in acetaldehyde and 1-butanol accumulation in the *ALD6/ACS2 adh1*Δ W303-1A strain remains to be seen.

### 10.5.2 Genes of the ergosterol biosynthesis pathway are downregulated in *adh1Δ* strains

The previously observed changes in expression of respiratory gene transcripts somewhat reflect the changes in the ability of the *adh1Δ* strains to produce 1-butanol when *ALD6* and *ACS2* are overexpressed, thus analysing other metabolic processes that depend on respiratory function could widen the picture on the physiology of the butanol-producing strains.

Ergosterol biosynthetic process is a GO term found enriched in the *adh1Δ* W303-1A strain, with 20 downregulated genes assigned to this category that spanned most of the ergosterol biosynthesis pathway (Figure 10.7). While this category was not enriched in the downregulated genes of the  $\Sigma$ 1278b strain, some of the *ERG* genes were found in the enriched cellular lipid metabolic process GO term, and additional genes belonging to the pathway were identified and found significantly downregulated (Figure 10.9 A), indicating that this pathway is repressed in the *adh1Δ* mutants regardless of genetic background.

Ergosterol biosynthesis gene transcripts were also found downregulated when *ALD6* and *ACS2* are overexpressed in each *adh1Δ* strain, but the degree of repression for many of the DEGs in the W303-1A was less than in the rest of the strains (Figure 10.9 A). This phenomenon can be easily seen when comparing transcript expression between the *ALD6/ACS2 adh1Δ* strains and the *adh1Δ* strains (Figure 10.9 B). In this comparison, expression of multiple DEGs in the  $\Sigma$ 1278b background did not change significantly, while the difference was much larger in the W303-1A background.

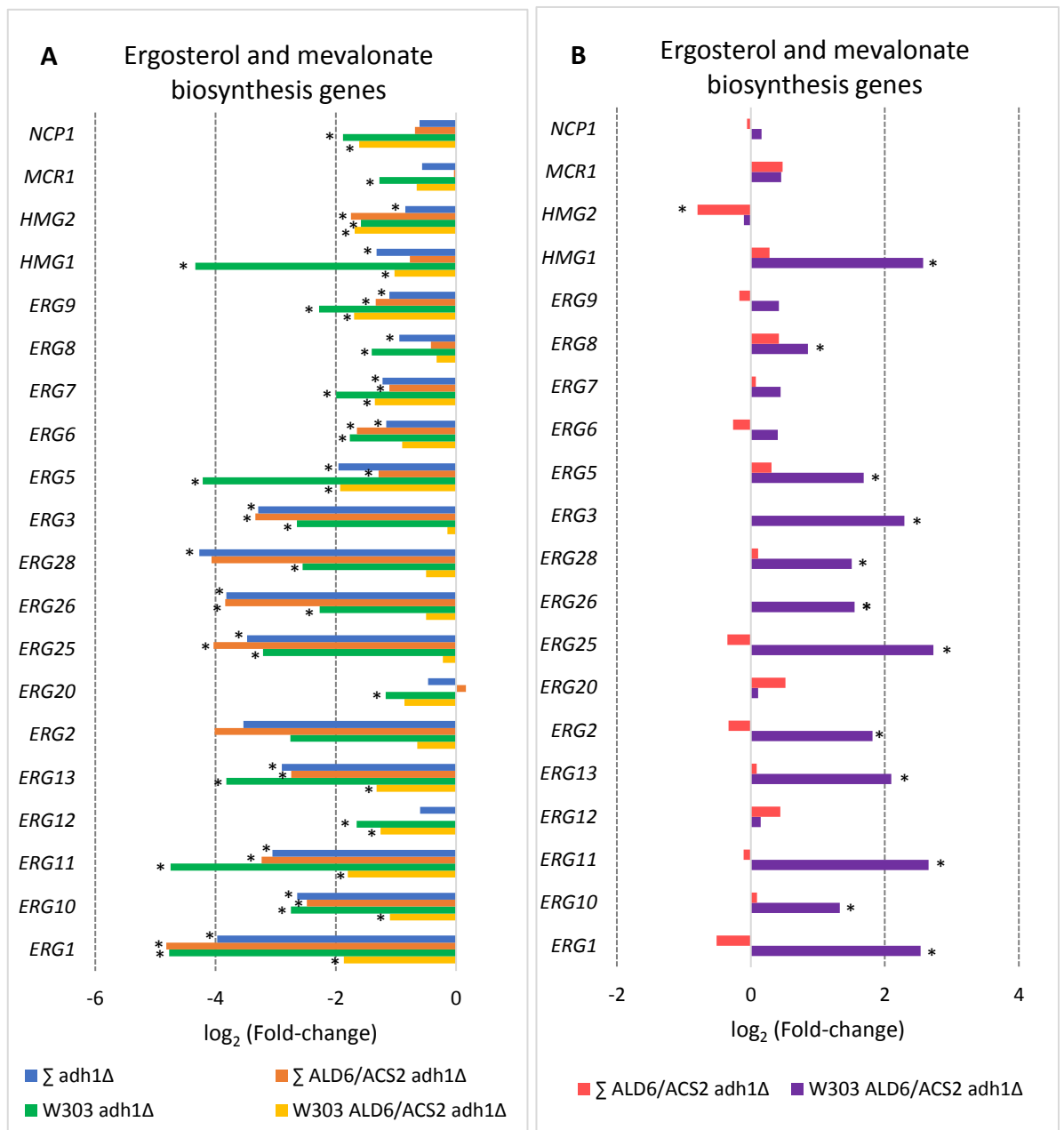


**Figure 10.9. Downregulation of the ergosterol biosynthesis pathway in the *adh1* $\Delta$  strains is reduced in the W303-1A strain when *ALD6* and *ACS2* are overexpressed.** A) Bar plot of  $\log_2$  of the fold-change in expression of ergosterol and mevalonate biosynthesis genes of the *adh1* $\Delta$  and *ALD6/ACS2 adh1* $\Delta$  strains, over their parental strains of the  $\Sigma 1278b$  and W303-1A backgrounds. B) Bar plot of fold-change expression of genes in the *ALD6/ACS2 adh1* $\Delta$  strains, over their respective *adh1* $\Delta$  strains. Asterisks (\*) over each bar indicate a DEG with an adjusted p-value less than 0.05.

Ergosterol is a steroid molecule that maintains the fluidity and integrity of fungal biological membranes, as well as contributing to a series of cellular stress responses including low temperatures, alcohol toxicity, and oxidative stress (Jordá and Puig, 2020).

Expression of sterol biosynthetic genes is induced by sterol depletion by the transcription factors Upc2p and Ecm22p (Davies and Rine, 2006), and under oxygen-limiting conditions by the heme-activated transcription factor Hap1p (Tamura et al., 2004). Differential expression data suggests that the *adh1Δ* strains do not follow this pattern when grown in anaerobic conditions for 9 days, as all of the enriched *ERG* genes were downregulated in both genetic backgrounds.

The above observations suggest that transcriptional expression of the ergosterol pathway under oxygen-limiting conditions is likely compromised in the *adh1Δ* strains. On the other hand, overexpression of *ALD6* and *ACS2* in the W303-1A *adh1Δ* reverted the repression of ergosterol biosynthesis gene transcripts of the ergosterol pathway. One explanation for this phenomenon is that due to the high ATP and NADPH requirements for ergosterol biosynthesis (Jordá and Puig, 2020), this process is repressed in the *adh1Δ* strains due of the low respiratory activity and the demand for NADPH in the acetaldehyde tolerance mechanisms.

### 10.5.3 Genes involved in glycolysis, glycogen metabolism, and the pentose phosphate pathway are downregulated in the *adh1Δ* W303-1A strain

Generation of precursor metabolites and energy is a broad GO term that includes genes involved in intermediary metabolism, concerned with energy production within cells. This term was found enriched in the list of downregulated genes of the *adh1Δ* W303-1A strain with 56 DEGs assigned to it (Figure 10.7). This category overlapped with the aerobic respiration GO term, and included previously examined DEGs such as *COX* genes, *QCR* genes, and *MDH* genes (Figure 10.8 A). Thus, only DEGs exclusive to this new GO term will be included in this analysis.

Genes in this category included genes of the glycolytic pathway (i.e. *CDC19*, *ENO2*, and *GLK1*), the glycogen debranching enzyme *GDB1*, and genes of the pentose phosphate pathway (PPP) (i.e. *GND1*, *SOLA*, and *ZWF1*). The most downregulated gene in the *adh1Δ* W303-1A, besides *ADH1*, was the cytochrome b5 gene *CYB5* with a  $\log_2(\text{fold-change})$  of -6.08, approximately 100-fold less than the parental strain (Figure 10.10 A). The other strains displayed less differential expression of many of the genes in this category than the *adh1Δ* W303-1A. Notable exceptions to this trend were the expression of *CYB5* which was found downregulated at the same level in every strain except the *ALD6/ACS2* W303-1A strain, the dihydroxyacetone kinase gene *DAK2*, which was downregulated in both W303-1A strains but upregulated up to 64-fold in the  $\Sigma$ 1278b strains, and the acyl-CoA desaturase gene *OLE1*, which was more robustly downregulated in the  $\Sigma$ 1278b strains (Figure 10.10 A).

The downregulation of glycolytic genes in the strains is an expected result, as research published by our laboratory demonstrated that in an anaerobic fermentation setup more

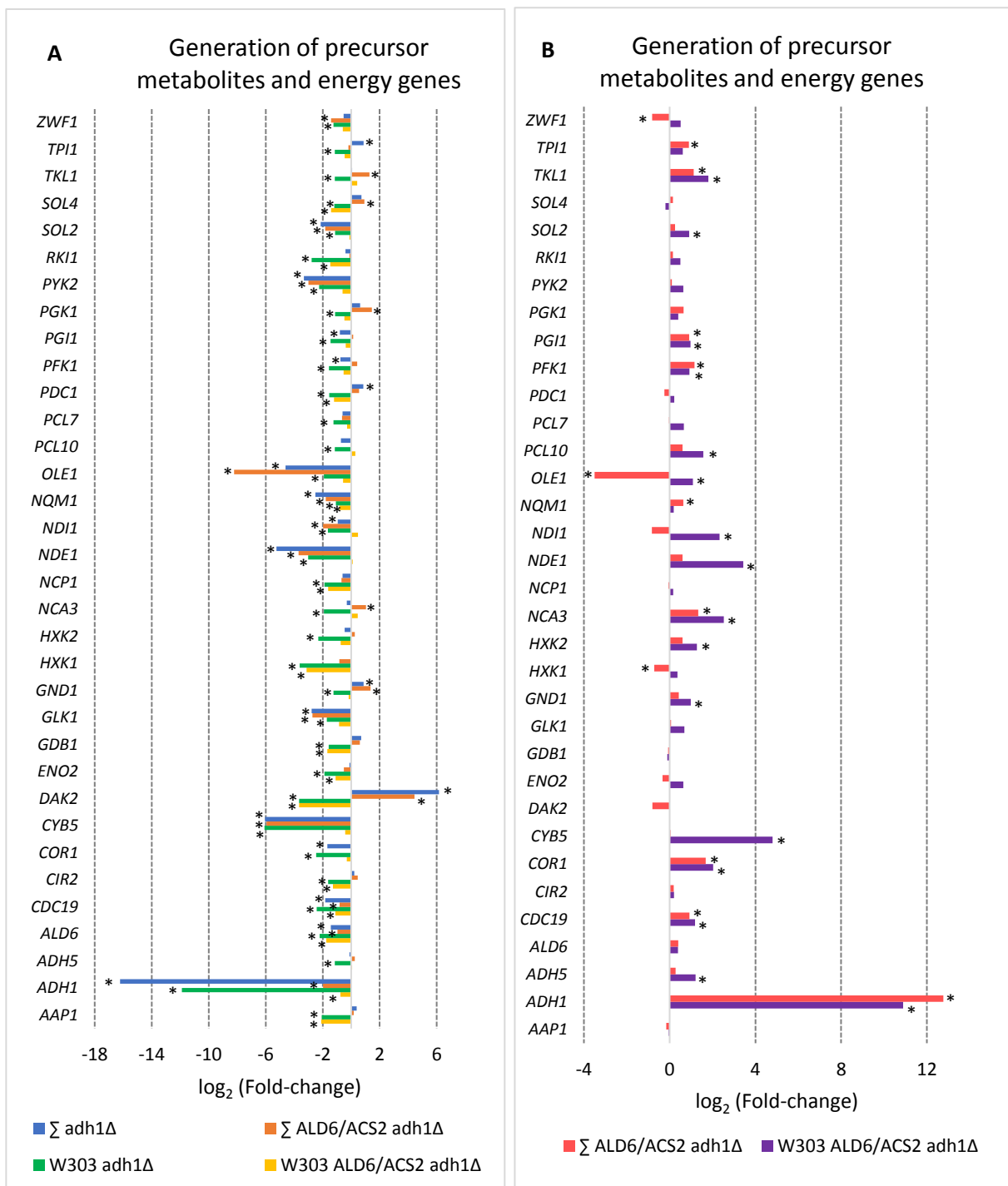


**Figure 10.10. Differential expression of glycolytic, glycogen, and pentose phosphate pathway genes in the *adh1*Δ strains.** A) Bar plot of  $\log_2$  of the fold-change in expression of genes involved in the generation of metabolic precursors and energy of the *adh1*Δ and *ALD6/ACS2 adh1*Δ strains, over their parental strains of the  $\Sigma$ 1278b and W303-1A backgrounds. B) Bar plot of fold-change expression of genes in the *ALD6/ACS2 adh1*Δ strains, over their respective *adh1*Δ strains. Asterisks (\*) over each bar indicate a DEG with an adjusted p-value less than 0.05.

than 80% of the available glucose is consumed by day 9 of fermentation by an *adh1Δ* W303-1A strain (Swidah et al., 2015).

The fact gene transcripts of the PPP are downregulated in the *adh1Δ* strains poses interesting questions regarding the redox state of the cells. The first three reactions of the PPP, catalyzed by Zwf1p, Sol3p and Sol4p, and Gnd1p and Gnd2p, convert one molecule D-glucose-6-phosphate into D-ribulose-5-phosphate, reducing two molecules of NADP<sup>+</sup> to NADPH in the process (Figure 10.11 A) (Bertels et al., 2021). NADPH is an enzymatic cofactor required for a series of biosynthetic pathways and for redox homeostasis. Biosynthetic pathways that utilise NADPH include fatty acid biosynthesis and elongation (Lomakin et al., 2007), ergosterol biosynthesis (Jordá et al., 2020), and 7,8-dihydrofolate reduction to tetrahydrofolate (Revuelta et al., 2018). NADPH is also needed for the restoration of reduced glutathione by yeast glutathione reductase Glr1p (Figure 10.14) thus participating in the maintenance of active glutathione required to protect the cell against reactive oxygen species (ROS) (Grant, 2001).

The observed downregulation of *ZWF1* implies that the initial step of the PPP is downregulated in all strains (Figure 10.11 A). Despite this, other genes involved in the oxidative part of the PPP presented varying levels of expression, some of them being upregulated during anaerobic growth. In particular, *SOL3* was significantly overexpressed in all strains except the *adh1Δ* W303-1A strain, indicating that some pathway activity is present (Figure 10.11 B). More importantly the transcriptional activator of oxidative stress genes and genes of the PPP, *STB5* (Larochelle et al., 2006) was upregulated in both  $\Sigma$ 1278b strains (Figure 10.11 B). Curiously, this increase in expression of *STB5* does not correlate with the levels of *ZWF1* in the  $\Sigma$ 1278b, nor with the increased expression of *SOL3* and *GND2* in the W303-1A strains, but it may be an indicator that the strains are inducing a response to oxidative stress.

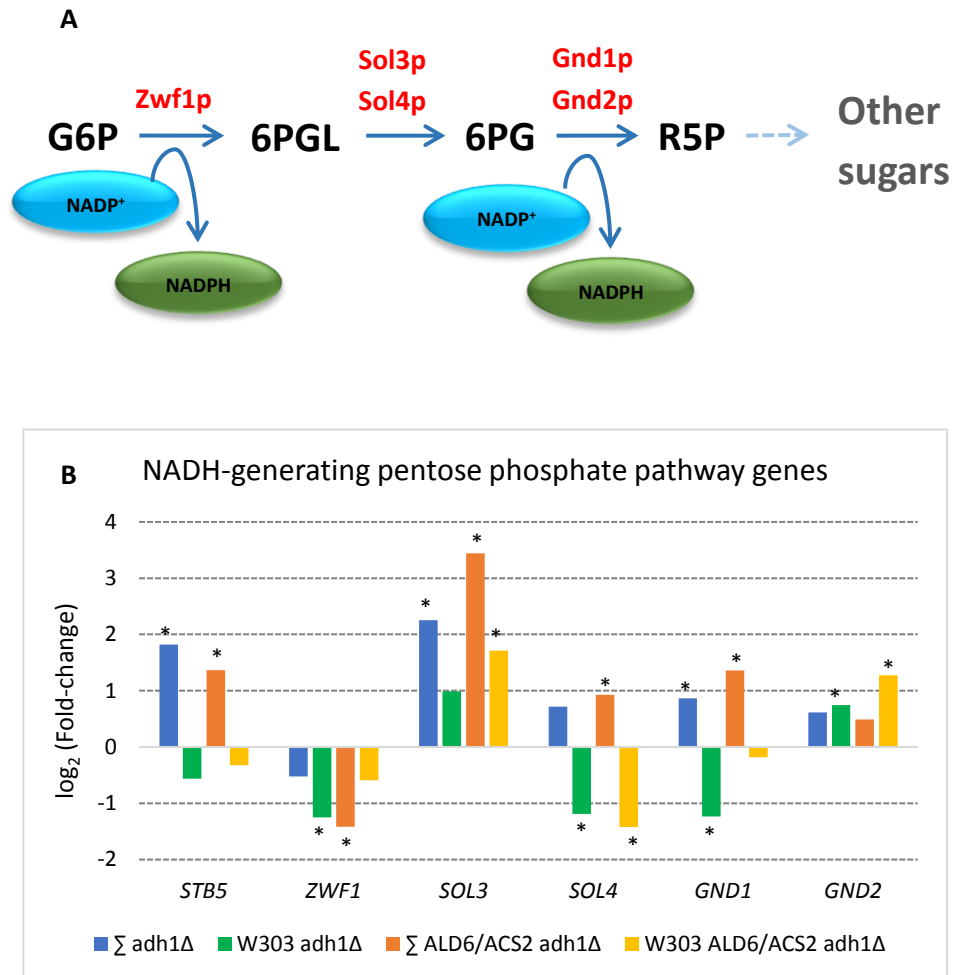


**Figure 10.11. NADH-producing reactions of the Pentose Phosphate Pathway in *S. cerevisiae*.**  
 A) Summarised diagram of the oxidative part of the pentose phosphate pathway. Metabolites and enzymes involved: glucose-6-phosphate (G6P), 6-phospho-gluconolactone (6PGL), 6-phospho-gluconate (6PG), ribulose-5-phosphate (R5P), glucose-6-phosphate dehydrogenase (Zwf1p), 6-phosphogluconolactonase (Sol3p, Sol4p), 6-phosphogluconate dehydrogenase (Gnd1p, Gnd2p).  
 B) Differential expression of the transcriptional activator *STB5* and enzymes of the oxidative part of the pentose phosphate pathway, expressed as  $\log_2$  fold-change relative to the parental strains. Asterisks (\*) over each bar indicate a DEG with an adjusted p-value less than 0.05.

Evidence in the literature points to *STB5* as an important transcription factor in acetaldehyde tolerance in *S. cerevisiae*. Yeast cells overexpressing *STB5* have increased acetaldehyde resistance, and exposure to this toxic agent induces the transcription of *STB5* (Matsufuji et al., 2010). A more recent publication performed a genome-wide study of the binding targets of Stb5p in different culture conditions, including aerobic and anaerobic growth in glucose-limited conditions. The study revealed that in all tested conditions, Stb5p was bound to promoters of genes involved in NADPH regeneration and the PPP, except for *ZWF1* (Ouyang et al., 2018), which is constitutively expressed in yeast (Minard and McAlister-Henn, 2005).

Considering the above studies, it is reasonable to argue that intracellular acetaldehyde accumulating in the *adh1Δ* and *ALD6/ACS2 adh1Δ*  $\Sigma$ 1278b strains is driving the Stb5p-dependent transcription of some of the genes of the PPP with the goal of increasing intracellular levels of NADPH to combat acetaldehyde toxicity. Whether intracellular NADPH concentrations are actually higher in the  $\Sigma$ 1278b strains or this is a factor contributing to enhanced 1-butanol production remains to be tested, but the obtained results have revealed that the  $\Sigma$ 1278b strains respond more robustly to some of the stressful conditions of anaerobic 1-butanol fermentation.

#### 10.5.4 Sulfur uptake, homocysteine biosynthesis, and glutathione conjugation genes are upregulated in butanol-producing strains

54 and 34 significantly upregulated genes in the *adh1Δ*  $\Sigma$ 1278b and W303-1A strains, respectively, were enriched for the sulfur compound metabolic process GO term (Figure 10.7). Genes in each list encoded a variety of enzymes involved in the utilization of extracellular sulfur sources, as well as the biosynthesis of amino-acids with sulfur, the biosynthesis and utilization of glutathione, and thiamine biosynthesis. Among the top significant upregulated genes in both backgrounds were glutathione s-transferase *GTT2* (Choi et al., 1998), omega-class glutathione transferase *GTO1* (Garcerá et al., 2006), Fe(II)-dependent sulfonate/2-oxoglutarate dioxygenase *JLP1* (Hogan et al., 1999), and sulfite reductase *MET10* (Hansen et al., 1994) (Figure 10.12 A).

Additionally, a series of transcription factors grouped in this category including the bi-functional transcriptional repressor of nitrogen utilization and glutathione peroxidase *URE2* (Bai et al., 2004; Coschigano and Magasanik, 1991), transcriptional activator of thiamine biosynthesis *THI2* (Nishimura et al., 1992), and the basic leucine zipper regulator of sulfur metabolism *MET28* (Kuras et al., 1996).

While this category was not significantly enriched in the list of differentially upregulated genes in the *ALD6/ACS2 adh1Δ*  $\Sigma$ 1278b strain, expression values were often close to that of the *adh1Δ* strain (Figure 10.12 A). This discrepancy occurred due to the calculated p-value of the enrichment for this category falling out of the accepted threshold by a small margin (p-value of 0.0503).

Interestingly, when comparing gene expression between the *ALD6/ACS2 adh1Δ* strains and the *adh1Δ* strains, this category was found enriched in the list of downregulated genes in the W303-1A strain (Figure 10.7).

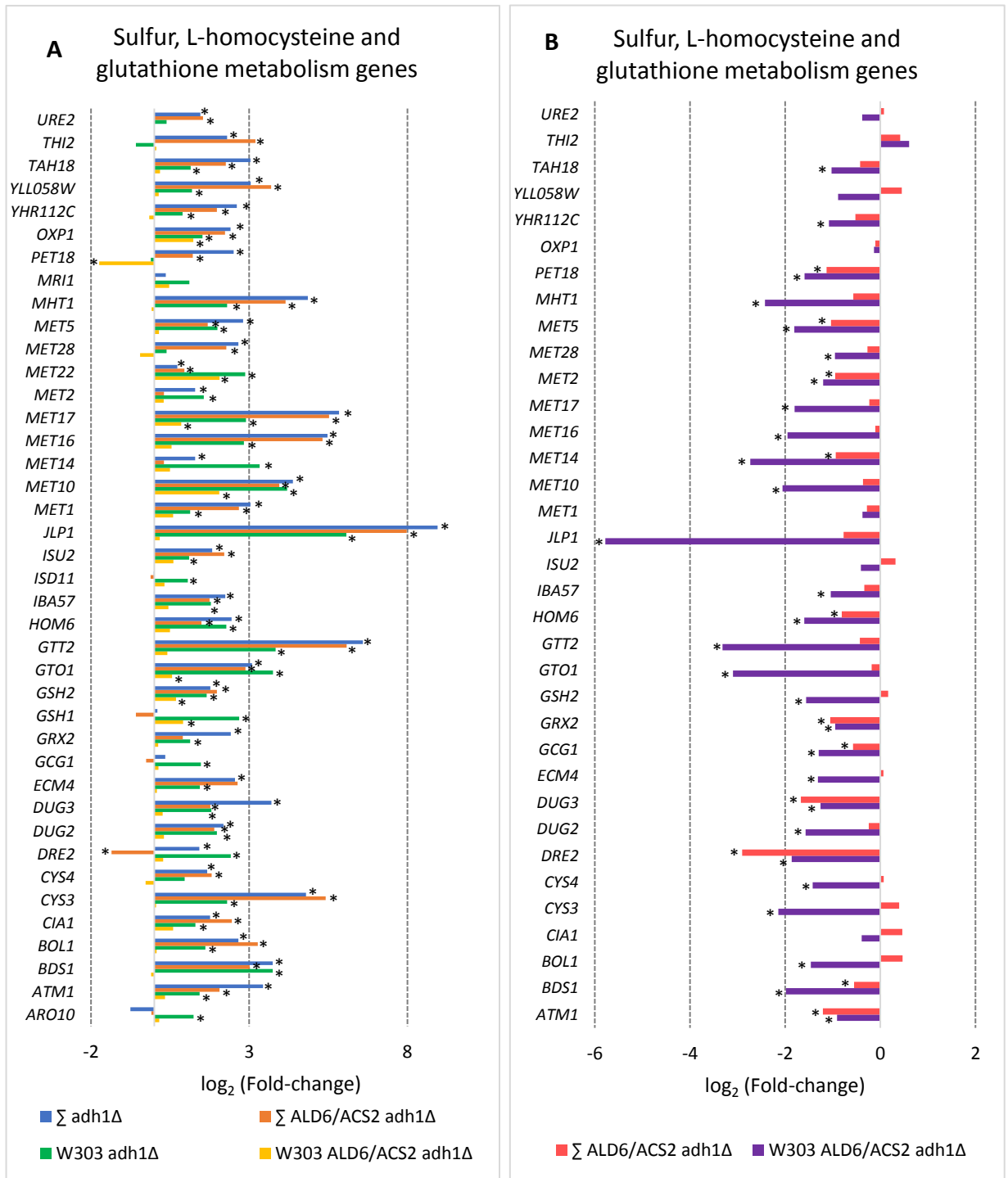


**Figure 10.12. Upregulation of sulfur metabolism genes in the *adh1Δ* strains decreases when *ALD6* and *ACS2* are overexpressed.** A) Bar plot of log<sub>2</sub> of the fold-change in expression of sulfur metabolism genes of the *adh1Δ* and *ALD6/ACS2 adh1Δ* strains, over their parental strains of the Σ1278b and W303-1A backgrounds. B) Bar plot of fold-change expression of genes in the *ALD6/ACS2 adh1Δ* strains, over their respective *adh1Δ* strains. Asterisks (\*) over each bar indicate a DEG with an adjusted p-value less than 0.05.

While this list contained only 26 genes, it included all of the top genes that were originally upregulated in the *adh1Δ* strains (Figure 10.12 B). Some of the genes suffered a drastic downregulation, such as *JLP1*, which changed from approximately 64-fold upregulation in the *adh1Δ* strain to almost a 100-fold decrease when *ALD6* and *ACS2* were overexpressed in the W303-1A background. While this trend was true for the W303-1A strain, the sulfur compound metabolic process term was not enriched in any of the DEG lists of the  $\Sigma$ 1278b strain in this comparison (Figure 10.7). Further examination of expression values of genes belonging to this category revealed weaker differential expression and multiple non-significant genes (Figure 10.12 B), reinforcing the observations made when mutant strains were compared with their respective parental strains (Figure 10.12 A).

The increased presence of sulfur metabolism transcripts in the *adh1Δ* mutant is an interesting finding that correlates with previous observations on the expression of genes belonging to the NADPH-producing pentose phosphate pathway (Figure 10.11 B). As mentioned above, DEGs assigned to this GO term can be separated into four categories depending on their metabolic function: uptake and reduction of sulfur to hydrogen sulfide (i.e. *MET14*, *MET16*, and *MET10*), biosynthesis of the sulfur-containing amino-acids cysteine, methionine, and homocysteine (i.e. *CYS3*, *CYS4*, and *MET6*), and glutathione biosynthesis and metabolism (i.e. *GSH2*, *GRX2*, and *GTT2*). Together, these genes form the sulfur assimilation and L-homocysteine biosynthesis pathway (Figure 10.13), and the glutathione biosynthesis and redox homeostasis reactions (Figure 10.14), two pathways that depend on NADPH for reductive power.

Glutathione is a ubiquitous antioxidant molecule involved in the detoxification of xenobiotics by its conjugation catalysed by glutathione-S-transferase enzymes Gtt1p and Gtt2p (Jakoby, 1985), as well as glutaredoxins Grx1p and Grx2p (Collinson and Grant,

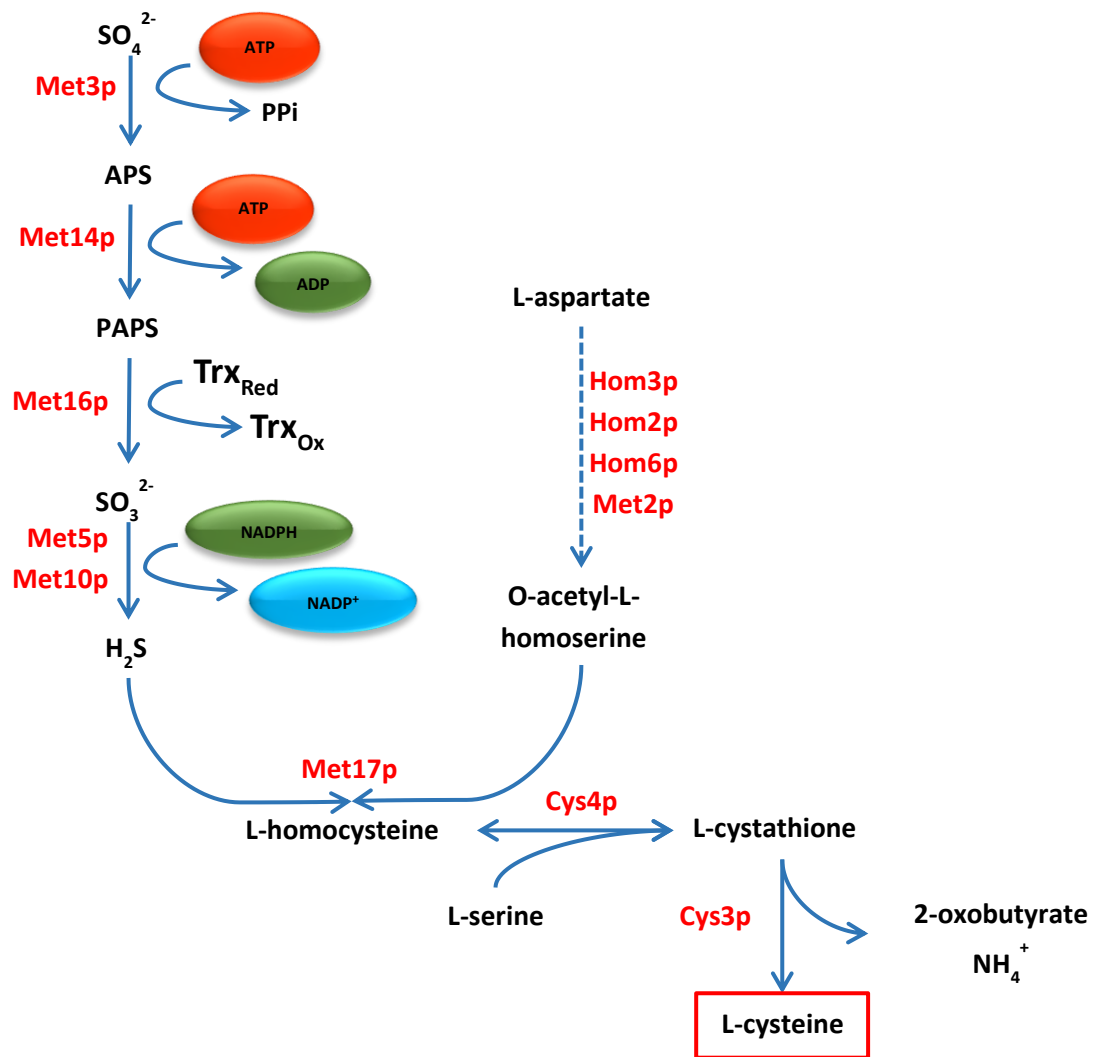


**Figure 10.13. Sulfate reduction and L-cysteine biosynthesis pathway in *S. cerevisiae*.** Diagram shows a summary of sulfate oxidation and biosynthesis of L-cysteine. Abbreviated metabolites and cofactors include adenosine triphosphate (ATP), adenosine diphosphate (ADP), adenosine-5'-phosphosulfate (APS), reduced nicotinamide adenine dinucleotide phosphate (NADPH), oxidised nicotinamide adenine dinucleotide phosphate (NAD<sup>+</sup>), 3'-phosphoadenylyl-sulfate (PAPS), reduced/oxidised thioredoxin (Trx<sub>Red</sub>/Trx<sub>Ox</sub>) Dashed line indicates multiple reactions. Enzymes involved: cystathione  $\gamma$ -lyase (Cys3p), cystathione  $\beta$ -synthase (Cys4p), aspartic  $\beta$  semi-aldehyde dehydrogenase (Hom2p), aspartate kinase (Hom3p), homoserine dehydrogenase (Hom6p), L-homoserine-O-acetyltransferase (Met2p), ATP sulfurylase (Met3p), sulfite reductase  $\beta$ -subunit (Met5p), sulfite reductase  $\alpha$ -subunit (Met10p), adenylyl sulfate kinase (Met14p), 3'-phosphoadenylylsulfate reductase (Met16p), O-acetyl homoserine-O-acetyl serine sulfhydrylase (Met17p).

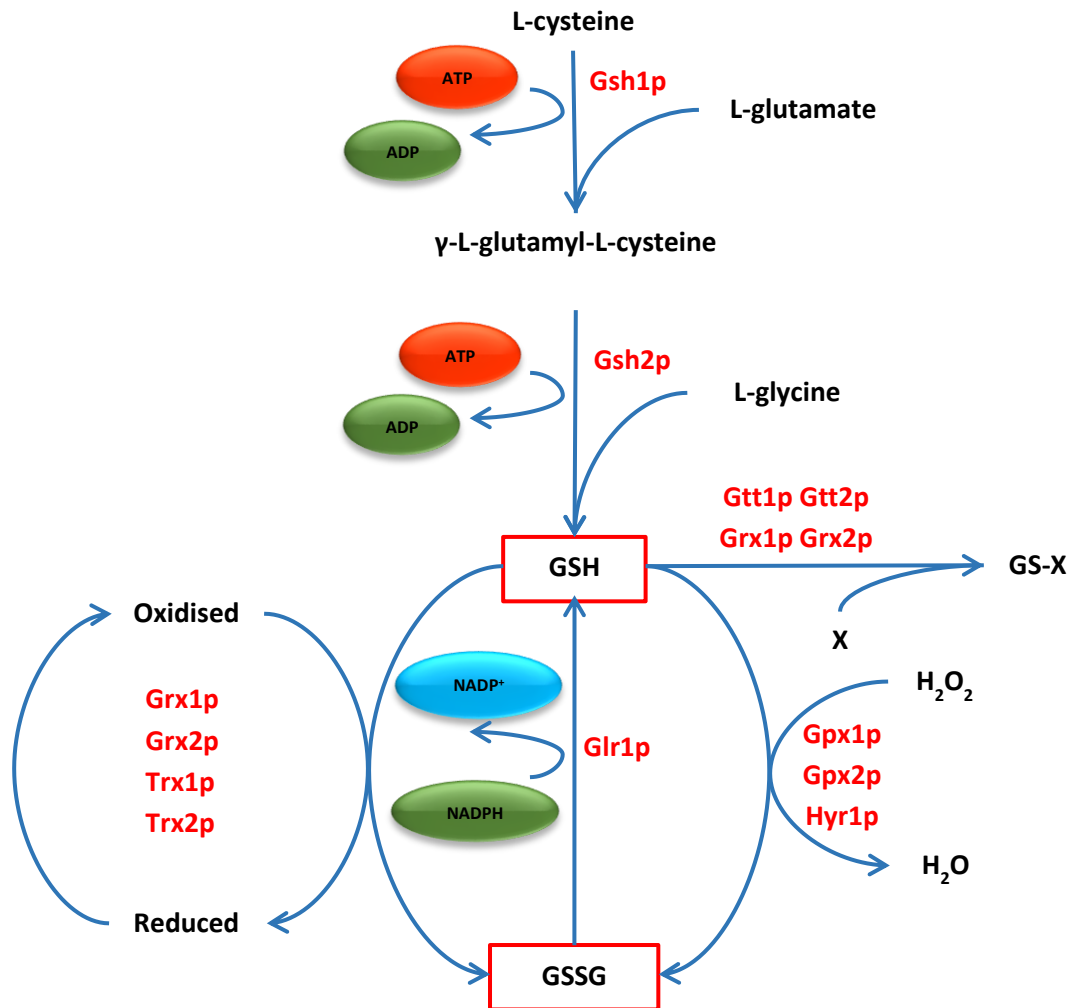


**Figure 10.14. Glutathione biosynthesis pathway and role of glutathione in the maintenance of redox homeostasis.** Diagram shows a summary of glutathione biosynthesis and its redox homeostasis reactions. Abbreviated metabolites and cofactors include adenosine triphosphate (ATP), adenosine diphosphate (ADP), glutathione (GSH), glutathione disulfide (GSSG), reduced nicotinamide adenine dinucleotide phosphate (NADPH), oxidised nicotinamide adenine dinucleotide phosphate (NAD<sup>+</sup>), a xenobiotic (X), and a xenobiotic-glutahtione gonjugate (GS-X). Enzymes involved: glutathione oxidoreductase (Glr1p), glutathione peroxidase (Gpx1p, Gpx2p, and Hyr1p),  $\gamma$ -glutamylcysteine synthetase (Gsh1p), glutathione synthetase (Gsh2p), glutaredoxin (Grx1p and Grx2p), glutathione S-transferase (Gtt1p and Gtt2p), thioredoxin (Trx1p and Trx2p).

2003) (Figure 10.14). Glutathione also serves as a scavenger of reactive oxygen species (ROS), protecting cellular structures such as membrane lipids from peroxidation by the action of glutathione peroxidases Grx1p, Grx2p, and Hyr1p (Muthukumar et al., 2011) and the glutaredoxin and thioredoxin enzymes (Trx1p and Trx2p) (Cnubben et al., 2001, Grant et al., 1996).

Evidence in the literature suggests that sulfur metabolism and glutathione are central in the acetaldehyde stress response of *S. cerevisiae*. One study reported the transcriptional upregulation of sulfur uptake, homocysteine biosynthesis, and thiamine biosynthesis genes after exposing yeast cells to a 1-hour acetaldehyde stress (Aranda and del Olmo, 2004). While the analytical technique and stress conditions are different between the above publication and this project, it is not surprising to see that the same group of genes is induced in the *adh1Δ* strains, as it was previously demonstrated that the deletion of *ADH1* causes the metabolic accumulation of acetaldehyde by disrupting its reduction into ethanol (Figure 9.5 A). It is also not surprising to see that the *ALD6/ACS2 adh1Δ* W303-1A did not exhibit the same upregulation of sulfur metabolism genes as the rest of the strains (Figures 10.12 A and B) given that it was not able to accumulate acetaldehyde in anaerobic culture.

Another study reported that yeast cells deleted for either *GSH1*, *GSH2*, or *GLR1* are more sensitive to acetaldehyde stress, suggesting that glutathione biosynthesis is required for acetaldehyde resistance in yeast (Matsifuji et al., 2013). The same study also found that one molecule of reduced glutathione was able to sequester up to four acetaldehyde molecules *in vitro*, revealing a plausible mechanism for its contribution to acetaldehyde tolerance within yeast cells.

In order to have a more complete view of the transcriptomic state of glutathione biosynthesis and the different reactions that use glutathione as a reductant in the tested strains, differential expression of genes belonging to each glutathione-related process was manually plotted (Figure 10.15).

Overall, the *adh1*Δ  $\Sigma$ 1278b displayed the highest level of gene upregulation across all of the categories, closely followed by the *ALD6/ACS2 adh1*Δ  $\Sigma$ 1278b strain (Figure 10.15). Many of the highly expressed genes in the *adh1*Δ  $\Sigma$ 1278b strain were expressed half as much in the *adh1*Δ W303-1A, such as *GTT2*, *MET3*, *GRX8*, and *MET17*, while expression of these genes was much less in the *ALD6/ACS2 adh1*Δ  $\Sigma$ 1278b strain (Figure 10.15).

Sulfate membrane transporter *SUL1* was highly induced in all strains, except in the *ALD6/ACS2 adh1*Δ W303-1A strain. On the other hand, while *SUL2* induction was about three times less than *SUL1*, its expression was more similar among all strains. One hypothesis explaining this phenomenon is that while *SUL1* is induced by acetaldehyde stress, *SUL2* is likely to be constitutively expressed. Additional experiments would be needed in order to test this hypothesis, but it could prove valuable to obtain new knowledge on the regulation of sulfate uptake in butanol-producing strains.

The expression of gene transcripts involved in glutathione-mediated oxidative stress responses and detoxification of chemicals showed a series of strain-dependent patterns. While the glutathione-S-transferase *GTT1* was found repressed in all four strains, *GTT2* was highly expressed in all strains, except the *ALD6/ACS2 adh1*Δ W303-1A strain (Figure 10.15), indicating that *GTT2* likely is the major isoform of the glutathione conjugation enzyme acting in these strains. At the same time, the glutathione-S-conjugate

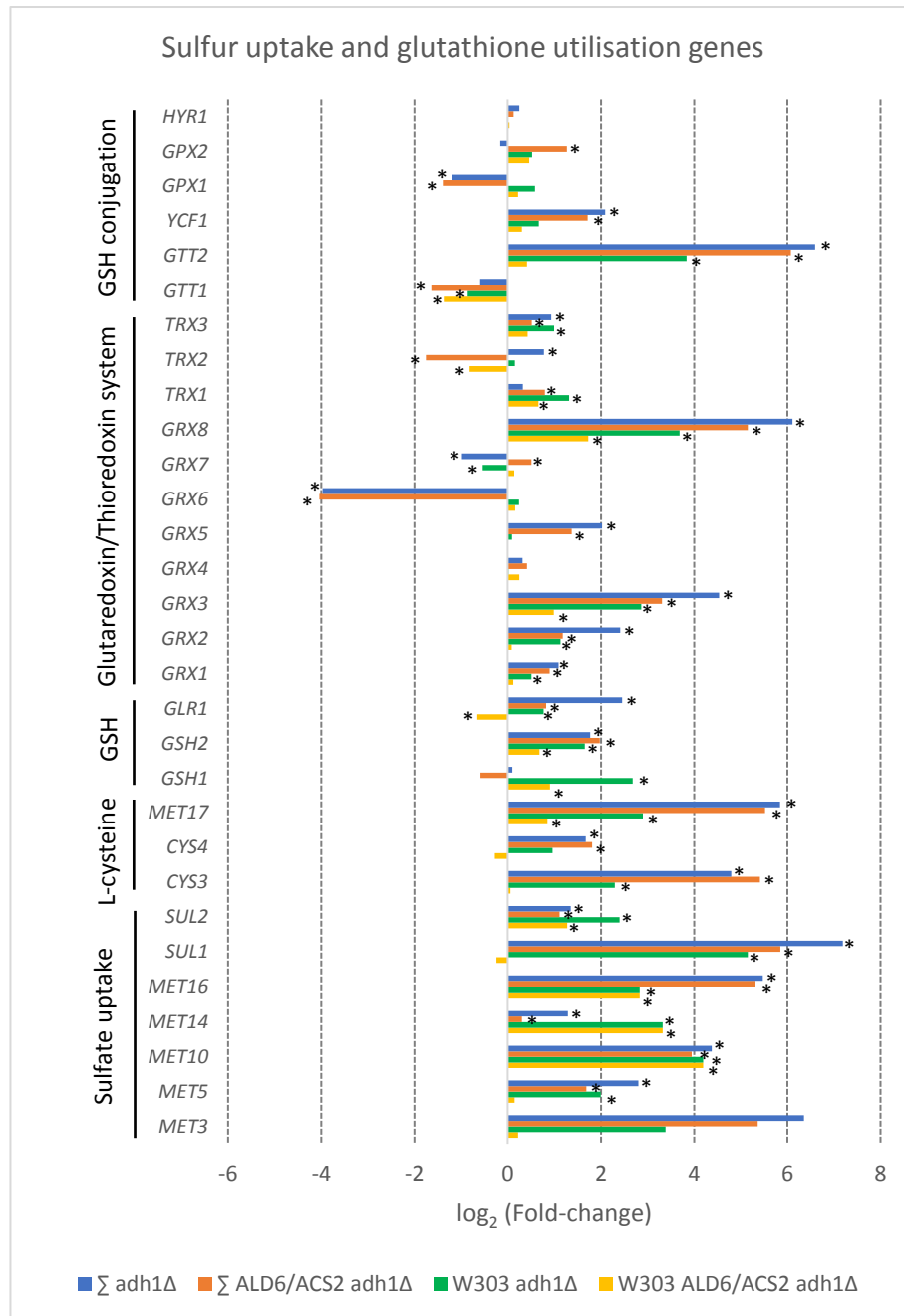


**Figure 10.15. Differential expression of genes involved in glutathione biosynthesis and cellular redox homeostasis.** Bar plot of  $\log_2$  of the fold-change in expression of sulfur uptake, L-cysteine biosynthesis, glutathione (GSH) biosynthesis, glutaredoxin/thioredoxin system, and glutathione conjugation genes of the  $adh1\Delta$  and  $ALD6/ACS2 adh1\Delta$  strains, over their parental strains of the  $\Sigma 1278b$  and W303-1A backgrounds. Asterisks (\*) over each bar indicate a DEG with an adjusted p-value less than 0.05.

vacuolar transporter *YCF1* was also induced in all strains (Figure 10.15), suggesting that detoxification of chemicals by glutathione conjugation is active in the strains during anaerobic growth. Expression of glutathione peroxidase genes varied among strains. While *GPX1* was significantly downregulated in both  $\Sigma$ 1278b strains, *GPX2* was significantly induced only in the *ALD6/ACS2 adh1Δ*  $\Sigma$ 1278b (Figure 10.15).

Glutaredoxins and thioredoxins also contribute to cellular protection against ROS. Glutaredoxins are able to reduce a series of oxidised substrates in order to revert oxidative damage done by ROS, and some participate in the synthesis of Fe/S clusters (Grant, 2001; Rodríguez-Manzaneque et al., 2002). There are eight identified *GRX* isoforms in *S. cerevisiae*, of which *GRX1*, *GRX2*, and *GRX8* are considered the “classical” glutaredoxins that contain two cysteine residues in their active site, while *GRX3-7* contain only one (Tang et al., 2014).

Among the multiple *GRX* gene transcripts that were induced in the yeast strains grown in anaerobic conditions, the *GXR8* gene transcript was induced the most, with *GRX3* and *GRX2* following it (Figure 10.14). Expression of these glutaredoxin genes followed the usual pattern of expression already seen in other induced DEGs, where the *adh1Δ*  $\Sigma$ 1278b had the most induction followed closely by its corresponding *ALD6/ACS2*-overexpressing version. The *ALD6/ACS2 adh1Δ* W303-1A had the lowest induction levels for these three glutaredoxins. Interestingly *GRX6*, encoding a glutaredoxin that localizes to the endoplasmic reticulum (ER) and Golgi apparatus, was the only isoform strongly repressed in both  $\Sigma$ 1278b strains (Figure 10.15). It has been proposed in the literature that *GRX6* participates in the maintenance of the redox state of enzymes and nascent proteins in the ER lumen (Izquierdo et al., 2008), thus its repression in the  $\Sigma$ 1278b strains could be suggestive of reduced secretory activity.

Besides participating in the defence against ROS, thioredoxins are also required as cofactors for PAPS reduction to sulfite by Met16p in the sulfate reduction pathway (Figure 10.13), and can catalyse deglutathionylation reactions (Greetham et al., 2010).

Thioredoxin gene transcript expression varied between the tested strains. *TRX1* expression was induced in all strains except the *adh1Δ*  $\Sigma$ 1278b strain, while *TRX2* was induced in the *adh1Δ*  $\Sigma$ 1278b mutant and repressed in both *ALD6/ACS2* strains (Figure 10.15). Finally, *TRX3*, encoding a mitochondrial thioredoxin, was increased in all strains except the *ALD6/ACS2 adh1Δ* W303-1A mutant.

Among L-cysteine biosynthesis genes, *MET17* and *CYS3* were expressed the most in the *adh1Δ* mutant, which encode the enzymes that catalyse the biosynthesis of L-homocysteine from O-acetyl-homoserine and hydrogen sulfide, and the breakdown of L-cystathione into L-cysteine, 2-oxobutyrate and ammonia, respectively (Figure 10.13). 2-oxobutyrate is a metabolite involved in the proposed threonine-dependent 1-butanol production pathway, where its metabolism by enzymes Leu4p, Leu1p, and Leu2p result in the synthesis of 2-oxoalate, the precursor of 1-butanol (Si et al., 2014).

While the accumulation of 2-oxobutyrate as a by-product of L-cysteine biosynthesis in the *adh1Δ*  $\Sigma$ 1278b strain is an attractive hypothesis for the increased 1-butanol production over the W303-1A strain, it is important to note that the  $\Sigma$ 1278b strain is *leu2Δ*. This enzyme is also theorized to participate in the glycine-dependent 1-butanol pathway to produce 2-oxoalate. The results obtained show that the  $\Sigma$ 1278b *adh1Δ* was able to accumulate 1-butanol despite lacking a functional *LEU2* gene, suggesting that either this strain uses a different pathway, or an unidentified gene is complementing the *leu2Δ* phenotype. A similar hypothesis was proposed by a previous study from our

laboratory, where neither deletion of *LEU1* or expression of *LEU2* had any impact on 1-butanol accumulation in the *adh1Δ* W303-1A strain (Swidah et al., 2018).

A quick and simple experiment that can be performed to test the oxidative stress response of the *adh1Δ* strains compared to the parental strains is a spot test on agar plates supplemented with hydrogen peroxide ( $H_2O_2$ ). Serial dilutions of cultures growing in exponential phase in liquid SCD were spotted on SCD agar plates either in the absence or presence of 0.5 mM  $H_2O_2$  and left to grow up for 4 days. Preliminary results showed that the *adh1Δ* mutant better tolerated the presence of  $H_2O_2$  compared with the wild-type strain (Figure 10.16), suggesting that the results of the transcriptomic analysis translated to an effective phenotypical advantage in the *adh1Δ* strains. Additional assays using different  $H_2O_2$  concentrations and sources of ROS should be used in future experiments to test antioxidant mechanisms in the *adh1Δ* strains.

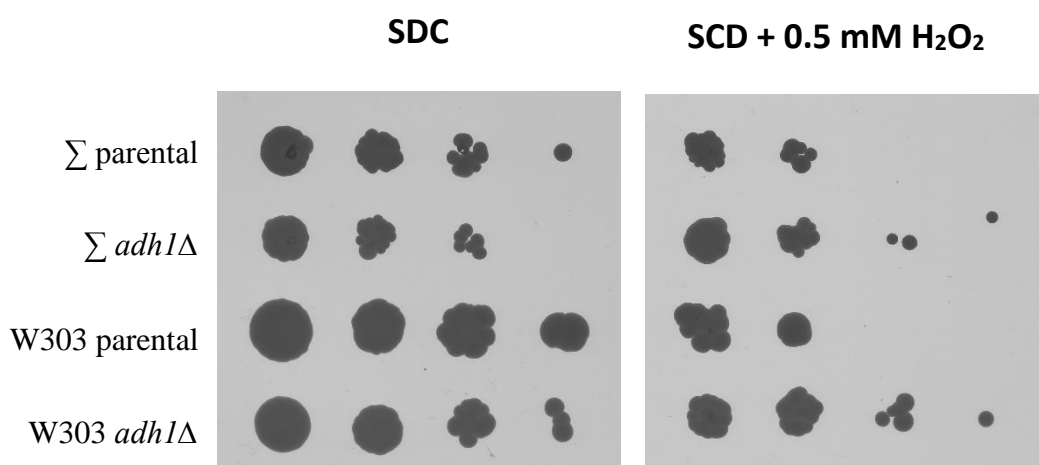


**Figure 10.16. *adh1* $\Delta$  strains are more resistant to hydrogen peroxide stress than the parental strains.** 1:10 serial dilutions of exponential phase cultures of *adh1* $\Delta$  and parental strains of the  $\Sigma$ 1278b and W303-1A background spotted on solid SCD media supplemented with amino-acids with or without 0.5 mM H<sub>2</sub>O<sub>2</sub> and grown at 30°C for 4 days.

## 10.6 Discussion

RNA-seq data for *adh1* $\Delta$  and *ALD6/ACS2 adh1* $\Delta$  strains of the  $\Sigma$ 1278b and W303-1A genetic backgrounds has revealed the regulation of a variety of cellular processes that may contribute to the differential accumulation of endogenous 1-butanol in these strains. Overall, repression of respiratory and ergosterol biosynthesis genes and induction of NADPH-generating reactions, sulfate uptake, glutathione biosynthesis and redox homeostasis genes correlated well with 1-butanol and acetaldehyde accumulation in these yeast strains.

Besides particular differences between the expression patterns observed in each genetic background, it is likely that a major contributing factor to the differences in 1-butanol production between the  $\Sigma$ 1278b and W303-1A background is the intensity of the differential expression of gene transcripts for each relevant cellular process. It may not be coincidental that the *ALD6/ACS2 adh1* $\Delta$  W303-1A strain, which were not able to accumulate 1-butanol, displayed a transcriptomic response which is lower, and in some cases, opposite to the response in the other strains.

While the above analysis did not yield any definitive answers as to how 1-butanol is effectively synthesised by the endogenous pathway, it revealed expression patterns that emphasise the importance of cellular defence mechanisms against acetaldehyde and other stresses present during anaerobic fermentation. Improvements in tolerance towards toxic metabolites has been a viable strategy towards increasing the yield of cellular metabolic products of industrial interest, hence further investigation of the role of NADPH-producing and glutathione metabolism genes in 1-butanol yields is a potential future avenue of research.

Finally, attempting to address the role of unidentified gene transcripts which show differential changes in expression such as *YML146W*, *YJL027C*, and *YLR257W* in the cellular response to anaerobic fermentation might result in the characterisation of new genes and an expansion of the knowledge of the actors involved in *S. cerevisiae* 1-butanol production.

## 11. General discussion

### 11.1 Overview

Butanol is a fusel alcohol that has attracted attention as a potential biofuel due to its higher energy density, lower volatility, reduced hygroscopicity and minimal corrosive properties relative to ethanol (Dürre, 2007). Butanol is naturally produced by anaerobic bacteria of the *Clostridia* genus through the ABE pathway (Zheng et al., 2009), but due to the challenges of using these microorganisms in industry, researchers have attempted to express this pathway in more industry-friendly hosts such as *S. cerevisiae*.

While early attempts at expressing the ABE pathway in *S. cerevisiae* resulted in low 1-butanol yields (Steen et al, 2008), improvements were made by deleting *ADHI*, the major yeast alcohol dehydrogenase. Curiously, as well as enhancing butanol production from an exogenously expressed metabolic pathway, deletion of the *ADHI* gene was also able to activate endogenous butanol production in yeast (Si et al., 2014; Swidah et al., 2015).

Additional research has demonstrated that enhancing cellular tolerance to 1-butanol stress can improve production (Ashe et al., 2001; Swidah et al., 2015), making this area of research attractive for biotechnology. One of the adaptive responses to fusel alcohols found in wild strains and the laboratory  $\Sigma$ 1278b strain is filamentation, a proposed scavenging response activated by nitrogen starvation and/or toxic microenvironments that result in drastic morphological changes (Lorenz et al., 2000).

The fact that filamentous strains respond in terms of their morphology and growth to fusel alcohols such as 1-butanol prompted an aim of this project, that was to study endogenous 1-butanol accumulation induced by the deletion of *ADHI* in the filamentous  $\Sigma$ 1278b strain with a view to the identification of methods for improving butanol production in yeast strains. In addition, it was recognised that in order to harness the

genetic advantages of yeast for optimised butanol production, a simple assay reporting increased butanol levels would be required.

## 11.2 Summary of the main findings of this project

The first objective of this project was to construct a fluorescent butanol-responding biosensors with the goal of generating new tools to screen for mutant strains demonstrating increased 1-butanol yields. To this end, six biosensor strains consisting of GFP fusions of *GAC1*, *GLC7*, *BDH2*, *RTS3*, *NRP1*, and *SHQ1*, were constructed in the W303-1A background, and their ability to respond to 1-butanol stress was tested in different assays.

Overall, none of the biosensor strains was able to produce a significant increase in fluorescence after exposure to 1-butanol. Western-blot analysis hinted at a failure to produce the fusion protein, suggesting that the candidate genes were not appropriate for the desired application. Hence, new strategies to construct fast and specific 1-butanol biosensors will have to be developed if yeast genetic screening is to be applied to butanol production.

In order to address another major objective of this thesis, *ADHI* was deleted in a  $\Sigma$ 1278b strain, resulting in a slow-growing strain that displayed complex colony morphology. When anaerobic 1-butanol accumulation of the *adh1* $\Delta$   $\Sigma$ 1278b strain was measured relative to an *adh1* $\Delta$  W303-1A by gas chromatography, the filamentous strain produced more 1-butanol than its non-filamentous counterpart, suggesting that the  $\Sigma$ 1278b possesses beneficial traits for this purpose.

In an attempt to improve butanol yields of the *adh1* $\Delta$   $\Sigma$ 1278b strain, *ALD6* and *ACS2* were overexpressed in order to decrease intracellular levels of the toxic metabolite acetaldehyde. In anaerobic fermentation, the *ALD6/ACS2 adh1* $\Delta$   $\Sigma$ 1278b strain had

impaired acetaldehyde and 1-butanol accumulation, while the *ALD6/ACS2 adh1Δ* W303-1A had its acetaldehyde and 1-butanol accumulation abolished. This experiment showed that both genetic backgrounds responded differently to the overexpression of *ALD6* and *ACS2* and hinted at a potential role for acetaldehyde in inducing 1-butanol accumulation in the *adh1Δ* mutants.

As an additional experiment to test alternative mutations leading to endogenous 1-butanol production, *PDC1* and *PDC5* were deleted to test if disrupting pyruvate decarboxylation could mimic the phenotype of *adh1Δ* mutants. Interestingly, neither *pdc1Δ*, *pdc5Δ*, or *pdc1,5Δ* deletions resulted in 1-butanol or acetaldehyde accumulation, suggesting that activation of endogenous butanol accumulation is specific to the deletion of *ADH1*.

Finally, in order to obtain a more complete picture of the mechanisms behind the observed differences in 1-butanol accumulation among the tested strains, transcriptomic analysis of *adh1Δ*, *ALD6/ACS2 adh1Δ*, and *pdc1Δ* strains of the  $\Sigma$ 1278b and W303-1A background was performed. Differential expression data showed that transcriptional induction of sulfur uptake and glutathione biosynthesis and the pentose phosphate pathway, as well as transcriptional repression of aerobic respiration and ergosterol biosynthesis correlated with the ability to produce 1-butanol in the *adh1Δ* strains. These results hint at a role for NADPH and glutathione as acetaldehyde tolerance mechanisms that may improve survival under stressful conditions, thus enabling increased 1-butanol production. The downregulation of aerobic metabolism and ergosterol biosynthesis may represent an adaptive strategy to redirect energy and NADPH to more critical processes, such as acetaldehyde tolerance.

### 11.3 Conclusions

The results obtained in this project have revealed some insights into the mechanisms behind endogenous 1-butanol production activated by the deletion of *ADH1* in *S. cerevisiae*. The correlation between acetaldehyde and butanol accumulation as well as the transcriptomic state during anaerobic fermentation in the *adh1Δ* strains imply that the acetaldehyde stress response plays a role in facilitating 1-butanol production. Hence, engineering yeast strains for enhanced glutathione biosynthesis is a promising strategy to achieve higher endogenous 1-butanol production in *S. cerevisiae*. Indeed even in *Clostridia*, where metabolism differs enormously to *S. cerevisiae*, the introduction of glutathione biosynthetic genes has been shown to increase 1-butanol yields, although the precise explanation for this observation is not clear (Hou et al., 2013; Zhu et al., 2011).

This project also demonstrated that endogenous butanol production was not activated by the deletion of two pyruvate decarboxylases (*PDC1* and *PDC5*), likely due to the ability of *PDC6* to compensate for the lack of enzymatic activity. On the other hand, despite presenting some residual ethanol production, the deletion of *ADH1* resulted in drastic metabolic changes, indicating that the other six *ADH* isoforms are not able to compensate for the loss of *ADH1* activity while potentially participating in the reduction of butyraldehyde to 1-butanol. Future deletion and overexpression analysis of the *ADH* isoforms and other alcohol dehydrogenases in an *adh1Δ* strain could reveal which gene is involved in 1-butanol production.

Despite its advantages, there is still a long way before *S. cerevisiae* can become a butanol-producing host able to compete with bacterial producers. Metabolic optimisation of both the endogenous and the ABE pathway and engineering of strains able to tolerate

higher concentrations of butanol and other metabolic intermediates will be paramount to minimise inhibitory effects on the butanol production pathways. Additionally, coupling the above modifications with pathways for the efficient utilisation of xylose is a high priority if the goal is to produce butanol using more sustainable sources of biomass such as agricultural lignocellulosic wastes.

One final question is if there is still value in the biological production of butanol and other biofuels in the advent of commercially viable electrical vehicles. While biofuels seem to be in disadvantage against the sustainability of electrical vehicle technologies, it is important to note that this is just one application for these chemicals. Aviation technologies still depend on liquid fuels to propel aircrafts, and efforts are being made to employ biojet fuels in order to decrease the environmental impact of flight (Bosch et al., 2017). Additionally, the applications of butanol and other chemical products is not limited to biofuels, but they can be employed in a series of industrial production processes. This flexibility grants biorefinery-based industries a value that cannot be matched by electric technologies, securing its place in humanity's toolkit to approach new challenges.

## 12. References

- Abdullah B., Muhammad S., Shokravi Z., Ismail S., Kassim K., Mahmood A., Aziz M. (2019). *Renew. Sustain. Energy Rev.* 107, pp. 37-50.
- Adeniyi O., Azimov U., Burluka A. (2018). Algae biofuel: Current status and future applications. *Renew. Sust. Energ. Rev.* 90, pp. 316-35.
- Alalwan H., Alminshid A., Aljafaari H. (2019). Promising evolution of biofuel generations. Subject review. *Renew. Energy Focus.* 28, pp. 127-39.
- Alberghina L., Cirulli C. (2010). Proteomics and systems biology to tackle biological complexity: Yeast as a case study. *Proteomics.* 10(24), pp. 4337-41.
- Alexandre A., Lehninger A. (1984). Bypasses of the antimycin a block of mitochondrial electron transport in relation to ubiquinone function. *Biochim. Biophys. Acta.* 767(1), pp. 120-9.
- Amodeo G., Momcilovic M., Carlson M., Tong L. (2010). Biochemical and functional studies on the regulation of the *Saccharomyces cerevisiae* AMPK homolog SNF1. *Biochem. Biophys. Res. Comm.* 397(2), pp. 197-201.
- Anders S., Huber W. (2010). Differential expression analysis for sequence count data. *Genome. Biol.* 11, R106.
- Aranda A., del Olmo M. (2003). Response to acetaldehyde stress in the yeast *Saccharomyces cerevisiae* involves a strain-dependent regulation of several *ALD* genes and is mediated by the general stress response pathway. *Yeast.* 20(8), pp. 747-59.
- Aranda A., del Olmo M. (2004). Exposure of *Saccharomyces cerevisiae* to acetaldehyde induces sulfur amino acid metabolism and polyamine transporter genes, which depend on Met4p and Haa1p transcription factors, respectively. *Appl. Environ. Microbiol.* 70(4), pp. 1913-22.
- Ashe M., Long S., Sachs A. (2000). Glucose Depletion Rapidly Inhibits Translation Initiation in Yeast. *Mol. Biol. Cel.* 11, pp. 833-48.
- Ashe M., Slaven J., De Long S., Ibrahim S., Sachs A. (2001). A novel eIF2B-dependent mechanism of translational control in yeast as a response to fusel alcohols. *EMBO J.* 20(22), pp. 6464-74.
- Ashrafi K., Lin S., Manchester J., Gordon J. (2001). Sip2p and its partner Snf1p kinase affect aging in *S. cerevisiae*. *Genes Dev.* 14(15), pp. 1872-85.
- Atsumi S., Cann A., Connor M., Shen C., Smith K., Brynildsen M., Chou K., Hanai T., Liao J. (2008). Metabolic engineering of *Escherichia coli* for 1-butanol production. *Metab. Eng.* 10(6), pp. 305-11.
- Bae S., Kim S., Kahn J. (2016). Efficient production of acetoin in *Saccharomyces cerevisiae* by disruption of 2,3-butanediol dehydrogenase and expression of NADH oxidase. *Sci. Rep.* 6(27667).

- Bai M., Zhou J., Perrett S. (2004). The Yeast Prion Protein Ure2 Shows Glutathione Peroxidase Activity in Both Native and Fibrillar Forms. *J. Biol. Chem.* 279(48), pp. 50025-30.
- Balleza E., Kim J., Cluzel P. (2018). Systematic characterization of maturation time of fluorescent proteins in living cells. *Nat. Methods.* 15, pp. 47-51.
- Barnett J. (1998). A History of Research on Yeasts 1: Work by Chemists and Biologists 1789-1850. *Yeast*, 14(16), pp. 1439-51.
- Barnett J. (2000). A History of Research on Yeasts 2: Louis Pasteur and his contemporaries, 1850–1880. *Yeast*, 16(8), pp. 755-71.
- Barnett J. (2003). A history of research on yeasts 5: the fermentation pathway. *Yeast*, 20(6), pp. 509-43.
- Bartowsky E., Henschke P. (2004). The 'buttery' attribute of wine--diacetyl--desirability, spoilage and beyond. *Int. J. Food. Microbiol.* 96(3), pp. 235-52.
- Bermejo C., Haerizadeh F., Takanaga H., Chermark D., Frommer W. (2011). Optical sensors for measuring dynamic changes of cytosolic metabolite levels in yeast. *Nat. Protoc.* 6(11), pp. 1806-17.
- Bertels L., Fernández L., Heinisch J. (2021). The Pentose Phosphate Pathway in Yeasts—More Than a Poor Cousin of Glycolysis. *Biomolecules.* 11(5), 725.
- Bhatnagar A., Chinnasamy S., Singh M., Das C. (2011). Renewable biomass production by mixotrophic algae in the presence of various carbon sources and wastewaters. *Appl. Energy.* 88, pp. 3425-31.
- Bidard F., Bony M., Blondin B., Dequin S., Barre P. (1995). The *Saccharomyces cerevisiae* *FLO1* flocculation gene encodes for a cell surface protein. *Yeast.* 11(9), pp. 809-22.
- Binder S., Schendzielorz G., Stäbler N., Krumbach K., Hoffmann K., Bott M., Eggeling L. (2012). *Genome. Biol* 12, R40.
- Bleoanca I., Bahrim G. (2013). Overview on Brewing Yeast Stress Factors. *Rom.Biotechnol. Lett.* 18(5), pp. 8559-72.
- Blackwood A., Simpson F., Wheat J., Leslie J., Ledingham G. (1949). Production and properties of 2,3-butanediol: XXXI. Pilot plant studies on the fermentation of whet by *Aerobacillus polymyxa*. *Can. J. Res.* 27F(4), pp. 199-210.
- Blázquez M., Gamo F., Gancedo C. (1995). A mutation affecting carbon catabolite repression suppresses growth defects in pyruvate carboxylase mutants from *Saccharomyces cerevisiae*. *FEBS Letters.* 377(2), pp. 197-200.
- Boer V., de Winde J., Pronk J., Piper M. (2003). The Genome-wide Transcriptional Responses of *Saccharomyces cerevisiae* Grown on Glucose in Aerobic Chemostat Cultures Limited for Carbon, Nitrogen, Phosphorus, or Sulfur. *J. Biol. Chem.* 278(5), pp. 3265-74.

Bosch J., De Jong S., Hoefnagels R., Slade R. (2017). *Aviation biofuels: strategically important, technically achievable, tough to deliver*. Available at: <https://www.imperial.ac.uk/media/imperial-college/grantham-institute/public/publications/briefing-papers/BP-23-Aviation-Biofuels.pdf> (Accessed: 29 September 2021).

Boy-Marcotte E., Ikonomi P., Jacquet M. (1996). SDC25, a dispensable Ras guanine nucleotide exchange factor of *Saccharomyces cerevisiae* differs from CDC25 by its regulation. *Mol. Biol. Cell.* 7(4), pp. 529-39.

BP p.l.c. (2020). *bp Statistical Review of World Energy 2020 69<sup>th</sup> edition*. Available at: <https://www.bp.com/content/dam/bp/business-sites/en/global/corporate/pdfs/energy-economics/statistical-review/bp-stats-review-2020-full-report.pdf> (Accessed: 24 September 2021).

Branduardi P., Longo V., Berterame N., Rossi G., Porro D. (2013). A novel pathway to produce butanol and isobutanol in *Saccharomyces cerevisiae*. *Biotechnol. Biofuels*, 6(68).

Braus G., Grundmann O., Brückner S., Mösch H. (2003). Amino Acid Starvation and Gcn4p Regulate Adhesive Growth and *FLO11* Gene Expression in *Saccharomyces cerevisiae*. *Mol. Biol. Cell.* 14(10), pp. 4272-84.

Brito A., Neuhäuser B., Wintjens R., Marini A., Boeckstaens M. (2020). Yeast filamentation signaling is connected to a specific substrate translocation mechanism of the Mep2 transceptor. *PLoS Genet.* 16(2): e1008634.

Bud R. (1993). *The uses of life: a history of biotechnology*. Cambridge: Cambridge University Press, pp. 299.

Budovskaya V., Stephan J., Deminoff S., Herman P. (2005). An evolutionary proteomics approach identifies substrates of the cAMP-dependent protein kinase. *Proc. Natl. Acad. Sci. U S A.* 102(39), pp. 13933-38.

Bui V., Thi Thu Huyen Nguyen, Mai C., Bettarel Y., Hoang T., Trinh T., Truong N., Chu H., Nguyen V., Nguyen H., Wöfl S. (2016). Procarcinogens – Determination and Evaluation by Yeast-Based Biosensor Transformed with Plasmids Incorporating *RAD54* Reporter Construct and Cytochrome *P450* Genes. *PLOS ONE.* 11(12), e0168721.

Bushnell B., Rood J., Singer E. (2017). BBMerge – Accurate paired shotgun read merging via overlap. *PLoS ONE.* 12(10), e0185056.

Cabrito T., Teixeira M., Singh A., Prasad R., Sá-Correia I. (2011). The yeast ABC transporter Pdr18 (ORF *YNR070w*) controls plasma membrane sterol composition, playing a role in multidrug resistance. *Biochem. J.* 440(2), pp. 195-202.

Campbell S., Hoyle N., Ashe M. (2005). Dynamic cycling of eIF2 through a large eIF2B-containing cytoplasmic body: implications for translation control. *J. Cell. Biol.* 170(6), pp. 925-34.

Cannon J. (2010). Function of protein phosphatase-1, Glc7, in *Saccharomyces cerevisiae*. *Adv. Appl. Microbiol.* 73, pp. 27–59.

- Cao Y., Fanning S., Proos S., Jordan K., Srikumar S. (2018). A Review on the Applications of Next Generation Sequencing Technologies as Applied to Food-Related Microbiome Studies. *Front. Microbiol.* doi: 10.3389/fmicb.2017.01829.
- Carbone D., Gargano I., Chiaiese P., Pollio A., Marotta R., Olivieri G., Pinto G. (2017). *Scenedesmus vacuolatus* cultures for possible combined laccase-like phenoloxidase activity and biodiesel production. *Annals. Microbiol.* 68, pp. 9-15.
- Carter Z., Delneri D. (2010). New generation of *loxP*-mutated cassettes for the genetic manipulation of yeast natural isolates. *Yeast*, 27, pp. 765-75.
- Celińska E., Grajek W. (2009). Biotechnological production of 2,3-butanediol--current state and prospects. *Biotechnol. Adv.* 27(6), pp. 715-25.
- Chang H., Kaiser C., Hartl F., Barral J. (2005). *De novo* Folding of GFP Fusion Proteins: High Efficiency in Eukaryotes but Not in Bacteria. *J. Mol. Biol.* 253(2), pp. 397-409.
- Chavel C., Dionne H., Birkaya B., Joshi J., Cullen P. (2010). Multiple Signals Converge on a Differentiation MAPK Pathway. *PLoS Genet.* 6(3).
- Chen G., Jordan F. (1984). Brewers' yeast pyruvate decarboxylase produces acetoin from acetaldehyde: a novel tool to study the mechanism of steps subsequent to carbon dioxide loss. *Biochem.* 23(16), pp. 3576-82.
- Chen H., Fink G. (2006). Feedback control of morphogenesis in fungi by aromatic alcohols. *Genes Dev.* 20(9), pp. 1150-61.
- Chen R., Thorner J. (2007). Function and Regulation in MAPK Signaling Pathways: Lessons Learned from the Yeast *Saccharomyces cerevisiae*. *Biochim Biophys. Acta.* 1773(8), pp. 1311-40.
- Choi J., Lou W., Vancura A. (1998). A Novel Membrane-bound Glutathione S-Transferase Functions in the Stationary Phase of the Yeast *Saccharomyces cerevisiae*. 273(45), pp. 29915-22.
- Colgan J. (2013). Fueling the Fire: Pathways from Oil to War. *Int. Secur.* 38(2), pp. 147-80.
- Collinson E., Grant C. (2003). Role of Yeast Glutaredoxins as Glutathione S-transferases. *J. Biol. Chem.* 25(20), pp. 22492-97.
- Conesa A., Madrigal P., Tarazona S., Gomez-Cabrero D., Cervera A., McPherson A., Wojciech Szcześniak M., Gaffney D., Elo L., Zhang X., Mortazavi A. (2016). A survey of best practices for RNA-seq data analysis. *Genome. Biol.* 17, 13.
- Coschigano P., Magasanik B. (1991). The *URE2* Gene Product of *Saccharomyces cerevisiae* Plays an Important Role in the Cellular Response to the Nitrogen Source and Has Homology to Glutathione S-Transferases. *Mol. Cell. Biol.* 11(2), pp. 822-32.
- Costessi A., van der Bogert B., May A., van Themaat E., Roubos J., Kolkman M., Butler D., Pirovano W. (2018). Novel sequencing technologies to support industrial biotechnology. *FEMS Microbiol. Lett.* 365(16). doi: 10.1093/femsle/fny103.

- Cranfill P., Sell B., Baird M., Allen J., Lavagnino Z., de Gruiter H., Kremers G., Davidson M., Usitone A., Piston D. (2016). Quantitative Assessment of Fluorescent Proteins. *Nat. Methods*. 13(7), pp. 557-62.
- Crutzen P., Mosier A., Smith K., Winiwarter W. (2016). N<sub>2</sub>O Release from Agro-biofuel Production Negates Global Warming Reduction by Replacing Fossil Fuels. In: Crutzen P., Brauch H., eds., *Paul J. Crutzen: A Pioneer on Atmospheric Chemistry and Climate Change in the Anthropocene*. Springer, Cham, pp. 227-238.
- Cullen P., Sprague Jr. G. (2000). Glucose depletion causes haploid invasive growth in yeast. *Proc. Natl. Acad. Sci. U S A*. 97(25), pp. 13619-24.
- Cullen P., Sprague Jr. G. (2002). The roles of bud-site-selection proteins during haploid invasive growth in yeast. *Mol. Biol. Cell*. 13(9), pp. 2990-3004.
- Cullen P., Sabbagh W., Graham Jr. E., Irick M., van Olden E., Neal C., Delrow J., Bardwell L., Sprague Jr. G. (2004). A signaling mucin at the head of the Cdc42- and MAPK-dependent filamentous growth pathway in yeast. *Genes Dev*. 18(14), pp.1695–1708.
- Cullen P., Sprague Jr. G. (2012). The Regulation of Filamentous Growth in Yeast. *Genetics*. 190(1), pp. 23-49.
- Cullen P. (2015). The Plate-Washing Assay: A Simple Test for Filamentous Growth in Budding Yeast. *Cold Spring Harb. Protoc*. 2, pp. 168-71.
- Cutler N., Pan X., Heitman J., Cardenas M. (2001). The TOR Signal Transduction Cascade Controls Cellular Differentiation in Response to Nutrients. *Mol. Biol. Cell*. 12(12), pp. 4103-13.
- Dacquay L., McMillen D. (2021). Improving the design of an oxidative stress sensing biosensor in yeast. *FEMS Yeast. Res*. 21(4), foab025.
- D'Ambrosio V., Jensen M. (2017). Lighting up yeast cell factories by transcription factor-based biosensors. *FEMS Yeasts. Res*. 17(7), fox076.
- Dang N., Hinch D. (2011). Identification of two hydrophilins that contribute to the desiccation and freezing tolerance of yeast (*Saccharomyces cerevisiae*) cells. *Cryobiology*. 62(3), pp. 188-93.
- Davies B., Rine J. (2006). A Role for Sterol Levels in Oxygen Sensing in *Saccharomyces cerevisiae*. *Genetics*. 174(1), pp. 191-201.
- Das B., Deka S. (2019). A cost-effective and environmentally sustainable process for phycoremediation of oil field formation water for its safe disposal and reuse. *Sci. Rep*. 9(15232).
- Davis A., Symington L. (2001). The Yeast Recombinational Repair Protein Rad59 Interacts With Rad52 and Stimulates Single-Strand Annealing. *Genetics*. 159(2), pp. 515-25.
- De Deken R. (1966). The Crabtree Effect: A Regulatory System in Yeast. *J. Gen. Microbiol*. 44, pp. 149-56.

- de Groot P., Hellingwerf K., Klis F. (2003). Genome-wide identification of fungal GPI proteins. *Yeast*. 20(9), pp. 781-96.
- Delneri D., Gardner D., Oliver S. (1999). Analysis of the Seven-Member AAD Gene Set Demonstrates That Genetic Redundancy in Yeast May Be More Apparent Than Real. *Genetics*. 153(4), pp. 1591-600.
- Demirbas A. (2015). Properties of Fuels from Crops. In: J. Speight, ed., *The Biofuels Handbook*. London: Royal Society of Chemistry, pp. 228-254.
- Demuyser L., Palmans I., Vandecruys P., Van Dijck P. (2020). Molecular Elucidation of Riboflavin Production and Regulation in *Candida albicans*, toward a Novel Antifungal Drug Target. *mSphere*. 5(4), e00714-20.
- de Smidt O., du Preez J., Albertyn J. (2008). The alcohol dehydrogenases of *Saccharomyces cerevisiae*: a comprehensive review. *FEMS. Yeast. Res.* 8(7), pp. 967-78.
- Dickinson J., Salgado L., Hewlins M. (2002). The Catabolism of Amino Acids to Long Chain and Complex Alcohols in *Saccharomyces cerevisiae*. *J. Biol. Chem.* 278(10), pp. 8034-34.
- Ding N., Zhou S., Deng Y. (2021). Transcription-Factor-based Biosensor Engineering for Applications in Synthetic Biology. *ACS. Synth. Biol.* 10(5), pp. 911-22.
- Dobbel C. (1923). A Protozoological Bicentenary: Antony van Leeuwenhoek (1632–1723) and Louis oblot (1645–1723). *Parasitology*, 15(3), pp. 308-319.
- Dobin A., Davis C., Schlesinger F., Drenkow J., Zaleski C., Jha S., Batut P., Chaisson M., Gingeras T. (2013). STAR: ultrafast universal RNA-seq aligner. *Bioinformatics*. 29(1), pp. 15-21.
- Donker H. (1926). Ph.D. Dissertation. Delft, Netherlands.
- Duina A., Miller M., Keeney J. (2014). Budding Yeast for Budding Geneticists: A Primer on the *Saccharomyces cerevisiae* Model System. *Genetics*. 197(1), pp. 33-48.
- Dunlop M., Dossani Z., Szmids H., Chu H., Lee T., Keasling J., Hadi M., Mukhopadhyay A. (2011). Engineering microbial biofuel tolerance and export using efflux pumps. *Mol. Syst. Biol.* 7, 487.
- Dürre P. (2007). Biobutnaol: an attractive biofuel. *Biotechnol. J.* 2, pp. 1525-34.
- Ehrlich F. (1907). Über die Bedingungen der Fuselölbildung und über ihren Zusammenhang mit dem Eiweissaufbau der Hefe. *Ber. Dtsch. Chem. Ges.* 40, pp. 1027–47.
- Elfström L., Widersten M. (2005). The *Saccharomyces cerevisiae* ORF YNR064c protein has characteristics of an ‘orphaned’ epoxide hydrolase. *Biochim. et. Biophys. Acta.* 1748(2), pp. 213-21.
- Ellington A. and Pollard J. (1999). Preparation and Analysis of DNA. In: F. Ausubel, R. Brent, R. Kingston, D. Moore, J. Seidman, J. Smith and K. Struhl, ed., *Short Protocols in Molecular Biology*, 4<sup>th</sup> ed. John Wiley & Sons, pp. 1104.

- ENCODE Project Consortium. (2011). A user's guide to the encyclopedia of DNA elements (ENCODE). *PLoS Biol.* 9, e1001046.
- Falco S., Dumas K., Livak K. (1985). Nucleotide sequence of the yeast ILV2 gene which encodes acetolactate synthase. *Nucleic. Acids. Res.* 13(11), pp. 4011-27.
- Feilmeier B., Iseminger G., Shroeder D., Webber H., Phillips G. (2000). Green fluorescent protein functions as a reporter for protein localization in *Escherichia coli*. *J. Bacteriol.* 182(14), pp. 4068-76.
- Fernández-Niño M., Marquina M., Swinnen S., Rodríguez-Porrata B., Nevoigt E., Ariño J. (2015). The Cytosolic pH of Individual *Saccharomyces cerevisiae* Cells Is a Key Factor in Acetic Acid Tolerance. *Appl. Environ. Microbiol.* 81(22), pp. 7813-21.
- Few N., Wen S., Tau C., Chon S., Beng T. (2009). Quantitation of green fluorescent protein using a gel-based imaging method. *Anal. Biochem.* 384, pp. 353-55.
- Fidalgo M., Barrales R., Ibeas J., Jimenez J. (2006). Adaptive evolution by mutations in the *FLO11* gene. *PNAS.* 103(30), pp. 11228-33.
- Fischer C., Klein-Marcuschamer D., Stephanopoulos G. (2008). Selection and optimization of microbial hosts for biofuels production. *Metabol Eng.* 10, pp. 295-304.
- Flickinger M. (1980). Current biological research in conversion of cellulosic carbohydrates into liquid fuels: how far have we come. *Biotechnol. Bioeng.* 22, pp. 27-48.
- Flickweert M., van der Zanden L., Janssen W., Steensma Y., van Dijken J., Pronk J. (1996). Pyruvate decarboxylase: An indispensable enzyme for growth of *Saccharomyces cerevisiae* on glucose. *Yeast.* 12(3), pp. 247-57.
- Flores I., Benetti R., Blasco M. (2006). Telomerase regulation and stem cell behaviour. *Curr Opin Cell Biol.* 18, pp 254–60.
- Forsburg S., Guarente L. (1989). Identification and characterization of HAP4: a third component of the CCAAT-bound HAP2/HAP3 heteromer. *Genes. Dev.* 3, pp. 166-78.
- Foury F. (1997). Human genetic diseases: a cross-talk between man and yeast. *Gene.* 195(1), pp. 1-10.
- Galanie S., Thodey K., Trenchard I., Interrante M., Smolke C. (2015). Complete biosynthesis of opioids in yeast. *Science.* 349, pp. 1095-100.
- Galdieri L., Mehrotra S., Yu S., Vancura A. (2010). Transcriptional Regulation in Yeast during Diauxic Shift and Stationary Phase. *OMICS.* 14(6), pp. 629-38.
- Galitski T., Saldanha A., Styles C., Lander E., Fink G. (1999). Ploidy regulation of gene expression. *Science.* 285(5425), pp. 251-4.
- Galloni E., Fontana G., Staccone S., Scala F. (2016). Performance analyses of a spark-ignition engine firing with gasoline–butanol blends at partial load operation. *Energy Convers. Manag.* 110, pp. 319-26.
- Gancedo J. (2008). The early steps of glucose signalling in yeast. *FEMS. Microbiol. Rev.* 32(4), pp. 673-704.

- Ganzhorn A., Green D., Hershey A., Gould R., Plapp B. (1987). Kinetic characterization of yeast alcohol dehydrogenases. Amino acid residue 294 and substrate specificity. *J. Biol. Chem.* 262(8), pp. 3754-61.
- Garcerá A., Barreto L., Piedrafita L., Tamarit J., Herrero E. (2006). *Saccharomyces cerevisiae* cells have three Omega class glutathione S-transferases acting as 1-Cys thiol transferases. *Biochem. J.* 398(2), pp. 187-196.
- Garg S., Jain A. (1995). Fermentative production of 2,3-butanediol: A review. *Biores. Technol.* 51, pp. 103-9.
- Ghiaci P., Norbeck J., Larsson C. (2013). Physiological adaptations of *Saccharomyces cerevisiae* evolved for improved butanol tolerance. *Biotechnol. Biofuels.* 6, 101.
- Gimeno C., Ljungadhi P., Styles C., Fink G. (1992). Unipolar Cell Divisions in the Yeast *S. cerevisiae* Lead to Filamentous Growth: Regulation by Starvation and RAS. *Cell*, 68, pp. 1077-90.
- Gomaa M., Al-Haj L., Abed R. (2016). Metabolic engineering of Cyanobacteria and microalgae for enhanced production of biofuels and high-value products. *J. Appl. Microbiol.* 121, pp. 919-31.
- Goodwin S., McPherson J., McCombie W. (2016). Coming of age: ten years of next-generation sequencing technologies. *Nat. Rev. Genet.* 17, pp. 333-51.
- González A., Hall M. (2017). Nutrient sensing and TOR signaling in yeast and mammals. *EMBO J.* 36(4), pp. 397-408.
- González E., Fernández R., Larroy C., Solà, Pericàs M., Parés X., Biosca J. (2000). Characterization of a (2R,3R)-2,3-Butanediol Dehydrogenase as the *Saccharomyces cerevisiae* YAL060W Gene Product: DISRUPTION AND INDUCTION OF THE GENE. 275 *J. Biol. Chem.* (46), pp. 3876-85.
- González B., Mas A., Beltran G., Cullen P., Torjilla M. (2017). Role of Mitochondrial Retrograde Pathway in Regulating Ethanol-Inducible Filamentous Growth in Yeast. *Mol. Cell. Biol.* 22(12), pp. 3994-4000.
- González-Ramos D., van den Broek M., van Maris A., Pronk J., Daran J. (2013). Genome-scale analyses of butanol tolerance in *Saccharomyces cerevisiae* reveal an essential role of protein degradation. *Biotechnol Biofuels.* 6(1), 48. doi:10.1186/1754-6834-6-48.
- Granek J., Magwene P. (2010). Environmental and Genetic Determinants of Colony Morphology in Yeast. *PLoS Genet.* 6(1), e1000823.
- Grant C., Maclver F., Dawes I. (1996). Glutathione is an essential metabolite required for resistance to oxidative stress in the yeast *Saccharomyces cerevisiae*. *Curr. Genet.* 29, pp. 511-15.
- Grant. C. (2001). Role of the glutathione/glutaredoxin and thioredoxin systems in yeast growth and response to stress conditions. *Mol. Microbiol.* 39(3), pp. 553-41.

- Grozdanov P., Roy S., Kittur N., Meier T. (2009). SHQ1 is required prior to NAF1 for assembly of H/ACA small nucleolar and telomerase RNPs. *RNA*. 15, pp. 1188-97.
- Haber J. (2012). Mating-Type Genes and *MAT* Switching in *Saccharomyces cerevisiae*. *GENETICS*. 191(1), pp. 33-64.
- Halligan. J. (2017). The use of diacetyl (2,3-butanedione) and related flavoring substances as flavorings added to foods—Workplace safety issues. *Toxicol.* 388, pp. 1-6.
- Harden A., Walpole G. (1906). 2,3-Butylene glycol fermentation by *Aerobacter aerogenes*. *Roy. Soc. Proc.* 77, pp. 399-405.
- Hardie, D. (2007). AMP-activated/SNF1 protein kinases: conserved guardians of cellular energy. *Nat. Rev. Mol. Cell. Biol.* 8, pp. 774–85.
- Hahne K., Rödel G., Ostermann K. (2021). A fluorescence-based yeast sensor for monitoring acetic acid. *Eng. Life. Sci.* 21(5), pp. 303-13.
- Hanko E., Minton N., Malys N. (2018). A Transcription Factor-Based Biosensor for Detection of Itaconic Acid. *ACS. Synth. Biol.* 7(5), pp. 1436-46.
- Hansen J., Cherest H., Kielland-Brandt M. (1994). Two Divergent *MET10* Genes, One from *Saccharomyces cerevisiae* and One from *Saccharomyces carlsbergensis*, Encode the  $\alpha$  Subunit of Sulfite Reductase and Specify Potential Binding Sites for FAD and NADPH. *J. Bacteriol.* 176(19), pp. 6050-58.
- Hartwell L. (2002). NOBEL LECTURE: Yeast and Cancer. *Biosci. Rep.* 22, pp. 373-94.
- Haynes W. (2014). Section 5: Thermochemistry, Electrochemistry and Solution Chemistry. In: W. Haynes, ed., *CRC Handbook of Chemistry and Physics*, 95<sup>th</sup> ed. Boca Ratón: CRC Press, pp. 2666.
- Hazelwood L., Daran J., van Maris A., Pronk J., Dickinson J. (2008). The Ehrlich Pathway for Fusel Alcohol Production: a Century of Research on *Saccharomyces cerevisiae* Metabolism. *Appl. Environ. Microbiol.* 74(8), pp. 2259-66.
- Hedbacker K., Carlson M. (2009). SNF1/AMPK pathways in yeast. *Front. Biosci.* 13, pp. 2408-20.
- Heppert J., Dickinson D., Pani A., Higgins C., Steward A., Ahringer J., Kuhn J., Goldstein B. (2016). Comparative assessment of fluorescent proteins for in vivo imaging in an animal model system. *Mol. Biol. Cell.* 27(22), pp. 3385-94.
- Herskowitz I. (1989). A regulatory hierarchy for cell specialization in yeast. *Nature*. 342, pp. 749-57.
- Higgins V., Rogers P., Dawes I. (2020). Application of Genome-Wide Expression Analysis To Identify Molecular Markers Useful in Monitoring Industrial Fermentations. *Appl. Environ. Microbiol.* 69(12), pp. 7535-40.

- Hinnebusch A. (2000). Mechanism and regulation of initiator methionyl-tRNA binding to ribosomes. In: N. Sonenberg, J. Hershey, M. Mathews, eds., *Translational Control of Gene Expression*. New York: Cold Spring Harbor Laboratory Press, pp. 185–244.
- Hogan D., Auchtung T., Hausinger R. (1999). Cloning and Characterization of a Sulfonate/ $\alpha$ -Ketoglutarate Dioxygenase from *Saccharomyces cerevisiae*. *J. Bacteriol.* 181(18), pp. 5876-79.
- Hohmann S. (1991). Characterization of *PDC6*, a third structural gene for pyruvate dehydrogenase in *Saccharomyces cerevisiae*. *J. Bacteriol.* 173(24), pp. 7963-69.
- Hong S., Leiper F., Woods A., Darling D., Carlson M. (2003). Activation of yeast Snf1 and mammalian AMP-activated protein kinase by upstream kinases. *PNAS*. 100(15), pp. 8839-43.
- Hong K., Nielsen J. (2012). Metabolic engineering of *Saccharomyces cerevisiae*: a key cell factory platform for future biorefineries. *Cell. Mol. Life Sci.* 69(16), pp. 2671-90.
- Hornby J., Jensen E., Lisek A., Tasto J., Jahnke B., Shoemaker R., Dussault P., Nickerson K. (2001). Quorum Sensing in the Dimorphic Fungus *Candida albicans* Is Mediated by Farnesol. *Appl. Environ. Microbiol.* 67(7), pp. 2982-92.
- Hou X., Peng W., Xiong L., Huang C., Chen X., Chen X., Zhang W. (2013). Engineering *Clostridium acetobutylicum* for alcohol production. *J. Biotechnol.* 166, pp. 25-33.
- Iizuka R., Yamagishi-Shirasaki M., Funatsu T. (2011). Kinetic study of *de novo* chromophore maturation of fluorescent proteins. *Anal. Biochem.* 414(2), pp. 173-8.
- Isken S., de Bont J. (1998). Bacteria tolerant to organic solvents. *Extremophiles*. 2(3), pp. 299-38.
- Izquierdo A., Casas C., Mühlenhoff U., Lillig C., Herrero E. (2008). *Saccharomyces cerevisiae* Grx6 and Grx7 Are Monothiol Glutaredoxins Associated with the Early Secretory Pathway. *Am. Soc. Microbiol.* 7(8), 1415-26.
- Jaff A., Ellass J. (2015). War and the Oil Price Cycle. *J. Int. Aff.* 69(1), pp. 121-137.
- Jang Y., Lee J., Malaviya A., Seung do Y., Cho J., Lee S. (2012). Butanol production from renewable biomass: rediscovery of metabolic pathways and metabolic engineering. *Biotechnol J.* 7(2), pp. 186-98.
- Janke C., Magiera M., Rathfelder N., Taxis C., Reber S., Maekawa H., Moreno-Borchart A., Doenges G., Schwob E., Schiebel E., Knop M. (2004). A versatile toolbox for PCR-based tagging of yeast genes: new fluorescent proteins, more markers and promoter substitution cassettes. *Yeast*. 21(11), pp. 947-62.
- Jansen N., Flickinger M., Tsao G. (1984). Production of 2,3-butanediol from d-xylose by *Klebsiella oxytoca* ATCC 8724. *Biotechnol. Bioeng.* 26, pp. 362-69.
- Jay J. (1982). Antimicrobial properties of diacetyl. *Appl. Environ. Microbiol.* 44(3), pp. 525-32.

- Jin R., Dobry C., McCown P., Kumar A. (2008). Large-Scale Analysis of Yeast Filamentous Growth by Systematic Gene Disruption and Overexpression. *Mol. Biol. Cell.* 19(1), pp. 284-96.
- Jones D., Shirley M., Wu X., Keis S. (2000). Bacteriophage infections in the industrial acetone butanol (AB) fermentation process. *J. Mol. Microbiol. Biotechnol.* 2(1), pp. 21-6.
- Jones R. (1989). Biological principles for the effects of ethanol. *Enzyme. Microbiol. Technol.* 11, pp. 130-53.
- Jones S., Vignais M., Broach J. (1991). The CDC25 protein of *Saccharomyces cerevisiae* promotes exchange of guanine nucleotides bound to ras. *Mol. Cell. Biol.* 11(5), pp. 2641-6.
- Jönsson L., Martín C. (2016). Pretreatment of lignocellulose: Formation of inhibitory by-products and strategies for minimizing their effects. *Biores. Tec.* 199, pp. 103-12.
- Jordá T., Puig S. (2020). Regulation of Ergosterol Biosynthesis in *Saccharomyces cerevisiae*. *Genes.* 11(7), 795.
- Kang C., Jiang Y. (2005). Genome-wide survey of non-essential genes required for slowed DNA synthesis-induced filamentous growth in yeast. *Yeast.* 22(2), pp. 79-90.
- Kern K., Dunn C., Pichová A., Dickinson R. (2004). Isoamyl alcohol-induced morphological change in *Saccharomyces cerevisiae* involves increases in mitochondria and cell wall chitin content. *FEMS Yeast Res.* 5(1), pp. 43-49.
- Kheirein K., Schilling, R., Möller-Hergt B., Wurm C., Jakobs S., Lamkemeyer T., Langer T., Ott M. (2015). Organization of Mitochondrial Gene Expression in Two Distinct Ribosome-Containing Assemblies. *Cell. Rep.* 10(6), pp. 843-53.
- Khmelniskii A., Meurer M., Duishoev N., Delhomme N., Knop M. (2011). Seamless Gene Tagging by Endonuclease-Driven Homologous Recombination. *PLoS One.* 6(8).
- Kim H., Lee S., Kang H., Oh G., Kim T. (2014). Two distinct domains of Flo8 activator mediates its role in transcriptional activation and the physical interaction with Mss11. *Biochem. Biophys. Res. Comm.* 499(2), pp. 202-7.
- Kim H., Ju J., Lee H., Chun H., Seong J. (2021). Genetically Encoded Biosensors Based on Fluorescent Proteins. *Sensors.* 21(3), 795.
- Kim S., Kahn J. (2015). Efficient production of 2,3-butanediol in *Saccharomyces cerevisiae* by eliminating ethanol and glycerol production and redox rebalancing. 31, pp. 94-101.
- Kiss T., Fayet-Lebaron N., Jány B. (2010). Box H/ACA Small Ribonucleoproteins. *Mol. Cell.* 37(5), pp. 597-606.
- Knop M., Siegers K., Pereira G., Zachariae W., Winsor B., Nasmyth K., Schiebel E. (1999). Epitope tagging of yeast genes using a PCR-based strategy: more tags and improved practical routines. *Yeast.* 15(10), pp. 963-72.

- Kohlwein S., Eder S., Oh C., Martin C., Gable K., Bacikova D., Dunn T. (2001). Tsc13p Is Required for Fatty Acid Elongation and Localizes to a Novel Structure at the Nuclear-Vacuolar Interface in *Saccharomyces cerevisiae*. *Am. Soc. Microbiol. Mol. Cell. Biol.* 21(1), pp. 109-25.
- Kroemer G., Galluzzi L., Brenner C. (2007). Mitochondrial Membrane Permeabilization in Cell Death. *Physiol. Rev.* 87(1), pp. 99-163.
- Kron S., Styles C., Fink G. (1994). Symmetric cell division in pseudohyphae of the yeast *Saccharomyces cerevisiae*. *Mol. Biol. Cel.* 5(9), pp. 1003-22.
- Kuchin S., Vyas V., Carlson M. (2002). Snf1 Protein Kinase and the Repressors Nrg1 and Nrg2 Regulate *FLO11*, Haploid Invasive Growth, and Diploid Pseudohyphal Differentiation. *Mol. Cell. Biol.* 22(12), pp. 3994-4000.
- Kuras L., Cherest H., Surdin-Kerjan Y., Thomas D. (1996). A heteromeric complex containing the centromere binding factor 1 and two basic leucine zipper factors, Met4 and Met28, mediates the transcription activation of yeast sulfur metabolism. *EMBO. J.* 15(10), pp. 2519-29.
- Lamuchhane G., Acharya A., Poudel D., Aryal B., Gyawali N., Niraula P. (2021). Recent advances in bioethanol production from Lignocellulosic biomass. *Int. J. Green. Energy.* 18(7), pp. 731-44.
- Landgraf D., Huh D., Hallacli E., Lindquist S. (2016). Scarless Gene Tagging with One-Step Transformation and Two-Step Selection in *Saccharomyces cerevisiae* and *Schizosaccharomyces pombe*. *PLoS One.* 11(10).
- Larochelle M., Drouin S., Robert F., Turcotte B. (2006). Oxidative Stress-Activated Zinc Cluster Protein Stb5 Has Dual Activator/Repressor Functions Required for Pentose Phosphate Pathway Regulation and NADPH Production. *Mol. Cell. Biol.* 26(17), pp. 6690-701.
- Ledingham G., Neish A. (1954). Fermentative production of 2,3-butanediol., In L.A. Underkofler, R.J. Hickey, eds, *Industrial Fermentations*, 2, Chemical Publ., New York, pp. 27-93
- Le T., Ju S., Lee H., Lee J., Oh S., Kwon K., Sung B., Lee S., Yeom S. (2021). Biosensor-Based Directed Evolution of Methanol Dehydrogenase from *Lysinibacillus xylanilyticus*. *Int. J. Mol. Sci.* 22(3), 1471.
- Lee J., Jang Y., Lee J., Papoutsakis E., Lee S. (2009). Metabolic engineering of *Clostridium acetobutylicum* M5 for highly selective butanol production. *Biotechnol J.* 4(10), pp. 1432-40.
- Lee Y., Seo J. (2019). Production of 2,3-butanediol from glucose and cassava hydrolysates by metabolically engineered industrial polyploid *Saccharomyces cerevisiae*. *Biotechnol. Biofuels.* 12(204).
- Letcher T. (2019). Why do we have global warming? In: Letcher T., ed. *Managing Global Warming, An Interface of Technology and Human Issues*. Academic Press, pp. 3-15.

- Levine B., Klionsky D. (2017). Autophagy wins the 2016 Nobel Prize in Physiology or Medicine: Breakthroughs in baker's yeast fuel advances in biomedical research. *PNAS*. 114(2), pp. 201-5.
- Lian J., Chao R., Zhao H. (2014). Metabolic engineering of a *Saccharomyces cerevisiae* strain capable of simultaneously utilizing glucose and galactose to produce enantiopure (2R,3R)-butanediol. *Metab. Eng.* 23, pp. 92-9.
- Li L., Kaplan J., Ward D. (2017). The glucose sensor Snf1 and the transcription factors Msn2 and Msn4 regulate transcription of the vacuolar iron importer gene CCC1 and iron resistance in yeast. *J. Biol. Chem.* 292, pp. 15577-86.
- Li Z., Lee I., Moradi E., Hung N., Johnson A., Marcotte E. (2009). Rational Extension of the Ribosome Biogenesis Pathway Using Network-Guided Genetics. *PLOS. Biol.* 7(10), e1000213.
- Liu J., Barrientos A. (2013). Transcriptional Regulation of Yeast Oxidative Phosphorylation Hypoxic Genes by Oxidative Stress. *Antiox. & Redox. Sig.* 19(16), pp. 1916-27.
- Liu H., Wang G., Zhang J. (2013). Chapter 6: The Promising Fuel-Biobutanol. In Fang Z., ed., *Liquid, Gaseous and Solid Biofuels - Conversion Techniques*. INTECH, [S.I.], pp. 552.
- Liu D., Evans T., Zhang F. (2015). Applications and advances of metabolite biosensors for metabolic engineering. *Metabol. Eng.* 31, pp. 35-43.
- Liu H., Yang S., Wang F., Bai C., Hu Y., Zhang X. (2016). Polymerization of 1,3-butadiene catalyzed by cobalt(II) and nickel(II) complexes bearing pyridine-2-imidate ligands. *Chin. J. Polym. Sci.* 34, pp. 1060-69.
- Lobas M., Tao R., Nagai J., Kronschläger M., Borden P., Marvin J., Looger L., Khakh B. (2019). A genetically encoded single-wavelength sensor for imaging cytosolic and cell surface ATP. *Nat. Commun.* 10, 711. doi: 10.1038/s41467-019-08441-5.
- Loewith R., Hall M. (2011). Target of Rapamycin (TOR) in Nutrient Signaling and Growth Control. *Genetics*. 189(4), pp. 1177-1201.
- Lomakin I., Xiong Y., Steitz T. (2007). The Crystal Structure of Yeast Fatty Acid Synthase, a Cellular Machine with Eight Active Sites Working Together. *Cell*. 129(2), pp. 319-32.
- Lorenz M., Heitman J. (1998). The MEP2 ammonium permease regulates pseudohyphal differentiation in *Saccharomyces cerevisiae*. *EMBO J.* 17(5), pp. 1236-47.
- Lorenz M., Cutler N., Heitman J. (2000). Characterization of Alcohol-induced Filamentous Growth in *Saccharomyces cerevisiae*. *Mol. Biol. Cel.* 11(1), pp. 183-199.
- Love M., Huber W., Anders S. (2014). Moderated estimation of fold change and dispersion for RNA-seq data with DESeq2. *Genome. Biol.* 15, 550.
- Maddox I. (1996). Microbial production of 2,3-butanediol, pp. 269–291. In Roehr M. ed., *Biotechnology: products of primary metabolism*, vol. 6. VCH, Weinheim, Germany.

- Madhani H., Styles C., Fink G. (1997). MAP Kinases with Distinct Inhibitory Functions Impart Signaling Specificity during Yeast Differentiation. *Cell*. 91(5), pp. 673-684.
- Mahr R., Frunzke K. (2016). Transcription factor-based biosensors in biotechnology: current state and future prospects. *Appl. Microbiol. Biotechnol.* 100, pp. 70-90.
- Mans R., Daran J., Pronk J. (2018). Under pressure: evolutionary engineering of yeast strains for improved performance in fuels and chemicals production. *Curr. Opin. Biotechnol.* 50, pp. 47-56.
- Marciniak S., Perry G. (2017). Harnessing ancient genomes to study the history of human adaptation. *Nat. Rev. Genet.* 18, pp. 659-74.
- Marcó M., Moineau S., Quiberoni A. (2012). Bacteriophages and dairy fermentations. *Bacteriophage*. 2(3), pp. 149-58.
- Martin C., Oh C., Jiang Y. (2007). Regulation of long chain unsaturated fatty acid synthesis in yeast. *Biochim. et Biophys. Acta.* 1771(3), pp. 271-85.
- Martínez Montañés F., Pascual-Ahuir A., Proft M. (2010). Repression of ergosterol biosynthesis is essential for stress resistance and is mediated by the Hog1 MAP kinase and the Mot3 and Rox1 transcription factors. *Mol. Microbiol.* 79(4), pp. 1008-23.
- Marx H., Mattanovich D., Sauer M. (2008). Overexpression of the riboflavin biosynthetic pathway in *Pichia pastoris*. *Microb. Cell. Fact.* 7, 23.
- Maslanka R., Kwolek-Mirek M., Zadrag-Tecza R. (2018). Autofluorescence of yeast *Saccharomyces cerevisiae* cells caused by glucose metabolism products and its methodological implications. *J. Microbiol. Methods.* 146, pp. 55-60.
- Mathieu L., Marsy S., Saint-Georges Y., Jacq C., Dujardin G. (2011). A transcriptome screen in yeast identifies a novel assembly factor for the mitochondrial complex III. *Mitochondrion*. 11(3), pp. 391-96.
- Matsifuji Y., Nakagawa T., Fujimura S., Tani A., Nakagawa J. (2010). Transcription factor Stb5p is essential for acetaldehyde tolerance in *Saccharomyces cerevisiae*. *J. Basic. Microbiol.* 50(5), pp. 494-98.
- Matsifuji Y., Yamamoto K., Yamauchi K., Mitsunaga T., Hayakawa T., Nakagawa T. (2013). Novel physiological roles for glutathione in sequestering acetaldehyde to confer acetaldehyde tolerance in *Saccharomyces cerevisiae*. *Appl. Microbiol. Biotechnol.* 97, pp. 297-303.
- Mayer F., Heath R., Underwood E., Sanders M., Carmena D., McCartney R., Leiper F., Xiao B., Jing C., Walker P., Haire L., Ogrodowicz R., Martin S., Schmidt M., Gamblin S., Carling D. (2011). ADP regulates *SNF1*, the *Saccharomyces cerevisiae* homolog of AMP-activated protein kinase. *Cell. Metab.* 14(5), pp. 707-714.
- Mayordomo I., Estruch F., Sanz P. (2002). Convergence of the Target of Rapamycin and the Snf1 Protein Kinase Pathways in the Regulation of the Subcellular Localization of Msn2, a Transcriptional Activator of STRE (Stress Response Element)-regulated Genes. *J. Biol. Chem.* 277(38), pp. 35650-56.

- McGovern P., Zhang J., Tang J., Zhang Z., Hall G., Moreau RA. Nuñez A., Butrym E., Richards M., Wang C., Cheng G., Zhao Z., Wang C. (2004). Fermented beverages of pre- and proto-historic China. *Proc Natl Acad Sci U S A*, 101(51), pp. 17593-8.
- McGovern P., Hartung U., Badler V., Glukser D., Exner L. (1997). The Beginnings of Winemaking and Viniculture in the Ancient Near East and Egypt. *Expedition*, 39(1), pp. 3-21.
- Mi H., Ebert D., Muruganujan A., Mills C., Albou L., Mushayamaha T., Thomas P. (2020). PANTHER version 16: a revised family classification, tree-based classification tool, enhancer regions and extensive API. *Nucl. Acids. Res.* 49(D1), pp. D394-403.
- Miceli M., Jiang J., Tiwari A., Rodriguez-Quiñones J., Jazwinski S. (2012). Loss of mitochondrial membrane potential triggers the retrograde response extending yeast replicative lifespan. *Front. Genet.* 10(2), 102.
- Minard K., McAlister-Henn L. (2005). Sources of NADPH in Yeast Vary with Carbon Source. *J. Biol. Chem.* 280(48), pp. 39890-96.
- Miller R., Sorrell S. (2014). The future of oil supply. *Phil. Trans. R. Soc. A.* 372(2006): 20130179.
- Mishra V., Goswami R. (2017). A review of production, properties and advantages of biodiesel. *Biofuels.* 9(2), pp. 273-89.
- Mitchell W. (1997). Physiology of Carbohydrate to Solvent Conversion by Clostridia. *Adv. Microb. Physiol.* 39, pp. 31-130.
- Mizushima N., Noda T., Yoshimori T., Tanaka Y., Ishii T., George M., Klionsky D., Ohsumi M., Ohsumi Y. (1998). A protein conjugation system essential for autophagy. *Nature.* 395, pp. 395-98.
- Molina M., Cid V., Martín H. (2010). Fine regulation of *Saccharomyces cerevisiae* MAPK pathways by post-translational modifications. *Yeast.* 27(8), pp. 503-511.
- Molin M., Norbeck J., Blomberg A. (2003). Dihydroxyacetone Kinases in *Saccharomyces cerevisiae* Are Involved in Detoxification of Dihydroxyacetone. *J. Biol. Chem.* 278(3), pp. 1415-23.
- Moravvej Z., Makarem M., Rahimpour M. (2019). The fourth generation of biofuel. In: Basile A., Dalena F., eds., *Second and Third Generation of Feedstocks*, 1<sup>st</sup> ed., Elsevier: Amsterdam, The Netherlands; Oxford, UK; Cambridge, MA, USA, pp. 557-597.
- Moriya H., Johnston M. (2004). Glucose sensing and signaling in *Saccharomyces cerevisiae* through the Rgt2 glucose sensor and casein kinase I. *Proc. Natl. Acad. Sci. USA.* 101(6), pp. 1572-7.
- Morrison D. (2012). MAP Kinase Pathways. *Cold Spring Harb Perspect Biol.* 4(11).
- Mösch H., Kübler E., Krappmann S., Fink GR., Braus GH. (1999). Crosstalk between the Ras2p-controlled mitogen-activated protein kinase and cAMP pathways during invasive growth of *Saccharomyces cerevisiae*. *Mol. Cel. Biol.* 10(5), pp. 1325-35.

- Muthukumar K., Rajakumar S., Sarkar, M., Nachiappan V. (2011). Glutathione peroxidase3 of *Saccharomyces cerevisiae* protects phospholipids during cadmium-induced oxidative stress. *Antonie van Leeuwenhoek*. 99, pp. 761–71.
- Nagai T., Sawano A., Park E., Atsushi Miyawaki A. (2001). Circularly permuted green fluorescent proteins engineered to sense Ca<sup>2+</sup>. *PNAS*. 98(6), pp. 3197-202.
- Narayanan V., Sánchez i Nogué V., van Niel E., Gorwa-Graslund M. (2016). Adaptation to low pH and lignocellulosic inhibitors resulting in ethanolic fermentation and growth of *Saccharomyces cerevisiae*. *AMB Expr*. 6(1), 59. doi: 10.1186/s13568-016-0234-8.
- Naresh V., Lee N. (2021). A Review on Biosensors and Recent Development of Nanostructured Materials-Enabled Biosensors. *Sensors*. 21(4), 1109.
- Nath N., McCartney R., Schmidt M. (2003). Yeast Pak1 kinase associates with and activates Snf1. *Mol. Cell. Biol*. 23(11), pp. 3909-17.
- National Center for Biotechnology Center. (2020). *Methyl ethyl ketone | C4H8O – PubChem*. Available at: <https://pubchem.ncbi.nlm.nih.gov/compound/Methyl-ethyl-ketone>. (Accessed: 16 May 2020).
- Nevoigt E. (2008). Progress in Metabolic Engineering of *Saccharomyces cerevisiae*. *Microbiol Mol. Biol. Rev.* 72(3), pp. 379-412.
- Nicolaou S., Gaida S., Papoutsakis E. (2010). A comparative view of metabolite and substrate stress and tolerance in microbial bioprocessing: From biofuels and chemicals, to biocatalysis and bioremediation. *Metabol. Eng.* 12(4), pp. 307-331.
- Nielsen J. (2001). Metabolic engineering. *Appl Microbiol Biotechnol*, 55(3), pp. 263-283.
- Nigavekar S., Tan Y., Cannon J. (2002). Glc8 is a glucose-repressible activator of Glc7 protein phosphatase-1. *Arch. Biochem. Biophys.* 404, pp. 71-9.
- Nishimura H., Kawasaki Y., Kaneko Y., Nosaka K., Iwashima A. (1992). Cloning and characteristics of a positive regulatory gene, *THI2 (PHO6)*, of thiamin biosynthesis in *Saccharomyces cerevisiae*. *FEBS*. 297(1,2), pp. 155-58.
- Oliveros, J. (2015) *Venny*. An interactive tool for comparing lists with Venn's diagrams. Available at: <https://bioinfogp.cnb.csic.es/tools/venny/index.html> (Accessed: 16 Aug 2021).
- Osiro K., Borgström C., Brink D., Fjölnisdóttir B., Gorwa-Grauslund M. (2019). Exploring the xylose paradox in *Saccharomyces cerevisiae* through in vivo sugar signalomics of targeted deletants. *Microb. Cell. Fact.* 18(88).
- Ouyang L., Holland P., Lu H., Bergenholm D., Nielsen J. (2018). Integrated analysis of the yeast NADPH-regulator Stb5 reveals distinct differences in NADPH requirements and regulation in different states of yeast metabolism. *FEMS. Yeast. Res.* 18(8), pp. foy091.
- Paddon C., Keasling J. (2014). Semi-synthetic artemisinin: a model for the use of synthetic biology in pharmaceutical development. *Nat. Rev. Microbiol.* 12(5), pp. 355-67.

- Palecek S., Parikh A., Kron S. (2000). Genetic analysis reveals that *FLO11* upregulation and cell polarization independently regulate invasive growth in *Saccharomyces cerevisiae*. *Genetics*. 156(3), pp. 1005-23.
- Pan X., Heitman J. (1999). Cyclic AMP-Dependent Protein Kinase Regulates Pseudohyphal Differentiation in *Saccharomyces cerevisiae*. *Mol. Cell. Biol.* 19(7), pp. 4874-87.
- Pan X., Heitman J. (2002). Protein Kinase A Operates a Molecular Switch That Governs Yeast Pseudohyphal Differentiation. *Mol. Cell. Biol.* 22(12), pp. 3981-93.
- Pannunzio N., Manthey G., Liddell L., Fu B., Roberts C., Bailis A. (2012). Rad59 regulates association of Rad52 with DNA double-strand breaks. *Microbiol. Open.* 1(3), pp. 285-97.
- Patakova P., Branksa B., Seldar K., Vasylykivska M., Jureckova K., Kolek J., Koscova P. (2019). Acidogenesis, solventogenesis, metabolic stress response and life cycle changes in *Clostridium beijerinckii* NRRL B-598 at the transcriptomic level. *Sci. Rep.* 9(1371).
- Patiño M., Ortiz J., Velásquez M., Stambuk B. (2019). d-Xylose consumption by nonrecombinant *Saccharomyces cerevisiae*: A review. *Yeast.* 36(9), pp. 541-556.
- Patriarchi T., Cho J., Merten K., Howe M., Marley A., Xiong W., Folk R., Broussard G., Liang R., Jang M., Zhong H., Dombeck D., von Zastrow M., Nimmerjahn A., Gradinaru V., Williams J., Tian L. (2018). Ultrafast neuronal imaging of dopamine dynamics with designed genetically encoded sensors. *Science.* 360(6396). doi: 10.1126/science.aat4422.
- Petranovic D., Nielsen J. (2008). Can yeast systems biology contribute to the understanding of human disease? *Trends Biotechnol.* 26(11), pp. 584-90.
- Pfeiffer T., Morley A. (2014). An evolutionary perspective on the Crabtree effect. *Front. Mol. Biosci.* doi: 10.3389/fmolb.2014.00017.
- Polevoda B., Martzen M., Das B., Phizicky E., Sherman F. (2000). Cytochrome c Methyltransferase, Ctm1p, of Yeast. *J. Biol. Chem.* 275(7), pp. 20508-13.
- Polvi E., Li X., O'Meara T., Leach M., Cowen L. (2015). Opportunistic yeast pathogens: reservoirs, virulence mechanisms, and therapeutic strategies. *Cell. Mol. Life Sci.* 72, 2261-87.
- Principi P., König R., Cuomo M. (2019). Anaerobic Digestion of Lignocellulosic Substrates: Benefits of Pre-Treatments. *Curr. Sustainable Renewable Energy Rep.* 6, pp. 61-70.
- Putman M., van Veen H., Konings W. (2000). Molecular properties of bacterial multidrug transporters. *Microbiol. Mol. Biol. Rev.* 64(4), pp. 672-93.
- Qi Y., Liu Z., Liu S., Cui L., Dai Q., He J., Dong W., Bai C. (2019). Synthesis of 1,3-Butadiene and Its 2-Substituted Monomers for Synthetic Rubbers. *Catalysts.* 9(1), 97.
- Qin D. (2019). Next-generation sequencing and its clinical application. *Cancer Biol. Med.* 16(1), pp. 4-10.

- Revuelta J., Serrano-Amatriain C., Ledesma-Amaro R., Jiménez A. (2018). Formation of folates by microorganisms: towards the biotechnological production of this vitamin. *Appl. Microbiol. Biotechnol.* 102(20), pp. 8613-20.
- Reynolds T., Fink G. (2001). Bakers' yeast, a model for fungal biofilm formation. *Science.* 291, pp. 878-81.
- Rieske J.S. (1967) Antimycin A. In: Gottlieb D., Shaw P.D., eds., *Mechanism of Action. Antibiotics*, vol 1. Springer, Berlin, Heidelberg.
- Robertson L., Fink G. (1998). The three yeast A kinases have specific signaling functions in pseudohyphal growth. *Proc. Natl. Acad. Sci. U S A.* 95(23), pp. 13783-7.
- Rodríguez-Manzanque M., Tamarit J., Bellí G., Ros J., Herrero E. (2002). Grx5 Is a Mitochondrial Glutaredoxin Required for the Activity of Iron/Sulfur Enzymes. *Mol. Biol. Cell.* 13(4), pp. 1109-21.
- Romano P., Suzzi G. (1996). Origin and Production of Acetoin during Wine Yeast Fermentation. *Appl. Environ. Microbiol.* 62(29), pp. 309-15.
- Rosado C., Mijaljica D., Hatzinisiriou I., Prescott M., Devenish R. (2007). Rosella: A fluorescent pH-biosensor for reporting vacuolar turnover of cytosol and organelles in yeast. *Autophagy.* 4(2), pp. 205-13.
- Roullion A., Surdin-Kerjan Y., Thomas D. (1999). Transport of sulfonium compounds. Characterization of the s-adenosylmethionine and s-methylmethionine permeases from the yeast *Saccharomyces cerevisiae*. *J. Biol. Chem.* 274(40), pp. 28096-105.
- Rubenstein E., McCartney R., Zhang C., Shokat K., Shirra M., Arndt K., Schmidt M. (2008). Access Denied: Snf1 Activation Loop Phosphorylation Is Controlled by Availability of the Phosphorylated Threonine 210 to the PP1 Phosphatase. *J. Biol. Chem.* 283, pp. 222-30.
- Rupp S. (2002). *LacZ Assays in Yeast*. In: Guthrie C., Fink G., eds., *Methods in Enzymology Volume 350, Guide to Yeast Genetics and Molecular and Cell Biology - Part B*, 1<sup>st</sup> ed. Elsevier, pp. 112-131.
- Russell D., Smith M. (1983). Nucleotide Sequence of the Yeast Alcohol Dehydrogenase I1 Gene. *J. Biol. Chem.* 258(4), pp. 2674-82.
- Rutherford J., Chua G., Hughes T., Cardenas M., Heitman J. (2008). A Mep2-dependent Transcriptional Profile Links Permease Function to Gene Expression during Pseudohyphal Growth in *Saccharomyces cerevisiae*. *Mol. Biol. Cell.* 19(7), pp. 3028-39.
- Sablayrolles J., Goma G. (1894). Butanediol production by *Aerobacter aerogenes* NRRL B199: effect of initial substrate concentration and aeration, agitation. *Biotechnol. Bioeng.* 26, pp. 148-55.
- Sallin O., Reymond L., Gondrand C. Raith F., Koch B., Jonsson K. (2018). Semisynthetic biosensors for mapping cellular concentrations of nicotinamide adenine dinucleotides. *eLife*. doi: 10.7554/eLife.32638.
- Sanger F., Nickler S., Coulson A. (1977). DNA sequencing with chain-terminating inhibitors. *Proc. Natl. Acad. Sci. USA.* 74(12), pp. 5463-67.

- Santos P., Simões T., Sa-Correira I. (2009). Insights into yeast adaptive response to the agricultural fungicide mancozeb: A toxicoproteomics approach. *Proteomics*. 9, pp. 657-70.
- Sardi M., Krause M., Heilberger J., Gasch A. (2018). Genotype-by-Environment-by-Environment Interactions in the *Saccharomyces cerevisiae* Transcriptomic Response to Alcohols and Anaerobiosis. *Genes Genomes Genetics*. 8(12), pp. 3881-90.
- Schaaff I., Heinisch J., Zimmermann F. (1989). Overproduction of glycolytic enzymes in yeast. *Yeast*. 5(4), pp. 285-90.
- Schiestl R., Gietz R. (1989). High efficiency transformation of intact yeast cells using single stranded nucleic acids as a carrier. *Curr. Genet.* 16, pp. 339-346.
- Schmidt M., McCartney R. (2000).  $\beta$ -subunits of Snf1 kinase are required for kinase function and substrate definition. *EMBO. J.* 19(18), pp. 4936-43.
- Sellmer S., Sievers M., Teuber M. (1992). Morphology, Virulence and Epidemiology of Bacteriophage Particles Isolated from Industrial Vinegar Fermentations. *Syst. Appl. Microbiol.* 15(4), pp. 610-16.
- Senejani A., Gogarten J. (2007) Structural stability and endonuclease activity of a PI-SceI GFP-fusion protein. *Int. J. Biol. Sci.* 3(4), pp. 205-11.
- Shashkova S., Wollman A., Hohmann S., Leake M. (2018). Characterising Maturation of GFP and mCherry of Genomically Integrated Fusions in *Saccharomyces cerevisiae*. *Bio-protocol*. 8(2), e2710.
- Shi S., Si T., Zhang H., Ang E., Zhao H. (2016). Metabolic engineering of a synergistic pathway for *n*-butanol production in *Saccharomyces cerevisiae*. *Sci. Rep.* 6.
- Shi S., Choi Y., Zhao H., Tan M., Ang E. (2017). Discovery and engineering of a 1-butanol biosensor in *Saccharomyces cerevisiae*. *Biores. Tech.* 245(B), pp. 1343-51.
- Shekhawat K., Patterton H., Bauer F., Setati M. (2019). RNA-seq based transcriptional analysis of *Saccharomyces cerevisiae* and *Lachancea thermotolerans* in mixed-culture fermentations under anaerobic conditions. *BMC Genomics*. 20, 145.
- Shen C., Lan E.,<sup>1</sup> Dekishima Y., Baez A., Myung Cho K., J. Liao. (2011). Driving Forces Enable High-Titer Anaerobic 1-Butanol Synthesis in *Escherichia coli*. *Appl. Environ. Microbiol.* 77(9), pp. 2905-15.
- Shimazu M., Sekito T., Akiyama K., Ohsumi Y., Kakinuma Y. (2005). A Family of Basic Amino Acid Transporters of the Vacuolar Membrane from *Saccharomyces cerevisiae*. *J. Biol. Chem.* 280(6), pp. 4851-57.
- Siemering K., Golbik R., Sever R., Haselhoff J. (1996). Mutations that suppress the thermosensitivity of green fluorescent protein. *Curr. Biol* 6(12), pp. 1653-63.
- Simpson-Lavy K., Kupiec M. (2019). Carbon Catabolite Repression in Yeast is Not Limited to Glucose. *Sci. Rep.* 9, 6491.
- Si T., Luo Y., Xiao H., ZHao H. (2014). Utilizing an endogenous pathway for 1-butanol production in *Saccharomyces cerevisiae*. *Metab. Eng.* 22, pp. 60-68.

- Simon J., Szankasi P., Nguyen D., Ludlow C., Dunstan H., Roberts C., Jensen E., Hartwell L., Friend S. (2000). Differential Toxicities of Anticancer Agents among DNA Repair and Checkpoint Mutants of *Saccharomyces cerevisiae*. *Cancer. Res.* 60(2), pp. 328-33.
- Skrzypek M., Nash R., Wong E., MacPherson K., Hellerstedt S., Engel S., Karra K., Weng S., Sheppard T., Binkley G., Simison M., Miyasato S., Cherry J. (2018). *Saccharomyces* genome database informs human biology. *Nucleic Acids Res.* 46, pp. 736-42.
- Smirnova J., Selley J., Sanchez-Cabo F., Carroll K., Eddy A., McCarthy J., Hubbard S., Pavitt G., Grant C., Ashe M. (2005). Global Gene Expression Profiling Reveals Widespread yet Distinctive Translational Responses to Different Eukaryotic Translation Initiation Factor 2B-Targeting Stress Pathways. *Mol. Cel. Biol.* 25(21), pp. 9340-49.
- Song Q., Kumar A. (2012). An Overview of Autophagy and Yeast Pseudohyphal Growth: Integration of Signaling Pathways during Nitrogen Stress. *Cells.* 1(3), pp. 263-83.
- Soltys K., Batta A., Koneru B. (2001). Successful Nonfreezing, Subzero Preservation of Rat Liver with 2,3-Butanediol and Type I Antifreeze Protein. *J. Surg. Ser.* 96(1), pp. 30-34.
- Stanley D., Bandara A., Fraser S., Chambers P., Stanley G. (2010). The ethanol stress response and ethanol tolerance of *Saccharomyces cerevisiae*. *J. Appl. Microbiol.* 109(1), pp. 13-24.
- Starovoytova A., Sorokin M., Sokolov S., Severin F., Knorre D. (2013). Mitochondrial signaling in *Saccharomyces cerevisiae* pseudohyphae formation induced by butanol. *FEMS Yeast Res.* 13(4), pp. 367-74.
- Steen E., Chan R., Prasad N., Myers S., Petzold C., Redding A., Ouellet M., Keasling J. (2008). Metabolic engineering of *Saccharomyces cerevisiae* for the production of n-butanol. *Microb. Cell Fact.* 7(36).
- Sung-Hee A., Acurio A. Kron S. (1999). Regulation of G2/M Progression by the STE Mitogen-activated Protein Kinase Pathway in Budding Yeast Filamentous Growth. *Mol. Biol. Cell.* 10(10), pp. 3301-16.
- Swidah R., Wang H., Reid P., Ahmed H., Pisanelli A., Persaud K., Grant C., Ashe M. (2015). Butanol production in *S. cerevisiae* via a synthetic ABE pathway is enhanced by specific metabolic engineering and butanol resistance. *Biotechnol. Biofuels.* 8(97).
- Swidah R., Ogunlabi O., Grant C., Ashe M. (2018). n-Butanol production in *S. cerevisiae*: co-ordinate use of endogenous and exogenous pathways. *Appl. Microbiol. Biotechnol.* 102, pp. 9857-66.
- Tamura K., Gu Y., Wang Q., Yamada T., Ito K., Shimoi H. (2004). A *hap1* mutation in a laboratory strain of *Saccharomyces cerevisiae* results in decreased expression of ergosterol-related genes and cellular ergosterol content compared to sake yeast. *J. Biosci. Bioeng.* 98(3), pp. 159-66.
- Tanaka K., Nakafuku M., Satoh T., Marshall M., Gibbs J., Matsumoto K., Kaziro Y., Toh-e A. (1990). *S. cerevisiae* genes *IRA1* and *IRA2* encode proteins that may be

- functionally equivalent to mammalian ras GTPase activating protein. *Cell*. 60(5), pp. 803-7.
- Tang Y., Zhang J., Yu J., Xu L., Wu J., Zhou C., Shi Y. (2014). Structure-Guided Activity Enhancement and Catalytic Mechanism of Yeast Grx8. *Biochem*. 53(13), pp. 2185-86.
- Tang R., Li L., Yuan H., He R., Wang Q. (2020). Biosensor-enabled droplet microfluidic system for the rapid screening of 3-dehydroshikimic acid produced in *Escherichia coli*.
- Tapia E., Anschau A., Coradini A., Franco T., Deckmann A. (2012). Optimization of lipid production by the oleaginous yeast *Lipomyces starkeyi* by random mutagenesis coupled to cerulenin screening. *AMB. Expr.* 2, 64.
- Taylor E., Campbell S., Griffiths C., Reid P., Slaven J., Harrison R., Sims P., Pavitt G., Delneri D., Ashe M. (2010). Fusel Alcohols Regulate Translation Initiation by Inhibiting eIF2B to Reduce Ternary Complex in a Mechanism That May Involve Altering the Integrity and Dynamics of the eIF2B Body. *Mol. Biol. Cel.* 21(13), pp. 2202-16.
- Teixeira M., Godinho C., Cabrito T., Mira N., Sá-Correia I. (2012). Increased expression of the yeast multidrug resistance ABC transporter Pdr18 leads to increased ethanol tolerance and ethanol production in high gravity alcoholic fermentation. *Microb. Cell. Fact.* 11, 98.
- Thevelein J., Voordeckers K. (2009). Functioning and Evolutionary Significance of Nutrient Transceptors. *Mol. Biol. Evol.* 26(11), pp. 2407-14.
- Tkach J., Yimit A., Lee A., Riffle M., Costanzo M., Jaschob D., Hendry J., Ou J., Moffat J., Boone C., Davis T., Nislow C., Brown G. (2012). Dissecting DNA damage response pathways by analysing protein localization and abundance changes during DNA replication stress. *Natl Cell. Biol.* 14, pp. 966-76.
- Toda T., Cameron S., Sass P., Zoller M., Wigler M. (1987). Three Different Genes in *S. cerevisiae* Encode the Catalytic Subunits of the cAMP-Dependent Protein Kinase. *Cell*. 50, pp. 277-87.
- Tran A., Chambers R. (1987). The dehydration of fermentative 2,3-butanediol into methyl ethyl ketone. *Biotechnol. Bioeng.* 29(3), pp. 343-51.
- Tresse O., Errampalli D., Kostrzynska M., Leung K., Lee H., Trevors J., van Elsas D. (1998). Green fluorescent protein as a visual marker in a p-nitrophenol degrading *Moraxella sp.* *FEMS. Microbiol. Lett.* 164(1), pp. 187-93.
- Trybek T., Kowalik A., Gózdź S., Kowalska A. (2020). Telomeres and telomerase in oncogenesis (Review). *Oncol Lett.* 20, pp. 1015-27.
- Tu J., Carlson M. (1995). REG1 binds to protein phosphatase type 1 and regulates glucose repression in *Saccharomyces cerevisiae*. *EMBO J.* 14(23), pp. 5939-46.
- Tu R., Li L., Yuan H., He R., Wang Q. (2020). Biosensor-enabled droplet microfluidic system for the rapid screening of 3-dehydroshikimic acid produced in *Escherichia coli*. *J. Ind. Microbiol. Biotechnol.* 47(12), pp. 1155-60.
- Váchová L., Čáp M., Palková Z. (2012). Yeast Colonies: A Model for Studies of Aging, Environmental Adaptation, and Longevity. *Oxid. Med. Cell Longev.* 2012, 601836.

- Vadaie N., Dionne H., Akajagbor D., Nickerson S., Krysan D., Cullen P. (2008). Cleavage of the signaling mucin Msb2 by the aspartyl protease Yps1 is required for MAPK activation in yeast. *J. Cell. Biol.* 181(7), pp. 1073-81.
- Vandenbol M., Jauniaux J., Grenson M. (1989). Nucleotide sequence of the *Saccharomyces cerevisiae* PUT4 proline-permease-encoding gene: similarities between CAN1, HIP1 and PUT4 permeases. *Gene.* 83(1), pp. 153-59.
- Van der Schaft P. (2015). Approaches to production of natural flavors. In: Balagiannis D., ed., *Flavour Development, Analysis and Perception in Food and Beverages*. Cambridge: Woodhead Publishing, pp. 448.
- Varela E., Blasco M. (2010). 2009 Nobel Prize in Physiology or Medicine: telomeres and telomerase. *Oncogene.* 29, pp. 1561-65.
- Villet R. (1981). Biotechnology for Producing Fuels and Chemicals from Biomass: Volume II - Fermentation Chemicals from Biomass. *Fermentation Chemicals from Biomass*. Solar Energy Research Institute, Golden, Colorado, pp. 621-54
- Vincent O., Townley R., Kuchin S., Carlson M. (2001). Subcellular localization of the Snf1 kinase is regulated by specific  $\beta$  subunits and a novel glucose signaling mechanism. *Genes Dev.* 15(9), pp. 1104-14.
- Vyas V., Berkey C., Miyao T., Carlson M. (2005). Repressors Nrg1 and Nrg2 regulate a set of stress-responsive genes in *Saccharomyces cerevisiae*. *Eukaryot. Cell.* 4(11), pp. 1882–91.
- Walker G., Basso T. (2020). Mitigating stress in industrial yeasts. *Fungal. Biol.* 124(5), pp. 387-97.
- Walker R., Pretorius I. (2018). Applications of Yeast Synthetic Biology Geared towards the Production of Biopharmaceuticals. *Genes.* 9(7), pp. 340.
- Wan-Sheng L., Dranginis. (1998). The Cell Surface Flocculin Flo11 Is Required for Pseudohyphae Formation and Invasion by *Saccharomyces cerevisiae*. *Mol. Biol. Cell.* 9(1), pp. 161-171.
- Warburg O., Wind F., Negelein E. (1926). Über den Stoffwechsel von Tumoren im Körper. *J. Mol. Med.* 5, pp. 829-32.
- Watts G. (2001). Three cell cycle scientists win Nobel prize. *BMJ.* 323(7317), pp. 823.
- Webb A., Ingraham J. (1963). Fusel Oil. *Adv. Appl. Microbiol.* 5, pp. 317-353.
- Weismann L., Bacallao R., Wickner W. (1987). Multiple methods of visualizing the yeast vacuole permit evaluation of its morphology and inheritance during the cell cycle. *J. Cell. Biol.* 105(4), pp. 1539-47.
- Wetterstrand K. (2021). DNA Sequencing Costs: Data from the NHGRI Genome Sequencing Program (GSP). Available at: [www.genome.gov/sequencingcostsdata](http://www.genome.gov/sequencingcostsdata). (Accessed: 1 January 2022).

- Williams T., Xu X., Ostrowski M., Pretorius I., Paulsen I. (2017). Positive-feedback, ratiometric biosensor expression improves high-throughput metabolite-producer screening efficiency in yeast. *Synth Biol (Oxf)*. 2(1), ysw002.
- Williams-Hart T., Wu X., Tatchell K. (2002). Protein Phosphatase Type 1 Regulates Ion Homeostasis in *Saccharomyces cerevisiae*. *Genetics*. 160(4), pp. 1423-37.
- Winey M., Mathison L., Soref C., Culbertson M. (1989). Distribution of introns in frameshift-suppressor proline-tRNA genes of *Saccharomyces cerevisiae*. *Gene*. 76(1), pp. 89-97.
- Wingett S., Andrews S. (2018). FastQ Screen: A tool for multi-genome mapping and quality control [version 2; peer review: 4 approved]. *F1000Research*. 7, 1338.
- Winzler E., Shoemaker D., Astromoff A., Liang H., Anderson K., Andre B., Bangham R., Benito R., Boeke J., Bussey H., Chu A., Connely C., Davis K., Dietrich F., Whelen Dow S., El Bakkoury M., Foury F., Friend S., Gentalen E., Giaever G., Hegemann J., Jones T., Laub M., Liao H., Liebundugth N., Lockhart D., Lucau-Danila A., Lussier M., M'Rabet N., Menard P., Mittmann M., Pai C., Rebischung C., Revuelta J., Riles L., Roberts C., Ross-MacDonald P., Scherens B., Snyder M., Sookhai-Mahadeo S., Storms R., Véronneau S., Voet M., Volckaert G., Ward T., Wysocki R., Yen G., Yu K., Zimmermann K., Philippsen P., Johnston M., Davis R. (1999). Functional Characterization of the *S. cerevisiae* Genome by Gene Deletion and Parallel Analysis. *Science*. 285, pp. 901-6.
- Xue Y., Battle M., Hirsch JP. (1998). GPR1 encodes a putative G protein-coupled receptor that associates with the Gpa2p Ga subunit and functions in a Ras-independent pathway. *EMBO. J*. 17, pp. 1996–2007.
- Yao Z., Delorme-Axford E., Backues S., Klionsky D. (2015). Atg41/Icy2 regulates autophagosome formation. *Autophagy*. 11(12), pp. 2288-99.
- Yao Z., Delorme-Axford E., Backues S., Klionsky D. (2016). Atg41/Icy2 regulates autophagosome formation. *Autophagy*. 11(12), pp. 2288-99.
- Yu L., Xu M., Tang I., Yang S. (2015). Metabolic engineering of *Clostridium tyrobutyricum* for n-butanol production through co-utilization of glucose and xylose. *Biotechnol. Bioeng*. 112(10), pp. 2134-41.
- Zahn J., Halter M. (2018). Surveillance and Elimination of Bacteriophage Contamination in an Industrial Fermentation Process. In: Savva R., ed., *Bacteriophages-Perspectives and Future*. IntechOpen, pp. 91-106.
- Zampar G., Kümmel A., Ewald J., Jol S., Niebel B., Picotti P., Aebbersold R., Sauer U., Zamboni N., Heinemann M. (2013). Temporal system-level organization of the switch from glycolytic to gluconeogenic operation in yeast. *Mol. Sys. Biol*. 9(1), 651.
- Zhang Y., Shi S. (2021). Transcription Factor-Based Biosensor for Dynamic Control in Yeast for Natural Product Synthesis. *Front. Bioeng. Biotechnol*. 9, 635265. doi: 10.3389/fbioe.2021.635265.
- Zheng Y., Li L., Xian M., Ma Y., Yang J., Xu X., He D. (2009). Problems with the microbial production of butanol. *J. Ind. Microbiol. Biotechnol*. 36(9), pp. 1127-38.

Zhu L., Dong H., Zhang Y., Li Y. (2011). Engineering the robustness of *Clostridium acetobutylicum* by introducing glutathione biosynthetic capability. *Metab. Eng.* 13(4), pp. 426-34.

Zenklusen D., Wells A., Condeelis J., Singer R. (2007). *Cold. Spring. Harb. Protoc.* doi:10.1101/pdb.prot4870.